DISSERTATION

CHARACTERIZING THE ROLE OF PLANT HORMONES DURING PLANT DEVELOPMENT AND PLANT IMMUNITY IN ARABIDOPSIS THALIANA AND SOLANUM LYCOPERSICUM CV. MICRO-TOM

Submitted by

Hannah Marie Berry

Graduate Degree Program in Cell and Molecular Biology

In partial fulfillment of the requirements

For the Degree of Doctor of Philosophy

Colorado State University

Fort Collins, Colorado

Summer 2022

Doctoral Committee:

Advisor: Cristiana Argueso

Daniel Bush
Patricia Bedinger
Timothy Stasevich

ABSTRACT

CHARACTERIZING THE ROLE OF PLANT HORMONES DURING PLANT DEVELOPMENT AND PLANT IMMUNITY IN ARABIDOPSIS THALIANA AND SOLANUM LYCOPERSICUM CV. MICRO-TOM

Plant hormones are major regulators of plant growth, development, and responses to biotic and abiotic stressors. Constitutive activation of immunity is commonly associated with stunted plant growth. This phenomenon, called the growth defense tradeoff, was previously thought to result from limitations in metabolic processes, where resources were redirected from plant growth toward energetically costly defense responses. However, recent studies have shown that metabolic limitations are not solely responsible for the growth defense tradeoff, and that growth and defense can be uncoupled, resulting in plants with increased immunity without compromising plant yield. While the effects on plant growth have been widely characterized in the context of constitutive immunity, developmental impacts such as changes to plant architecture, reproductive development, and leaf morphology, have been studied to a lesser extent.

Cytokinin is one of nine major plant hormone families and its role in plant growth, meristematic maintenance, cell division, and senescence are widely known. In conjunction with salicylic acid (SA), a primarily defense related hormone, cytokinin acts to promote SA-dependent defense responses, thus demonstrating a role for cytokinin in plant immunity. Perception of cytokinin initiates a two-component signaling phosphorelay leading to the activation of downstream transcription factors to induce the transcription of cytokinin-responsive genes. One group of these transcription factors is the CYTOKININ RESPONSE FACTORS (CRFs), which is found in all land plant species. In Chapter 2, I show that CRFs are negative regulators of plant growth and positively regulate plant defense responses. To further elucidate

the role of CRFs in growth and immunity, I quantified growth and development in crosses between constitutive immunity mutants with elevated SA and *CRF* overexpressing (hereafter *CRFox*) lines. Here, these data show that *CRFox* enhances the growth restriction phenotypes previously characterized in the constitutive immunity mutants. I propose a model with CRF5 at the intersection of CK and SA crosstalk, acting as a regulator of the growth defense tradeoff.

How constitutive immunity alters plant development as well as plant growth is not well understood. In Chapter 3, I characterize changes in plant architecture in constitutive immunity mutants *SUPPRESSOR OF NPR1-1 (NONEXPRESSER OF PATHOGENESIS RELATED GENES 1), CONSTITUTIVE 1* (*snc1*) and *CONSTITUTIVE EXPRESSION OF PR GENES 5* (*cpr5*). Both *snc1* and *cpr5* have elevated levels of endogenous SA and elevated disease resistance. While the reduced growth phenotypes (measured as biomass) of these mutants have been characterized, phyllotaxy has not previously been quantified. Phyllotaxy describes the consistent arrangement or pattern of consecutive organs around a central point. Arabidopsis has a spiral phyllotactic pattern where each consecutive organ is separated by approximately 137.5°. Phyllotactic analysis of shoot apical meristems (SAMs) using scanning electron microscopy and the arrangement of siliques on inflorescence stems in *snc1* mutants showed a change in phyllotactic divergence angle originating from reduced shoot apical meristem size and increased plastochron ratio. The plastochron describes the amount of time between organ initiations but can be shown as a ratio when the edge of two consecutive inflorescence primordia to the SAM center is quantified using imaging software. To mimic the phenotypes of constitutive immunity, I inoculated wild type Arabidopsis Col-0 plants with high concentrations of *Pseudomonas syringae* pv. *tomato* (*Pst*) strains: (1) *Pst* hrcC^{-}, which is lacks the type-III secretion system necessary to introduce bacterial effectors into the plant cell but initiates plant basal immune responses, thus inducing pattern triggered immunity (PTI); (2) *Pst* DC3000, which causes plant disease via introduction of bacterial effector proteins into the plant cell to change plant metabolism and dampen plant immune responses causing effector triggered susceptibility

(ETS); and (3) *Pst* ArvRpm1 where the bacterial effector protein Rpm1 is recognized by the plant, initiating a high level of defense responses called effector triggered immunity (ETI). Only multiple, concentrated inoculations of *Pst* DC3000 were able to induce changes to silique phyllotactic patterns. Notably, the SAM was unaltered after *Pst* DC3000 inoculations, demonstrating, that phyllotactic patterns originating at the meristem are very robust upon infection, and this change in silique patterning was determined to be a result of post-meristematic stem torsion. I conclude that elevated SA throughout the plant life in the constitutive immunity mutants shows a role for SA in regulating meristematic maintenance and/or patterning, but elevated SA after pathogen attack is not sufficient to overcome the tight regulation of the meristem.

Arabidopsis has been a primary source of knowledge for elucidating hormone crosstalk during plant development and immunity. However, Arabidopsis cannot inform us about the roles of hormones during fleshy fruit development. Tomatoes are an important agricultural crop species, have a fully sequenced genome, and many genetic resources are available, making tomatoes a model crop species. In my last research chapter, I quantified plant hormones in *Solanum lycopersicum* cv. Micro-Tom in above- and below-ground plant tissues at four stages of plant development. I selected plant developmental stages based on easily definable traits: the seedling stage was defined as the presence of cotyledons before the emergence of true leaves; the young developmental stage was characterized by the presence of four true leaves before the transition to flowering; the adult or flowering stage was determined by the opening of the first flower; and the fruiting stage was identified by fruit set and fully expanded, breaker, and ripe fruit development stages. While the data collected in this chapter is primarily descriptive, we showed that a single extraction protocol could be used to extract and quantify 18 plant hormones representing 5 of the 9 major hormone families in multiple tissue types including roots, leaves, and fruits. Plant hormone data were integrated into botanical illustrations to create the Plant Hormone Atlas, which was presented at the Art Lab Fort Collins, in Fort Collins, CO.

ACKNOWLEDGEMENTS

First, thank you to everyone who has supported me over the years during graduate school. This feat cannot be accomplished without a network of friends, family, and mentors. Thank you.

Thank you so much to my graduate advisor, Dr. Cris Argueso. Even through rough times, you have been there to give me advice and help me grow as a scientist and person, and I appreciate your dedication to your students and your desire to help us succeed. Thank you to my other graduate advising committee members, Dr. Dan Bush, Dr. Pat Bedinger, and Dr. Tim Stasevich. Though our meetings were infrequent, I valued all the input you have contributed to my projects.

I have had the honor of receiving funding from multiple sources from the start of my graduate career. Thank you to Dr. Lucas Argueso for submitting an application on my behalf to the Program in Molecular Plant Biology before I officially joined the CMB program, which funded my stipend as a GRA for my first two semesters. Thank you to the School of Global Environmental Sciences (SoGES) Sustainable Leadership Fellowship program. I learned so much from the training programs and I really believe they improved my scientific communication skills that will be an invaluable skill throughout my career. In the spring of 2019, I received the USDA NIFA Pre-Doctoral Fellowship, which funded me and my research on tomato hormones for two years. This funding also allowed me to travel to Paris to attend the International Plant Growth Society Association conference in 2019, and other conferences remotely in the summers of 2020 and 2021. Thank you to everyone who gave me feedback while writing this grant. It was a huge honor to receive this special recognition.

Thank you to the Graduate Program in Cell and Molecular Biology (CMB). During my interview weekend in February 2015, I instantly felt the strong bond the first-year students at the time had with one another and was eager to join the community. The interdisciplinary nature of

CMB has allowed me to expand my knowledge of subjects outside of my field and introduced me to other students across campus I would not have otherwise met. Thank you to the Department of Agricultural Science for being my home base and bringing me into another community of researchers more aligned with my research interests. This department is full of warmth and support, I have really enjoyed being part of it.

I cannot thank my friends I have met in graduate school enough. You all have gone through this challenge with me, and I know these are friendships that will last long beyond graduate school. A special thank you to Hailey Conover Sedam, James Curlin, Chase Calvi, Jaz Donkoh, and Jemma Fadum. Not only have I had an amazing group of friends in graduate school but have kept in touch with friends from the past milestones of my life. Thank you to Anita Nagavalli, Sarah Butz Schubel, Fiona Baker, Kathryn Kinser, and Nelly Bellamy. Even though we now live all over the country, thanks for keeping in touch and having zoom baking dates while we catch up. From the bottom of my heart, I love you all.

Lastly, thank you to my family, especially Mom and Dad. You have always believed in my ability to excel in anything I do and have been so supportive along the way. Thank you for convincing me I could rearrange my college classes to fit in that freshman-only biotechnology class, I would not be where I am today without that experience. Thank you for teaching me to be compassionate, resilient, independent, and creative.

DEDICATION

This is dedicated to all the strong, intelligent, creative, and supportive women that have guided me through each stage of my life. You all have been such an inspiration and I couldn't have done it without you. I am forever grateful to be the person you have helped shape me to be.

TABLE OF CONTENTS

CHAPTER 1

More than growth: Phytohormone-regulated transcription factors mediating plant development and immunity[1]

1.1 SUMMARY

Activation of immunity by exogenous signals or mutations leading to autoimmunity have long been associated with decreased plant growth, known as the growth-defense tradeoff. Originally thought to be a redirection of metabolic resources towards defense and away from growth, recent studies have demonstrated that growth and defense can be uncoupled, indicating that metabolic regulation is not solely responsible for the growth-defense tradeoff. Immunity activation has effects on plant development beyond reduction of plant biomass, including changes in plant architecture. Phytohormone signaling pathways and crosstalk between these pathways are responsible, in part, for regulating plant growth, development, and defense responses. Here we review the hormonal regulation of transcription factors that play roles in both defense and development, with a focus on their effects on plant architecture, and suggest the targeting of these transcription factors to increase plant immunity and change plant form, for enhancement of agricultural traits.

1.2 INTRODUCTION

When plant immunity is activated by pathogen perception, treatment with chemical activators of defense, or mutations inducing autoimmunity, a negative effect on plant growth is often observed (Huot et al. 2014; van Wersch, Li, and Zhang 2016). This phenomenon, known as the growth-defense tradeoff, is observed in model plants such as *Arabidopsis thaliana*

[1] This chapter has been resubmitted to Current Opinions of Plant Biology (under review) with the following authors: Hannah M. Berry and Cristiana T. Argueso.

(hereafter, Arabidopsis), as well as crop plant species. Such suppression of growth is detrimental to overall plant yield and is a barrier for the use of mutations leading to constitutive immunity in plant breeding programs (Dwivedi, Reynolds, and Ortiz 2021).

Early studies on characterization of plants with activated states of immunity led to the hypothesis that the growth-defense tradeoff was attributed to a redirection of the plant's metabolism to defense, at the expense of growth. Support for such mechanism includes evidence of decreased rates of photosynthesis (Bilgin et al. 2010), and changes in plant primary and specialized metabolisms after defense activation (Zhou et al. 2015). However, metabolism redirection for production of defense compounds is not the entire cause of this suppression of growth by immunity (reviewed in (Kliebenstein 2016)). Recent studies have shown that growth and defense can be uncoupled, resulting in plants with increased defense without severe compromises to plant growth (Campos et al. 2016; Major et al. 2017; Xu, Uan, et al. 2017; Xu, Greene, et al. 2017; Liu et al. 2019).

In general, the growth-defense tradeoff has been mostly documented at the level of overall plant growth, i.e., by observations of reduction of biomass and yield (van Wersch, Li, and Zhang 2016; Heidel et al. 2004). However, plant architecture also has an essential role in plant yield. Reduced plant stature, leaf length or width, or even leaf angle, can have a substantial effect on light capture and photosynthesis, changing overall plant performance. Similarly, altered root architecture, with a reduction in root length, or the number or structure of root hairs and lateral roots, prevent plants from properly obtaining water and capturing essential nutrients from the soil for growth. Defense activated plants not only have reduced growth but can also display changes in plant development such as ectopic meristem development (Igari et al. 2008), changes in apical dominance and internode length (Bowling et al. 1997), as well as changes in flowering time (Martinez et al. 2004; Glander et al. 2018). Therefore, immunity activation modulates more than growth (defined as changes in cell division and expansion) to involve

changes in development, which encompass changes in patterns of cell division and expansion resulting in altered organ shape and plant architecture.

Phytohormone signaling pathways, and their extensive crosstalk, help plants integrate signals from the environment and determine whether developmental programs begin, continue or arrest (Scheres and van der Putten 2017). As such, phytohormones are obvious mediators of this growth-defense tradeoff. After attack by biotrophic or necrotrophic pathogens, plants respond by increasing the levels of the phytohormones salicylic acid (SA) or jasmonic acid (JA), respectively. Once over a threshold, high levels of SA or JA can result in negative impacts on plant growth, through their interplays with other phytohormonal pathways (Huot et al. 2014). In this review we focus on phytohormone-regulated transcriptional factors mediating plant immunity and plant development, and their resulting effects on plants. Understanding of these transcriptional mediators and the growth, immune, and developmental processes they control, together with engineering of their expression and activity, can lead to plants not only with increased resistance to pathogens and increased biomass, but also with altered plant architecture, which can be important for traits of agricultural importance.

1.3 PHYTOHORMONE-REGULATED TRANSCRIPTION FACTORS AFFECTING PLANT IMMUNITY AND DEVELOPMENT

Transcription factors (TFs) are responsible for transducing signals into gene expression, and transcriptional regulation plays a major role in the processes of plant development and defense activation. As such, several TFs have been identified as regulators of both plant development and immunity (Figure 1.1 and Table 1.1). In most cases these TFs are transcriptionally regulated in opposing ways by phytohormones involved in defense or growth. While primary TFs of phytohormonal pathways are major regulators of these processes, changes in their function lead to substantial changes in plant growth and immunity with vast pleiotropic effects, making them less than optimal targets for manipulation to achieve favorable

outcomes of resistance to pathogens and increased plant yield. Manipulation of non-primary phytohormone-regulated TFs, on the other hand, allows for more precise manipulation of the processes of immunity and development. Here we highlight select non-primary phytohormone-regulated TFs whose regulation and function in both immune responses and plant development have been recently elucidated, with consequences to plant architecture.

Among phytohormonal pathways, signaling of the phytohormone brassinosteroid (BR) is tightly intertwined with plant growth immunity. The basic helix-loop-helix (bHLH) HOMOLOG OF BRASSINOSTEROID ENHANCED EXPRESSION2 INTERACTING WITH IBH 1 (HBI1) was one of the first TFs identified regulating plant immunity and growth. BR signaling and perception of microbial patterns (Pattern Triggered Immunity, or PTI) opposingly regulate the expression of *HBI1* (Fan et al. 2014; Malinovsky et al. 2014). Induction of *HBI1* expression by BR directly changes the expression of genes involved in reactive oxygen species (ROS) homeostasis, as seen in the up-regulation of *RbohC* resulting in leaf cell expansion, and repression of *RbohA*, a critical component of bacterial resistance response (Neuser et al. 2019). Not surprisingly, overexpression of *HBI1* is associated with increased rosette, leaf, and cell area, and *HBI*-overexpressing plants are more susceptible to infection by the bacterial pathogen *Pseudomonas syringae* pv. *tomato* (Malinovsky et al. 2014; Neuser et al. 2019). However, plants overexpressing *HBI1* also display a change in plant architecture, with a reduction in the angle of stem-branch junctions (Malinovsky et al. 2014; Neuser et al. 2019), a phenotype that is associated with BR signaling (Vert and Chory 2011). The mediation of plant growth by HBI1 may be linked to regulation of nitrate signaling and ROS homeostasis (Chu et al. 2021). Nitrate-induced plant growth is reduced in a quadruple mutant of *hbi1* and its three closest homologues in Arabidopsis, while overexpression of *HBI1* results in the opposite phenotype with increased shoot and root growth under nitrate (Chu et al. 2021). In wild type plants, HBI1-induced expression of antioxidant genes reduces the inhibitory effects of ROS on nitrate signaling, promoting plant growth (Chu et al. 2021). Whether nitrate signaling is also involved in the HBI1-

mediated regulation of root architecture is unknown, but of note, nitrate is a major regulator of root architecture, through mechanisms that also involve BR signaling (Song et al. 2021).

The TEOSINTE BRANCHED1/CYCLOIDEA/PCF (TCP) is a TF family involved in the regulation of plant development and immunity. TCPs mediate plant immunity through direct binding of TCP8 and TCP9 to the promoter of the SA biosynthesis gene *ISOCHORISMATE SYNTHASE 1* (*ICS1*), driving *ICS1* expression during pathogen infection, resulting in increased SA levels necessary for defense responses (Wang et al. 2015). TCP8, TCP14, and TCP15 also play a role in PTI, through regulation of the gene encoding the pattern recognition receptor (PRR) EF-TU RECEPTOR (EFR), and *tcp8,14,15* mutants are deficient in *EFR*-dependent PTI (Spears et al. 2019). For their role in plant growth, TCPs have been linked to BR biosynthesis (Guo et al. 2010), however the contribution of individual TCPs in plant development differs. Overexpression of *TCP8* results in delayed flowering compared to wild type (Wang et al. 2019). Because *tcp8* mutants do not display obvious morphological changes, a *35S::TCP8-EAR* transcriptional repressor line was used to evaluate the role of TCP8 in plant development (Wang et al. 2019). *35S::TCP8-EAR* plants have severe developmental defects including arrested growth, and surviving seedlings have abnormal development with dark green leaves, hyponastic cotyledons, and shorter primary roots (Wang et al. 2019). Seedlings that reach reproductive stage are considerably smaller than wild type and have three outer fused floral whorls, resulting in exposed, irregular gynoecia that fail to develop viable seeds (Wang et al. 2019). Lines overexpressing *TCP15* (*35S::TCP15*) have irregular flower development including fused carpel defects, increased number of seeds per silique, and reduced auxin content (Lucero et al. 2015), and acts to balance cytokinin and auxin responses to regulate gynoecium development (Lucero et al. 2015). *tcp15-3* has a significant reduction in silique pedicel length and inflorescence height resulting from reduced internode length, and increased trichome branching in leaves and stems (Kieffer et al. 2011; Camoirano et al. 2020). Pedicel and internode length are further reduced in *tcp14-4, tcp15-3* double mutants (Kieffer et al. 2011). Furthermore, *tcp14-4, tcp15-3* has

reduced expression of cuticle biosynthesis genes, leading to a more permeable cuticle layer (Camoirano et al. 2020), potentially contributing to increased plant susceptibility. The dominant repressor *pTCP14:TCP14-SRDX* plants have a larger reduction in stem height and pedicel length compared to the double mutant, and show leaf development defects, including a broader leaf base, reduced leaf tip elongation, and increased trichome branching, as well as severe defects in floral development, including ectopic tissue proliferation on the carpel valve boundaries and flower receptacle (Kieffer et al. 2011). Of interest is the fact that TCPs are targeted by effectors from a variety of pathogens, highlighting their importance to plant immunity (Lopez et al. 2015).

WRKY TFs make up a large family of TFs in plants that contain the WRKY (Trp-Arg-Lys-Tyr) domain and are widely associated with responses to pathogens, however their role in the regulation of plant development is less known. The rice TF OsWRKY53 is induced by fungal elicitors, and overexpression of *OsWRKY53* leads to increased expression of several genes encoding proteins involved in defense, such as PATHOGENESIS-RELATED (PR) proteins, chitinases and peroxidases, and also to increased resistance to the fungal pathogen *Magnaporthe oryzae* (Chujo et al. 2007; Chujo et al. 2014). However, overexpression of *OsWRKY53* leads to thinner sclerenchyma cell walls and increased susceptibility to the bacterial pathogen *Xanthomonas oryzae* pv. *oryzae* (*Xoo*) (Xie et al. 2021). Notably, overexpression of *OsWRKY53* also has a positive effect in rice reproductive development, leading to increased seed size and increased lamina angle of the flag leaf, while *oswrky53* plants have erect leaves and exhibits many BR-deficient phenotypes including reduced plant and seed size (Tian et al. 2017). BR reduces expression of *OsWRKY53* but increases OsWRKY53 protein stability, indicating a fine-tuning mechanism for WRKY53 regulation (Tian et al. 2017).

An APETALA2/ETHYLENE RESPONSIVE FACTOR (AP2/ERF) TF in cotton, GhTINY2, mediates SA-dependent defense response and suppresses BR-dependent growth responses

(Xiao et al. 2021). Infection by fungus *Verticillium dahliae* or treatment with SA induces expression of *GhTINY2*, which directly activates expression of *WRKY51*, leading to increased SA accumulation and signaling and increased defense responses (Xiao et al. 2021). Overexpression of *GhTINY2* in Arabidopsis results in increased resistance to *V. dahliae*, however, these lines have stunted growth, with reduced petiole elongation, shortened hypocotyl cell length, and fewer rosette leaves compared to wild type (Xiao et al. 2021). Similarly, overexpression of *GhTINY2* in cotton results in increased disease resistance, due to upregulation of genes associated with defense responses, including SA biosynthesis and signaling genes, and decreased plant growth, in part due to reduced expression of genes associated with BR-dependent signaling (Xiao et al. 2021). In Arabidopsis lines overexpressing *GhTINY2*, repression of BR-mediated growth occurs by direct interaction between GhTINY2 and the Arabidopsis bHLH TF BRASSINAZOLE RESISTANT 1 (BZR1), resulting in suppression of BZR1-mediated gene expression of BR-regulated genes (Xiao et al. 2021).

In cucumber, the *IRREGULAR VASCULAR PATTERNING* (*CsIVP*) gene encodes a bHLH transcription factor that regulates vascular development and is also involved in plant immunity (Yan et al. 2020). RNAi lines specifically silencing *CsIVP* show defects in vascular differentiation and reduced plant growth. CsIVP directly binds to the promoters of several vascular developmental regulators and auxin-related genes, and *CsIVP* RNAi lines show increased auxin content. This is also accompanied by an increased expression of SA-regulated genes, including the SA-marker *PR-1*, and decreased susceptibility to downy mildew. Furthermore, the CsIVP protein interacts with CsNIMIN1, a cucumber orthologue of the Arabidopsis NIMIN1 protein involved in SA signaling, consolidating that an alteration in a developmental program affects SA signaling, and consequently, plant immunity. And in tomato, the expression of another bHLH TF, bHLH132, is up-regulated after SA or JA treatment and infection by the bacterial pathogen *Xanthomonas euvesicatoria* containing the effector XopD (Kim and Mudgett 2019). Overexpression of *bHLH132* leads to increased resistance to *X.*

euvesicatoria, but also to narrower leaves with sharp, serrated edges, while silenced lines have stunted growth, shorter internodes, smaller leaves, and also show increased disease susceptibility (Kim and Mudgett 2019).

While most of the examples of TFs regulating plant development and immunity described have roles in the plant shoot, roots are also the site of pathogen attack and defense, and immunity activation can also have developmental effects on roots (Smakowska et al. 2016). The atypical transcription factor dimerization partner (DP)-E2F-like 1 (DEL1) is expressed in actively dividing cells to promote endoreduplication, and acts as a transcriptional repressor of the SA transporter ENHANCED DISEASE SUSCEPTIBILITY 5 (EDS5), restricting SA accumulation in actively growing shoots, as well as roots (Chandran et al. 2014; Nakagami et al. 2020). The knockout mutant *del1-1* is more resistant to infection by powdery mildew, resulting from increased total SA, but has reduced rosette and leaf size compared to wildtype (Chandran et al. 2014). Additionally, *del1-1* mutant plants show ectopic patterns of lignification of root cells, which become more resistant to root knot nematodes, and display an altered pattern of lateral root initiation (Nakagami et al. 2020).

Evidence for JA and SA regulating meristematic activity in roots is also supported by the AP2-domain transcription factors PLETHORA (PLT) 1 and 2, which mediate an auxin gradient that is essential for proper root apical meristem (RAM) patterning and root growth. The expression of *PLT1* and *PLT2* is repressed by JA, through direct binding of the main JA transcriptional regulator, the bHLH transcription factor MYC2, to their promoters. Repression of *PLT1* and *PLT2* promotes division of the cells of quiescent center (QC) in the RAM, and deregulated differentiation of the columella stem cells during root development (Chen et al. 2011). Similarly, accumulation of SA also down-regulates *PLT1* and *PLT2* expression, and the expression of a QC marker, the homeodomain transcription factor WUSCHEL-RELATED 5 HOMEOBOX (WOX5), leads to increased ratios of QC cell division and decreased root growth (Wang et al. 2021). This action of SA in the RAM is likely mediated by ROS production, is

dependent on the main regulator of SA signaling NPR1 (NONEXPRESSOR OF PATHOGENESIS RELATED PROTEINS 1), and is associated with increased pathogen resistance (Wang et al. 2021).

WUSCHEL (WUS) is a homeodomain transcription factor required for stem cell maintenance in the shoot apical meristem (SAM). Proper spatial expression of *WUS* in the SAM is regulated by phytohormones including cytokinin and is essential for the regulation of cell proliferation and differentiation in the SAM, resulting in primordia initiation (Somssich et al. 2016). The SAM has widely been known to be free from disease, so much so that culture of meristems is a known way to make plants virus-free. A role for WUS in maintaining a virus-free SAM was recently identified (Wu et al. 2020). During infection of Arabidopsis with Cucumber Mosaic Virus (CMV), WUS functions to prevent viral infection in the cells comprising the SAM where WUS is expressed (WUS expression domain). Genetic and transgenic alteration of the WUS expression domain allows for CMV proliferation in WUS-free cells and the ability of the virus to take over the SAM. Gene expression profiling of the WUS domain identified genes encoding *S*-adenosyl-L-methionine-dependent methyl transferases (MTases), some of which had their expression induced by CMV, but repressed by WUS, through direct binding of WUS to their promoters (Wu et al. 2020). Because MTases are essential for global protein synthesis, the hypothesis put forward is that WUS represses global protein synthesis to prevent viral takeover of the SAM, thus preventing infection. Whether this function of WUS is regulated by plant hormones, and whether WUS also modulates immune signaling in the SAM, remains untested. The correlation between total protein synthesis and pathogen proliferation provides a link between plant metabolism and growth to immunity, via a central transcriptional regulator of plant development.

Another important connection between WUS and immunity has been uncovered in tomato, where a Receptor-Like Kinase (RLK) was recently identified to regulate resistance to necrotrophic fungi, as well as plant development (Jaiswal et al. 2022). TRK1, a RLK from the

RLK-VII subfamily, interacts with SlLYK1, the tomato orthologue of Arabidopsis CERK1 involved in fungal chitin perception that results in PTI activation. *TRK1* RNAi plants display decreased defense responses upon chitin perception and increased susceptibility to *B. cinerea*, by mechanisms that involve suppression of JA signaling, through the transcriptional and post-transcriptional regulation of MYC2 by TRK1. Pointing again to an intersection of plant immunity and development, TRK1 is required for chitin-induced growth suppression, and was also shown to physically interact with SlWUS and SlCLV1, phosphorylating SlWUS. As expected, given this interaction of TRK1 with key developmental regulators, *TRK1* RNAi lines also show altered reproductive developmental patterns, displaying ectopic meristems, and flowers with increased number of flowers organs, including carpels. Of further interest is the fact that the function of TRK1 is spatially regulated, functioning to promote chitin-induced PTI in leaves, while suppressing it in meristematic tissue (Jaiswal et al. 2022). Finally, the MADS-domain transcription factor SHORT VEGETATIVE PHASE (SVP) is directly associated with a developmentally-regulated type of resistance, known as Age-Related Resistance (ARR), which is expressed in plants at the late adult vegetative and reproductive transition (Wilson et al. 2017). SVP is a major negative regulator of flowering, acting both in the SAM and in leaves. While SVP is not transcriptionally regulated by defense phytohormones, it mediates the transcriptional regulation of SA biosynthesis for direct defense against biotrophs, while acting at the same time as regulator of flowering initiation (Wilson et al. 2017).

1.4 ENGINEERING TRANSCRIPTION FACTORS FOR REGULATION OF PLANT IMMUNITY AND PLANT ARCHITECTURE

Given the complexity of phytohormonal signaling networks, and the extensive crosstalk amongst them, engineering hormonal networks for specific outcomes is a challenging endeavor. Thus, relying on regulators with specific roles, such as TFs, can be an attractive alternative to engineer hormonal-regulated processes. The identification of phytohormone-regulated

transcription factors involved in the control of plant immunity and development opens the door to the manipulation of their expression and activity for specific outcomes of defense and development, with consequences to plant architecture and therefore yield. One of the strategies successfully used has been the optimization of transcriptional levels of regulatory TFs. WRKY45 is a well characterized rice TF induced by SA (Goto et al. 2015). Overexpression of *WRKY45* leads to robust defense to *M. oryzae*, mediated by SA and cytokinin synergism (Akagi et al. 2014), and to *Xoo*, however, these lines have decreased height and reduced number of flowers (Goto et al. 2015). In an effort to optimize defense and growth, candidate promoters were identified and used to drive expression of *WRKY45* (Goto et al. 2015). Transgenic lines using the rice *UBIQUITIN7* promoter driving *WRKY45* resulted in increased disease resistance to both types of pathogens, and plant height, number of panicles and seed number that were comparable to wild type plants, thus eliminating tradeoffs due to increased immunity (Goto et al. 2015). Regulation of levels of protein translation by the use of upstream open reading frames of the transcription factor *TL1*-BINDING FACTOR 1 ($uORFs_{TBF1}$) were used to drive expression of defense regulators resulting in increased immune responses without compromising plant yield (Xu, Uan, et al. 2017), however this approach has not been used to change the translation levels of TFs themselves.

In addition to manipulation of transcriptional expression, post-translational modifications can also have a role in regulating TF activity, and therefore can be used to change TF function. In rice, a member of the SQUAMOSA PROMOTER BINDING PROTEIN-LIKE (SPL) family of TFs, Ideal Plant Architecture 1 (IPA1), is regulated at the post-translational level, with effects in reproductive yield and plant immunity, depending on its phosphorylation state (Wang et al. 2018). In the non-phosphorylated state, IPA1 promotes vegetative growth and seed set (Wang et al. 2018). Upon pathogen perception, IPA1 is phosphorylated, resulting in altered DNA binding specificity and IPA1-induced expression of *WRKY45* and resistance to *M. oryzae* (Wang et al. 2018). Lines overexpressing *IPA1* are more resistant to *Xoo,* however, these transgenic

plants are dwarfed, have delayed germination associated with reduced sensitivity to gibberellic acid, and have significantly reduced seed set compared to wild type (Liu et al. 2019). Because overexpression of *IPA1* resulted in increased disease resistance with negative impacts to plant growth, expression under an inducible promoter was used to drive expression of *IPA1* (Liu et al. 2019). The promoter of the RNA methyltransferase homolog of Arabidopsis HUA ENHANCER 1 (HEN1), containing a binding site for the *Xoo* TAL effector Tal9a, was used to drive expression of *IPA1* (Liu et al. 2019). This resulted in a further increase in disease resistance to *Xoo* but also enhanced yield-related phenotypes, including phenotypes associated with reproductive development such as increased number of primary branches per panicle and increased grain number (Liu et al. 2019).

Another example of post-translational modification of a TF controlling development and immunity is the Arabidopsis TF WRKY70. WRKY70 acts as an activator of defense responses upon SA treatment or pathogen infection (Li, Brader, and Palva 2004) and as a transcriptional repressor of defense genes under naive conditions (Zhou et al. 2018). The phosphorylation state of WRKY70 is responsible for its opposing roles in plant growth and immunity (Liu et al. 2021). WRKY70 is phosphorylated in response to SA treatment or pathogen infection and promotes defense-related gene expression (Liu et al. 2021). After accumulation of phosphorylated WRKY70 acts to promote defense responses, it is ubiquitinated by the E3 ligase CHY ZINC FINGER AND RING PROTEIN 1 (CHYR1), leading to WRKY70 degradation and reduction of defense-related gene expression (Liu et al. 2021). Unphosphorylated WRKY70, on the other hand, acts as a transcriptional repressor of defense gene expression, allowing for normal plant growth (Liu et al. 2021). In the absence of pathogen signals, lines overexpressing *WRKY70* display reduced stature, reduced tiller and panicle number, and leaf phenotypes associated with altered BR signaling (Tang et al. 2022).

Finally, synthetic biology approaches have also been recently used to alter hormone-regulated gene expression, such as the use of transgene or viral-mediated sgRNA and Cas9-

based technologies to create transcription activators and repressors with programmable binding domains responsive to specific phytohormones. Such approaches have been successful in changing patterns of root branching and phyllotaxy and overall plant growth (Khakhar et al. 2021; Khakharn et al. 2018). Similar concepts could be useful to manipulate phytohormone-regulated TFs in the context of plant immunity and development.

1.5 DISCUSSION

Beyond the normally characterized parameters of plant biomass, immunity activation also changes plant development that change plant architecture. The severity of these developmental alterations can vary after immunity triggered by pathogen attack depending on the pathogen and pathogen inoculum (Korves and Bergelson 2003), or can be induced by mutations that lead to constitutive immunity, or through immunity activation with chemicals. Because plant architecture can have a substantial impact in plant productivity, it is critical to consider these developmental effects, along with the typical biomass phenotypes, when discussing tradeoffs of immunity.

In the past decade, several TFs regulating plant immunity but also with roles in plant development have been identified (highlighted here). It is likely that that other TFs also play a role in the integration of immunity and plant development, whose roles in plant development have yet to be uncovered or may have been overlooked due to incomplete characterization of resulting phenotypes. As expected, many of these TFs have their expression regulated by phytohormones, underscoring the central role of these molecules in regulating both processes. Of note, many of the phenotypic outcomes from manipulation of these TFs result from experiments using overexpression approaches, which may not reflect the native temporal and/or spatial regulation of these TFs, and therefore their inherent function. However, these experiments also demonstrate that the altered expression of these TFs can change plant development and immunity, and thus they may be used to change plant architecture in the

context of immunity for better growth and yield, even in tissues in which their expression, or even pathogen infection, are not normally present.

Proper balance of immunity and development requires perception of specific pathogen and growth signals, followed by transcriptional reprogramming mediated by TFs, culminating in plant physiological changes. Engineering of transcription and translation of TFs, along with uncovering of post-translational modifications that change their regulation and DNA binding specificity, may be used to optimize plant architecture in active states of immunity, and consequently, plant productivity. While the contribution of the TFs mentioned here to immunity and plant development may have been defined, the identity of the upstream regulators that control their function and activation are mostly unknown. Similarly, the discovery of the transcriptional targets of these TFs, under native or overexpression conditions, is of paramount importance, as it may allow for more precise manipulation of the resulting traits. Unveiling the connection between perception of growth and pathogen signals, and the resulting transcriptional reprograming, will be an important step to understand and manipulate developmental changes upon immunity activation, to control and optimize plant productivity.

1.6 FIGURES

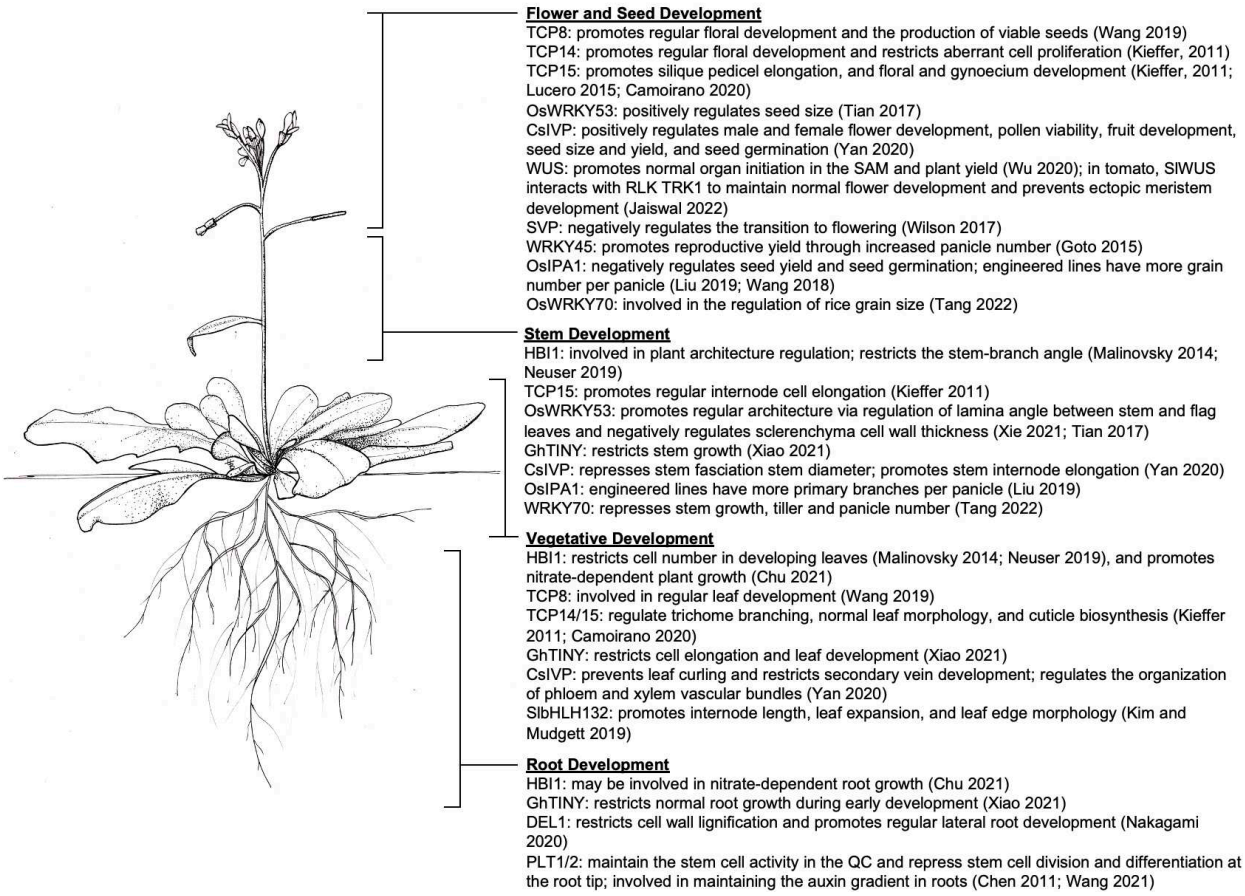

Figure 1.1: Effects of transcription factors associated with regulation of plant immunity on plant developmental processes. Several plant transcription factors (TF) play roles in plant immunity and development. Altered TF activity leads to changes not only in plant immunity, but also in plant developmental processes in various plant tissues, changing overall plant architecture, with consequences to plant yield. SAM: shoot apical meristem; RLK: receptor-like kinase; QC: quiescent center. Scientific illustration of *Arabidopsis thaliana* by Hannah M. Berry.

1.7 TABLES

Table 1.1: Phytohormone-mediated transcription factors and their role in plant immunity

Transcription Factor	Regulating Hormone	Effect on Plant Defense	Reference
HBI1	BR	Differentially regulates *NOX* and *POX* gene expression to regulate apoplastic ROS Represses expression of *RbohA* to repress immunity to bacterial pathogens Negatively regulates *POX* in response to PTI to restrict ROS accumulation	(Malinovsky et al. 2014; Neuser et al. 2019)
TCP8	SA	Directly binds to the promoter of *ICS1* to promote SA biosynthesis during pathogen infection Promotes PTI by driving the expression of pattern recognition receptor EFR Promotes ETI responses	(Wang et al. 2015; Spears et al. 2019)
TCP14/TCP15	SA	Promotes PTI by driving the expression of pattern recognition receptor EFR Promotes ETI responses	(Spears et al. 2019)
OsWRKY53	SA, BR, JA	Transcription is induced during pathogen infection Acts as a transcriptional activator to enhance defense responses Is a negative regulator of JA and JA-Ile accumulation in response to herbivory Promotes *PR* gene expression and resistance to *M. oryzae* Promotes susceptiblity to *Xoo*	(Chujo et al. 2007; Chujo et al. 2014; Xie et al. 2021)
GhTINY2	SA, JA	Expression is induced by SA and JA Promotes *WRKY51* expression leading to increased SA accumulation and immunity Promotes resistance to *V. dahliae*	(Xiao et al. 2021)
CsIVP	SA, Auxin	Promotes susceptibility of cucumber to powdery mildew Negatively regulates SA accumulation via a strong interaction with SA repressor CsNIMIN1	(Yan et al. 2020)
SlbHLH132	SA, JA	Expression is moderately upregulated by SA or JA treatment Expression is significantly induced by the effector XopD during *X. euvesicatoria* infection Promotes ETI responses and resistance to *X. euvesicatoria*	(Kim and Mudgett 2019)
DEL1	SA	Acts as a transcriptional repressor of the SA transporter *EDS5* Restricts SA accumulation in growing tissues Promotes plant susceptibility to powdery mildew and root knot nematodes	(Chandran et al. 2014; Nakagami et al. 2020)
PLT1/PLT2	SA, JA, Auxin	SA-induced ROS down-regulates expression, thus promoting pathogen resistance Transcriptionally regulated by binding of MYC2 to its promoter	(Chen et al. 2011; Wang et al. 2021)
WUS	CK, Auxin, JA	WUS prevents viral infection of pluripotent cells in the SAM WUS may act to prevent viral infection by repressing *MTases* and global protein synthesis Tomato SlWUS interacts with and is phosphorylated by RLK TRK1 during chitin-triggered PTI	(Wu et al. 2020; Jaiswal et al. 2022)
SVP	none	Promotes SA biosynthesis during ARR to *P. syringae* pv. *tomato* Promotes plant immunity to bacterial pathogens	(Wilson et al. 2017)
WRKY45	SA, CK	Promotes defense to *M. oryzae* and *Xoo* Transgenic line *pOsUbi7::WRKY45* results in further increase of disease resistance	(Goto et al. 2015; Akagi et al. 2014)
OsIPA1	SA	Is phosphorylated upon pathogen perception leading to altered DNA binding specificity In the phosphorylated state, induces *WRKY45* expression to promote immunity Promotes resistance to *M. oryzae* Reduces GA-mediated plant susceptibility and promotes resistance to *Xoo* *pHEN1::IPA1* enhances plant disease resistance	(Liu et al. 2019; Wang et al. 2018)
WRKY70	SA	In the unphosphorylated state, WRKY70 represses expression of defense-related genes Is phosphorylated in response to SA treatment or pathogen infection leading to its ubiquitination and degradation, and reduction of defense gene expression	(Li, Brader, and Palva 2004; Zhou et al. 2018; Liu et al. 2021)

BR: brassinosteroids; SA: salicylic acid; JA: jasmonic acid; CK: cytokinin; GA: gibberellic acid; NOX: NAPDH oxidase; POX: peroxidase; ROS: reactive oxygen species; PTI: pattern-triggered immunity; ETI: effector-triggered immunity; MTase: *S*-adenosyl-L-methionine-dependent methyltransferase; SAM: shoot apical meristem; ARR: age-related resistance.

REFERENCES

Akagi, A., S. Fukushima, K. Okada, C. J. Jiang, R. Yoshida, A. Nakayama, M. Shimono, S. Sugano, H. Yamane, and H. Takatsuji. 2014. 'WRKY45-dependent priming of diterpenoid phytoalexin biosynthesis in rice and the role of cytokinin in triggering the reaction', *Plant Molecular Biology*, 86: 171-83.

Bilgin, D. D., J. A. Zavala, J. Zhu, S. J. Clough, D. R. Ort, and E. H. DeLucia. 2010. 'Biotic stress globally downregulates photosynthesis genes', *Plant Cell and Environment*, 33: 1597-613.

Bowling, S. A., J. D. Clarke, Y. D. Liu, D. F. Klessig, and X. N. Dong. 1997. 'The *cpr5* mutant of Arabidopsis expresses both NPR1-dependent and NPR1-independent resistance', *Plant Cell*, 9: 1573-84.

Camoirano, A., A. L. Arce, F. D. Ariel, A. L. Alem, D. H. Gonzalez, and I. L. Viola. 2020. 'Class I TCP transcription factors regulate trichome branching and cuticle development in Arabidopsis', *Journal of Experimental Botany*, 71: 5438-53.

Campos, M. L., Y. Yoshida, I. T. Major, D. D. Ferreira, S. M. Weraduwage, J. E. Froehlich, B. F. Johnson, D. M. Kramer, G. Jander, T. D. Sharkey, and G. A. Howe. 2016. 'Rewiring of jasmonate and phytochrome B signalling uncouples plant growth-defense tradeoffs', *Nature Communications*, 7.

Chandran, D., J. Rickert, Y. X. Huang, M. A. Steinwand, S. K. Marr, and M. C. Wildermuth. 2014. 'Atypical E2F transcriptional repressor DEL1 acts at the intersection of plant growth and immunity by controlling the hormone salicylic acid', *Cell Host & Microbe*, 15: 506-13.

Chen, Q., J. Q. Sun, Q. Z. Zhai, W. K. Zhou, L. L. Qi, L. Xu, B. Wang, R. Chen, H. L. Jiang, J. Qi, X. G. Li, K. Palme, and C. Y. Li. 2011. 'The basic helix-loop-helix transcription factor MYC2 directly represses *PLETHORA* expression during jasmonate-mediated modulation of the root stem cell niche in Arabidopsis', *Plant Cell*, 23: 3335-52.

Chu, X. Q., J. G. Wang, M. Z. Li, S. J. Zhang, Y. Y. Gao, M. Fan, C. Han, F. N. Xiang, G. Y. Li, Y. Wang, X. Yu, C. B. Xiang, and M. Y. Bai. 2021. 'HBI transcription factor-mediated ROS homeostasis regulates nitrate signal transduction', *Plant Cell*, 33: 3004-21.

Chujo, T., K. Miyamoto, S. Ogawa, Y. Masuda, T. Shimizu, M. Kishi-Kaboshi, A. Takahashi, Y. Nishizawa, E. Minami, H. Nojiri, H. Yamane, and K. Okada. 2014. 'Overexpression of phosphomimic mutated OsWRKY53 leads to enhanced blast resistance in rice', *PLOS ONE*, 9.

Chujo, T., R. Takai, C. Akimoto-Tomiyama, S. Ando, E. Minami, Y. Nagamura, H. Kaku, N. Shibuya, M. Yasuda, H. Nakashita, K. Umemura, A. Okada, K. Okada, H. Nojiri, and H. Yamane. 2007. 'Involvement of the elicitor-induced gene *OsWRKY53* in the expression of defense-related genes in rice', *Biochimica et Biophysica Acta*, 1769: 497-505.

Dwivedi, S. L., M. P. Reynolds, and R. Ortiz. 2021. 'Mitigating tradeoffs in plant breeding', *iScience*, 24.

Fan, M., M. Y. Bai, J. G. Kim, T. N. Wang, E. Oh, L. Chen, C. H. Park, S. H. Son, S. K. Kim, M. B. Mudgett, and Z. Y. Wang. 2014. 'The bHLH transcription factor HBI1 mediates the trade-off between growth and pathogen-associated molecular pattern-triggered immunity in Arabidopsis', *Plant Cell*, 26: 828-41.

Glander, S., F. He, G. Schmitz, A. Witten, A. Telschow, and J. de Meaux. 2018. 'Assortment of flowering time and immunity alleles in natural *Arabidopsis thaliana* populations suggests immunity and vegetative lifespan strategies coevolve', *Genome Biology and Evolution*, 10: 2278-91.

Goto, S., F. Sasakura-Shimoda, M. Suetsugu, M. G. Selvaraj, N. Hayashi, M. Yamazaki, M. Ishitani, M. Shimono, S. Sugano, A. Matsushita, T. Tanabata, and H. Takatsuji. 2015. 'Development of disease-resistant rice by optimized expression of *WRKY45*', *Plant Biotechnology Journal*, 13: 753-65.

Guo, Z. X., S. Fujioka, E. B. Blancaflor, S. Miao, X. P. Gou, and J. Li. 2010. 'TCP1 modulates brassinosteroid biosynthesis by regulating the expression of the key biosynthetic gene *DWARF4* in *Arabidopsis thaliana*', *Plant Cell*, 22: 1161-73.

Heidel, A. J., J. D. Clarke, J. Antonovics, and X. N. Dong. 2004. 'Fitness costs of mutations affecting the systemic acquired resistance pathway in *Arabidopsis thaliana*', *Genetics*, 168: 2197-206.

Huot, B., J. Yao, B. L. Montgomery, and S. Y. He. 2014. 'Growth-defense rradeoffs in plants: A balancing act to optimize fitness', *Molecular Plant*, 7: 1267-87.

Igari, K., S. Endo, K. Hibara, M. Aida, H. Sakakibara, T. Kawasaki, and M. Tasaka. 2008. 'Constitutive activation of a CC-NB-LRR protein alters morphogenesis through the cytokinin pathway in Arabidopsis', *Plant Journal*, 55: 14-27.

Jaiswal, N., C. J. Liao, B. Mengesha, H. Han, S. Lee, A. Sharon, Y. Zhou, and T. Mengiste. 2022. 'Regulation of plant immunity and growth by tomato receptor-like cytoplasmic kinase TRK1', *New Phytologist*, 233: 458-78.

Khakhar, A., C. Wang, R. Swanson, S. Stokke, F. Rizvi, S. Sarup, J. Hobbs, and D. F. Voytas. 2021. 'ViparíNama: RNA viral vectors to rapidly elucidate the relationship between gene expression and phenotype', *Plant Physiology*, 186: 2222-38.

Khakharn, A., A. R. Leydon, A. C. Lemmex, E. Klavins, and J. L. Nemhauser. 2018. 'Synthetic hormone-responsive transcription factors can monitor and reprogram plant development', *eLife*, 7.

Kieffer, M., V. Master, R. Waites, and B. Davies. 2011. 'TCP14 and TCP15 affect internode length and leaf shape in Arabidopsis', *Plant Journal*, 68: 147-58.

Kim, J. G., and M. B. Mudgett. 2019. 'Tomato bHLH132 transcription factor controls growth and defense and is activated by *Xanthomonas euvesicatoria* effector XopD during pathogenesis', *Molecular Plant-Microbe Interactions*, 32: 1614-22.

Kliebenstein, D. J. 2016. 'False idolatry of the mythical growth versus immunity tradeoff in molecular systems plant pathology', *Physiological and Molecular Plant Pathology*, 95: 55-59.

Korves, T. M., and J. Bergelson. 2003. 'A developmental response to pathogen infection in Arabidopsis', *Plant Physiology*, 133: 339-47.

Li, J., G. Brader, and E. T. Palva. 2004. 'The WRKY70 transcription factor: A node of convergence for jasmonate-mediated and salicylate-mediated signals in plant defense', *Plant Cell*, 16: 319-31.

Liu, H. H., B. Liu, S. L. Lou, H. Bi, H. Tang, S. F. Tong, Y. Song, N. N. Chen, H. Zhang, Y. Z. Jiang, and J. Q. Liu. 2021. 'CHYR1 ubiquitinates the phosphorylated WRKY70 for degradation to balance immunity in *Arabidopsis thaliana*', *New Phytologist*, 230: 1095-109.

Liu, M. M., Z. Y. Shi, X. H. Zhang, M. X. Wang, L. Zhang, K. Z. Zheng, J. Y. Liu, X. M. Hu, C. R. Di, Q. Qian, Z. H. He, and D. L. Yang. 2019. 'Inducible overexpression of *Ideal Plant Architecture1* improves both yield and disease resistance in rice', *Nature Plants*, 5: 389-400.

Lopez, J. A., Y. Sun, P. B. Blair, and M. S. Mukhtar. 2015. 'TCP three-way handshake: linking developmental processes with plant immunity', *Trends in Plant Science*, 20: 238-45.

Lucero, L. E., N. G. Uberti-Manassero, A. L. Arce, F. Colombatti, S. G. Alemano, and D. H. Gonzalez. 2015. 'TCP15 modulates cytokinin and auxin responses during gynoecium development in Arabidopsis', *Plant Journal*, 84: 267-82.

Major, I. T., Y. Yoshida, M. L. Campos, G. Kapali, X. F. Xin, K. Sugimoto, D. D. Ferreira, S. Y. He, and G. A. Howe. 2017. 'Regulation of growth-defense balance by the JASMONATE ZIM-DOMAIN (JAZ)-MYC transcriptional module', *New Phytologist*, 215: 1533-47.

Malinovsky, F. G., M. Batoux, B. Schwessinger, J. H. Youn, L. Stransfeld, J. Win, S. K. Kim, and C. Zipfel. 2014. 'Antagonistic Regulation of Growth and Immunity by the Arabidopsis Basic Helix-Loop-Helix Transcription Factor HOMOLOG OF BRASSINOSTEROID ENHANCED EXPRESSION2 INTERACTING WITH INCREASED LEAF INCLINATION1 BINDING bHLH1', *Plant Physiology*, 164: 1443-55.

Martinez, C., E. Pons, G. Prats, and J. Leon. 2004. 'Salicylic acid regulates flowering time and links defence responses and reproductive development', *Plant Journal*, 37: 209-17.

Nakagami, S., K. Saeki, K. Toda, T. Ishida, and S. Sawa. 2020. 'The atypical E2F transcription factor DEL1 modulates growth-defense tradeoffs of host plants during root-knot nematode infection', *Scientific Reports*, 10.

Neuser, J., C. C. Metzen, B. H. Dreyer, C. Feulner, J. T. van Dongen, R. R. Schmidt, and J. H. M. Schippers. 2019. 'HBI1 mediates the trade-off between growth and immunity through its impact on apoplastic ROS homeostasis', *Cell Reports*, 28: 1670-+.

Scheres, B., and W. H. van der Putten. 2017. 'The plant perceptron connects environment to development', *Nature*, 543: 337-45.

Smakowska, E., J. X. Kong, W. Busch, and Y. Belkhadir. 2016. 'Organ-specific regulation of growth-defense tradeoffs by plants', *Current Opinion in Plant Biology*, 29: 129-37.

Somssich, M., B. Je, R. Simon, and D. Jackson. 2016. 'CLAVATA-WUSCHEL signaling in the shoot meristem', *Development*, 143: 3238-48.

Song, X. Y., J. F. Li, M. L. Lyu, X. Z. Kong, S. Hu, Q. W. Song, and K. J. Zuo. 2021. 'CALMODULIN-LIKE-38 and PEP1 RECEPTOR 2 integrate nitrate and brassinosteroid signals to regulate root growth', *Plant Physiology*, 187: 1779-94.

Spears, B. J., T. C. Howton, F. Gao, C. M. Garner, M. S. Mukhtar, and W. Gassmann. 2019. 'Direct regulation of the EFR-dependent immune response by arabidopsis TCP transcription factors', *Molecular Plant-Microbe Interactions*, 32: 540-49.

Tang, J. Q., E. Y. Mei, M. L. He, Q. Y. Bu, and X. J. Tian. 2022. 'Functions of OsWRKY24, OsWRKY70 and OsWRKY53 in regulating grain size in rice', *Planta*, 255.

Tian, X. J., X. F. Li, W. J. Zhou, Y. K. Ren, Z. Y. Wang, Z. Q. Liu, J. Q. Tang, H. N. Tong, J. Fang, and Q. Y. Bu. 2017. 'Transcription factor OsWRKY53 positively regulates brassinosteroid signaling and plant architecture', *Plant Physiology*, 175: 1337-49.

van Wersch, R., X. Li, and Y. L. Zhang. 2016. 'Mighty dwarfs: Arabidopsis autoimmune mutants and their usages in genetic dissection of plant immunity', *Frontiers in Plant Science*, 7.

Vert, G., and J. Chory. 2011. 'Crosstalk in Cellular Signaling: Background Noise or the Real Thing?', *Developmental Cell*, 21: 985-91.

Wang, J., L. Zhou, H. Shi, M. Chern, H. Yu, H. Yi, M. He, J. J. Yin, X. B. Zhu, Y. Li, W. T. Li, J. L. Liu, J. C. Wang, X. Q. Chen, H. Qing, Y. P. Wang, G. F. Liu, W. M. Wang, P. Li, X. J. Wu, L. H. Zhu, J. M. Zhou, P. C. Ronald, S. G. Li, J. Y. Li, and X. W. Chen. 2018. 'A single transcription factor promotes both yield and immunity in rice', *Science*, 361: 1026-28.

Wang, X. Y., J. Gao, Z. Zhu, X. X. Dong, X. Lei Wang, G. D. Ren, X. Zhou, and B. K. Kuai. 2015. 'TCP transcription factors are critical for the coordinated regulation of *ISOCHORISMATE SYNTHASE 1* expression in *Arabidopsis thaliana*', *Plant Journal*, 82: 151-62.

Wang, Xiaoyan, Xintong Xu, Xiaowei Mo, Luyao Zhong, Jiancong Zhang, Beixin Mo, and Benke Kuai. 2019. 'Overexpression of *TCP8* delays Arabidopsis flowering through a FLOWERING LOCUS C-dependent pathway', *Bmc Plant Biology*, 19.

Wang, Z. Q., D. Y. Rong, D. X. Chen, Y. Xiao, R. Y. Liu, S. Wu, and C. Yamamuro. 2021. 'Salicylic acid promotes quiescent center cell division through ROS accumulation and down-regulation of *PLT1*, *PLT2*, and *WOX5*', *Journal of Integrative Plant Biology*, 63: 583-96.

Wilson, D. C., C. J. Kempthorne, P. Carella, D. K. Liscombe, and R. K. Cameron. 2017. 'Age-related resistance in *Arabidopsis thaliana* involves the MADS-domain transcription factor SHORT VEGETATIVE PHASE and direct action of salicylic acid on *Pseudomonas syringae*', *MPMI*, 30: 919-29.

Wu, H. J., X. Y. Qu, Z. C. Dong, L. J. Luo, C. Shao, J. Forner, J. U. Lohmann, M. Su, M. C. Xu, X. B. Liu, L. Zhu, J. Zeng, S. M. Liu, Z. X. Tian, and Z. Zhao. 2020. 'WUSCHEL triggers innate antiviral immunity in plant stem cells', *Science*, 370: 227-+.

Xiao, S. H., Q. Hu, X. J. Zhang, H. Si, S. M. Liu, L. Chen, K. Chen, S. Berne, D. J. Yuan, K. Lindsey, X. L. Zhang, and L. F. Zhu. 2021. 'Orchestration of plant development and defense by indirect crosstalk of salicylic acid and brassinosteorid signaling via transcription factor GhTINY2', *Journal of Experimental Botany*, 72: 4721-43.

Xie, W. Y., Y. G. Ke, J. B. Cao, S. P. Wang, and M. Yuan. 2021. 'Knock out of transcription factor *WRKY53* thickens sclerenchyma cell walls, confers bacterial blight resistance', *Plant Physiology*, 187: 1746-61.

Xu, G. Y., G. H. Greene, H. J. Yoo, L. J. Liu, J. Marques, J. Motley, and X. N. Dong. 2017. 'Global translational reprogramming is a fundamental layer of immune regulation in plants', *Nature*, 545: 487-+.

Xu, G. Y., M. Y. Uan, C. R. Ai, L. J. Liu, E. Zhuang, S. Karapetyan, S. Wang, and X. N. Dong. 2017. 'uORF-mediated translation allows engineered plant disease resistance without fitness costs', *Nature*, 545: 491-+.

Yan, S. S., K. Ning, Z. Y. Wang, X. F. Liu, Y. T. Zhong, L. Ding, H. L. Zi, Z. H. Cheng, X. X. Li, H. Y. Shan, Q. Y. Lv, L. X. Luo, R. Y. Liu, L. Y. Yan, Z. Y. Zhou, W. J. Lucas, and X. L. Zhang. 2020. 'CsIVP functions in vasculature development and downy mildew resistance in cucumber', *Plos Biology*, 18.

Zhou, M., Y. Lu, G. Bethke, B. T. Harrison, N. Hatsugai, F. Katagiri, and J. Glazebrook. 2018. 'WRKY70 prevents axenic activation of plant immunity by direct repression of *SARD1*', *New Phytologist*, 217: 700-12.

Zhou, S. Q., Y. R. Lou, V. Tzin, and G. Jander. 2015. 'Alteration of plant primary metabolism in response to insect herbivory', *Plant Physiology*, 169: 1488-98.

CHAPTER 2

CYTOKININ RESPONSE FACTOR 5 is a mediator of plant growth and defense through regulation of cytokinin and salicylic acid responses[2]

2.1 SUMMARY

Cytokinin (CK) was first identified as regulator of plant cell division. Since then, this plant hormone has been shown to be a critical regulator of many aspects of plant growth and development. More recently, CK has been shown to play a role in plant defense responses against pathogens, through crosstalk with other defense plant hormones, notably salicylic acid (SA). Activation of the CK signaling cascade results in the expression of genes encoding a family of transcription factors, CYTOKININ RESPONSE FACTORS (CRFs), which carry out downstream CK signaling responses. CRFs belong to the family of APETALA2/ETHYLENE RESPONSE FACTOR (AP2/ERF) transcription factors, are defined by a conserved N-terminal CRF domain and are found across all land plant species. Based on phenotypic and genetic analysis, CRFs have been proposed to be modulators of plant growth and immunity in Arabidopsis and agricultural plant species. Here, we show that *CRFs* are differentially regulated by CK, SA, and pathogen attack, and that there is extensive functional genetic redundancy in this gene family. Overexpression of *CRF5* suppresses plant growth and accelerates senescence, and this is associated with an increase in SA biosynthesis and signaling, reduced CK biosynthesis, and increased CK degradation. Epistatic analyses revealed that CRF5 functions independently of other known pathways that regulate immunity and plant growth, and thus is a new player in the regulation of the growth-defense tradeoff. We propose a model where CRF5 acts in the crosstalk between CK and SA, to regulate plant growth and defense.

[2] Data from this chapter will be used in a future publication with the following authors: Hannah M Berry, Tessa A Albrecht, Dawn Hajdu, Ruth A Watson, Felipe Vicentino Salvador, and Cristiana T Argueso.

2.2 INTRODUCTION

The plant hormone CK has been shown to play a major role in plant growth and development as a regulator of cell division, meristematic maintenance, cell differentiation, flower development, and leaf senescence (Mok and Mok 2001; Hwang, Sheen, and Muller 2012; Wybouw and De Rybel 2019). Perception of CK in plant cells is mediated by a phosphorelay signaling system, resembling the bacterial two-component signaling system (TCS) (Kieber and Schaller 2018). The endoplasmic reticulum-localized ARABIDOPSIS HISTIDINE KINASES (AHKs) function as CK receptors in plants, and upon binding to CK undergo autophosphorylation of specific histidine and aspartic acid amino acid residues (Figure 2.1) (Kieber and Schaller 2018). This phosphorylation signal is then transferred to ARABIDOPSIS HISTIDINE PHOSPHOTRANSFER PROTEINS (AHPs), which carry the phosphorylation signal from the cytoplasm to the nucleus (Figure 2.1) (Kieber and Schaller 2018). Transfer of the phosphoryl group from AHPs to Type-B Arabidopsis Response Regulator (Type-B ARRs) transcription factors promotes expression of Type-A ARRs, which act as negative regulators of CK signaling to fine-tune CK responses (Figure 2.1) (Kieber and Schaller 2018). Type-B ARRs also transcriptionally activate the expression of CK-responsive genes, including Cytokinin Response Factors (CRFs) (Figure 2.1) (Argueso, Ferreira, and Kieber 2009; Rashotte et al. 2006; Kieber and Schaller 2018).

The plant hormone SA plays a negative role in plant growth and development with high levels of exogenous SA application, or mutations leading to constitutive activation of defense or accumulation of SA, showing severe growth restriction, dwarfed phenotype, and reduced seed yield (Vicente and Plasencia 2011; van Wersch, Li, and Zhang 2016). This growth suppression, known as the growth-defense tradeoff, is commonly observed in Arabidopsis and other plant species. However, SA is critical for initiating plant defense responses to biotrophic and hemi-biotrophic pathogens. Prior to pathogen attack, SA concentrations are relatively low in plant cells. The SA receptor NONEXPRESSER OF PR-GENES 1 (NPR1) (Wu et al. 2012) forms an

oligomer in the cytoplasm and the NPR1 paralogues, NPR3 and NPR4, act as transcriptional co-repressors of TGA b-zip transcription factors, thus inhibiting SA-dependent gene expression (Figure 2.2A) (Ding et al. 2018). In response to pathogen infection, SA is synthesized via the isochorismate synthase (ICS) pathway (Wildermuth et al. 2001). As SA concentrations increase, SA inhibits the repressor activity of NPR3 and NPR4, thus removing inhibition on TGA transcription factors (Figure 2.2B) (Ding et al. 2018). Additionally, changes in the cellular redox state cause NPR1 oligomers to monomerize and move into the nucleus (Fan and Dong 2002; Rochon et al. 2006; Vlot, Dempsey, and Klessig 2009). Nuclear NPR1 then acts as a transcriptional co-activator via physical interaction with members of the TGA transcription factor family (TGA2, TGA3, and TGA4), leading to the expression of SA-response genes and immunity activation (Figure 2.2B) (Fan and Dong 2002; Rochon et al. 2006).

In the last decade, CK has been shown to participate in plant immunity, primarily through crosstalk with hormones associated with plant defense, such as SA (Shigenaga and Argueso 2016; Shigenaga et al. 2017). Mutations or transgenes resulting in increased CK signaling, or application of exogenous CK to plants, promotes the expression of SA-regulated genes, and significantly reduces pathogen growth, demonstrating that CK signaling promotes SA-mediated defense (Choi et al. 2010; Argueso et al. 2012; Naseem et al. 2012). This crosstalk between the CK and SA signaling pathways is mediated by the CK-regulated Type-B ARR transcription factor ARR2, and the SA-regulated transcription factor TGA3 (Figure 2.3A-C) (Choi et al. 2010). ARR2 and TGA3 physically interact and together bind to the promoter of the SA marker and defense gene *PATHOGENESIS-RELATED GENE 1* (*PR-1*), enhancing its expression (Figure 2.3A-C) (Choi et al. 2010). While CK promotes plant immunity through SA-dependent defense responses, SA has been shown to inhibit CK signaling, forming a feedback loop to tightly regulate SA-mediated defense responses (Argueso et al. 2012), however, potential mediators of this crosstalk are currently unknown.

CRFs are a group of transcription factors in the APETALA2/ETHYLENE RESPONSE FACTOR (AP2/ERF) protein family, characterized by an AP2 DNA binding domain present in the center of the protein (Figure 2.4A). CRFs are further defined by a CRF domain, a conserved amino acid (AA) sequence of about 40AA at the N-terminal end, often immediately preceded by the TEH (threonine, glutamic acid, histidine) region, another conserved sequence of about 13AA (Figure 2.4A) (Rashotte et al. 2003; Rashotte and Goertzen 2010; Rashotte et al. 2006). Additionally, about half of the CRFs with full-length sequences contain a putative MAP kinase phosphorylation site at the C-terminal end (Figure 2.4A) (Rashotte and Goertzen 2010). Investigation into the function of the CRF domain revealed that CRFs form homo- and heterodimers with each other and with AHPs via the CRF domain (Cutcliffe et al. 2011). CRFs are found in all land plant species (Rashotte and Goertzen 2010) and can be divided into five distinct clades (Figure 2.4B) (Rashotte and Goertzen 2010; Zwack et al. 2012; Hallmark and Rashotte 2019). In Arabidopsis, six main CRFs (*CRF1 to CRF6*) have been identified and genetic analyses have shown that these CRFs play roles in root and shoot development (Raines et al. 2016). Of these six, gene expression analysis shows that *CRF2* and *CRF5* are both rapidly and robustly induced upon treatment with CK, and *CRF6* expression is induced by CK at later time and to a lesser extent (Rashotte et al. 2006). The three other main CRFs were not found to be transcriptionally regulated by CK, showing little to no changes in expression after CK treatment (Rashotte et al. 2006).

Identification of *crf* T-DNA insertion mutations in Arabidopsis (Figure 2.4C) allowed for the evaluation of the role *CRFs* in plant growth and development (Raines et al. 2016). Single mutants did not show obvious shoot growth phenotypes, while combinations of double, triple, and quadrupole mutants had reduced root length and number of cells in the root meristematic zone, increased vegetative growth, and delayed senescence (Raines et al. 2016). Arabidopsis transgenic lines overexpressing *CRF1*, *CRF3*, or *CRF5* under the *35S Cauliflower Mosaic Virus* constitutive promoter (named *CRF1ox*, *CRF3ox*, or *CRF5ox*, respectively) had significantly

reduced rosette growth and early onset of leaf senescence, suggesting *CRFs* are negative regulators of plant growth (Raines et al. 2016). Notably, not all *CRFs* have the same effect on senescence, as CRF6 is a negative regulator of leaf senescence (Zwack et al. 2013; Zwack and Rashotte 2013), thus indicating that CRFs can play somewhat independent roles in plant responses. Similarly to the effect of CK on plant growth, CRFs have the opposite effect on the regulation of root growth, functioning as positive regulators (Raines et al. 2016). *CRF5ox* roots were significantly longer than Col-0 resulting from significantly more cells in the meristematic zone (Raines et al. 2016). Loss of four *CRFs* in the *crf1,3,5,6* quadruple mutant had the opposite phenotype, with fewer cells in the root meristem and shorter roots than Col-0, (Raines et al. 2016). Beyond plant growth, *CRFs* play roles in embryogenesis and female reproductive organ development (Rashotte et al. 2006; Cucinotta et al. 2016). Loss-of-function of some multiple *crf* mutants leads to delayed embryogenesis or complete lethality at the embryonic stage, reduced ovule number, and reduced placenta length (Rashotte et al. 2006; Cucinotta et al. 2016).

Arabidopsis transgenic overexpressing *CRF* genes were inoculated with the hemi-biotrophic bacterial pathogen *Pseudomonas syringae* pv. *tomato* DC3000 (*Pst* DC3000), to which Col-0 Arabidopsis is susceptible (Liang et al. 2010; Kwon 2016). Overexpression of *CRF5* led to increased expression of *PR* genes and reduced disease symptoms compared to Col-0 plants (Liang et al. 2010). Similarly, overexpressing *CRF2* resulted in increased expression of SA-responsive genes (Kwon 2016). These plants had a high mortality rate, accelerated leaf senescence, and developed lesion-mimic phenotypes (Kwon 2016).

In this study, we show that CRF5 is positive regulator of plant defense responses by promoting expression of SA biosynthesis and signaling genes and is a negative regulator of plant growth and CK biosynthesis and signaling. We show that overexpression of *CRF5* in combination with autoimmunity mutants results in severe growth reduction and delayed flowering compared to either parental line, placing CRF5 in a new pathway. We used RNA-seq

to evaluate transcriptional changes of *CRF5ox* plants and found an increase the expression of genes involved in SA biosynthesis and signaling, increased CK degradation, and decreased CK biosynthesis. Furthermore, gene ontology (GO) analysis showed a significant increase in expression of genes associated with defense responses to bacterial and fungal pathogens. We propose a model for the role of CRF5 in mediating the crosstalk between CK and SA, and thus the balance between plant growth and defense mediated by these plant hormones.

2.3 METHODS

Plant materials and growth conditions

Arabidopsis thaliana ecotype Columbia (Col-0, wild-type), mutants, and transgenic lines in the Col-0 background were used for all experiments. T-DNA insertional *crf* mutant alleles *crf1-2*, *crf2-3*, *crf3-2*, *crf5-5*, and *crf6-3*, as well as multiple mutant lines, have been previously described (Figure 2.4C) (Raines et al. 2016). Genotypes were confirmed by PCR using primer pairs listed in Table 2.1. *CRF* overexpressing lines, *35S:CRF1-GFP* (*CRF1ox*) and *35S:CRF5-GFP* (*CRF5ox*) have been previously described (Raines et al. 2016). Homozygosity of transgenic lines was confirmed by antibiotic selection (kanamycin resistance) and detection of the *35S* promoter via PCR (For 5'-GCTCCTACAAATGCCATC-3'; Rev 5'-GATAGTGGGATTGTGCGTC-3'). All CK mutant and overexpressing lines were obtained from Joseph J. Kieber, University of North Carolina, Chapel Hill, NC (Raines et al. 2016). The CK signaling mutant *ahk2-7 ahk3-2* (*ahk2,3*). Constitutive immunity mutant *cpr5-1* (Bowling et al. 1997) was obtained from the Arabidopsis Biological Resource Center (ABRC). Mutant *cpr5-1* was genotyped to confirm homozygosity by Cleaved Amplified Polymorphic Sequence (CAPS) assays (Table 2.2).

Seeds were stratified for 2-4 days at 4°C before germination on Sunshine Growing Mix 4 (Sunshine) soilless media. For *in planta* bacterial growth assays, plants were grown in short-day conditions, in a controlled environment plant growth chamber (Conviron, ATC-60) with a

photoperiod of 10:14 hour day:night at 160 ± 20 µmol $m^{-2}s^{-1}$, 22°C, and 66%:75% relative humidity. For hormone induction and antibiotic selection, seeds were gas sterilized, plated on 1X Murashige and Skoog (MS) plant growth medium (Murashige and Skoog 1962) (PhytoTech Labs) with 1% sucrose and 0.8% bactoagar (US Biological Life Sciences, Catalogue Number (CN): A0930), and germinated in long-day conditions, in a controlled environment plant growth room, with a photoperiod of 16:8 hour day:night at 160 ± 20 µmol $m^{-2}s^{-1}$, 22°C, and 55%:65% relative humidity. Overexpressing *CRF* lines were selected for antibiotic resistance on 1X MS agar with 1% sucrose and 50 mg/mL kanamycin.

Rosette area quantification

Rosettes were photographed 5-7 weeks post germination, unless otherwise noted, in short-day conditions. Area measurements were done using Fiji imaging software (Schindelin et al. 2012) by drawing the smallest circle encompassing all leaves in a single rosette. Data was normalized for each genotype to Col-0. Normalizing was done by averaging area measurements from control Col-0 measurements, followed by dividing each raw data point by the control average and multiplying by 100. Percent growth reduction was calculated from normalized data by taking the difference between the Col-0 average and the average of each genotype.

Hormone induction experiments

Two-week old Col-0 seedlings germinated on 1X MS media plates were transferred to flasks with 1X MS liquid media and allowed to adjust for 1 hour, with constant shaking at 75 rpm, in a controlled environment plant growth room, under long-day conditions as described previously. Flasks were supplemented with the synthetic CK benzyl adenine (BA) (Sigma-Aldrich; Catalogue Number (CN): B3408), SA (Sigma-Aldrich; CN: S7401), or control in 0.1% dimethyl sulfoxide (DMSO) (Sigma-Aldrich; CN: 472301). Seedlings from each treatment were

removed from the MS liquid media after hormone induction at 15 minutes post induction, 1 hour post induction (hpi), or 6 hpi. Harvested tissue was briefly rinsed with deionized water, patted dry, frozen in liquid nitrogen, and stored at -80°C before RNA extraction.

Bacterial growth assays and plant inoculation

Pseudomonas syringae pv. *tomato* DC3000 strains used were as follows: *Pst* DC3000 EV *(Pst* DC3000), carrying an empty vector selectable by kanamycin resistance; or *Pst* DC3000 hrcC$^-$ (*Pst* hrcC$^-$), a nonpathogenic deletion mutant lacking the type III secretion system necessary for delivery of bacterial effectors into the plant cell to cause disease (Deng et al. 1998), selectable by kanamycin resistance. Both strains harbor chromosomal resistance to rifampicin.

For bacterial *in planta* growth assays, *Pseudomonas syringae* pv. *tomato* DC3000 EV (*Pst* DC3000) was streaked on King's B (KB) media supplemented with Rifampicin (50mg/mL) and kanamycin (50mg/mL) and incubated at 28°C for 48 hours. Colonies were re-streaked for a lawn plate onto new $KB_{Rif/Kan}$ plates 24 hours before plant inoculation. On the day of inoculation, bacteria were resuspended in 10 mM $MgCl_2$ and adjusted to OD_{600} = 0.05, equal to 5 x 10^7 colony forming units (CFU)/mL, with 0.025% Silwett L-77. For gene expression experiments, bacteria were sprayed onto whole rosettes of five-week-old Col-0 plants grown in short-day conditions, using a Prevall sprayer (Prevall, Inc.). After inoculation, plants were covered with a dome lightly sprayed with water, which was removed 24 hours after inoculation.

For bacterial *in planta* growth assays, stratified seedlings were germinated on domed pots covered with mesh in short-day conditions. Two weeks post germination, seedlings were dip inoculated with a bacterial suspension of 5 x 10^7 CFU/mL in 10 mM $MgCl_2$ with 0.025% Silwett L-77, following published methods (Tornero and Dangl 2001; Yao, Withers, and He 2013). After inoculation, plants were covered with a water-sprayed dome, which was removed

24 hours post inoculation (hpi). *In planta* bacterial growth was quantified 1 hpi and 3 days post inoculation (dpi) by plating serial dilutions onto KB media, followed by colony counting (Yao, Withers, and He 2013). Day 0 dilutions were plated on $KB_{Rif/Kan}$ while day 3 bacterial dilutions were plated on $KB_{Rif/Chx}$ (cycloheximide) plates. Dilution plates were incubated for 24 hours at 28°C before colony counting.

RNA extraction and qRT-PCR

Total RNA was extracted from collected plant tissue using a RNeasy Plant kit (QIAGEN), following manufacturer's protocols. RNA quality was evaluated using A_{260}/A_{280} and A_{260}/A_{230} ratios. Samples meeting quality control ratios were treated with Invitrogen Turbo DNase-Free (Thermo Fisher Scientific) treatment and checked for the absence of genomic DNA by qRT-PCR using Actin (AT5G66770) primers. cDNA was synthesized from DNase-treated RNA using qScript cDNA SuperMix (QuantaBio) and checked for complete cDNA amplification with qRT-PCR using primers for *GLYCERALDEHYDE 3-PHOSPHATE DEHYDROGENASE, GAPDH* (AT1G13320). Ct/Cq differences between each GAPDH primer of less than 1.5 were indicative of complete cDNA synthesis. qRT-PCR reactions were quantified using a BioRad CFX Connect Real-Time System (Bio-Rad) using PerfeCTa SYBR Green SuperMix (QuantaBio). *UBIQUITIN 10, UBQ10* (AT4G05320), primers were used as a housekeeping gene in all reactions. All quality control and gene specific primers used for gene expression analysis are listed in Table 2.3. Three biological replicates, at minimum, were done for each experiment.

RNA-seq

Col-0, *CRF5ox* 3G, *cpr5-1*, and *cpr5, CRF5ox* F2 seeds were stratified as above before germination on Sunshine Mix #4 soilless media in short-day conditions. Two weeks after germination, seedlings were transplanted; three plants each Col-0, *CRF5ox*, and *cpr5*, and fertilized with Miracle-Gro Water Soluble All Purpose Plant Food (Miracle-Gro), NPK 24-18-16

(1/2 tsp. per gallon). Any germinating *cpr5, CRF5ox* seedlings were transplanted to identify homozygous individuals through phenotyping. At seven weeks, whole rosettes were collected from each genotype and flash frozen in liquid nitrogen. Col-0, *CRF5ox*, and *cpr5* whole rosettes were ground by mortar and pestle while *cpr5, CRF5ox* rosettes were ground in 2 mL tubes with stainless steel beads using a TissueLyserII (QIAGEN) to minimize tissue loss. RNA was extracted from all plant material using the QIAGEN RNeasy Plant Mini Kit (QIAGEN). Sample quality was evaluated by Nanodrop and TapeStation 2200 (Agilent) with High Sensitivity RNA materials (Agilent Screentape 5067-5579, Agilent Sample Buffer 5067-5580). Samples were sequenced by Novogene (Sacramento, CA, USA), using the Illumina Novoseq platform paired-end 150bp reds, sequenced at a 40 million read pairs (mrp) per sample depth. Raw data were cleaned using Novogene perl scripts for quality control before mapping to the *Arabidopsis thaliana* reference genome (ensemblplants_arabidopsis_thaliana_tair10_gca_000001735_1) using Hisat2 v2.0.5. Mapped reads were assembled using StringTie v1.3.3b (Pertea et al. 2015) and quantified using featureCounts v1.5.0-p3. The fragments per kilobase of transcript per million mapped reads (FPKM) of each gene was calculated based on the read counts mapped to each gene, taking into account the sequencing depth and gene length. Differential expression was done using the DESq2 R package (1.20.0) and adjusted p-values using Benjamini and Hochberg's approach to control for false discovery rate. A p-value ≤ 0.05 was used to identify genes as differentially expressed. Panther (http://pantherdb.org) was used to identify gene ontology (GO) enrichment of differentially expressed genes (DEGs) in *CRF5ox* 3G, *cpr5*, and *cpr5, CRF5ox* genotypes relative to Col-0.

Protein extraction and western blot

Col-0, *CRF1ox*, and *CRF5ox* 3G two-week-old seedlings germinated on MS media in long-day conditions in a controlled environment plant growth room were pooled, weighted, frozen in liquid nitrogen and stored at -80°C before protein extraction. Whole leaves from Col-0

and *CRF5ox* 3A grown in short-day conditions in a controlled environment growth plant chamber (Conviron, ATC-60) were collected in a similar manner. Protein extracts were prepared as previously described (To et al. 2007). Protein extracts were separated by SDS-PAGE (Bio-Rad) and transferred to a nitrocellulose membrane (Thermo Fisher Scientific). GFP-tagged proteins were detected with a mixture of two monoclonal mouse anti-GFP (Roche; CN: C755C12) primary antibodies and secondary goat anti-mouse (Boster Biological Technology; CN: bs-0296G) antibody. Antibodies were developed with SuperSignal™ West Pico PLUS Chemiluminescent Substrate (Thermo Scientific; CN: 34580) and imaged by chemiluminescence on an Azure imager (Azure Biosystems).

Statistical Analysis

Three biological replicates were done for each assay, minimum, for each experiment. Sample sizes for each experiment are noted in figure legends. Statistical significance was determined using a one-WAY ANOVA with a p-value ≤ 0.05.

2.4 RESULTS

CRFs are differentially regulated by cytokinin, salicylic acid, and pathogen infection

The crosstalk between the plant hormones CK and SA (Figure 2.3A-C) and their participation in plant growth and immunity, led to us to hypothesize that proteins in these signaling pathways could be mediators of the growth-defense tradeoff. Because patterns of gene expression can be indicative of gene function, we addressed the gene expression regulation of members of the *CRF* family by SA and CK. We mined publicly available microarray data using the e-Northern tool of The Bio-Analytic Resource for Plant Biology (BAR, http://bar.utoronto.ca/) (Toufighi et al. 2005) for CRF expression after CK or SA treatments. Compared to a mock control treatment, *CRF2* and *CRF5* were robustly up-regulated (6.2 and 14.8 fold-change (FC), respectively) 3 hours after treatment with 20 μM of the biologically active

form of CK, *trans* (*t*)-zeatin (Figure 2.5), matching previously published data (Rashotte et al. 2006; Raines et al. 2016). Both *CRF1* and *CRF3* were only slightly up regulated at this timepoint (1.4 and 1.5 FC, respectively), and while *CRF6* has previously been shown to be induced after CK treatment (Raines et al. 2016), at 3 hours after with *t*-zeatin *CRF6* expression remained low (1.1 FC). Expression of all *CRFs* was down-regulated by 10 μM SA treatment, except for *CRF6* (Figure 2.5). These data show that *CRFs* are differentially regulated by CK and SA treatments.

To have a better understanding of *CRF* hormone-regulated expression patterns over time, we performed a time-course experiment using 2-week-old seedlings in liquid MS media supplemented with 100 μM of the synthetic CK benzyl adenine (BA) or 100 μM SA, dissolved in 0.1% DMSO (Figure 2.6). All gene expression was normalized to *UBQ10* for each sample and *CRF* expression was evaluated in comparison to their corresponding 0.1% DMSO control treatments at each timepoint. Within 15 minutes after treatment, *CRF2*, *CRF3*, *CRF4*, and *CRF5* were all up-regulated by BA (1.70, 1.82, 1.66, and 2.42 FC, respectively), with *CRF5* expression being the most induced (Figure 2.6). At one hour, all *CRFs* but *CRF1* were significantly up-regulated by BA, with *CRF6* being the most highly expressed (Figure 2.6), confirming published data that expression of these *CRFs* are induced by CK treatment (Raines et al. 2016). At six hours, *CRF6* was most robustly up-regulated, again, supporting published data of delayed induction of *CRF6* after BA treatment. All other *CRFs* were down-regulated at six hours after BA (Figure 2.6). Overall, the expression of *CRF2*, *CRF3*, *CRF4*, and *CRF5* followed a pattern of strong expression after an initial CK signaling burst, suggesting that they are likely primary transcriptional targets of CK signaling. In comparison, across all timepoints, SA treatment resulted in down-regulation of *CRF* expression, with *CRF2* expression decreasing the most out of all *CRFs* (Figure 2.6). The only exception was *CRF6*, which was slightly up-regulated at 15 minutes post SA treatment (Figure 2.6). These results confirmed that CRF genes are differentially regulated by SA and CK.

Given the importance of the plant hormones SA and CK to plant immunity, we decided to ask how the expression of *CRFs* changed upon inoculation with the bacterial pathogen *Pst* DC3000, a well-established pathogen of Arabidopsis. In addition to the *Pst* DC3000 wild-type strain, we used also the *Pst* hrcC$^-$ mutant strain, which is less virulent on Arabidopsis. Rosettes of five-week-old Col-0 plants grown in short-day conditions were spray-inoculated with either strain, or a mock control treatment ($MgCl_2$), and differential expression was calculated in relation to $MgCl_2$ control plants. Inoculation with *Pst* DC3000 induced the expression of *CRF* genes, particularly of *CRF1*, *CRF4* and *CRF5* (Figure 2.7), indicating that in addition to their regulation by plant hormones, *CRF* genes are also regulated by pathogen stress. Of note, the expression of these *CRF* genes by *Pst* DC3000 was observed mostly at the 6h timepoint, which is later than the observed induction of expression by CK (Figure 2.6), indicating that *CRF* genes are not primary transcriptional targets of immunity-regulated transcription processes (Figure 2.7). Interestingly, the expression of *CRF1*, *CRF4* and *CRF5*, was even further induced by the *Pst* hrcC$^-$ mutant, which is a mutant that lacks the type III secretion system necessary to introduce pathogen effector proteins into the plant cell and cause disease (Tsuda et al. 2008). Because one of the main functions of pathogen effector proteins is to suppress immune responses to allow for disease development, these results suggest that CRF1, CRF4 and CRF5 may be involved in the transcriptional regulation of immune responses. Moreover, they suggest that expression of these *CRF* genes may be down-regulated, directly or indirectly, by pathogen effectors to suppress defense responses.

To further understand the transcriptional regulation of *CRF* genes after pathogen attack, the CK signaling double mutant *ahk2,3*, deficient in two of the three CK signaling receptors (ARABIDOPSIS HISTIDINE KINASE 2 and ARABIDOPSIS HISTIDINE KINASE 3), was used for *CRF* gene expression after *Pst* DC3000 or *Pst* hrcC$^-$. The experimental conditions were the same as described above. For both strains, lack of CK signaling in the *ahk2,3* mutant resulted in the down-regulation of *CRFs* at all timepoints (Figure 2.7), suggesting that CK signaling is

necessary for the induction of *CRF* expression upon pathogen inoculation. These data support previously published data that CK signaling plays a role in mediating plant defense responses to pathogens (Choi et al. 2010; Argueso et al. 2012). Further, these results suggest that an activation of CK signaling upon pathogen attack precedes *CRF* expression, a result that is also supported by previously published data that shows changes in CK signaling upon pathogen exposure (Argueso et al. 2012). Gene expression data was not available for *ahk2,3* plants inoculated with *Pst* DC3000 at 72 hpi, as this genotype displays high susceptibility to pathogens, which results in poor RNA quality of pathogen-treated samples, especially at later timepoints when disease progression is extensive.

CRFs act mostly redundantly in the regulation of plant growth under short-day conditions

Our gene expression results showed that *CRF* gene expression is regulated by the plant hormones SA and CK, and by pathogen treatment in a manner that is dependent on CK signaling. Given the involvement of these two plant hormones in plant growth, we decided to address whether *CRF* genes contribute to this process, using genetic analyses.

To do so, we took advantage of a collection of T-DNA insertion null mutants on *CRF* genes, which has been previously characterized (Figure 2.4C) (Raines et al. 2016). This previous study used combinations of single, double, triple and quadruple *crf* mutants, and analyzed them for total growth by measuring total rosette area. The results of this study showed that other than a specific combination of a *crf* multiple mutant (*crf1*$^{+/-}$*2,5,6*), all other single and multiple combinations did not show any strong phenotypes of altered plant growth (Raines et al. 2016). However, these experiments were performed in long-day conditions, which are different from the short-day conditions normally used for pathogen assays. Furthermore, different genotypes may have different phenotypes in long- versus short-day conditions, particularly in relation to time of flowering and vegetative growth. Thus, wild-type Col-0 plants and a selection of single and multiple *crf* mutants were grown in short-day conditions for comparison of growth

parameters. At seven weeks post germination, the rosette areas of all genotypes were measured (Figure 2.8A-B). Average rosette areas of all genotypes were comparable to Col-0, although *crf1* and *crf5* displayed a small but non-significant increase and decrease of rosette area, respectively (Figure 2.8A-B). *crf5* plants also showed a slight but significant decrease in the number of leaves produced (Figure 2.8C). Like previously published results, *crf1,3,5,6* rosette size was comparable to Col-0 under short-day conditions (Figure 2.8A-B) (Raines et al. 2016). These results showed that for the most part, mutations in *CRF* genes did not change plant growth significantly, and that with the exception of *CRF1* and *CRF5*, *CRF* genes act mostly redundantly on plant growth in short day-conditions. Because T-DNA insertional mutants are not available for *CRF4,* the contribution of this gene was never analyzed.

CRF5 and CRF1 are positive regulators of immunity against Pst DC3000

The up-regulation of *CRF1*, *CRF4*, and *CRF5* in response to *Pst* DC3000, led us to address whether these *CRFs* play a role in immunity against this pathogen. Because T-DNA insertion mutants are not available for *CRF4* (Figure 2.4C), we chose to focus on the possible contributions of *CRF1* and *CRF5* to plant immunity. Given the indication of genetic redundancy amongst these genes in relation to plant growth (Figure 2.8A-C), we chose to address whether CRFs play a role in immunity by also using a gain-of-function approach.

Homozygous transgenic lines overexpressing cDNAs of *CRF1* or *CRF5* fused to GFP at their C-terminus (*35S::CRF1-GFP* or *CRF1ox;* and *35S::CRF5-GFP* or *CRF5ox*, respectively) have been generated and previously characterized (Raines et al. 2016). We further characterized these lines, which included one *CRF1ox* and two *CRF5ox* independent lines (*CRF5ox* 3G and *CRF5ox* 3A), by determining the gene expression and protein abundance of their *CRF* transgenes. Gene expression of *CRF1* was increased by 385-fold in *CRF1ox* relative to Col-0, while *CRF5* gene expression in the *CRF5ox* 3G and *CRF5ox* 3A lines was up-regulated by approximately 100-fold and 500-fold, respectively (Figure 2.9A-C). A Western-blot

using an α-GFP antibody showed the presence of bands matching the size of the predicted CRF-GFP fusion proteins in all *CRFox* lines, and these bands were absent in control non-transformed Col-0 plants (Figure 2.9D-E). Importantly, these transgenic lines all showed a reduced growth phenotype when compared to Col-0, further implicating these genes in the control of plant growth. For simplicity, *CRF1ox* and *CRF5ox* 3G were then chosen for subsequent experiments.

The *crf1* and *crf5* single mutants, as well as *CRF1ox*, and *CRF5ox* 3G lines, were then used to evaluate plant susceptibility to *Pst* DC3000 through *in planta* bacterial growth quantification. Two-week-old seedlings of Col-0, *crf1*, *crf5*, *CRF1ox*, and *CRF5ox* 3G grown under short-day conditions were dip-inoculated with *Pst* DC3000 at a concentration of 5 x 10^7 CFU/mL (Tornero and Dangl 2001). At 1 hour post inoculation (hpi), tissue was collected from each genotype to confirm equal inoculation between genotypes (Figure 2.10). Three days post inoculation (dpi), tissue was again collected, and bacteria quantified from each genotype. Single mutants *crf1* and *crf5* had comparable bacterial growth to Col-0 at 3 dpi (7.54, 7.40, and 7.32 CFU/mL, respectively) indicating that the loss-of-function of a single *CRF* does not change plant susceptibility to *Pst* DC3000 (Figure 2.10). *CRF1ox* had a slight but non-significant reduction in bacterial growth at 3 dpi (7.17 CFU/mL), however *CRF5ox* 3G allowed for significantly less bacterial growth (6.82 CFU/mL) compared to Col-0 (Figure 2.10). These data show that CRF5, and possibly CRF1, positively contribute to plant immunity against *Pst* DC3000.

CRF1 and CRF5 differentially regulate genes involved in CK and SA metabolism and signaling

Our transcriptional and genetic analyses revealed a possible role for CRF1, and a more prominent role for CRF5, in the processes of plant growth and immunity. However, genetic redundancy in this gene family complicated our ability to determine whether these individual *CRFs* genes have independent roles in plant growth and immunity. To further discern the contributions of these two genes to these processes, we then decided to address whether these

two transcription factors could play different roles in the regulation of genes involved in CK and SA metabolism and signaling.

To do so, we quantified the expression of CK and SA metabolism and signaling genes in *CRF1ox* and *CRF5ox* 3G lines, in comparison to control Col-0 plants. Leaves from five-week-old rosettes grown in short-day conditions were collected for RNA extraction, cDNA synthesis, and quality control following the methods previously described. For CK, two genes involved in CK biosynthesis (*ISOPENTENYLTRANSFERASE 3, IPT3*; *ISOPENTENYLTRANSFERASE 7, IPT7*), one involved in CK degradation (*CYTOKININ OXIDASE 4, CKX4*) and one involved in CK signaling (*ARABIDOPSIS RESPONSE REGULATOR 7, ARR7*) were tested. For SA, one gene involved in SA biosynthesis (*ISOCHORISMATE SYNTHASE 1* or *ICS1*) and two genes involved in SA signaling (*NIM1-INTERACTING 1, NIMIN1* and *PATHOGENESIS-RELATED GENE 1, PR-1*), were tested (Figure 2.11B). Overall, expression patterns of the genes tested indicated that both CRF1 and CRF5 play an inhibitory role in CK biosynthesis (with the exception of *IPT7* expression in *CRF1ox*) and signaling, while only CRF5 has a positive effect in promoting SA biosynthesis and signaling. These results indicate that CRF1 and CRF5 play overlapping, but different, roles in CK and SA metabolism and signaling.

The combination of overexpression of CRF5 and constitutive immunity mutant cpr5 results in severe growth reduction and delayed transition to reproductive development

In Arabidopsis, mutants displaying constitutive activation of plant immunity often display stunted plant growth, a phenotype that is frequently associated with high levels SA (van Wersch, Li, and Zhang 2016). The *CPR5* gene (*CONSTITUTIVE EXPRESSION OF PR GENES 5)* encodes a nucleoporin that influences plant immunity via a role in nuclear transportation and regulation of the cell cycle and mRNA splicing (Peng et al. 2022). *CPR5* loss-of-function mutants have elevated SA levels and increased resistance to multiple pathogens, but also reduced rosette area, reduced seed size, and early senescence (Bowling et al. 1997), all

phenotypes that are also shared by *CRF5ox* plants. We therefore decided to test whether CRF5 and CPR5 are part of the same signaling pathway controlling plant growth and immunity.

We crossed *cpr5* to the *CRF5ox* 3G line and obtained F1 progeny. F1 plants were allowed to self, and F2 seed obtained. F2 plants were screened for the combination of the *cpr5* mutation and the *CRF5ox* transgene by a CAPS assay developed for the *cpr5* mutation and by amplification of the *35S* promoter, respectively. Next, we evaluated the resulting growth phenotypes of this combination line, *cpr5, CRF5ox*, in comparison to its parental genotypes (*cpr5* and *CRF5ox* 3G) and wild-type Col-0 plants. Compared to Col-0, *cpr5* had a 49.5% reduction in rosette area, and was significantly larger than *CRF5ox* 3G, which was reduced by 64.6% (Figure 2.12A-B). However, *cpr5* had significantly fewer leaves than both Col-0 and *CRF5ox* 3G (Figure 2.12C). The combination of *cpr5* and *CRF5ox* 3G resulted in further reduction of rosette area, which was decreased by 94.3% in *cpr5, CRF5ox* compared to Col-0, and reduced rosette leaf number (Figure 2.12A-C). These results demonstrate that *cpr5*-dependent constitutive immunity and constitutive expression of *CRF5* lead to a dramatic restriction of plant growth. Most importantly, the additive effect of these genetic perturbations on plant growth indicates that *CRF5* and *CPR5* operate in two distinct genetic pathways to regulate plant growth.

In addition to reduced growth, *cpr5* has reduced trichome number and reduced trichome branching (Bowling et al. 1997) resulting from improper trichome development (Brininstool et al. 2008), causing the leaves to appear smooth without magnification. Because this phenotype is tightly genetically linked to *cpr5*, we noticed that the *cpr5, CRF5ox* plants also had reduced trichome number and branching (data not shown). This was one phenotypic marker used to identify homozygous individuals in segregating populations. Furthermore, *cpr5* spontaneously forms lesions (Bowling et al. 1997), which was also seen in *cpr5, CRF5ox*, however, the pattern of cell death was different between *cpr5* and *cpr5, CRF5ox* (data not shown).

Reproductive development of *cpr5* is stunted compared to Col-0 with reduced stem height and seed yield (Bowling et al. 1997). While *CRF5ox* shoot phenotypes have been characterized to some extent (Raines et al. 2016), we noticed that *CRF5ox* 3G had a dramatic reduction in seed yield due to reduced pollen fertility, and most siliques did not develop viable seeds (data not shown). To evaluate the contributions of *CRF5* and *CPR5* to reproductive development, we grew all these genotypes to flowering and seed set. Representative photos of each genotype were taken at 16 weeks after germination (Figure 2.12D). At this time, *cpr5, CRF5ox* had not transitioned to reproductive development and was still extremely small (Figure 2.12E). Eventually, these plants did transition to reproductive development and flowering, however this transition was significantly delayed and occurred 120 dpg compared to 71.1 dpg, 85.6 dpg, and 83.2 dpg for Col-0, *CRF5ox* 3G*,* and *cpr5*, respectively (Figure 2.12F). After flowering, *cpr5, CRF5ox* had reduced pollen fertility, similar to the reduced fertility phenotype seen in *CRF5ox* 3G and set very few seeds (data not shown).

CRF5 activates immunity and suppresses plant growth independently of CPR5, but through the regulation of overlapping sets of genes

To better understand the role of CRF5 in the regulation of plant growth we performed an RNA-seq experiment of Col-0, *CRF5ox* 3G, *cpr5*, and *cpr5, CRF5ox* to evaluate transcriptional changes potentially linked to growth, development, and defense. Col-0, *CRF5ox* 3G, *cpr5*, and *cpr5, CRF5ox* plants were grown in short-day conditions, as described above. Seven weeks after germination, three whole rosettes of Col-0, *CRF5ox* 3G, and *cpr5*, and three to five whole rosettes of *cpr5, CRF5ox* were collected for RNA extraction. The rosettes of each genotype were pooled prior to grinding and RNA extraction, as described previously, for three biological replicates per genotype. The samples were sequenced using the Novoseq platform paired-end 150bp reads with depth of 40 mrp per sample. Differential expression between samples was

done using the DESq2 R package (1.20.0). An adjusted p-value ≤ 0.05 was used to identify differentially expressed genes (DEGs) compared to Col-0.

As a quality control, we performed a principal component analysis (PCA), which showed that the three biological replicates for each genotype were clustered together, suggesting little variation between biological replicates (Figure 2.13A). Furthermore, *cpr5* and *cpr5, CRF5ox* groups were close together, indicating that *cpr5* had a greater influence on gene expression in *cpr5, CRF5ox* than *CRF5ox* (Figure 2.13A). For an additional quality control, the expression of *CRF5 and CPR5* were evaluated in each genotype. As expected, *CRF5* expression was elevated in *CRF5ox* and *cpr5, CRF5ox,* and was unchanged in *cpr5* (Figure 2.13B). Also, the expression of *CPR5* was unchanged in the *CRF5ox* 3G background (Figure 2.13C). These results further confirm the results of our epistatic analyses, which indicate that *CRP5* and *CRF5* work independently to control plant growth.

Hierarchical clustering of the sets of differentially regulated genes (DEG) showed that there was more similarity between *cpr5* and *cpr5, CRF5ox* samples compared to *CRF5 ox 3G* and Col-0 (Figure 2.14). Notably, up-regulated genes in Col-0 were strongly down-regulated in *CRF5ox* and *cpr5, CRF5ox* and moderately down-regulated in *cpr5*, and down-regulated genes in Col-0 were generally up-regulated in *CRF5*, *cpr5*, *cpr5, CRF5ox* (Figure 2.14), showing there were robust transcriptional changes in each of these genotypes.

Gene ontology (GO) analyses of *CRF5ox* 3G, *cpr5*, and *cpr5, CRF5ox* DEGs compared to Col-0 were conducted, using the PANTHER Classification System (Version 17.0) (Mi, Muruganujan, and Thomas 2013; Thomas et al. 2003). In relation to Col-0, *CRF5ox* 3G, *cpr5*, and *cpr5, CRF5ox* had many up-regulated GO categories associated with plant immune responses and responses to abiotic stimuli (Figure 2.15A). Furthermore, there was an up-regulation of genes associated with hormone responses (Figure 2.15A), which included sub-categories related to SA and jasmonic acid (JA) biosynthesis, signaling, and responses, contributing to increased plant immunity. As a plant defense-related hormone, JA promotes

plant defense responses to necrotrophic pathogens and insect herbivory (Shigenaga and Argueso 2016). There were fewer GO terms associated with down-regulated genes and there was little commonality between the three genotypes, however, GO terms that were present were associated with embryo development, cell cycle, and DNA repair (Figure 2.15B). The only GO term associated with down-regulated genes in *cpr5, CRF5ox* was RNA-related processes and was also a broad category of down-regulated genes in *cpr5* and *CRF5ox* (Figure 2.15B). Looking across genotypes, we identified specific GO categories shared between *cpr5*, *CRF5ox*, and *cpr5, CRF5ox* (Figure 2.15C). Here, all GO terms identified were related to defense responses to bacterial and fungal pathogens (Figure 2.15C), further showing a robust up-regulation of defense responses in these backgrounds.

Because *cpr5, CRF5ox* parental lines *cpr5* and *CRF5ox* are associated with SA-dependent immunity and CK signaling, respectively, we identified genes in SA and CK biosynthesis, signaling, and metabolism that were differentially regulated in these genotypes. SA biosynthesis (*ICS1*), and signaling (*PAD4*, *NPR3, PR1*, and *WRKY18*) were up-regulated in all genotypes, supporting GO analysis results associated with increased defense response terms (Figure 2.16A; Table 2.4). SA signaling has been shown to inhibit CK (Argueso et al. 2012), though it is unclear if CK biosynthesis, signaling, or downstream responses are inhibited. In these genotypes, CK biosynthesis (*IPT3* and *IPT7*) and Type-A ARR (*ARR6* and *ARR15*) expression were down-regulated compared to Col-0 (Figure 2.16B; Table 2.4). CK degradation (*CKX2*, *CKX3*, and *CKX5*) genes were up-regulated along with Type-B ARR (*ARR2* and *ARR18*) (Figure 2.16B; Table 2.4). Taken together, *cpr5*, *CRF5ox*, and *cpr5, CRF5ox* have reduced CK biosynthesis and increased CK degradation, suggesting there are low concentrations of CK in these genotypes. As CK is known to be required for plant growth, and given these gene expression changes, it is likely that the reduced growth phenotypes of *CRF5ox*, *cpr5*, and *cpr5, CRF5ox* are, in part, due to reduced CK accumulation and signaling compared to Col-0.

To further evaluate transcriptional changes associated with CK in *CRF5ox* 3G, *cpr5*, and *cpr5, CRF5ox*, we compared DEGs to the "Golden List," a group of 226 DEGs robustly regulated by CK (Bhargava et al. 2013). The genes within the Golden List were identified through microarray meta-analysis of 13 independent data sets using CK-treated samples and an RNA-seq experiment to validate CK-regulated gene expression (Bhargava et al. 2013). Of these genes, 158 were up-regulated and 68 were down regulated (Bhargava et al. 2013). Of the 158 up-regulated Golden List genes, 18 (11.39%), 44 (27.85%), and 46 (29.11%) were differentially expressed in *cpr5*, *CRF5ox* 3G, and *cpr5, CRF5ox*, respectively. 59.09% of *cpr5, CRF5ox* DEGs were shared with *CRF5ox* 3G, while 61.11% of *cpr5* DEGs overlapped with both *CRF5ox* 3G and *cpr5, CRF5ox*. This suggests that the effects of *cpr5* and *CRF5ox* 3G are enhanced when these genetic backgrounds are combined. Furthermore, many of the Golden List genes that are positively regulated by CK were inhibited in *cpr5, CRF5ox* (Figure 2.20A-B; Table 2.5). In contrast, 17 (25%), 17 (25%), and 24 (35.29%) of the down regulated Golden List genes were differentially expressed in *cpr5*, *CRF5ox* 3G, and *cpr5, CRF5ox*, respectively, with most of these DEGs being up-regulated in *cpr5, CRF5ox* (Figure 2.21A-B; Table 2.5). Because of the opposite expression patterns between *cpr5, CRF5ox* and the Golden List, these data further support the roles of *CPR5 and CRF5* on the inhibition of CK and CK-associated responses.

2.5 DISCUSSION

Previous data have suggested that CRFs are mediators of plant growth and defense responses; here, we have added to this growing body of evidence. Overexpression of *CRF5* leads to repressed vegetative and reproductive plant growth and, in combination with *cpr5*, SA-dependent growth inhibition is enhanced. Based on these experimental results and gene expression patterns, we have developed a model of CRF5 regulation of CK-dependent growth and SA-mediated defense responses (Figure 2.19). Pathogen perception initiates defense

responses including CK-dependent expression of *CRF5*. CRF5 plays an inhibitory role on plant growth via inhibition of CK biosynthesis and signaling (Figure 2.11A and Figure 2.16B). CRF5 up-regulates transcription of SA biosynthesis genes, thus promoting SA, and further promotes SA-dependent signaling by up-regulating genes associated with SA signaling responses and defense markers, ultimately promoting SA-associated defense responses (Figure 2.11B and Figure 2.16A). Therefore, CRF5 acts as a negative regulator of CK-dependent growth and positive regulator of SA-mediated defense, placing CRF5 at the intersection of the CK-SA crosstalk.

The constitutive immunity mutant *cpr5* has distinct phenotypes including spontaneous lesion formation, early senescence, and reduced rosette area (Bowling et al. 1997), all of which are seen in *CRF5ox* lines (Raines et al. 2016). Additionally, both *cpr5* and *CRF5ox* 3G have increased resistance to *Pst* DC3000 (Bowling et al. 1997) and increased *PR-1* gene expression. To address if *CPR5* and *CRF5* act in the same pathway, we crossed *cpr5* and *CRF5ox* 3G, establishing the *cpr5, CRF5ox* line. *cpr5, CRF5ox* was dramatically reduced in vegetative growth and had a severe delay in the time to flowering compared to either parental line or Col-0, indicating that *CPR5* and *CRF5* act in different pathways.

To further characterize *cpr5, CRF5ox*, we performed an RNA-seq experiment. Here, we found that CK biosynthesis and signaling were generally down-regulated while SA biosynthesis and signaling were up-regulated in *cpr5, CRF5ox* compared to Col-0. Additionally, GO analysis revealed that genes associated with defense responses, including those to bacterial and fungal pathogens, and responses to defense-related hormones SA and JA were up-regulated in *cpr5*, *CRF5ox* 3G, and *cpr5, CRF5ox* compared to Col-0. Because of the overlap of DEGs in *cpr5* and *CRF5ox* 3G, the gene expression patterns in *cpr5, CRF5ox* are likely a result of a combinatorial effect of *cpr5* and *CRF5ox* 3G. As *cpr5, CRF5ox* has increased expression of defense-related genes, it will be interesting to evaluate susceptibility phenotypes compared to *cpr5* and *CRF5ox*

3G to further evaluate if *cpr5, CRF5ox* has an additive effect on plant immunity compared to parental lines.

There was little overlap between *cpr5*, *CRF5ox* 3G, and *cpr5, CRF5ox* in GO terms that were down-regulated, with the only similarity being RNA related processes between these three genotypes. CPR5 is a negative regulator of plant immunity and has recently been identified as an RNA-binding protein to regulate plant immune responses (Peng et al. 2022). In the *cpr5-1* loss of function mutant, the regulation of RNA processes is decreased and likely further decreased by *CRF5ox* 3G in the *cpr5, CRF5ox* mutant, as this is the only GO term enriched in down-regulated genes of *cpr5, CRF5ox*. As *cpr5* and *CRF5ox* 3G are more resistant to pathogens than Col-0 and have decreased gene expression of RNA-related processes, it is likely that the down-regulation of RNA related processes in *cpr5, CRF5ox* is a result of combinatorial effect from the parental lines. Taken together, these data show that *CPR5* and *CRF5* regulate similar genes associated with plant growth and defense, but act in separate pathways, and have a combinatorial effect on gene expression in *cpr5, CRF5ox*.

Because *CRF5* is induced by CK treatment and our interest in CK-SA crosstalk, we evaluated the gene expression patterns of the Golden List in *cpr5*, *CRF5ox* 3G, and *cpr5, CRF5ox* compared to Col-0. The Golden List is a set of genes robustly regulated by CK treatment (Bhargava et al. 2013). Of the genes up-regulated by CK in the Golden List, only 29.11% were differentially expressed in *cpr5, CRF5ox* compared to Col-0, most of which were down-regulated in *cpr5, CRF5ox*. A group of up-regulated Golden List genes that were also up-regulated in *cpr5, CRF5ox* were multiple members of the glutaredoxin (ROXY) family, which have been shown to interact with TGA transcription factors. Because TGAs are involved in SA-mediated gene expression, this suggests that elevated defense responses in *cpr5, CRF5ox* are, in part, associated with the up-regulation of *ROXY* genes. More genes that are down-regulated by CK in the Golden List were up-regulated in *cpr5, CRF5ox* (35.29%). Because *cpr5, CRF5ox* has increased expression of defense- and SA-associated genes, these Golden List gene

expression trends in *cpr5, CRF5ox* support the previous findings that SA inhibits CK signaling (Argueso et al. 2012).

Beyond association with plant growth and SA-associated defense responses, Arabidopsis CRFs have been shown to play a role in responses to abiotic stressors (Hallmark and Rashotte 2019). Studies have revealed the roles of CRFs in cold and freezing tolerance (Zwack, Compton, et al. 2016), oxidative stress response (Hughes et al. 2021; Zwack, De Clercq, et al. 2016), and potassium transport (Hughes et al. 2020). Taken together, these results demonstrate that CRFs play diverse roles in response to abiotic stressors, in addition to their roles as CK-responsive genes in plant growth and biotic defenses.

CRFs are found in all land plant species (Rashotte and Goertzen 2010) and studies have evaluated the role of CRFs in multiple species of agricultural importance including tomato (*Solanum lycopersicum*) (Shi, Gupta, and Rashotte 2012, 2014; Gupta and Rashotte 2014), Brassica (Liu et al. 2013), and Asteraceae (Melton et al. 2019). Because overexpression of *CRFs* result in reduced plant growth in Arabidopsis (Liang et al. 2010; Raines et al. 2016), antisense transgenic lines were established in tomato to evaluate the effect of reduced *SlCRFs* in plant growth (Gupta and Rashotte 2014). Multiple antisense lines, *SlCRF5* AS, had stunted primary root growth, lack of lateral root development, and a severe delay in the development of true leaves at the seedling stage (Gupta and Rashotte 2014). These developmental abnormalities persisted throughout plant growth with poorly developed leaves, shortened petiole length, thin stems, delayed flowering, and reduced seed set (Gupta and Rashotte 2014). These data show that CRFs play critical roles in plant growth and development in multiple plant species.

To further solidify CRFs in the crosstalk between CK and SA, identifying primary gene targets of CRFs will be indispensable. The data presented here shows that the SA biosynthesis gene *ICS1* is robustly up-regulated in *CRF5ox* lines. However, we do not know if this increase in *ICS1* expression is a directly mediated by CRF5, or if intermediate regulators are present to

initiate this part of CK-SA crosstalk. *CRF5* and *CRF2* were identified to be early and robustly up-regulated after CK application (Rashotte et al. 2003; Rashotte et al. 2006; Raines et al. 2016) and evidence exists for both *CRF5* and *CRF2* promoting plant immunity (Liang et al. 2010; Kwon 2016). It is therefore of interest to further investigate the role of CRF2 in the crosstalk between CK and SA and as a mediator of plant growth and defense responses.

2.6 FIGURES

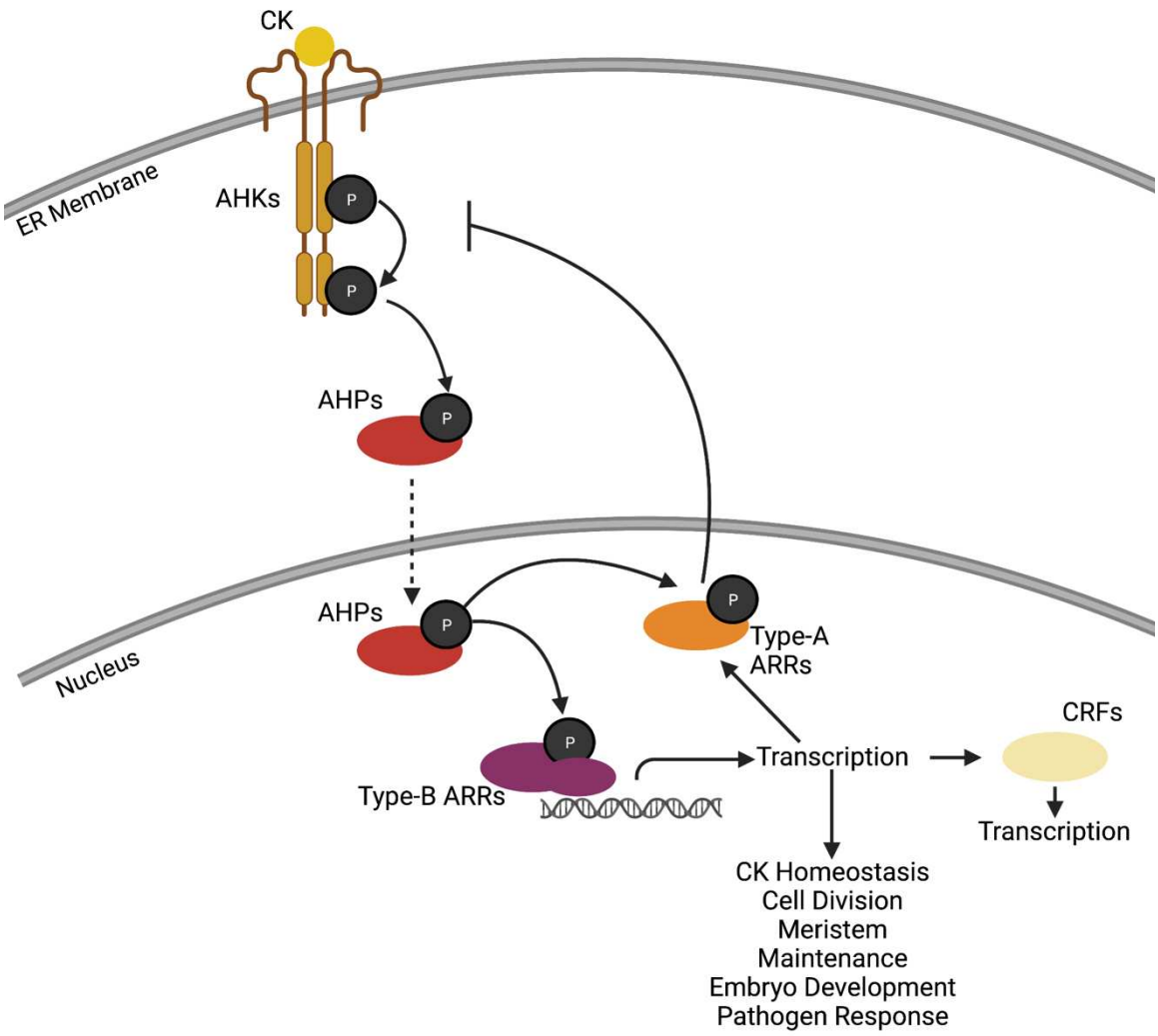

Figure 2.1: The CK signaling pathway in Arabidopsis. The CK receptors, ARABIDOPSIS HISTIDINE KINASES (AHKs), are located on the endoplasmic reticulum (ER) membrane. Upon CK perception, specific residues of the AHKs are autophosphorylated. The phosphate group is transferred to ARABIDOPSIS HISTIDINE PHOSPHOTRANSFERASES (AHPs), which translocate to the nucleus where the phosphate group is transferred to Type-A ARABIDOPSIS RESPONSE REGULATORS (ARRs) and Type-B ARRs. Type-A ARRs act as negative regulators of CK signaling. As transcription factors, the Type-B ARRs induce transcription of CK response genes, including Type-A ARRs and CYTOKININ RESPONSE FACTORS (CRFs). This figure was adapted from Hwang et al. 2012 and created using BioRender.com.

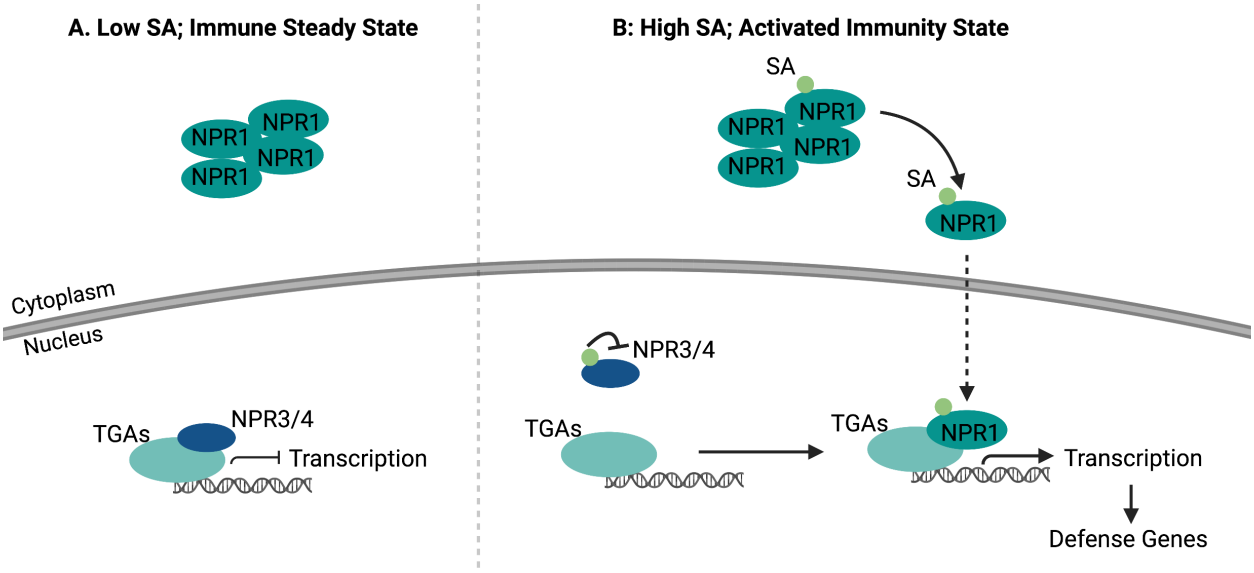

Figure 2.2: SA signaling pathway in Arabidopsis. A. During an immune steady state, there are low concentrations of SA within the cell and NONEXPRESSOR OF PR-GENES 1 oligomers reside in the cytoplasm. NPR3 and NPR4 act as transcriptional repressors, inhibiting the activity of TGA transcription factors. **B.** Upon pathogen perception and immunity activation, SA concentrations increase. Upon perception of SA, NPR1 monomerizes and is translocated into the nucleus, where it interacts with TGAs and induces transcription of SA-dependent gene expression. This figure was adapted from Vlot et al. 2009, Ding and Ding 2020, and Pokotylo et al. 2021, and created using BioRender.com.

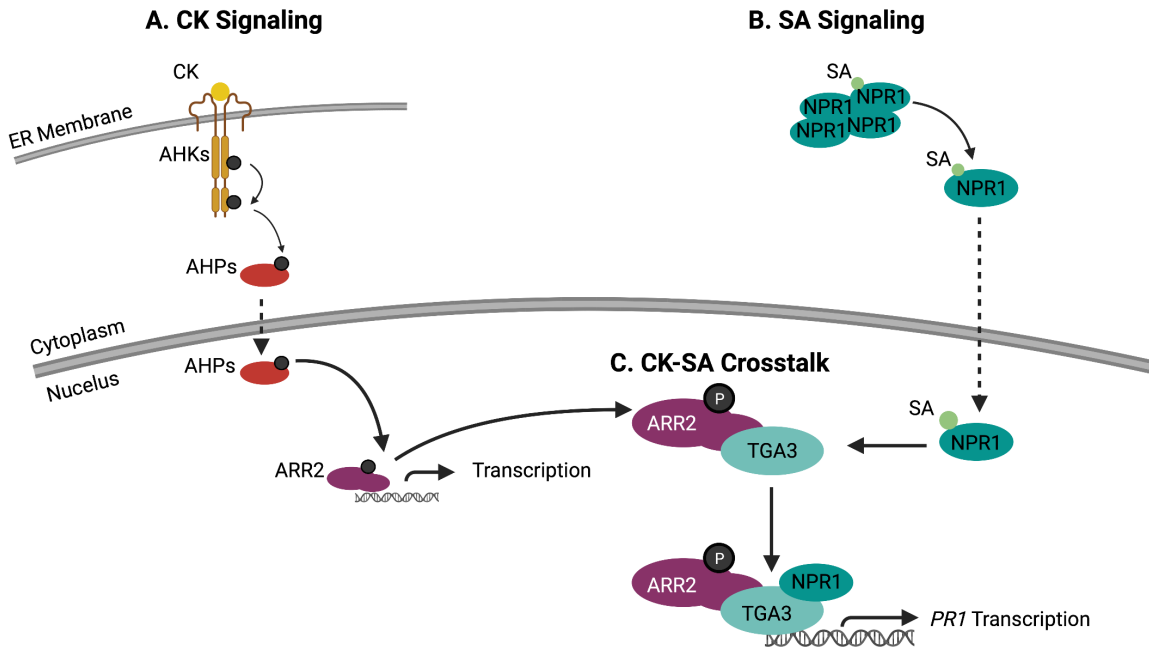

Figure 2.3: CK-SA crosstalk in Arabidopsis. A. The CK signaling pathway leads to phosphorylation and activation of Type-B ARR, ARR2. See Figure 2.1 for more detail. **B.** The SA signaling pathway leads to the destabilization of NPR1 polymers into NPR1 monomers. NPR1 monomers are translocated into the nucleus and interact with TGA transcription factors. See Figure 2.2A-B for more detail. **C.** The SA-responsive TGA transcription factor, TGA3 directly interacts with ARR2. NPR1 associates with TGA3 and induces *PR-1* gene expression. This figure was adapted from Choi et al. 2010 and created using BioRender.com.

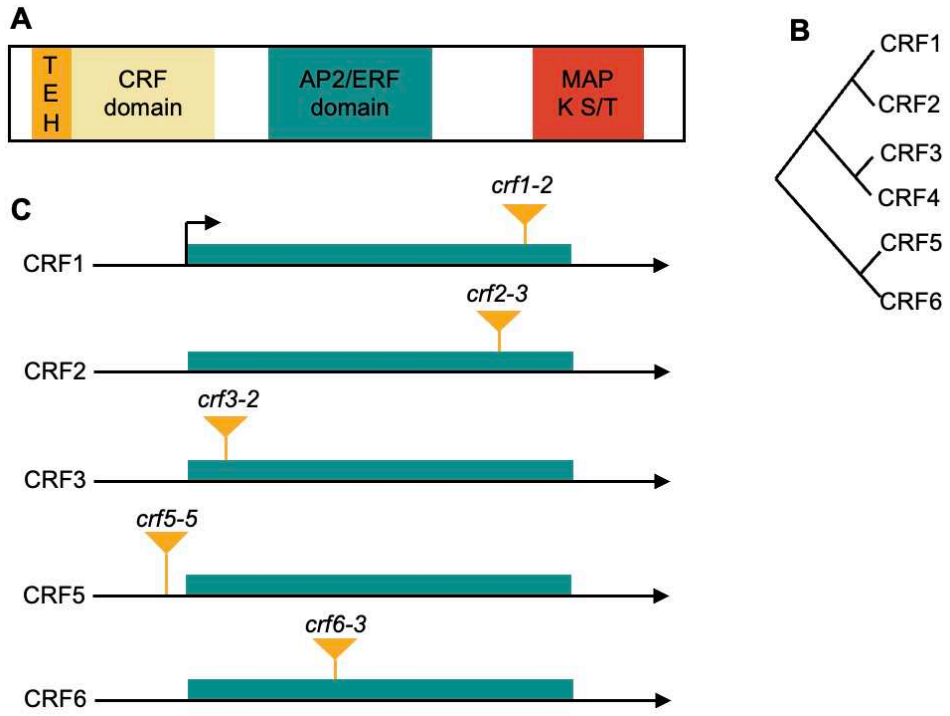

Figure 2.4: CRF protein structure, phylogeny, and T-DNA insertion mutant alleles. A. The domains of CRF proteins. All CRFs contain the conserved CRF domain at the N-terminus, which is immediately preceded by a TEH domain in about half of all CRFs. In the center of the protein, all CRFs contain an AP2/ERF DNA binding domain. At the C-terminal end, some CRFs contain a putative MAP kinase phosphorylation site. This figure was adapted from Rashotte and Goertzen 2010. **B.** An unrooted phylogenetic tree of Arabidopsis CRFs. This figure was adapted from Rashotte et al., 2006**. C.** T-DNA insertion mutant alleles, denoted with yellow arrows, used in this study. This figure was adapted from Raines et al. 2016.

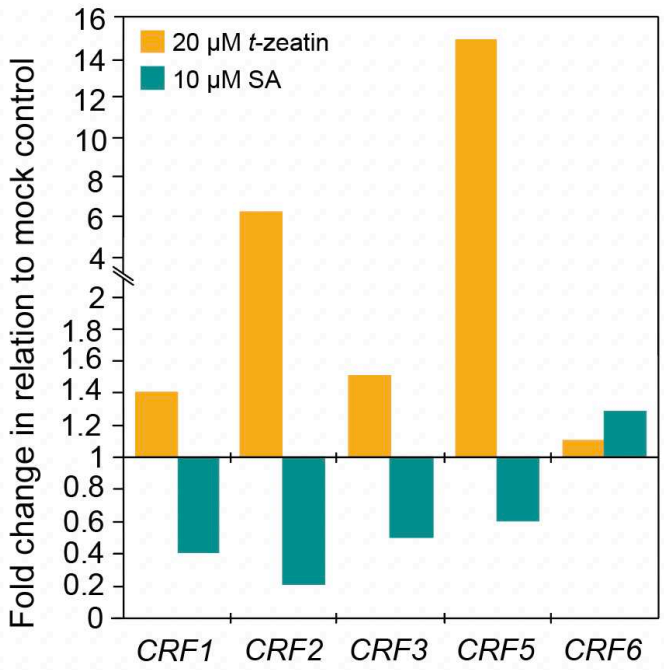

Figure 2.5: *CRF* gene expression is differentially regulated by *t*-zeatin and SA. *CRF* gene expression data from The Bio-Analytic Resource for Plant Biology (BAR, http://bar.utoronto.ca/) (Toufighi et al. 2005) of Arabidopsis seedlings treated with 20 µM *t*-zeatin (yellow) or 10 µM SA (teal), 3 hours post treatment. Expression data is relative to the mock control. No data is available for *CRF4*.

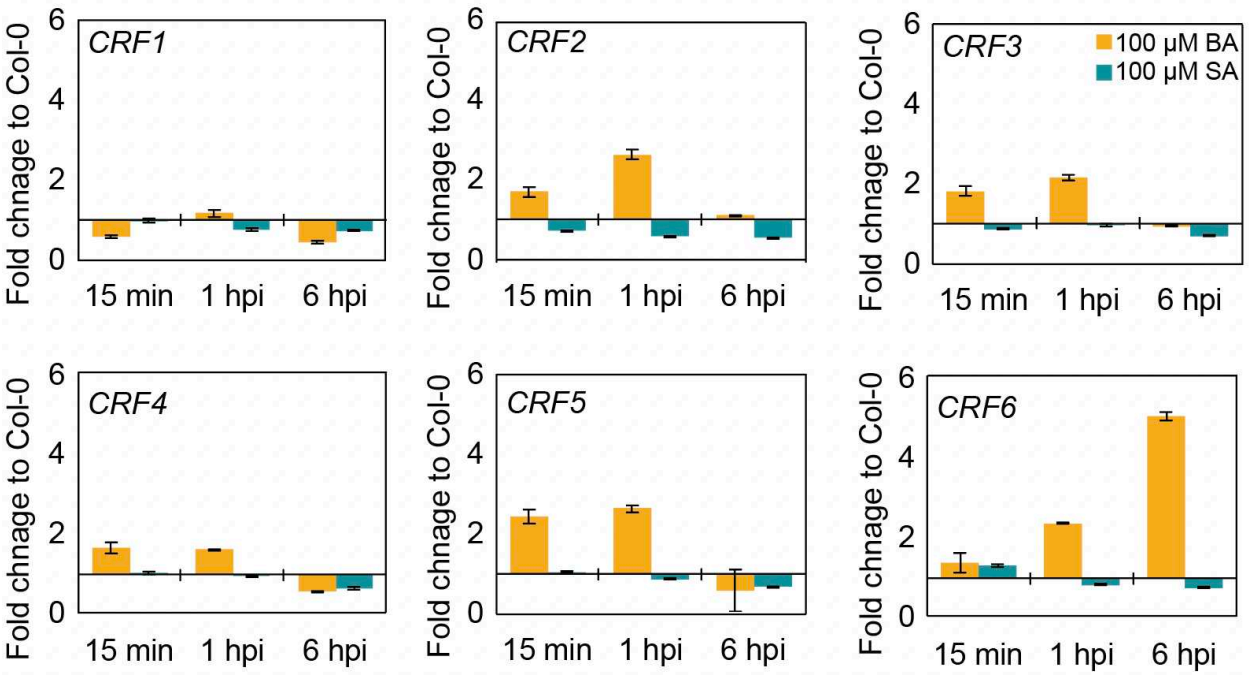

Figure 2.6: *CRF* gene expression is differentially regulated by BA and SA. *CRF* gene expression 15 minutes (min) post induction, 1 hour post induction (hpi), and 6 hpi with 100 µM BA (yellow) or 100 µM SA (teal) of a single experiment. All gene expression was graphed relative to the 0.1% DMSO control at each timepoint.

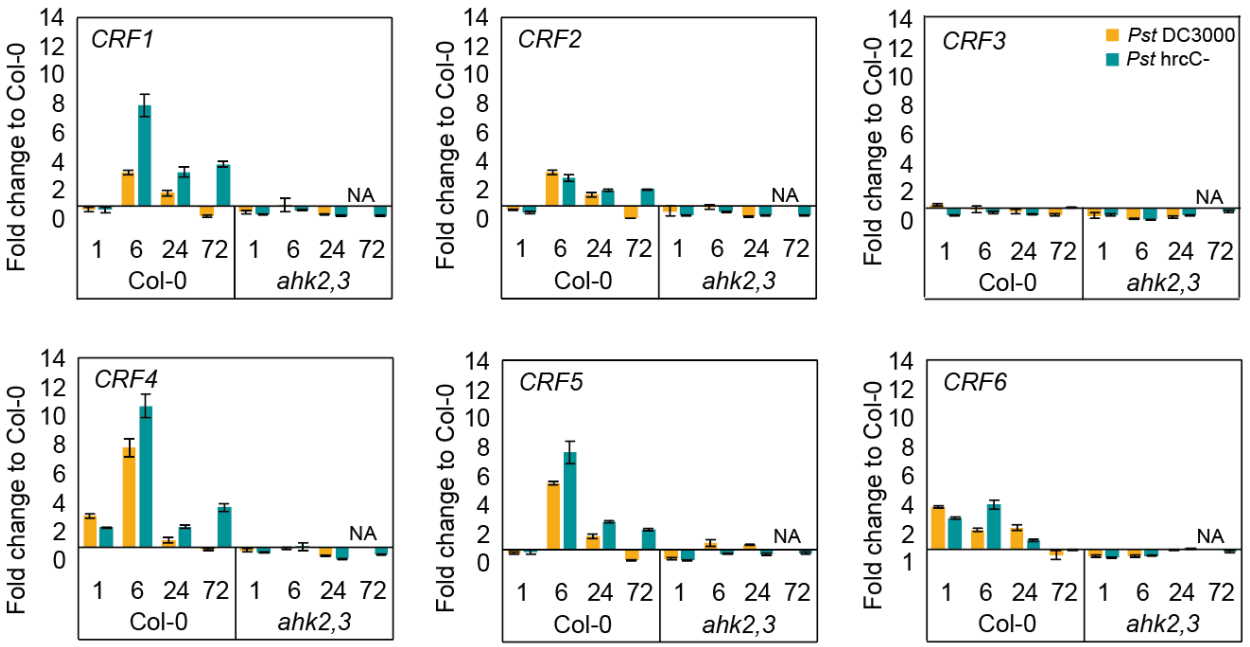

Figure 2.7: *CRF* gene expression is induced by *Pst* DC3000 and *Pst* hrcC⁻. *CRF* gene expression at 1, 6, 24, and 72 hours post inoculation (hpi) with *Pst* DC3000 (yellow) or *Pst* hrcC- (teal) in Col-0 and *ahk2,3* genotypes. Each genotype was graphed in relation to the corresponding uninoculated control. Similar trends were seen in three biological replicates per treatment. No data is available (NA) for *ahk2,3 Pst* DC3000 72 hpi due to increased plant susceptibility and resulting poor RNA quality.

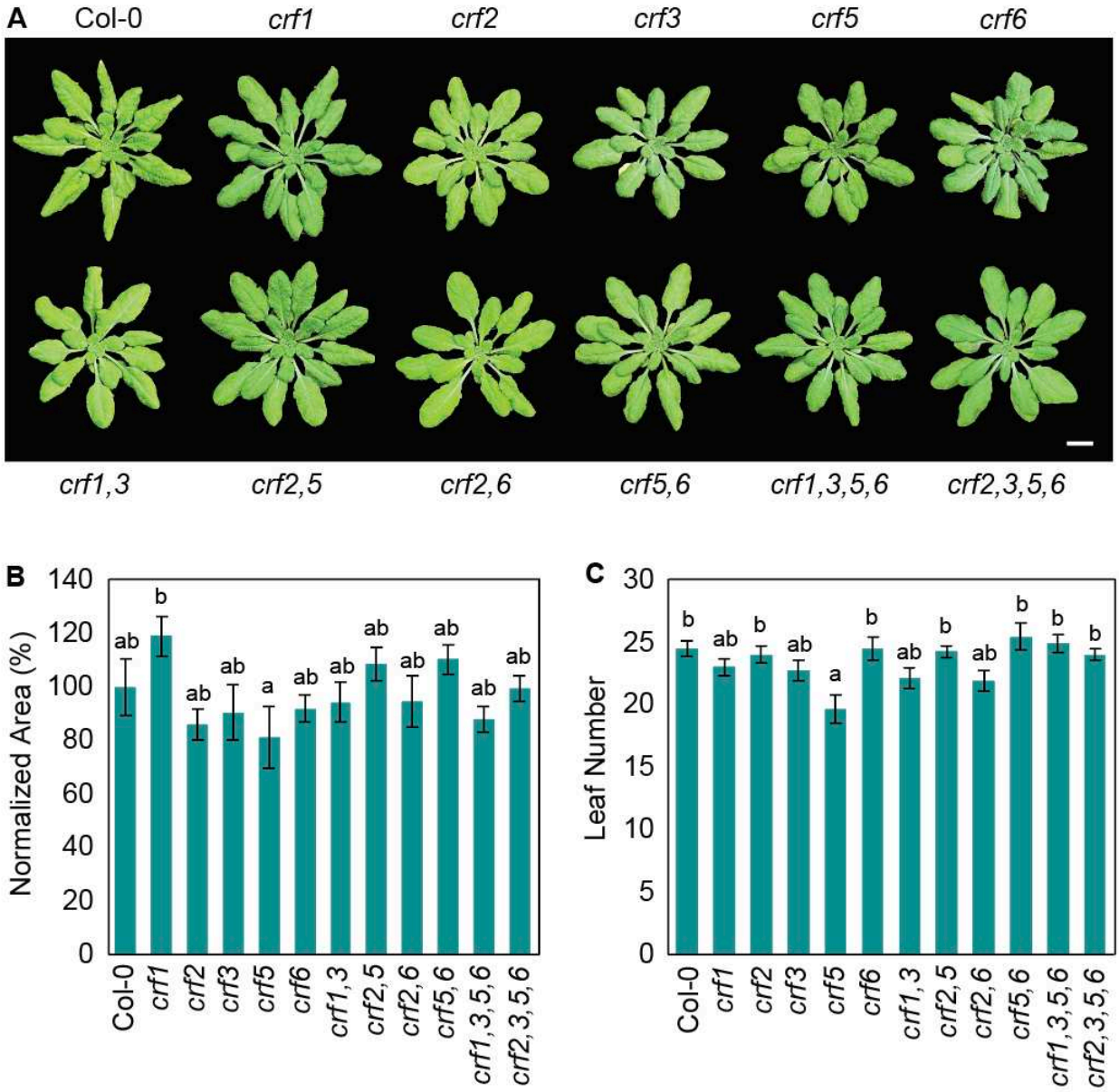

Figure 2.8: CRFs act redundantly and *crf* mutants show few growth phenotypes. A. Representative rosettes of single, double, and quadrupole *crf* mutant lines, at 7 weeks after germination of a single biological replicate. Scale bar represents 1 cm. **B.** Normalized rosette area to Col-0 control of *crf* mutant lines. n = 9 per genotype. Percent change in growth compared to Col-0, + indicates increased normalized area, - indicates decreased normalized area: *crf1* +18.79%; *crf2* -14.13%; *crf3* -9.61%; *crf5* -18.73%; *crf6* -8.12%; *crf1,3* -5.80%; *crf2,5* +8.68%; *crf2,6* -5.46%; *crf5,6* +10.30%; *crf1,3,5,6* -12.16%; and *crf2,3,5,6* -0.64%. **C.** Average number of leaves per rosette at the time of rosette area measurements. Error bars represent standard error of the mean. Significance determined using one-way ANOVA with p-value ≤ 0.05.

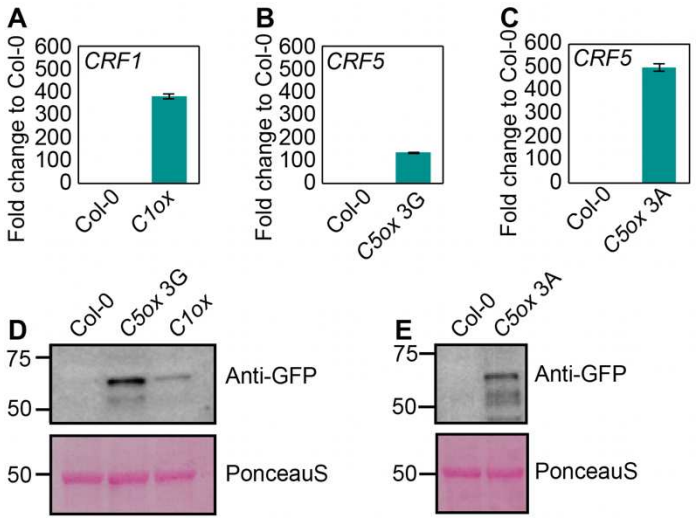

Figure 2.9: Characterizing *CRF1ox* and *CRF5ox* lines. A. *CRF1* gene expression in *CRF1ox* (*C1ox*) compared to Col-0. **B.** *CRF5* gene expression in *CRF5ox* line 3G (*C5ox* 3G) compared to Col-0. **C.** *CRF5* gene expression in *CRF5ox* line 3A (*C5ox* 3A) compared to Col-0. Gene expression was quantified using qRT-PCR. Error bars represent standard error of the mean. **D.** Protein blot of Col-0, *C5ox* 3G, and *C1ox* detected with α-GFP antibodies. Expected band size of CRF5-GFP: 60.16 kDa and CRF1-GFP: 58.55 kDa. **E.** Protein blot of Col-0 and *C5ox* 3A detected with α-GFP antibodies. Expected band size of CRF5-GFP: 60.16 kDa.

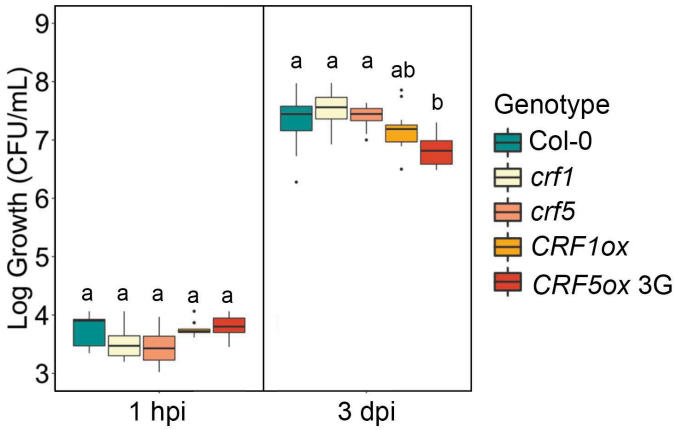

Figure 2.10: *CRFs* are positive regulators of plant defense responses to *Pst* DC3000 infection. Three pooled experiments of *Pst* DC3000 log growth (CFU/mL) at 1 hour post inoculation (hpi) and 3 days post inoculation (dpi) in Col-0, *crf1*, *crf5*, *CRF1ox*, and *CRF5ox* 3G genotypes. n=4 for each biological replicate per timepoint. Error bars represent standard error of the mean. Significance between genotypes at T3 was determined by one-way ANOVA with p-value ≤ 0.05.

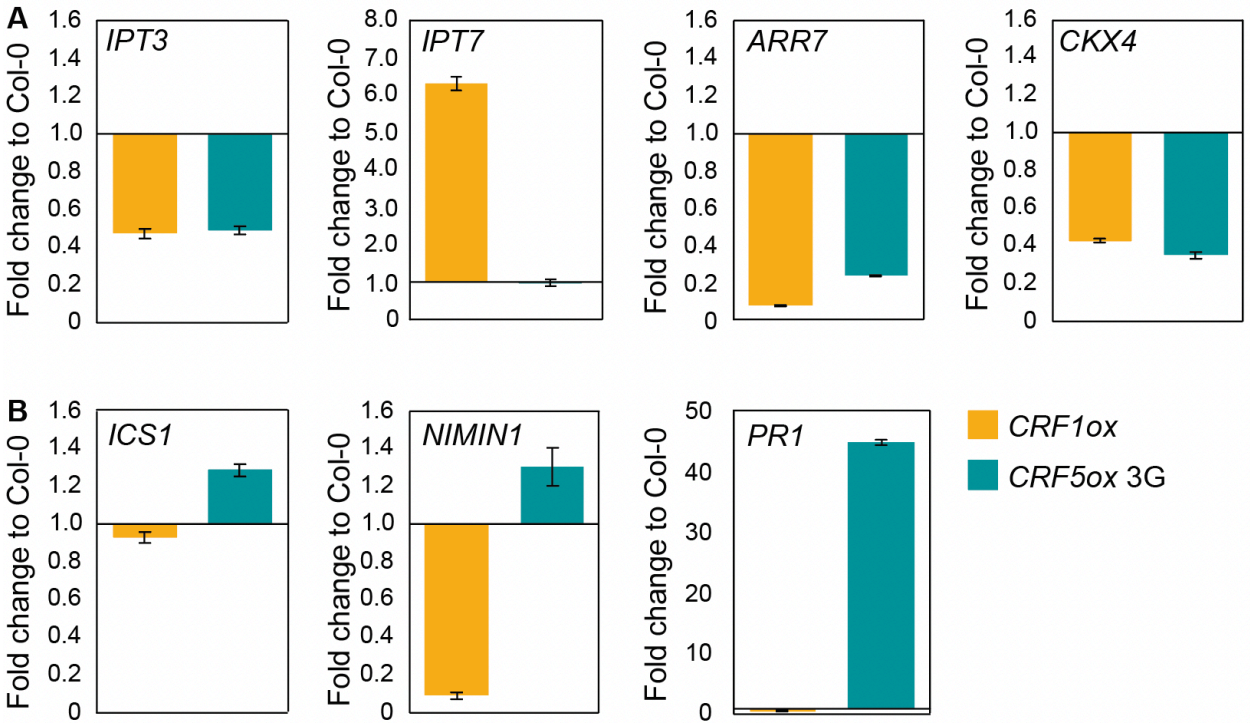

Figure 2.11: CK and SA biosynthesis and signaling genes are differentially regulated in *CRF1ox* and *CRF5ox* lines. A. CK biosynthesis (*IPT3, IPT7*), signaling (*ARR7*), and catabolism (*CKX4*) expression in *CRF1ox* (yellow) and *CRF5ox* 3G (teal). **B.** SA biosynthesis (*ICS1*), and SA-signaling markers (*NIMIN1* and *PR1*) expression in *CRF1ox* and *CRF5ox* lines. All genes are graphed relative to expression in Col-0. Error bars represent standard error of the mean.

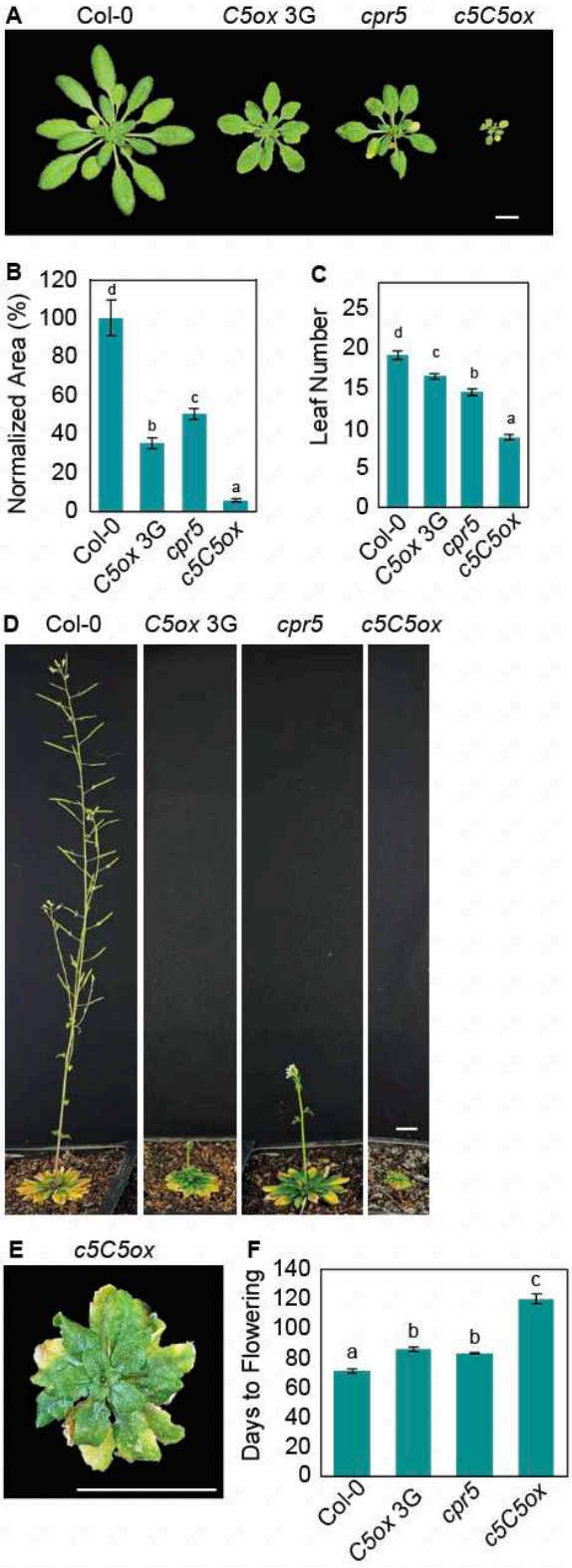

Figure 2.12: The *cpr5, CRF5ox* combinatorial line has a significant reduction in growth and delayed transition to flowering compared to parental lines. A. Representative rosettes

of each genotype from two experiments: Col-0, *CRF5ox* 3G (*C5ox* 3G), *cpr5*, and *cpr5, CRF5ox* (*c5C5ox*), at 7 weeks after germination in short-day conditions. Scale bar represents 1 cm. **B.** Average rosette area normalized to Col-0 of data pooled from two experiments. *C5ox* 3G: 64.64% rosette growth reduction; *cpr5*: 49.45%; *c5C5ox*: 94.31%. Percent growth reduction was determined by finding the difference between normalized average rosettes of each genotype compared to Col-0; $n \geq 5$ for each genotype. **C.** Average number of rosette leaves at the time of rosette measurements. **D.** Representative photos of flowering lines, approximately 16 weeks after germination. Scale bar represents 1 cm. **E.** The *c5C5ox* individual plant at 16 weeks after germination, at the time all other plants had transitioned to flowering. Scale bar represents 1 cm. **F.** Average number of days to flowering after germination. Error bars represent standard error of the mean. Significance determined by one-way ANOVA, p-value ≤ 0.05.

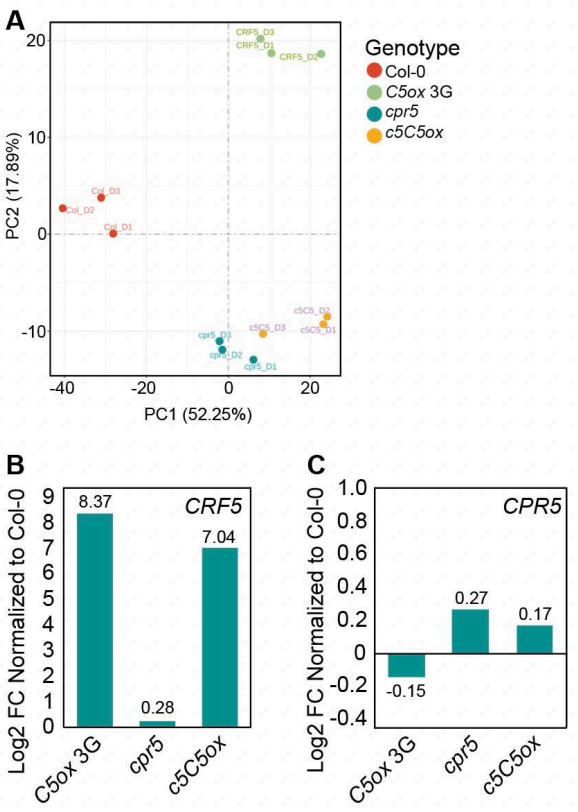

Figure 2.13: Confirming RNA-seq data quality. A. The PCA plot of three biological replicates for each genotype: Col-0 (pink), *CRF5ox* 3G (green), *cpr5* (blue), and *cpr5, CRF5ox* (*c5C5ox*) (purple). **B.** Average *CRF5* gene expression based on mapped reads for each genotype. **C.** *CPR5* gene expression in *CRF5ox* 3G. Differential expression was based on log fold change (±1.5 threshold) and adjusted p-value ≤ 0.05 of three biological replicates per genotype.

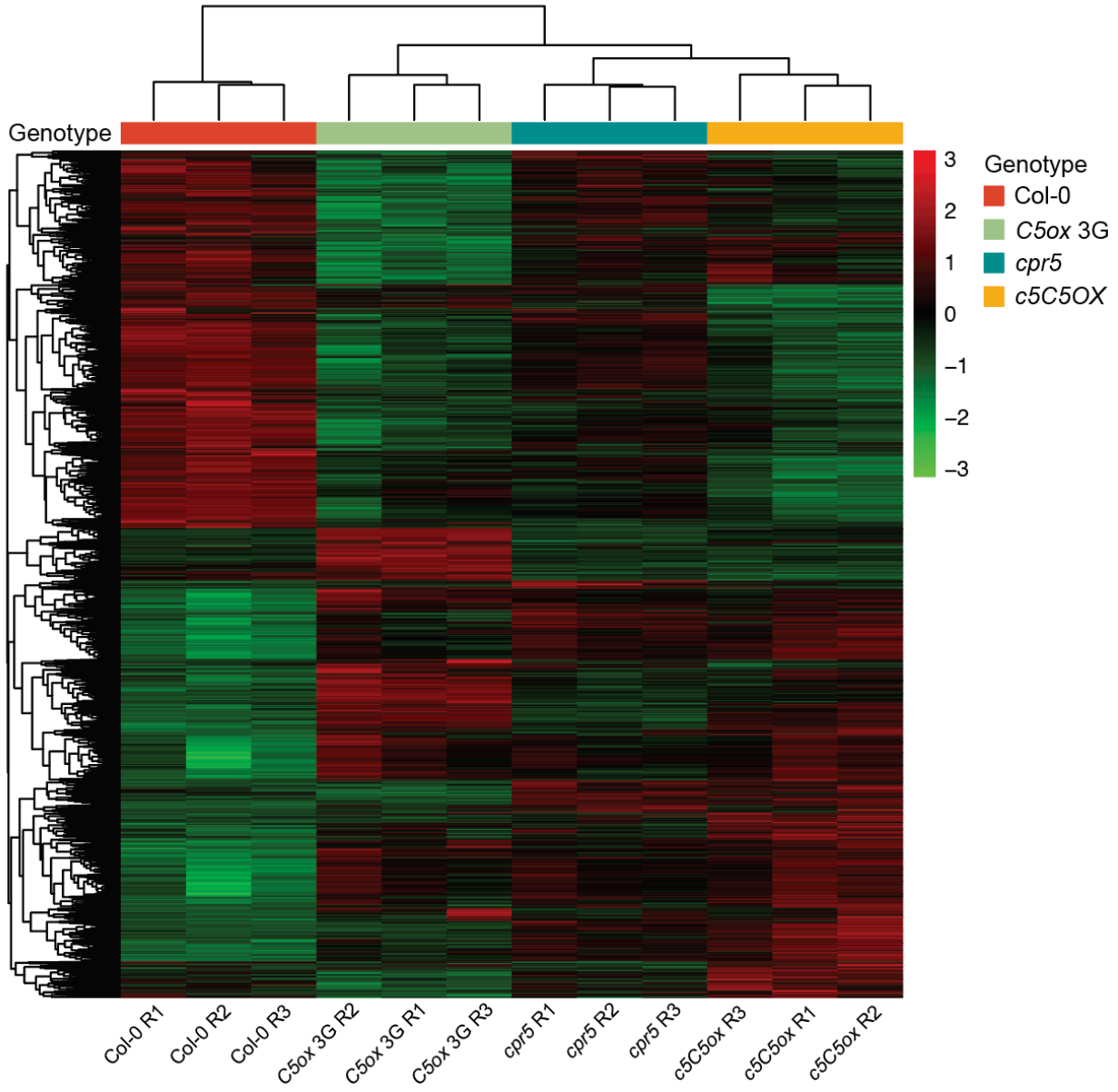

Figure 2.14: Hierarchical clustering of DEGs in Col-0, *CRF5ox* 3G, *cpr5*, and *cpr5, CRF5ox* (*c5C5ox*) genotypes. A heat map was constructed based on Log2 FC values relative to Col-0. Up-regulated genes are represented in red, down-regulated genes are represented in green.

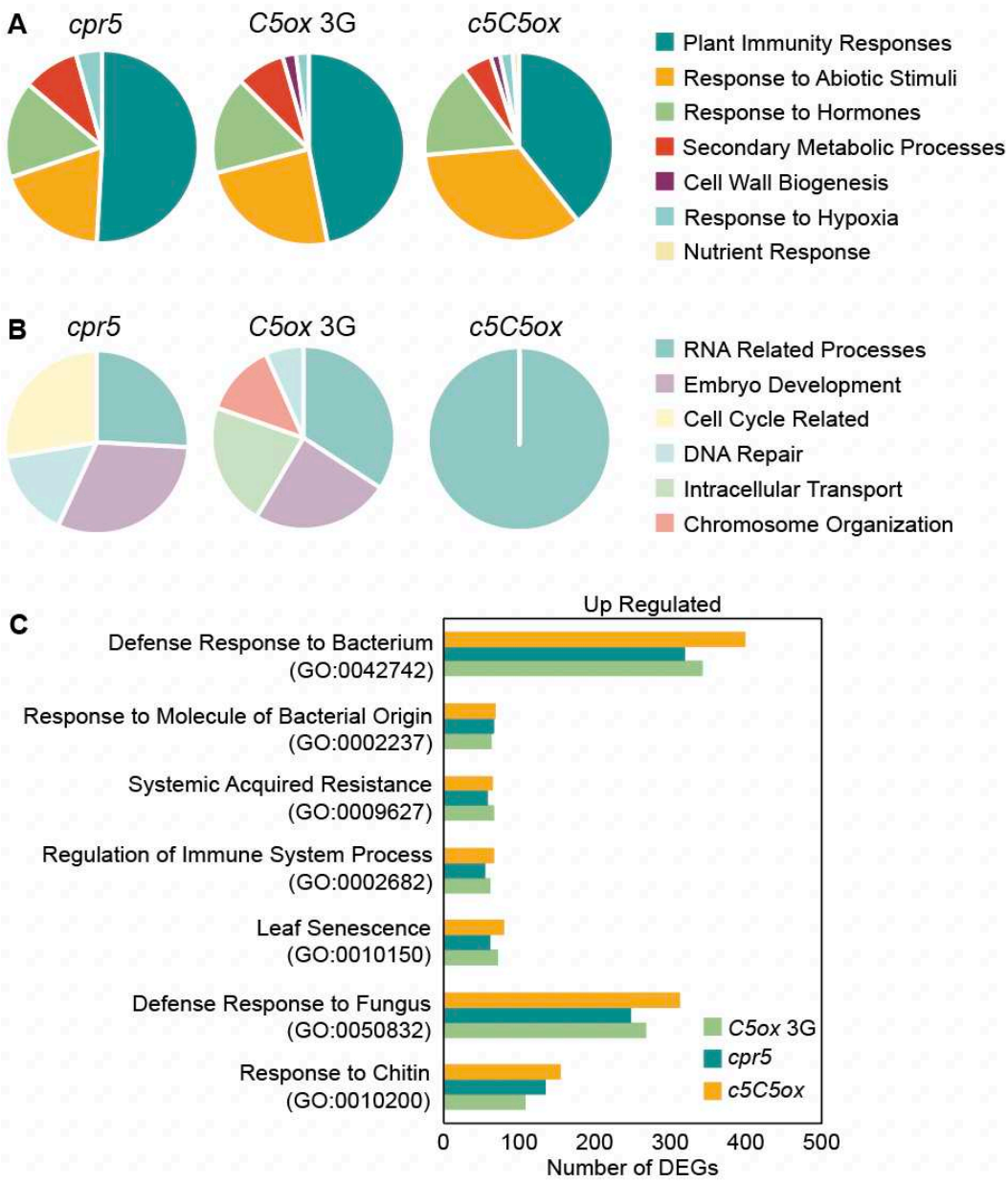

Figure 2.15: *CRF5ox* 3G, *cpr5*, and *cpr5, CRF5ox* (*c5C5ox*) have an increase in defense related genes compared to Col-0. A. Gene ontology (GO) analysis of biological processes differentially expressed genes (DEGs) shows an increase in genes associated with plant immune responses, responses to abiotic stimuli, and response to plant hormones. **B.** GO: Biological Processes analysis of DEGs shows decreased expression of genes related to RNA related processes, embryo development, cell cycle, and DNA repair. **C.** GO: Biological Processes terms found in all three genotypes shows increased expression of genes associated with responses to bacterial and fungal pathogens. The GO: Biological Processes genes were identified with differential expression of log fold change (±1.5 threshold) and adjusted p-value ≤ 0.05 of three biological replicates per genotype.

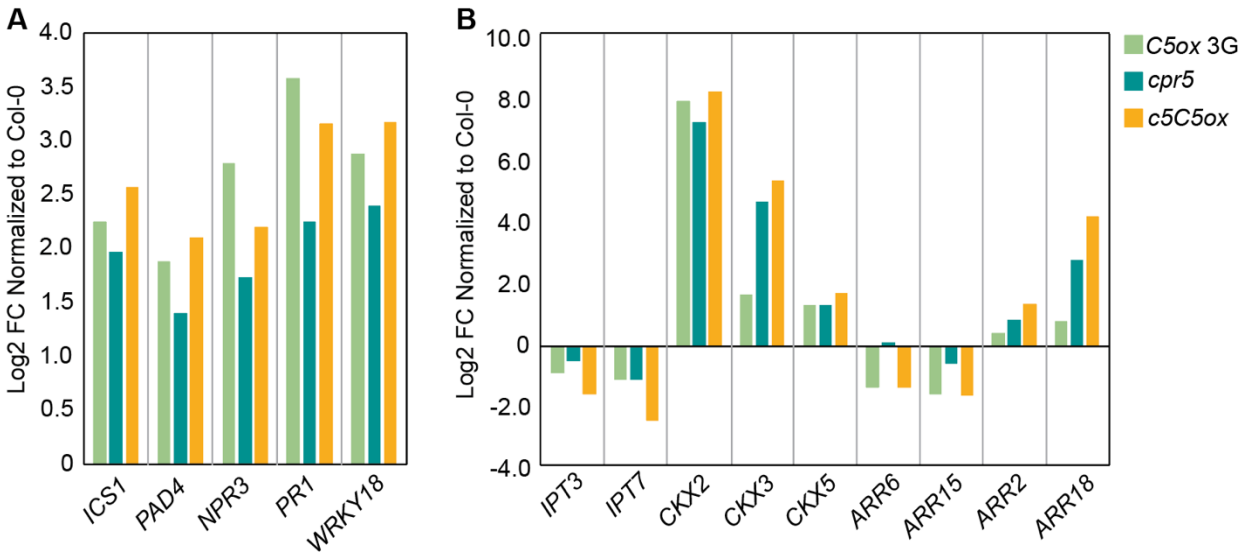

Figure 2.16: Characterizing differential gene expression in *cpr5, CRF5ox* of SA and CK biosynthesis and signaling genes. A. Log2 fold change (FC) normalized to Col-0 in *CRF5ox* 3G, *cpr5*, and *cpr5, CRF5ox* (*c5C5ox*) of SA biosynthesis and signaling genes. **B.** Log2 FC normalized to Col-0 in *CRF5ox* 3G, *cpr5*, and *c5C5ox* of CK biosynthesis, signaling, and metabolism genes. Differential expression was based on log fold change (±1.5 threshold) and adjusted p-value ≤ 0.05 of three biological replicates per genotype.

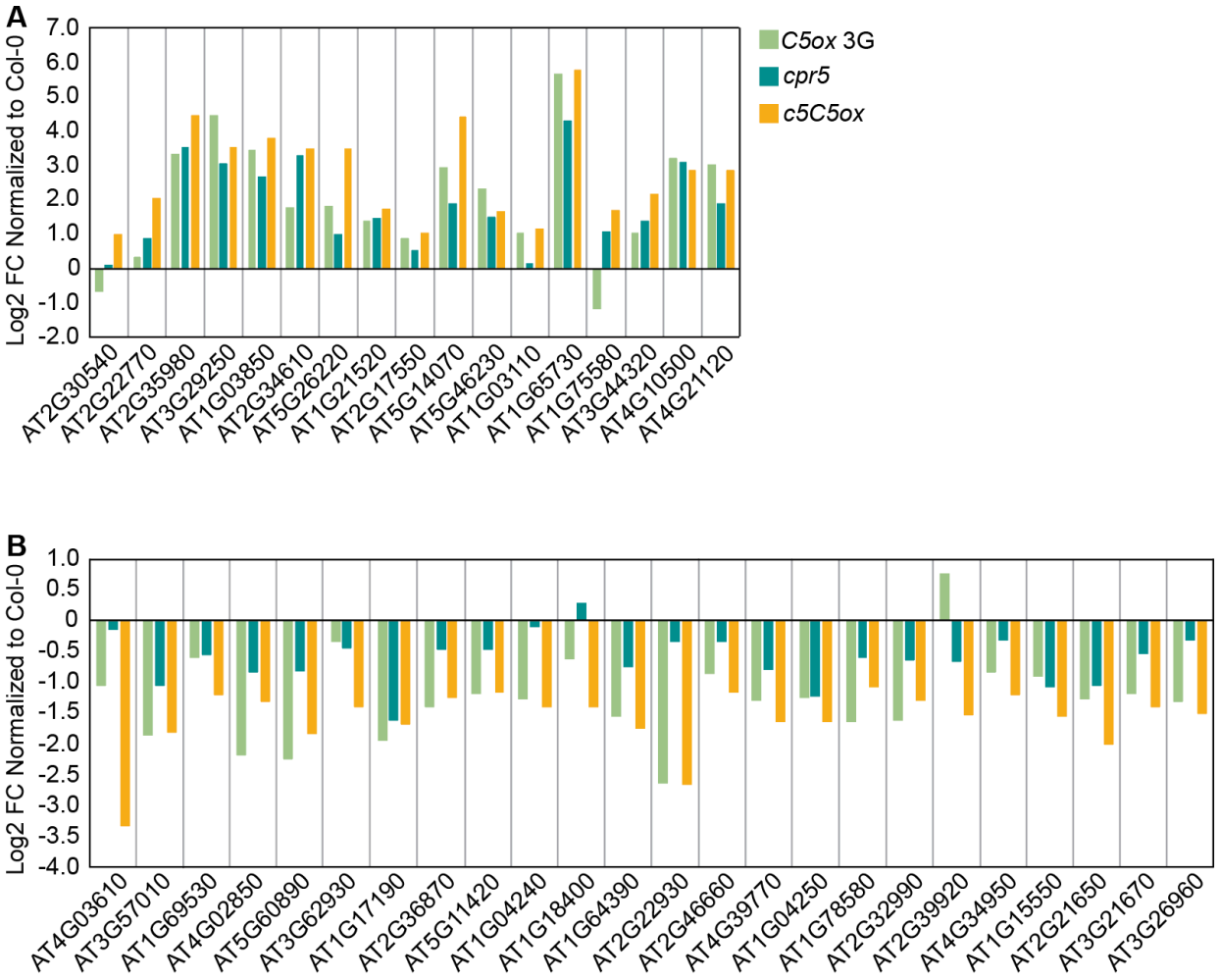

Figure 2.17: Differential gene expression analysis of Golden List up-regulated genes in *cpr5*, *CRF5ox* 3G, and *cpr5, CRF5ox* (*c5C5ox*). A. Log2 FC of genes significantly up-regulated in *c5C5ox* from the up-regulated Golden List relative to Col-0. **B.** Log2 FC of up-regulated genes from the Golden List that are significantly down-regulated in *c5C5ox* compared to Col-0. Differential expression was based on log fold change (±1.5 threshold) and adjusted p-value ≤ 0.05 of three biological replicates per genotype.

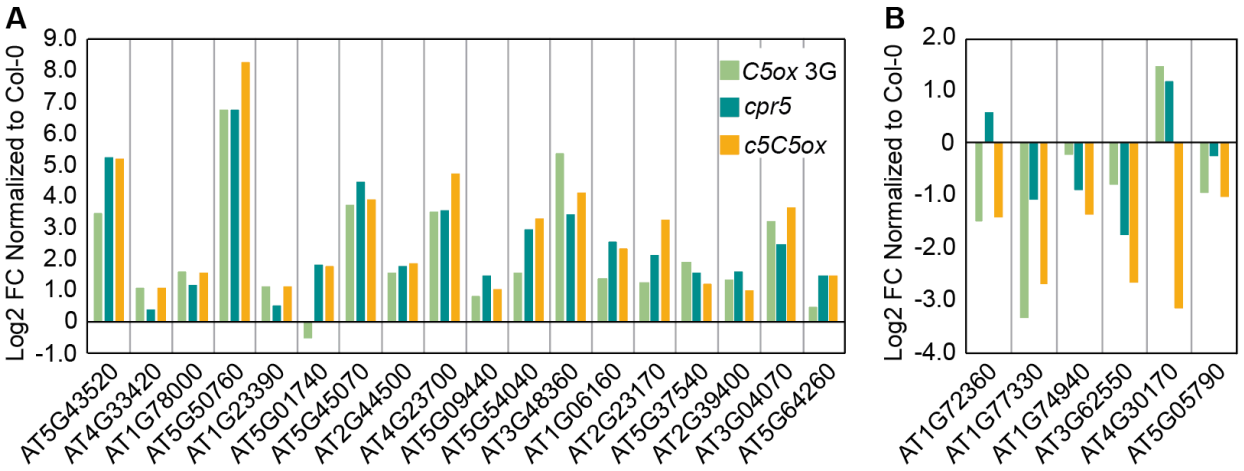

Figure 2.18: Differential gene expression analysis of Golden List down-regulated genes in *cpr5*, *CRF5ox* 3G, and *cpr5, CRF5ox* (*c5C5ox*). A. Log2 FC of genes significantly up-regulated in *c5C5ox* from the down-regulated Golden List relative to Col-0. **B.** Log2 FC of down-regulated genes from the Golden List that are significantly down-regulated in *c5C5ox* compared to Col-0. Differential expression was based on log fold change (±1.5 threshold) and adjusted p-value ≤ 0.05 of three biological replicates per genotype.

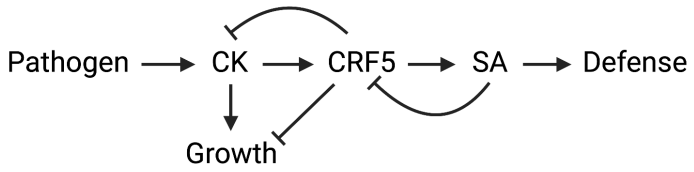

Figure 2.19: A proposed mechanism of CRF5 regulation of CK and SA to mediate plant growth and defense responses. CK promotes plant growth. Upon pathogen perception, *CRF5* expression is induced via CK signaling. In turn, CRF5 acts as an inhibitor of plant growth and CK biosynthesis and signaling. Further, CRF5 promotes biosynthesis of SA and expression of SA-responsive genes to promote SA-associated plant defense responses and SA reduces *CRF5* expression. This figure was created using BioRender.com.

2.7 TABLES

Table 2.1: *CRF* genotyping primers for T-DNA insertion and wild-type fragments.

Gene ID	Gene Name	Fragment	Forward (5' → 3')	Reverse (5' → 3')	PCR product (bp)
AT4G11140	*CRF1*	*CRF1* WT	TCCTTACGCAAC AGATTCGTC	CGTGAGACAACA CGTGATACG	1113 bp
		crf1-2 T-DNA*	TCCTTACGCAAC AGATTCGTC	*ATATTGACCATC ATACTCATTGC	602-909 bp
		crf1-2 T-DNA*	*ATATTGACCATC ATACTCATTGC	CGTGAGACAACA CGTGATACG	
AT4G23750	*CRF2*	*CRF2* WT	ATCACACGTGCC TCTACCAAC	ATGTGTGGTCAA ATGGAGTCG	1131 bp
		crf2-3 T-DNA+	ATCACACGTGCC TCTACCAAC	+GCCTTTTCAGAA ATGGATAAATA	587-887 bp
		crf2-3 T-DNA+	+GCCTTTTCAGAA ATGGATAAATA	ATGTGTGGTCAA ATGGAGTCG	
AT5G53290	*CRF3*	*CRF3* WT	TTCTGACCGGTG ATTGAGAAC	TACCCGAAACTA CCCTTGGAG	1193 bp
		crf3-2 T-DNA+	TTCTGACCGGTG ATTGAGAAC	+GCCTTTTCAGAA ATGGATAAATA	582-882 bp
		crf3-2 T-DNA+	+GCCTTTTCAGAA ATGGATAAATA	TACCCGAAACTA CCCTTGGAG	
AT2G46310	*CRF5*	*CRF5* WT	CCAGTCTCACGT GAGAGAAGG	GTGAGAAAATTC GTCTGAGCG	1015 bp
		crf5-5 T-DNA-	CCAGTCTCACGT GAGAGAAGG	-ATTTTGCCGATT TCGGAAC	478-778 bp
		crf5-5 T-DNA-	-ATTTTGCCGATT TCGGAAC	GTGAGAAAATTC GTCTGAGCG	
AT3G61630	*CRF6*	*CRF6* WT	AAACAACGAAAG GTCCAAACC	CGAACGAGACGA GTGAAGTTC	1164 bp
		crf-36 T-DNA*	AAACAACGAAAG GTCCAAACC	*ATATTGACCATC ATACTCATTGC	537-837 bp
		crf6-3 T-DNA*	*ATATTGACCATC ATACTCATTGC	CGAACGAGACGA GTGAAGTTC	

ID: Identification Number; *CRF*: *CYTOKININ RESPONSE FACTOR*; WT: wild-type; bp: base pairs. *GABI T-DNA primer; +SAIL T-DNA primer; -SAIL T-DNA primer. T-DNA insertion primers can be used in combination with either forward or reverse primers for detection of the T-DNA fragment.

Table 2.2: Gene specific primers and restriction enzymes for SA immunity mutant genotyping.

Gene ID	Gene Name	Forward (5' → 3')	Reverse (5' → 3')	RE	Digestion Products (bp)
AT5G64930	*constitutive expresser of PR genes 5, cpr5-1*	CGAGTTTGGGTG CAGATATTTTTGG	GGAAACATACTG TTACAACGGTTCG	FokI	320 bp (WT); 283 bp (*cpr5*)

ID: Identification Number; RE: Restriction Enzyme; bp: base pairs.

Table 2.3: qRT-PCR gene specific primers for gene expression analysis.

Gene ID	Gene Name	Forward (5' → 3')	Reverse (5' → 3')
AT4G11140	*CYTOKININ RESPONSE FACTOR 1, CRF1*	CGGAGATTAGA GATCCGAGTA	GTTAGGACCACG TAGCTGAATAG
AT4G23750	*CYTOKININ RESPONSE FACTOR 2, CRF2*	CAGTGACGACGA AGAAGAAGA	AGCACCGGAATC GAGATAGAC
AT5G53290	*CYTOKININ RESPONSE FACTOR 3, CRF3*	CGAGTCGTCAAC GTCCTAATAAC	GTTGCTCCGGAT CTCTAATCTC
AT4G27950	*CYTOKININ RESPONSE FACTOR 4, CRF4*	TTGGTTCGGGTC TCAATGAC	GCTCGACTCTGA TCTCGTTAATC
AT2G46310	*CYTOKININ RESPONSE FACTOR 5, CRF5*	CCCATGCGCTAC TGATTCTT	CCGGTTTAGGTT CGTCATCTT
AT3G61630	*CYTOKININ RESPONSE FACTOR 6, CRF6*	TGGTTCAAGAG TGAAACGATAC	CTTTCCTCCTCC TTGTGCTTAC
AT3G63110	*ISOPENTENYLTRANSFERASE 3, IPT3*	CGGTTTCTGCTG GACATTGC	CACTAGACACCG CGACAACT
AT3G23630	*ISOPENTENYLTRANSFERASE 7, IPT7*	TCCGAAGCCGGA AACCTAAC	TCCACCGGCTAC TATGGGAA
AT1G19050	*ARABIDOPSIS RESPONSE REGULATOR 7, ARR7*	ACTGTAGAGAGT GGAACTAGGGCT	AGTCCTGGCATT GAGTAATCCGTC
AT4G29740	*CYTOKININ OXIDASE/ DEHYDROGENASE 4, CKX4*	CACCCACAAGGG TGAAATGGTCTC	TGCGACTCTTGT TTGATCGGAGAG
AT1G74710	*ISOCHORISMATE SYNTHASE 1, ICS1*	TGCATCCAACTC CAGCTGTTTGTG	AGCTGATCTGAT CCCGACTGCAAA
AT2G14610	*PATHOGENESIS-RELATED PROTEIN 1, PR1*	ACAGTGCAATG GAGTTTGTGGTC	TACACCTCACTT TGGCACATCCGA
AT1G02450	*NIM1-INTERACTING 1, NIMIN1*	GCACGGAAACGT AGACGAGAAG	GACCTTTCTCCG CCGTTAGATT

Table 2.4: SA biosynthesis and signaling, and CK degradation genes are up-regulated and CK biosynthesis genes are down-regulated in *cpr5, CRF5ox* (*c5C5ox*). Log2 FC values of each genotype compared to expression in Col-0 calculated from RNA-seq data. These data are associated with Figure 2.19A-B.

Gene ID	Gene Name	Log2 FC Normalized to Col-0		
		***CRF5ox* 3G**	***cpr5***	***c5C5ox***
AT1G74710	*ISOCHORISMATE SYNTHASE 1* (*ICS1*)	2.25	1.97	2.57
AT3G52430	*PHYTOALEXIN DEFICIENT 4* (*PAD4*)	1.88	1.40	2.10
AT5G45110	*NPR1-LIKE PROTEIN 3* (*NPR3*)	2.80	1.73	2.20
AT2G14610	*PATHOGENESIS-RELATED GENE 1* (*PR-1*)	3.58	2.25	3.16
AT4G31800	*WRKY DNA BINDING PROTEIN 18* (*WRKY18*)	2.88	2.40	3.18
AT3G63110	*ISOPENTENYLTRANSFERASE 3* (*IPT3*)	-0.84	-0.44	-1.56
AT3G23630	*ISOPENTENYL TRANSFERASE 7* (*IPT7*)	-1.05	-1.06	-2.42
AT2G19500	*CYTOKININ OXIDASE/DEHYDROGENASE 2* (*CKX2*)	8.02	7.34	8.31
AT5G56970	*CYTOKININ OXIDASE/DEHYDROGENASE 3* (*CKX3*)*	1.72	4.73	5.44
AT1G75450	*CYTOKININ OXIDASE/DEHYDROGENASE 5* (*CKX5*)*	1.36	1.34	1.73
AT5G62920	*ARABIDOPSIS RESPONSE REGLATOR 6* (*ARR6*)*	-1.33	0.15	-1.34
AT1G74890	*ARABIDOPSIS RESPONSE REGLATOR 15* (*ARR15*)*	-1.55	-0.54	-1.57
AT4G16110	*ARABIDOPSIS RESPONSE REGLATOR 2* (*ARR2*)	0.45	0.89	1.39
AT5G58080	*ARABIDOPSIS RESPONSE REGLATOR 18* (*ARR18*)	0.84	2.82	4.26

*These genes are also part of the CK Golden List up-regulated genes but are included here because of their association with CK signaling and metabolism.

Table 2.5: Differential expression patterns of CK Golden List genes in each genotype reveal up-regulation of defense-related genes in *cpr5, CRF5ox* (*c5C5ox*) compared to Col-0. Log2 FC relative to Col-0 calculated from RNA-seq data. These data are associated with Figure 2.20A-B and Figure 2.21A-B.

	CK Golden List Up-Regulated Genes				
	Gene ID	Gene Name	Log2 FC Normalized to Col-0		
			CRF5ox 3G	*cpr5*	*c5C5ox*
Up-regulated in *c5C5ox* relative to Col-0	AT2G30540	*ROXY7*	-0.65	0.12	1.01
	AT2G22770	*NAI1*	0.32	0.89	2.04
	AT2G35980	*YELLOW-LEAF-SPECIFIC GENE 9* (*YSL9*)	3.35	3.53	4.47
	AT3G29250	*SHORT-CHAIN DEHYDROGENASE REDUCTASE 4* (*SDR4*)	4.47	3.05	3.55
	AT1G03850	*GLUTAREDOXIN 13* (*GRXS13*); *ROXY18*	3.46	2.69	3.82
	AT2G34610	unknown	1.77	3.31	3.47
	AT5G26220	*GAMMA-GLUTAMYL CYCLOTRANSFERASE 2;1* (*GGCT2;1*)	1.81	0.98	3.49
	AT1G21520	unknown	1.38	1.47	1.72
	AT2G17500	*PIN-LIKES 5* (*PILS5*)	0.89	0.54	1.03
	AT5G14070	*ROXY2*	2.93	1.91	4.44
	AT5G46230	*SVB3*	2.34	1.49	1.67
	AT1G03110	*TRNA MODIFICATION 82* (*TRM82*)	1.05	0.14	1.17
	AT1G65730	*YELLOW STRIPE LIKE 7* (*YSL7*)	5.65	4.31	5.78
	AT1G75580	*SMALL AUXIN UPREGULATED RNA 51* (*SAUR51*)	-1.19	1.06	1.72
	AT3G44320	*NITRILASE 3* (*NIT3*)	1.04	1.40	2.16
	AT4G10500	*DMR6-LIKE OXYGENASE 1* (*DOL1*)	3.22	3.09	2.86
	AT4G21120	*CATIONIC AMINO ACID TRANSPORTER 1* (*CAT1*)	3.02	1.90	2.87
Down-Regulated in *c5C5ox* relative to Col-0	AT4G03610	unknown	-1.06	-0.15	-3.32
	AT3G57010	unknown	-1.87	-1.07	-1.81
	AT1G69530	*EXPANSIN 1* (*EXP1*)	-0.61	-0.57	-1.20
	AT4G02850	*D-AMINO ACID RACEMASE 1* (*DAAR1*)	-2.19	-0.84	-1.33
	AT5G60890	*MYB DOMAIN PROTEIN 34* (*MYB34*)	-2.26	-0.83	-1.84
	AT3G62930	*GLUTAREDOXIN 6* (*GRXS6*); *ROXY17*	-0.35	-0.45	-1.40
	AT1G17190	*GLUTATHIONE S-TRANSFERASE TAU 26* (*GSTU26*)	-1.96	-1.62	-1.69
	AT2G36870	*XYLOGLUCAN ENDOTRANSGLUCOSYLASE/ HYDROLASE 32* (*XTH32*)	-1.40	-0.47	-1.25
	AT5G11420	unknown	-1.20	-0.48	-1.17
	AT1G04240	*SHORT HYPOCOTYL 2* (*SHY2*); *INDOLE-3-ACETIC ACID INDUCIBLE 3* (*IAA3*)	-1.28	-0.11	-1.42
	AT1G18400	*BR-ENHANCED EXPRESSION 1* (*BEE1*)	-0.62	0.29	-1.40
	AT1G64390	*GLYCOSYL HYRDOLASE 9C2* (*GH9C2*)	-1.56	-0.75	-1.76
	AT2G22930	unknown	-2.65	-0.35	-2.65
	AT2G46660	*CYTOCHROME P450, FAMILY 78, SUBFAMILY A, POLYPEPTIDE 6* (*CYP78A6*)	-0.88	-0.35	-1.17
	AT4G39770	*TREHALOSE-6-PHOSPHATE PHOSPHATASE H* (*TPPH*)	-1.30	-0.80	-1.65
	AT1G04250	*AUXIN RESISTANT 3* (*AXR3*); *INDOLE-3-ACETIC ACID INDUCIBLE 17* (*IAA17*)	-1.25	-1.22	-1.65
	AT1G78580	*TREHALOSE-6-PHOSPHATE SYNTHASE 1* (*TSP1*)	-1.64	-0.62	-1.09
	AT2G32990	*GLYCOSYL HYDROLASE 9B8* (*GH9B8*)	-1.62	-0.66	-1.30
	AT2G39920	unknown	0.76	-0.66	-1.53
	AT4G34950	*MAJOR FACILITATOR SUPERFAMILY 1* (*MFS1*)	-0.84	-0.34	-1.20
	AT1G15550	*GIBBERELLIN 3-OXIDASE 1* (*GA3OX1*); *GA REQUIRING 4* (*GA4*)	-0.91	-1.08	-1.57
	AT2G21650	*MATERNAL EFFECT EMBRYO ARREST 3* (*MEE3*)	-1.29	-1.06	-2.01
	AT3G21670	*NRT1/PTR FAMILY 6.4* (*NPF6.4*)	-1.18	-0.55	-1.40
	AT3G26960	unknown	-1.33	-0.32	-1.52

Table 2.4 continued from above.

	CK Golden List Down-Regulated Genes				
	Gene ID	Gene Name	Log2 FC Normalized to Col-0		
			***CRF5ox* 3G**	***cpr5***	***c5C5ox***
Up-Regulated in *c5C5ox* relative to Col-0	AT5G43520	unknown	3.47	5.24	5.19
	AT4G33420	*PEROXIDASE 47* (*PRX47*)	1.11	0.42	1.10
	AT1G78000	*SULFATE TRANSPORTER 1;2* (*SULTR1;2*)	1.60	1.19	1.58
	AT5G50760	*SMALL AUXIN UPREGULATED RNA 55* (*SAUR55*)	6.76	6.75	8.29
	AT1G23390	*KELCH DOMAIN-CONTAINING F-BOX PROTEIN* (*KFB*)	1.12	0.52	1.12
	AT5G01740	unknown	-0.49	1.81	1.80
	AT5G45070	*PHLOEM PROTEIN 2-A8* (*PP2-A8*)	3.76	4.47	3.92
	AT2G44500	unknown	1.58	1.79	1.86
	AT4G23700	*CATION/H+ EXCHANGER 17* (*CHX17*)	3.52	3.54	4.73
	AT5G09440	*EXPRDIUM LIKE 4* (*EXL4*)	0.86	1.46	1.07
	AT5G54040	unknown	1.56	2.94	3.31
	AT3G48360	*BTB AND TAZ DOMAIN PROTEIN 2* (*BT2*)	5.39	3.43	4.13
	AT1G06160	*ETHYLENE RESPONSIVE FACTOR 59* (*ERF59*)	1.42	2.58	2.34
	AT2G23170	*GH3.3*	1.25	2.15	3.28
	AT5G37540	unknown	1.91	1.57	1.21
	AT2G39400	unknown	1.36	1.62	1.01
	AT3G04070	*NAC DOMAIN CONTAINING PROTEIN 47* (*NAC047*)	3.22	2.50	3.34
	AT5G64260	*EXPRDIUM LIKE 2* (*EXL2*)	0.47	1.48	1.48
Down-Regulated in *c5C5ox* relative to Col-0	AT1G72360	*ETHYLENE RESPONSE FACTOR 73* (*ERF73*)	-1.50	0.57	-1.41
	AT1G77330	*ACC OXIDASE 5* (*ACO5*)	-3.34	-1.08	-2.69
	AT1G74940	unknown	-0.21	-0.90	-1.37
	AT3G62550	unknown	-0.79	-1.77	-2.67
	AT4G30170	unknown	1.47	1.19	-3.16
	AT5G05790	unknown	-0.95	-0.24	-1.02

ID: Identification Number.

REFERENCES

Argueso, C. T., F. J. Ferreira, P. Epple, J. P. C. To, C. E. Hutchison, G. E. Schaller, J. L. Dangl, and J. J. Kieber. 2012. 'Two-Component Elements Mediate Interactions between Cytokinin and Salicylic Acid in Plant Immunity', *Plos Genetics*, 8.

Argueso, C. T., F. J. Ferreira, and J. J. Kieber. 2009. 'Environmental perception avenues: the interaction of cytokinin and environmental response pathways', *Plant Cell and Environment*, 32: 1147-60.

Bhargava, Apurva, Ivory Clabaugh, Jenn P To, Bridey B Maxwell, Yi-Hsuan Chiang, G Eric Schaller, Ann Loraine, and Joseph J Kieber. 2013. 'Identification of cytokinin-responsive genes using microarray meta-analysis and RNA-Seq in Arabidopsis', *Plant Physiology*, 162: 272-94.

Bowling, S. A., J. D. Clarke, Y. D. Liu, D. F. Klessig, and X. N. Dong. 1997. 'The *cpr5* mutant of Arabidopsis expresses both NPR1-dependent and NPR1-independent resistance', *Plant Cell*, 9: 1573-84.

Brininstool, G., R. Kasili, L. A. Simmons, V. Kirik, M. Hulskamp, and J. C. Larkin. 2008. '*Constitutive Expressor of Pathogenesis-Related Genes 5* affects cell wall biogenesis and trichome development', *Bmc Plant Biology*, 8.

Choi, J., S. U. Huh, M. Kojima, H. Sakakibara, K. H. Paek, and I. Hwang. 2010. 'The Cytokinin-Activated Transcription Factor ARR2 Promotes Plant Immunity via TGA3/NPR1-Dependent Salicylic Acid Signaling in Arabidopsis', *Developmental Cell*, 19: 284-95.

Cucinotta, M., S. Manrique, A. Guazzotti, N. E. Quadrelli, M. A. Mendes, E. Benkova, and L. Colombo. 2016. 'Cytokinin response factors integrate auxin and cytokinin pathways for female reproductive organ development', *Development*, 143: 4419-24.

Cutcliffe, J. W., E. Hellmann, A. Heyl, and A. M. Rashotte. 2011. 'CRFs form protein-protein interactions with each other and with members of the cytokinin signalling pathway in Arabidopsis via the CRF domain', *Journal of Experimental Botany*, 62: 4995-5002.

Deng, W. L., G. Preston, A. Collmer, C. J. Chang, and H. C. Huang. 1998. 'Characterization of the hrpC and hrpRS operons of Pseudomonas syringae pathovars syringae, tomato, and glycinea and analysis of the ability of hrpF, hrpG, hrcC, hrpT, and hrpV mutants to elicit the hypersensitive response and disease in plants', *Journal of Bacteriology*, 180: 4523-31.

Ding, Y. L., T. J. Sun, K. Ao, Y. J. Peng, Y. X. Zhang, X. Li, and Y. L. Zhang. 2018. 'Opposite Roles of Salicylic Acid Receptors NPR1 and NPR3/NPR4 in Transcriptional Regulation of Plant Immunity', *Cell*, 173: 1454-+.

Fan, W. H., and X. N. Dong. 2002. 'In vivo interaction between NPR1 and transcription factor TGA2 leads to salicylic acid-mediated gene activation in Arabidopsis', *Plant Cell*, 14: 1377-89.

Gupta, S., and A. M. Rashotte. 2014. 'Expression patterns and regulation of SICRF3 and SICRF5 in response to cytokinin and abiotic stresses in tomato (Solanum lycopersicum)', *Journal of Plant Physiology*, 171: 349-58.

Hallmark, H. T., and A. M. Rashotte. 2019. 'Review - Cytokinin Response Factors: Responding to more than cytokinin', *Plant Science*, 289.

Hughes, A. M., H. T. Hallmark, L. Plackova, O. Novak, and A. M. Rashotte. 2021. 'Clade III cytokinin response factors share common roles in response to oxidative stress responses linked to cytokinin synthesis', *Journal of Experimental Botany*, 72: 3294-306.

Hughes, A. M., P. J. Zwack, P. A. Cobine, and A. M. Rashotte. 2020. 'Cytokinin-regulated targets of Cytokinin Response Factor 6 are involved in potassium transport', *Plant Direct*, 4.

Hwang, I., J. Sheen, and B. Muller. 2012. 'Cytokinin signaling networks.' in S. S. Merchant (ed.), *Annual Review of Plant Biology, Vol 63*.

Kieber, J. J., and G. E. Schaller. 2018. 'Cytokinin signaling in plant development', *Development*, 145.

Kwon, T. 2016. 'Cytokinin Response Factor 2 positively regulates salicylic acid-mediated plant immunity in Arabidopsis thaliana', *Plant Biotechnology*, 33: 207-+.

Liang, Y. S., N. Ermawati, J. Y. Cha, M. H. Jung, M. Su'udi, M. G. Kim, S. H. Ha, C. G. Park, and D. Son. 2010. 'Overexpression of an AP2/ERF-type Transcription Factor CRF5 Confers Pathogen Resistance to Arabidopsis Plants', *Journal of the Korean Society for Applied Biological Chemistry*, 53: 142-48.

Liu, Z. N., L. J. Kong, M. Zhang, Y. X. Lv, Y. P. Liu, M. H. Zou, G. Lu, J. S. Cao, and X. L. Yu. 2013. 'Genome-Wide Identification, Phylogeny, Evolution and Expression Patterns of AP2/ERF Genes and Cytokinin Response Factors in Brassica rapa ssp pekinensis', *Plos One*, 8.

Melton, A. E., P. J. Zwack, A. M. Rashotte, and L. R. Goertzen. 2019. 'Identification and functional characterization of the Marshallia (Asteraceae) Clade III Cytokinin Response Factor (CRF)', *Plant Signaling & Behavior*, 14.

Mi, H., A. Muruganujan, and P. D. Thomas. 2013. 'PANTHER in 2013: modeling the evolution of gene function, and other gene attributes, in the context of phylogenetic trees', *Nucleic Acids Res*, 41: D377-86.

Mok, D. W. S., and M. C. Mok. 2001. 'Cytokinin metabolism and action', *Annual Review of Plant Physiology and Plant Molecular Biology*, 52: 89-118.

Murashige, Toshio, and Folke Skoog. 1962. 'A revised medium for rapid growth and bio assays with tobacco tissue cultures', *Physiologia Plantarum*, 15: 473-97.

Naseem, M., N. Philippi, A. Hussain, G. Wangorsch, N. Ahmed, and T. Dandekar. 2012. 'Integrated Systems View on Networking by Hormones in Arabidopsis Immunity Reveals Multiple Crosstalk for Cytokinin', *Plant Cell*, 24: 1793-814.

Peng, Shun, Dongbei Guo, Yuan Guo, Heyu Zhao, Jun Mei, Yakun Han, Rui Guan, Tianhua Wang, Teng Song, and Keke Sun. 2022. 'CONSTITUTIVE EXPRESSER OF PATHOGENESIS-RELATED GENES 5 is an RNA-binding protein controlling plant immunity via an RNA processing complex', *The Plant Cell*, 34: 1724-44.

Pertea, Mihaela, Geo M Pertea, Corina M Antonescu, Tsung-Cheng Chang, Joshua T Mendell, and Steven L Salzberg. 2015. 'StringTie enables improved reconstruction of a transcriptome from RNA-seq reads', *Nature Biotechnology*, 33: 290-95.

Raines, T., C. Shanks, C. Y. Cheng, D. McPherson, C. T. Argueso, H. J. Kim, J. M. Franco-Zorrilla, I. Lopez-Vidriero, R. Solano, R. Vankova, G. E. Schaller, and J. J. Kieber. 2016. 'The cytokinin response factors modulate root and shoot growth and promote leaf senescence in Arabidopsis', *Plant Journal*, 85: 134-47.

Rashotte, A. M., S. D. B. Carson, J. P. C. To, and J. J. Kieber. 2003. 'Expression profiling of cytokinin action in Arabidopsis', *Plant Physiology*, 132: 1998-2011.

Rashotte, A. M., and L. R. Goertzen. 2010. 'The CRF domain defines Cytokinin Response Factor proteins in plants', *Bmc Plant Biology*, 10.

Rashotte, A. M., M. G. Mason, C. E. Hutchison, F. J. Ferreira, G. E. Schaller, and J. J. Kieber. 2006. 'A subset of Arabidopsis AP2 transcription factors mediates cytokinin responses in concert with a two-component pathway', *PNAS*, 103: 11081-85.

Rochon, A., P. Boyle, T. Wignes, P. R. Fobert, and C. Despres. 2006. 'The coactivator function of Arabidopsis NPR1 requires the core of its BTB/POZ domain and the oxidation of C-terminal cysteines', *Plant Cell*, 18: 3670-85.

Schindelin, Johannes, Ignacio Arganda-Carreras, Erwin Frise, Verena Kaynig, Mark Longair, Tobias Pietzsch, Stephan Preibisch, Curtis Rueden, Stephan Saalfeld, Benjamin Schmid, Jean-Yves Tinevez, Daniel James White, Volker Hartenstein, Kevin Eliceiri, Pavel Tomancak, and Albert Cardona. 2012. 'Fiji: an open-source platform for biological-image analysis', *Nature Methods*, 9: 676-82.

Shi, X. L., S. Gupta, and A. M. Rashotte. 2012. 'Solanum lycopersicum cytokinin response factor (SlCRF) genes: characterization of CRF domain-containing ERF genes in tomato', *Journal of Experimental Botany*, 63: 973-82.

Shi, X. L., S. Gupta, and A. M. Rashotte. 2014. 'Characterization of two tomato AP2/ERF genes, SlCRF1 and SlCRF2 in hormone and stress responses', *Plant Cell Reports*, 33: 35-45.

Shigenaga, A. M., and C. T. Argueso. 2016. 'No hormone to rule them all: Interactions of plant hormones during the responses of plants to pathogens', *Seminars in Cell & Developmental Biology*, 56: 174-89.

Shigenaga, A. M., M. L. Berens, K. Tsuda, and C. T. Argueso. 2017. 'Towards engineering of hormonal crosstalk in plant immunity', *Current Opinion in Plant Biology*, 38: 164-72.

Thomas, Paul D, Michael J Campbell, Anish Kejariwal, Huaiyu Mi, Brian Karlak, Robin Daverman, Karen Diemer, Anushya Muruganujan, and Apurva Narechania. 2003.

'PANTHER: a library of protein families and subfamilies indexed by function', *Genome research*, 13: 2129-41.

To, J. P. C., J. Deruere, B. B. Maxwell, V. F. Morris, C. E. Hutchison, F. J. Ferreira, G. E. Schaller, and J. J. Kieber. 2007. 'Cytokinin regulates type-A Arabidopsis response regulator activity and protein stability via two-component phosphorelay', *Plant Cell*, 19: 3901-14.

Tornero, P., and J. L. Dangl. 2001. 'A high-throughput method for quantifying growth of phytopathogenic bacteria in *Arabidopsis thaliana*', *Plant Journal*, 28: 475-81.

Toufighi, K., S. M. Brady, R. Austin, E. Ly, and N. J. Provart. 2005. 'The Botany Array Resource: e-Northerns, Expression Angling, and Promoter analyses', *Plant Journal*, 43: 153-63.

Tsuda, K., M. Sato, J. Glazebrook, J. D. Cohen, and F. Katagiri. 2008. 'Interplay between MAMP-triggered and SA-mediated defense responses', *Plant Journal*, 53: 763-75.

van Wersch, R., X. Li, and Y. L. Zhang. 2016. 'Mighty Dwarfs: Arabidopsis Autoimmune Mutants and Their Usages in Genetic Dissection of Plant Immunity', *Frontiers in Plant Science*, 7.

Vicente, M. R. S., and J. Plasencia. 2011. 'Salicylic acid beyond defence: its role in plant growth and development', *Journal of Experimental Botany*, 62: 3321-38.

Vlot, A. C., D. A. Dempsey, and D. F. Klessig. 2009. 'Salicylic Acid, a Multifaceted Hormone to Combat Disease', *Annual Review of Phytopathology*, 47: 177-206.

Wildermuth, M. C., J. Dewdney, G. Wu, and F. M. Ausubel. 2001. 'Isochorismate synthase is required to synthesize salicylic acid for plant defence', *Nature*, 414: 562-65.

Wu, Y., D. Zhang, J. Y. Chu, P. Boyle, Y. Wang, I. D. Brindle, V. De Luca, and C. Despres. 2012. 'The Arabidopsis NPR1 Protein Is a Receptor for the Plant Defense Hormone Salicylic Acid', *Cell Reports*, 1: 639-47.

Wybouw, B., and B. De Rybel. 2019. 'Cytokinin - A Developing Story', *Trends in Plant Science*, 24: 177-85.

Yao, Jian, John Withers, and Sheng Yang He. 2013. '*Pseudomonas syringae* infection assays in Arabidopsis.' in Alain Goossens and Laurens Pauwels (eds.), *Jasmonate Signaling: Methods and Protocols* (Humana Press: Totowa, NJ).

Zwack, P. J., M. A. Compton, C. I. Adams, and A. M. Rashotte. 2016. 'Cytokinin response factor 4 (CRF4) is induced by cold and involved in freezing tolerance', *Plant Cell Reports*, 35: 573-84.

Zwack, P. J., I. De Clercq, T. C. Howton, H. T. Hallmark, A. Hurny, E. A. Keshishian, A. M. Parish, E. Benkova, M. S. Mukhtar, F. Van Breusegem, and A. M. Rashotte. 2016. 'Cytokinin Response Factor 6 Represses Cytokinin-Associated Genes during Oxidative Stress', *Plant Physiology*, 172: 1249-58.

Zwack, P. J., and A. M. Rashotte. 2013. 'Cytokinin inhibition of leaf senescence', *Plant Signaling & Behavior*, 8.

Zwack, P. J., B. R. Robinson, M. G. Risley, and A. M. Rashotte. 2013. 'Cytokinin Response Factor 6 Negatively Regulates Leaf Senescence and is Induced in Response to Cytokinin and Numerous Abiotic Stresses', *Plant and Cell Physiology*, 54: 971-81.

Zwack, P. J., X. L. Shi, B. R. Robinson, S. Gupta, M. A. Compton, D. M. Gerken, L. R. Goertzen, and A. M. Rashotte. 2012. 'Vascular Expression and C-Terminal Sequence Divergence of Cytokinin Response Factors in Flowering Plants', *Plant and Cell Physiology*, 53: 1683-95.

CHAPTER 3

Robust shoot apical meristematic patterning is overcome by constitutive activation of immunity, leading to perturbed phyllotaxis in *Arabidopsis thaliana*[3]

3.1 SUMMARY

Phyllotaxy is the study of the arrangement of plant organs, such as leaves, around an axis in relation to one another. In *Arabidopsis thaliana* (hereafter Arabidopsis), leaf and floral primordia have a predictable spiral phyllotaxis, where each primordium is initiated separated from the next primordium by an angle of 137.5°. Phyllotactic patterns are initiated in the shoot apical meristem (SAM) and are mediated by proper signaling and distribution of the plant hormones cytokinin (CK) and auxin (Aux) within the SAM. Similar to other aspects of plant development, phyllotactic patterns are robust, withstanding environmental perturbations. Here, we have investigated whether activation of plant immunity could impact plant development, focusing on silique phyllotaxis and meristematic patterns as developmental parameters. We used bacterial infection assays, as well as mutations with different levels of content and/or signaling of the defense hormone salicylic acid (SA), to induce altered states of plant immunity, and determine perturbations in phyllotactic patterns and plant growth. We show that constitutively elevated SA content significantly changes plant phyllotactic patterning resulting from reduced meristem size and increased plastochron, but that transient perturbations in immunity or SA content are not enough to change these patterns. Additionally, plant susceptibility to a bacterial pathogen reduces growth and changes phyllotactic patterning from post-meristematic development processes that are likely independent of SA. These data

[3] Data from this chapter will be used for a future publication with the following authors: Hannah M. Berry and Cristiana T. Argueso.

suggest that in addition to CK and Aux, SA also plays a role in phyllotactic patterning and meristematic regulation.

3.2 INTRODUCTION

The establishment of plant form requires precise developmental programs, determined by conserved genetic networks. Maintenance of plant form requires these developmental programs to be robust and to withstand environmental perturbations. Plant hormones are essential regulators of plant development and response to biotic and abiotic stressors. In plants, longitudinal growth originates from apical meristems, which are tightly regulated by transcriptional feedback loops and hormonal crosstalk, primarily between CK and Aux (Gaillochet and Lohmann 2015; Zhao et al. 2010; Chickarmane et al. 2012; Gordon et al. 2009). The SAM is responsible for above ground plant growth. In the SAM, CK maintains a pluripotent stem cell niche as dividing cells enter an Aux gradient signaling for cell differentiation, thus establishing primordial organ tissues (Gaillochet and Lohmann 2015; Zhao et al. 2010; Chickarmane et al. 2012; Gordon et al. 2009). The regular patterning of organ primordia around the SAM establishes the phyllotactic pattern that is maintained throughout plant development. Arabidopsis has a spiral phyllotaxis where each organ primordia is initiated approximately 137.5° from the previous one (Adler, Barabe, and Jean 1997; Kuhlemeier 2017). In Arabidopsis, mutations that lead to phyllotaxis deviating from the spiral pattern, or divergence angles, have been associated with disrupted CK and Aux crosstalk in the SAM, mis-regulation of SAM stem cell populations, and post-meristematic development (Gallois et al. 2002; Byrne et al. 2003; Peaucelle et al. 2007; Goldshmidt et al. 2008; Szczesny, Routier-Kierzkowska, and Kwiatkowska 2009; Landrein et al. 2013; Besnard, Rozier, and Vernoux 2014; Mandel et al. 2014; Burian et al. 2015; Landrein et al. 2015; Yang et al. 2015).

Plants must balance responses to abiotic and biotic stressors in their environment with plant growth and development. Phytohormones are critical regulators of these responses,

including responses to pathogens (Bernoux, Ellis, and Dodds 2011). It has long been known that plant pathogens can change plant morphology and decrease productivity. These changes in plant growth by plant pathogens are achieved through the use of effectors, which are molecules of pathogen origin that change plant physiology to promote infection (Jiang et al. 2017). For example, phytoplasmas are bacterial plant pathogens that can alter plant architecture, including increased shoot branching, and abnormal inflorescence development (MacLean et al. 2014; Pecher et al. 2019). These shoot growth phenotypes result from manipulation of plant host machinery by pathogen effectors, such as degradation of MADS-box proteins associated with floral development, and destabilization of transcription factors associated with shoot branching (MacLean et al. 2014; Pecher et al. 2019). In Arabidopsis, susceptibility to the oomycete *Hyaloperonospora arabidopsidis* Noco2 or the bacterial pathogen *Xanthomonas campestris* results in altered shoot branching and reduced time to flowering (Korves and Bergelson 2003). Furthermore, infection with high inoculums of the bacterial pathogen *Pseudomonas syringae* pv. *tomato* DC3000 (hereafter *Pst* DC3000) also positively correlates with a reduction in time to flowering, and negatively correlates with the number of stem branches (Korves and Bergelson 2003).

In addition to changes in plant growth and development during disease, mutations resulting in constitutive activation of immunity can show developmental abnormalities, including loss of apical dominance and ectopic meristem development (Bowling et al. 1997; Clarke et al. 1998; Li et al. 2001; Igari et al. 2008). Such changes are most often due to increased accumulation or signaling of defense-related plant hormones such as SA. However, immunity activation is a complex process (Figure 3.1A-C). Pathogen recognition by plant cells starts with the perception of pathogen-associated molecular patterns (PAMPs) by cell surface plant transmembrane pattern recognition receptors, initiating a low level of defense response associated with a moderate increase in SA called pattern triggered immunity (PTI) (Figure 3.1A) (Jones and Dangl 2006). To evade plant immune responses, pathogens can introduce effector

proteins into the plant cell to dampen plant defenses, including PTI and SA accumulation, and alter plant metabolism to better suit the growth of the pathogen, termed effector triggered susceptibility (ETS) (Figure 3.1B). The second branch of plant immunity is through recognition of pathogen effectors by plant cells via intracellular nucleotide binding-leucine rich repeat (NB-LRR) proteins, leading to a more robust defense response, called effector triggered immunity (ETI), which is associated with strong increase in SA accumulation and signaling (Figure 3.1C). How changes in these different layers of immunity could affect plant development is still unknown.

Here, we address whether activation of plant immunity by pathogen infection, or by mutations that lead to constitutive activation of plant immunity, change Arabidopsis developmental patterns, focusing on patterns of phyllotaxy, and probe the role of the plant hormones CK and SA in this process. We show that phyllotaxy patterns are robust, but that this phyllotactic robustness can be overcome by constitutive activation of immunity over the lifetime of the plant, leading to changes in silique phyllotaxis that originate in the SAM.

3.3 METHODS

Plant materials and growth conditions

Arabidopsis thaliana accession Columbia (Col-0) was used as wild-type. The following mutants in SA signaling and biosynthesis in the Col-0 background, *ENHANCED DISEASE SUSCEPTIBILITY 16* (*eds16*) (Dewdney et al. 2000), *NONEXPRESSER OF PR GENES 1* (*npr1-1*) (Cao et al. 1994), *CONSTITUTIVE EXPRESSION OF PR GENES 5* (*cpr5-1*) (Bowling et al. 1997), and *SUPPRESSOR OF NPR1-1, CONSTITUTIVE 1* (*snc1-1*) (Li et al. 2001), were obtained from the Arabidopsis Biological Resource Center (ABRC). Mutants were genotyped to confirm homozygosity by Cleaved Amplified Polymorphic Sequence (CAPS) assays (Table 3.1). For plant growth, seeds were stratified for 2-4 days at 4°C before germination on Pro-Mix HP+, Mycorrhizae and Biofungicide soilless media. For most assays, plants were grown in long-day

conditions, in a controlled environment plant growth room with a photoperiod of 16:8 hour day:night at 160 ± 20 µmol $m^{-2}s^{-1}$, 22°C and 55%:65% relative humidity. Plants grown in short-day conditions were grown in a controlled environment plant growth chamber (Conviron, ATC-60) with a photoperiod of 10:14 hour day:night at 160 ± 20 µmol $m^{-2}s^{-1}$, 22°C and 66%:75% relative humidity. Light intensity was set at 150µE for both photoperiods.

Rosette area quantification

Rosettes were photographed just before bolting in all cases, around 4 weeks post germination in long-day conditions. Area measurements were done using Fiji imaging software (Schindelin et al. 2012) by drawing the smallest circle encompassing all leaves in a single rosette. Data was normalized for each genotype and control treatment, where indicated. Normalizing was done by averaging area measurements from the control group, followed by dividing each raw data point by the control average and multiplying by 100. Percent growth reduction was calculated from normalized data by taking the difference between control average and the average of other genotypes and treatments.

Silique phyllotaxy measurements

Primary stems of each plant were marked with a piece of tape shortly after bolting, approximately 5 weeks post germination, and kept separate from secondary stems throughout reproductive growth. Silique angles of the primary stem were measured as previously described (Landrein et al. 2013; Peaucelle and Laufs 2007). The device used to measure silique phyllotaxy angles was made based on images from Landrein, 2013 with slight modifications to the center stage opening (Figure 3.2). Primary stem height, internode length, and silique number along the primary stem were measured prior to taking divergence angle measurements.

Tissue dissection and preparation for scanning electron microscopy

Plants for scanning electron microscopy were grown under long-day conditions for 4 to 5 weeks. For SAM imaging, SAMs were dissected shortly after bolting, as previously described (Reddy et al. 2004), with slight modifications: floral buds of developmental stage 6 and older (Smyth, Bowman, and Meyerowitz 1990) were removed to expose meristem tissue. Tissue was fixed in 100% methanol for 10 minutes followed by 100% ethanol for 1 hour as described (Talbot and White 2013). For stem torsion imaging and analysis, internodes 1, 2, 3, 5, and 10 were collected, as previously described (Landrein et al. 2013). Samples were fixed in 100% methanol for 30 minutes followed by 100% ethanol for 1 hour. All samples were critically dried using a SPI-DRY Critical Point Dryer (Structure Probe, Inc) and stored in a desiccator prior to imaging.

Scanning electron microscopy

Prepared samples were coated in 20nm gold using a Denton Vacuum Desk II Gold Sputter Coater (Denton Vacuum, LLC) and imaged on a JEOL JSM-6500 Field Emission Scanning Electron Microscope (JEOL USA, Inc) at Colorado State University. Images were taken with an accelerating voltage of 5.0kV, working distance of 9.4 mm, and magnification of 220X (SAMs) or 150X (stems).

Meristematic and stem torsion measurements

SEM images of the SAM were used to collect meristematic phyllotaxy, area, and plastochron measurements as previously described (Landrein et al. 2015). Stem torsion analysis was performed using SEM stem images as described (Landrein et al. 2013).

SA treatment for phyllotaxy analysis

SA (Sigma-Aldrich; Catalogue Number: S7401) was dissolved into water for a final concentration of 100 μM SA. Plants were grown in long-day conditions, as above. Beginning at 14 days after germination, whole plant rosettes were spray-inoculated with 100 μM SA or water with 0.025% Silwett L-77, until runoff using a Prevall sprayer (Prevall, Inc). Plants were covered with a dome lightly sprayed with water for 24 hours, at which point the dome was removed. Plants were treated with SA or water every other day over 10 days. Approximately 8 weeks after germination, silique phyllotactic measurements were collected, as above.

Bacterial growth assays and plant inoculation

Pseudomonas syringae pv. *tomato* DC3000 (*Pst* DC3000) strains used were as follows: *Pst* DC3000 EV, carrying an empty vector selectable by kanamycin resistance; *Pst* DC3000 AvrRpm1, carrying a vector harboring the *Pst* DC3000 effector AvrRpm1 (Kim et al. 2009) and selectable by kanamycin resistance; or *Pst* DC3000 hrcC$^-$, a nonpathogenic deletion mutant lacking the type III secretion system necessary for delivery of bacterial effectors into the plant cell to cause disease (Deng et al. 1998), selectable by kanamycin resistance (Table 3.2). All strains harbor chromosomal resistance to rifampicin.

For bacterial *in planta* growth assays, bacteria were streaked on King's B (KB) media supplemented with rifampicin (50mg/mL) and kanamycin (50mg/mL) and incubated at 28°C for 48 hours. Colonies were re-streaked for a lawn plate onto new $KB_{Rif/Kan}$ plates, 24 hours before plant inoculation. On the day of inoculation, bacteria were resuspended in 10 mM $MgCl_2$ and adjusted for a concentration of $5x10^7$ colony forming units (CFU)/mL or $5x10^8$ CFU/mL (OD_{600} =0.1 and 1.0, respectively) with 0.025% Silwett L-77. Bacteria were sprayed onto whole rosettes using a Prevall sprayer (Prevall, Inc.). After inoculation, plants were covered with a dome lightly sprayed with water, which was removed 24 hours after inoculation. *In planta* bacterial growth

was quantified 1 hour (day 0) and 3 days (day 3) later by plating serial dilutions onto KB media, followed by colony counting (Yao, Withers, and He 2013). Day 0 dilutions were plated on $KB_{Rif/Kan}$ while day 3 bacterial dilutions were plated on $KB_{Rif/Chx}$ (cycloheximide) plates. Dilution plates were incubated for 24 hours at 28°C before colony counting.

For phyllotaxy experiments, bacterial inoculation of plants began 14 days post germination (dpg), unless otherwise indicated, in long-day conditions. Bacterial suspensions were prepared as above, using the concentrations of 10^7 CFU/mL, 10^8 CFU/mL, or 10^9 CFU/mL (OD_{600} =0.02, 0.2, or 2.0, respectively) with 0.025% Silwett L-77. Whole plant rosettes were spray-inoculated until run-off using a Prevall sprayer (Prevall, Inc.). Plants were covered with a dome lightly sprayed with water for 24 hours, at which point the dome was removed.

RNA extraction and qRT-PCR

Total RNA was extracted from frozen plant tissue using a RNeasy Plant kit (QIAGEN), following manufacturer's protocols. RNA quality was evaluated using A_{260}/A_{280} and A_{260}/A_{230} ratios using a nanodrop. Samples meeting quality ratios were treated with Invitrogen Turbo DNase-Free (Thermo Fisher Scientific) treatment and checked for the absence of genomic DNA by qRT-PCR using Actin (AT5G66770) primers. cDNA was synthesized from DNase-treated RNA using qScript cDNA SuperMix (QuantaBio) and checked for complete cDNA amplification with qRT-PCR using primers for *GLYCERALDEHYDE 3-PHOSPHATE DEHYDROGENASE, GAPDH* (AT1G13320). Ct/Cq differences between each GAPDH primer of less than 1.5 were indicative of complete cDNA synthesis. qRT-PCR reactions were quantified using a Bio-Rad CFX Connect Real-Time System (Bio-Rad) using PerfeCTa SYBR Green SuperMix (QuantaBio). *UBIQUITIN 10, UBQ10* (AT4G05320), primers were used as a housekeeping gene in all reactions. All quality control and gene specific primers used for gene expression analysis are listed in Table 3.3. Three biological replicates, at minimum, were done for each experiment.

Statistical Analysis

Three biological replicates were done for each assay, minimum, for each experiment. Sample sizes for each experiment are noted in figure legends. For each experiment, samples were compared to appropriate genotype or treatment controls and statistical significance was determined using a One-way ANOVA with a p-value ≤ 0.05.

3.4 RESULTS

Constitutive activation of SA-associated plant immunity alters plant growth and phyllotactic patterns

Previous research characterizing growth of Arabidopsis mutants with altered states of immunity has been mostly limited to general aspects of plant growth, including plant biomass, stem height, rosette diameter, and seed yield (Heidel et al. 2004; Bowling et al. 1997; Bowling et al. 1994; Clarke et al. 2000; Clarke et al. 1998; Dietrich et al. 1994; Dietrich et al. 1997; van Wersch, Li, and Zhang 2016; Zhang et al. 2003). The presence of plant growth alterations in mutants expressing constitutive immunity led us to hypothesize that immunity activation could have an effect on developmental patterns in plants. Phyllotactic patterns are developmental patterns that are well established in plants and known for their robustness against environmental perturbation. In Arabidopsis, silique (fruit) phyllotactic patterns along the main infloresence stem are reminiscent of rosette phyllotactic patterns, and thus can be used to determine overall plant phyllotaxis. Furthermore, the number of siliques produced by a single wild-type plant in normal growth conditions is far higher than the number of rosette leaves produced, allowing for good statistical analyses and determination of subtle changes. Thus, mutants with altered levels of immunity, expressing either constitutive or reduced immunity, were used to characterize the effects of altered immunity on SAM development and silique phyllotaxis.

Given the importance of the plant hormone SA on immunity against biotrophic and hemi-biotrophic pathogens, we concentrated on mutants that differed in SA content and/or signaling. The SA biosynthesis mutant *eds16* (*ENHANCED DISEASE SUSCEPTIBILITY 16)* contains a point mutation in the SA biosynthesis gene *ISOCHORISMATE SYNTHASE 1 (ICS1)*, resulting in reduced SA production and increased susceptibility to pathogens (Dewdney et al. 2000). A second mutant with increased disease susceptibility, *npr1*, contains a point mutation resulting in inactivity of the SA signaling protein NPR1 *(NONEXPRESSER OF PR GENES 1)* (Cao et al. 1994). Conversely, a point mutation in the *SUPPRESSOR OF NPR1-1, CONSTITUTIVE 1* (*SNC1*) gene, encoding an NB-LRR resistance protein, causes constitutive immunity activation in *snc1* plants, causing increased disease resistance that is associated with elevated SA content, and constitutive expression of pathogen-related (PR) genes (Li et al. 2001). A point mutation in *CONSTITUTIVE EXPRESSION OF PR GENES 5* (*cpr5-1*) (Bowling et al. 1997) causes loss-of-function of the encoded RNA binding protein, leading to SA accumulation, constitutive expression of *PR* genes, and increased disease resistance (Bowling et al. 1997; Meng et al. 2017). While both *snc1* and *cpr5* have constitutively activated immunity, shoot growth is significantly reduced in both mutants, however, developmental patterns beyond plant size have not been previously characterized for these mutants (Li et al. 2001; Bowling et al. 1997).

To confirm previously published data on overall plant size, we grew all of the mutants described above, plus the wild-type accession Col-0, at the same time under long-day conditions that promote plant flowering. Both *npr1* and *eds16* had increased rosette area compared to Col-0, while *cpr5* and *snc1* rosettes were smaller (Figure 3.3A-B). Even with these changes in rosette growth, the number of leaves between genotypes was the same, except for *cpr5*, which had fewer rosette leaves (Figure 3.3C). The overall height of adult *cpr5* and *snc1* was reduced compared to Col-0, and both had a reduced number of siliques on primary stems (Figure 3.4A, C, and D). Flowering time analysis revealed there was a slight delay in the number

of days to flowering after germination in *npr1* and *cpr5* plants (Figure 3.4B). While the internodes of *snc1* were much shorter than Col-0, the internodes of *cpr5* were longer and thus contributed to the increased height of *cpr5* compared to *snc1* (Figure 3.4E). Taken together, these data show that constitutive activation of SA-dependent immunity (*snc1* and *cpr5*) negatively impacts plant growth, supporting previously published data.

To further evaluate the effects of immunity on plant development, silique phyllotaxis along primary stems of each genotype was quantified 8 weeks post germination. Divergence angle measurements between consecutive siliques along the primary stem were taken using a tool previously described (Landrein et al. 2013) and displayed on histograms to evaluate changes in phyllotactic angle distributions. Representative stem photos of Col-0, *eds16*, *npr1*, *cpr5*, and *snc1* showed typical silique patterns along the primary stem for each genotype (Figure 3.5A). There was a slight visual difference in phyllotaxy in *cpr5* and a more pronounced change in *snc1* compared to Col-0, as indicated by white arrows, while *eds16* and *npr1* were similar to Col-0 (Figure 3.5A). Decreased SA biosynthesis and signaling in the *eds16* and *npr1* mutants, respectively, did not result in a significant change in divergence angle distributions compared to Col-0 (Figure 3.5B-C). On the other hand, both *cpr5* and *snc1* divergence angle distributions were different from Col-0 (Figure 3.5B-C). While the divergence angle distribution and overall average of *cpr5* (137°) was close to the Col-0 average, there were fewer silique angles around the 137° line than in Col-0 (Figure 3.5B). Furthermore, analysis of *cpr5* successive siliques showed the pattern of silique angles was different compared to Col-0 (Figure 3.5A, C), indicating that constitutive immunity in *cpr5* does lead to altered phyllotactic patterning. The divergence angle distribution of *snc1* was significantly different in comparison to Col-0, with an overall angle of 125° (Figure 3.5B). Because *snc1* was so small with an average of eight siliques per primary stem, it was impossible to conclude how the successive silique pattern compares to Col-0 (Figure 3.5C). We therefore plotted the first eight successive siliques

of each genotype (Figure 3.5C inserts) for comparison to *snc1*. The first eight siliques in the Col-0 and *cpr5* graphs showed that the successive silique pattern of *snc1* resembled that of Col-0 but was different from *cpr5* (Figure 3.5C). These data indicate that constitutive activation of defense and elevated SA content in *snc1* and *cpr5* is enough to overcome robust regulation of silique phyllotactic patterning.

Altered phyllotactic patterns due to constitutive activation of SA-associated plant immunity result from reduced SAM size and increased plastochron

Given that organ primordia originate at the SAM, we investigated if the phyllotactic patterns seen in these mutants are a result of changes in meristematic development and/or primordial patterning. Four to five weeks post germination, floral buds stages 6 to 12 were removed from SAMs to expose the inflorescence meristem (Smyth, Bowman, and Meyerowitz 1990) and prepared for SEM imaging (Talbot and White 2013) (Figure 3.6A-B). While the meristem size of both *eds16* and *npr1* were comparable to Col-0, *cpr5* and *snc1* were significantly smaller than Col-0 (Figure 3.7A, C). Furthermore, the divergence angle distributions measured between successive inflorescence primordia showed slight differences in *snc1* and *cpr5* compared to Col-0, however, the average angles were not significantly different (Figure 3.7B). The plastochron is the relative timing between primordia initiation represented as a ratio (R) of distances of two consecutive inflorescence primordia from the center of the SAM (Landrein et al. 2015). Previous studies have linked a larger meristem size to a shorter plastochron, increased organ permutation frequency, and reduced phyllotactic robustness (Landrein et al. 2015). To address if altered plastochron plays a role in silique phyllotactic patterns of *cpr5* and *snc1*, we quantified the plastochron ratio (R) of the SAM (Figure 3.7C-D). These data showed that both *cpr5* and *snc1* had significantly increased plastochron compared to Col-0, ultimately leading to the altered phyllotactic patterning seen in siliques of these mutants along their stem (Figure 3.7C). These data show that constitutive activation of immunity

throughout plant life does change meristematic growth and regulation, leading to perturbed silique patterning.

In some cases, post-meristematic development is responsible for changes in silique phyllotactic patterning (Peaucelle et al. 2007; Guedon et al. 2013; Burian et al. 2015). To confirm the phyllotactic patterning seen in constitutive immunity mutants was due to meristematic changes, we imaged stem segments to evaluate potential stem torsion that could contribute to altered phyllotaxis (Figure 3.8A). Quantification of stem torsion showed no change between any of the tested genotypes, indicating that the phyllotactic pattern changes of *snc1* and *cpr5* were not influenced by post-meristematic development. Critically, these data show that activated SA-dependent immunity in *cpr5* and *snc1* leads to altered silique phyllotactic patterning, reduced SAM size, and increased plastochron. To our knowledge this is the first time that the plant hormone SA has been linked to altered shoot meristem function.

Exogenous application of SA does not change silique phyllotaxis

Because constitutive immunity mutants with elevated endogenous levels of SA had perturbed silique phyllotactic patterns, we next addressed if application of SA could change silique phyllotaxis. Beginning at 14 dpg, Col-0 rosettes were sprayed with 100 μM SA in water or water control until runoff, every other day for 10 days, for a total of five applications. Silique phyllotaxis was quantified revealing there was no change in divergence angle distribution or overall average angle between control and SA treated plants (Figure 3.9A-B). Furthermore, the additional shoot phenotypes of internode length and silique number along the primary stem were unchanged (Figure 3.9D-E). The exogenous SA treatment did reduce the overall stem height, and prior to measuring the stems the plants were visually indistinguishable from the water treated control group. These data suggest that application of exogenous SA, at least at the levels and timing tested here, cannot overcome robust phyllotactic patterning.

ETS caused by a foliar pathogen perturbs silique phyllotactic patterning

The lack of altered phyllotaxis in response to SA led us to hypothesize that pathogen-induced immune responses present in the constitutive immunity mutants, which is more complex than activation of the SA pathway alone, could be responsible for changes in phyllotactic patterning in those backgrounds. Therefore, we decided to use the well-established bacterial pathogen of Arabidopsis, *Pst* DC3000 EV strain (hereafter *Pst* DC3000), to activate plant immunity. *Pst* DC3000 causes disease (ETS) in Col-0 Arabidopsis plants through the delivery of bacterial protein effectors into plant cells, through the use of its type III secretion system (Figure 3.1B). ETS activation leads to a mild increased in SA content and signaling.

Pst DC3000 is a foliar pathogen and thus bacterial growth assays are typically done in short-day conditions, to prolong the vegetative growth stage and increase the plant tissue available for bacterial analysis (Yao, Withers, and He 2013). Given that phyllotaxy experiments are performed in long-day conditions, which favor plant reproductive growth, we first performed *in planta* bacterial growth assays using plants grown in long-day conditions, to address whether bacterial growth proceeded similarly to what is observed in short-day conditions. At 24 dpg, plants grown under long-day conditions were spray-inoculated with 10^7, 10^8, or 10^9 colony forming units (CFU)/mL of *Pst* DC3000 suspended in 10mM $MgCl_2$. Inoculated plants developed disease symptoms (chlorosis and water-soaked lesions) consistent with *Pst* DC3000 infection in short-days (Figure 3.10A). At 3 days post inoculation (dpi), quantification of bacterial colonies showed a 1.6 to 3-fold increase in bacterial growth (Figure 3.10B), comparable to the bacterial growth normally seen in experiments performed in short-day conditions (Choi et al. 2010). In order to check whether molecular defense patterns in long-day grown plants were similar to short-day grown plants, we checked the expression of the immunity marker gene *PATHOGENESIS-RELATED 1* (*PR-1*), a gene known to be up-regulated after pathogen infection in short-day grown plants. *PR-1* expression at 3 dpi increased 19 to 23-fold after *Pst* DC3000 inoculation (Figure 3.10C). These experiments confirmed that plant infection by *Pst*

DC3000 in long-day conditions result in bacterial growth and disease progression that is comparable to plants grown in short-day conditions.

To identify the ideal concentration of *Pst* DC3000 inoculum that could lead to developmental changes, we inoculated plants grown in long-day conditions with three different inoculum concentrations (10^7, 10^8 or 10^9 CFU/mL) or a 10mM $MgCl_2$ mock control and observed the effect of these inoculations on plant growth. We hypothesized that a *Pst* DC3000 inoculation close to the transition of vegetative to reproductive development would result in perturbed phyllotactic patterning, and thus plants were inoculated just before bolting, at 25 dpg (Figure 3.11A). In order to confirm that the bacterial inoculations were having an effect on plants, the rosette area and leaf number of inoculated and mock control plants were quantified at 10 dpi. Rosette growth inhibition and reduced leaf number was observed in the *Pst* DC3000-inoculated plants in comparison to $MgCl_2$ mock control, especially when the two higher inoculum concentrations were used, with the inoculum of 10^9 CFU/mL leading to the highest decrease in rosette leaf number and highest suppression of rosette growth (Figure 3.11B-C). This growth suppression effect is part of the growth-defense tradeoff and is commonly observed in pathogen-treated short-day grown plants (Li et al. 2019). These results confirmed that our bacterial inoculation assays were replicating previously described physiological processes associated with suppression of growth by immunity activation.

Pst DC3000-inoculated and $MgCl_2$ mock controls plants were allowed to continue to grow under long-days and shift to reproductive growth, and then silique phyllotaxis along primary stems was quantified 8 weeks post germination. Phyllotactic patterning of Col-0 $MgCl_2$ control treated plants had a normal distribution of divergence angles with an average of 139° (Figure 3.12A-B). Inoculation with *Pst* DC3000 at 10^7 or 10^8 CFU/mL did not result in a change in divergence angle distribution or a significant change in average angle compared to $MgCl_2$ treated plants (Figure 3.12A-B). Plants inoculated with the highest concentration of *Pst* DC3000 at 10^9 CFU/mL had a shift in divergence angle distribution to the right and an increased overall

average angle of 143° (Figure 3.12A-B). Additional shoot phenotypes after *Pst* DC3000 included decreased stem height and silique number along the primary stem, in all concentrations used (Figure 3.12C, E). Additionally, increasing concentrations of *Pst* DC3000 resulted in increased internode length where plants inoculated with *Pst* DC3000 10^9 CFU/mL had the longest internodes compared to all treatments (Figure 3.12D). Notably, we observed some variation between these dose-dependent experiments, with the highest inoculum not always causing the most effect on phyllotaxis. Because of our interest in inducing developmental changes in response to immunity activation, we continued with treatments using 10^9 CFU/mL *Pst* DC3000 in our subsequent experiments.

Prolonged ETS to Pst DC3000, but not prolonged PTI or ETI, substantially changes silique phyllotaxis

A single inoculation of plants with *Pst* DC3000 at 25 dpg resulting in ETS did result in a change in phyllotactic pattern, however, these changes were subtle (Figure 3.12A-B). Because disease caused by *Pst* DC3000 initiates a low level of immune responses, we hypothesized that increased immune activation could lead to a stronger effect on phyllotaxis. The *Pst* DC3000 hrcC$^-$ strain (hereafter *Pst* hrcC$^-$) lacks the type III secretion system necessary to deliver bacterial effector proteins into the plant cell to suppress immunity, and thus activates PTI and basal SA-dependent defense responses (Deng et al. 1998; Tsuda et al. 2008). The *Pst* DC3000 AvrRpm1 strain (hereafter *Pst* AvrRpm1) contains a vector carrying the AvrRpm1 effector protein that is recognized by a NB-LRR protein in the Col-0 background, thus causing ETI and an even stronger activation of immunity and SA accumulation (Kim et al. 2009). Therefore, we investigated whether activation of higher levels of immunity, by triggering other layers of the plant immune system (PTI and ETI), changed silique phyllotactic patterns. Furthermore, we decided to perform repeated infections during an extended period of the plant's life. While we recognize that repeated inoculations at a very high concentration does not resemble a normal

infection in the natural environment, it allowed us to simulate conditions of constitutive immunity activation.

Arabidopsis Col-0 plants were grown in long-day conditions. Beginning at 14 dpg, Col-0 plants were inoculated every other day for 10 days with 10^9 CFU/mL *Pst* DC3000, *Pst* hrcC$^-$, or *Pst* AvrRpm1 for a total of five inoculations (Figure 3.13A). Two days after the last inoculation, 24 dpg, photos of the plants were taken for rosette area quantification. While rosette area was reduced by 30.2% and 53.5% after multiple inoculations of *Pst* hrcC$^-$ and *Pst* AvrRpm1, respectively, rosette growth was severely reduced after repeated *Pst* DC3000 inoculation, resulting in an 82.7% decrease compared to the control $MgCl_2$ treatment (Figure 3.13B-C). Only plants inoculated with *Pst* DC3000 had fewer leaves per rosette compared to $MgCl_2$ (Figure 3.13B-D), suggesting prolonged ETS dramatically reduces rosette and leaf growth. Repeated *Pst* DC3000 inoculations also led to a significant reduction in stem height, silique number per primary stem, and seed weight (Figure 3.14C, E-F). As seen in previous inoculations, the internode length of plants inoculated with *Pst* DC3000 was significantly longer than any other inoculation group (Figure 3.14D), suggesting plant susceptibility may result in increased cell elongation or cell division leading to longer internodes. Stem phenotypes of *Pst* hrcC$^-$ and *Pst* AvrRpm1 inoculated plants were not as dramatic; *Pst* hrcC$^-$ inoculations resulted in decreased stem height and reduced seed weight while *Pst* AvrRpm1 inoculations were comparable to each other *Pst* inoculation and $MgCl_2$ (Figure 3.14C-F).

Plants were then evaluated for silique phyllotactic patterns 8 weeks post germination, which revealed that repeated inoculations of *Pst* DC3000 causes a noticeable shift in divergence angle distribution and significant increase in overall average angle of 146° compared to the $MgCl_2$ treatment with an average divergence angle of 135° (Figure 3.14A-B). However, *Pst* hrcC$^-$ and *Pst* AvrRpm1 inoculations did not result in a significant change in phyllotactic distribution or average angle (Figure 3.14A-B), revealing that activation high levels of immunity

during PTI or ETI do not alter phyllotaxis. Because of these data, we hypothesized that perhaps the effects of *Pst* inoculations could cause only a transient change in phyllotaxis of siliques that developed closer to the time of inoculation, which could be masked by analysis of all of the siliques along stem. Therefore, we analyzed the divergence angles of the first 10 siliques of each inoculation group. There was no difference in the divergence angle distributions or average angle between any *Pst* inoculation and control (data not shown). This confirms that ETS, but not PTI or ETI, can change silique phyllotaxis. Because pathogen effectors can overcome plant defense responses and SA does not accumulate to high levels during ETS, the phyllotaxis changes observed during repeated *Pst* DC3000 inoculations are likely caused by SA-independent processes.

ETS perturbation of phyllotactic patterning results from post-meristematic stem torsion development

As above-ground plant developmental patterns originate at the SAM, we imaged the SAMs of Col-0 plants that were repeatedly inoculated with *Pst* hrcC$^-$, *Pst* DC3000, *Pst* AvrRpm1, or $MgCl_2$, to determine whether any changes were associated with altered SAM patterning. SAMs were dissected and prepared for imaging with SEM as previously described. Images of SAMs (Figure 3.15A) were used for quantification of inflorescence primordia phyllotaxy, SAM area, and plastochron ratio, following methods described by (Landrein et al. 2015). Analysis of inflorescence primordia phyllotactic patterns showed no difference between any treatment, suggesting repeated inoculation inducing PTI, ETS, or ETI cannot change the robust regulation of meristem patterning (Figure 3.15B). Additionally, quantification of SAM area and plastochron ratio showed no change between treatments, further indicating that developmental patterns are not changed in the SAM after any *Pst* inoculation (Figure 3.15C-D). While inoculation with *Pst* DC3000 or *Pst* AvrRpm1 did result in a significant difference in plastochron between these two treatments, statistical analysis revealed that there was no

difference between each treatment and $MgCl_2$ (Figure 3.15D), indicating that neither *Pst* strain results in a biological difference in plastochron.

As phyllotactic angles at the meristem were not different, particularly in *Pst* DC3000-treated SAMs, the change of silique divergence angles seen after repeated *Pst* DC3000 inoculations may be due to post-meristematic developmental changes. We therefore imaged stem segments after repeated inoculation with $MgCl_2$, *Pst* hrcC-, *Pst* DC3000, or *Pst* AvrRpm1 (Figure 3.16A). Quantification of stem torsion revealed a significant change in *Pst* DC3000 inoculated stems, compared to $MgCl_2$, *Pst* hrcC-, and *Pst* AvrRpm1 treatments (Figure 3.16A-B). Taken together, these data suggest that initiation of plant susceptibility after *Pst* inoculation at a high concentration changes silique phyllotactic patterning due to post-meristematic stem torsion, and thus is likely due to the action of pathogenic effectors. However, activation of high levels of immunity repeated inoculations of *Pst* strains initiating PTI or ETI associated with increased SA, are still not robust enough to change plant development.

CK signaling is necessary to limit the effects of Pst DC3000-dependent growth inhibition

Application of CK has been shown to promote SA-dependent defense responses and reduce pathogen growth (Choi et al. 2010; Argueso et al. 2012; Naseem et al. 2012). Additionally, mutations leading to reduced CK signaling are more susceptible to disease (Choi et al. 2010; Argueso et al. 2012; Naseem et al. 2012). To evaluate if CK plays a role in pathogen-induced vegetative growth reduction and phyllotaxy pattern change, we used the CK signaling mutant *ahk2,3* defective in two of the three CK receptors, *ARABIDOPSIS HISTIDINE KINASE 2 and ARABIDOPSIS HISTIDINE KINASE 3*. Two concentrations of *Pst* DC3000, 10^8 and 10^9 CFU/mL, were used to inoculate 10-day old Col-0 and *ahk2,3* plants to evaluate vegetative growth reduction in short-day conditions. At 10 dpi, rosettes were photographed and quantified. Because *ahk2,3* rosettes are normally smaller than Col-0 (Higuchi et al. 2004), rosette area was normalized for each genotype to the $MgCl_2$ control-treated rosettes to compare

growth reduction after *Pst* DC3000 treatment. Rosette area reduction in the absence of CK signaling was more severe after *Pst* DC3000 inoculation at both concentrations compared to Col-0 (Figure 3.17A-B). After inoculation with *Pst* DC3000 10^8 CFU/mL, Col-0 rosette area was reduced by 39.0%, while *ahk2,3* rosettes were reduced by 68.6% (Figure 3.17B). At 10^9 CFU/mL, *Pst* DC3000 inoculation led to a 73.1% decrease in *ahk2,3* rosette area compared to a 51.8% decrease in Col-0 (Figure 3.17B). Both *Pst* DC3000 concentrations resulted in a reduction of rosette leaf number in both genotypes, however, the reduction of leaf number was further reduced in *ahk2,3* (Figure 3.17C). These data indicate that CK signaling is necessary to limit the effects of *Pst* DC3000-induced vegetative growth inhibition in short-day conditions.

CK signaling is required for normal phyllotactic patterning and ETS-induced phyllotactic changes

Cytokinin has been shown to play an important role in meristematic maintenance and regular phyllotactic patterning (Chickarmane et al. 2012; Gordon et al. 2009; Besnard et al. 2014). Therefore, we investigated the role of CK signaling in phyllotactic robustness after repeated inoculations with *Pst* DC3000 in long-day conditions. We first characterized phyllotaxy of the *ahk2,3* CK signaling mutant compared to Col-0 to determine baseline patterns before pathogen treatments. The distribution of divergence angles in *ahk2,3* was increased with an average angle of 146° compared to the average Col-0 angle of 137° (Figure 3.18A-B). As these plants are known to be smaller and produce fewer seed than Col-0, it was expected that the overall stem height would be reduced and fewer siliques would be present along the primary stem (Figure 3.18B, D). Notably, the internode length of *ahk2,3* was significantly longer than Col-0 (Figure 3.18C), indicating *ahk2,3* height is, in part, due to increased internode length and may be a result of loss of hormone crosstalk regulating cell elongation. These data support previously reported data showing reduced CK signaling leads to perturbed phyllotactic patterning (Besnard et al. 2014), and further suggest that normal phyllotactic patterning is

dependent on the functioning of CK signaling receptors AHK2 and AHK3 and downstream CK signaling.

CK is known to play a role in increasing plant defense responses to biotic stressors by promoting SA-dependent defense responses (Argueso et al. 2012; Choi et al. 2010). Because of this hormonal crosstalk, we addressed if CK signaling is necessary to limit the effect of *Pst* DC3000-induced perturbed phyllotaxy. Col-0 and *ahk2,3* plants were inoculated five times, every other day (Figure 3.13A) with control $MgCl_2$ or *Pst* DC3000 10^9 CFU/mL and grown through reproductive development. Col-0 control $MgCl_2$ plants had a normal divergence angle distribution and an overall average angle of 138° (Figure 3.19A, E). As in Figure 3.13A, the divergence angle distribution of *Pst* DC3000 inoculated Col-0 plants was skewed with an increase in overall average angle to 142°, however, in this experiment, the changes were not significant (Figure 3.19E). On the other hand, both *ahk2,3* $MgCl_2$ and *Pst* DC3000-inoculated plants had increased average angles of 144° and 142°, respectively (Figure 3.19A, E). Because there is no change in patterning or average angle in *ahk2,3* $MgCl_2$ and *ahk2,3 Pst* DC3000-inoculated plants (Figure 3.19A, E), it is possible that ETS-induced changes in phyllotactic patterning require a function of CK in cell growth leading to stem torsion. Alternatively, given that phyllotactic pattern is already perturbed in uninoculated control *ahk2,3* (Figure 3.19A, E), it is possible that addition of a pathogen stress cannot further change phyllotactic patterns in the CK signaling mutant background. Other shoot phenotypes quantified do not show significant changes between treatments within each genotype except for increased internode of Col-0 *Pst* DC3000 inoculated plants (Figure 3.19B-D), as seen previously.

3.5 DISCUSSION

Mathematical modeling and experimental data have shown that meristem size and plastochron contribute to phyllotactic robustness, where larger meristems are associated with

decreased plastochron and perturbed phyllotactic pattern (Mirabet et al. 2012; Landrein et al. 2015). Additionally, interacting inhibitory fields associated with CK and auxin crosstalk at the SAM regulate primordia initiation, thus contributing to phyllotaxis (Mirabet et al. 2012; Besnard et al. 2014; Besnard, Rozier, and Vernoux 2014). A mutation in the CK signaling inhibitor, *ARABIDOPSIS HISTIDINE PHOSPHOTRANSFER PROTEIN 6* (*ahp6-1*), leads to change in meristematic maintenance and phyllotactic patterning, in part through altered crosstalk with Aux to establish inhibitory fields for primordia initiation (Besnard et al. 2014; Besnard, Rozier, and Vernoux 2014). Furthermore, the SAM is tightly guarded from pathogen infection. Recently, the homeobox transcription factor that maintains the stem cell population in the SAM, WUSCHEL (WUS), was shown to play a role in antiviral immunity, thus protecting cells within the SAM from infection (Wu et al. 2020). CK (Kyozuka 2007; Gordon et al. 2009; Chickarmane et al. 2012; Gruel et al. 2016), Aux (Vernoux et al. 2011), and their crosstalk (Zhao et al. 2010; Gaillochet and Lohmann 2015), have been well characterized in maintaining stem cell populations and promoting cell differentiation as cells exit the meristematic region.

The plant hormone SA has previously been shown to play a role in meristematic regulation and patterning in the root apical meristem (RAM) via crosstalk with Aux (Pasternak et al. 2019), however, SA has not yet been linked to SAM regulation. The data presented here suggest that SA plays a role in SAM processes, possibly through crosstalk with CK and/or Aux. Mutations in *CPR5* and *SNC1* leading to constitutive immunity and elevated levels of SA throughout plant development have an impact on plant growth and development from the very start of the plant's life. The effects of elevated SA from embryogenesis in these mutants results in reduced meristem size, increased plastochron, and altered phyllotactic patterning, linking increased SA with SAM regulation and shoot development.

To address if a transient increase in SA accumulation and signaling could alter phyllotactic development, we inoculated plants with *Pst* hrcC^{-}, *Pst* DC3000, or *Pst* AvrRpm1 to induce plant immunity (PTI, ETS, ETI). Defense responses to hemibiotrophic and biotrophic

pathogens, such as *Pst,* are dependent on SA accumulation and signaling (Glazebrook 2005). While PTI responses cause a moderate increase in SA accumulation (Tsuda et al. 2008), ETI potentiates PTI responses resulting in a further increase in SA accumulation, biosynthesis, and signaling (Castel et al. 2019; Ngou et al. 2021). We therefore hypothesized that activation of plant immunity by inoculation with *Pst* hrcC$^-$ or *Pst* AvrRpm1 could change silique phyllotaxis. However, only after repeated high inoculum infections with *Pst* DC3000 inducing ETS did we see changes in phyllotaxis. Furthermore, analysis of SAM size, plastochron, and inflorescence primordia revealed that *Pst* treatments had no effect on SAM developmental patterns, and changes in phyllotaxis in *Pst* DC3000 treatment resulted from post-meristematic effects on stem torsion.

Because we found that the SAM size was significantly reduced and plastochron was increased in the immunity mutants *snc1* and *cpr5* leading to perturbed silique phyllotaxis, we investigated SAM phenotypes after inoculation with *Pst* strains. Notably, our data show that even after multiple inoculations of any *Pst* strain, at a very high concentration, SAM size or plastochron does not change. This is likely a result of the tight regulation of the meristem and that a transient increase in SA accumulation and signaling during infection cannot overcome robust meristematic maintenance and developmental patterns. Post-meristematic development has been identified as a contributing source to phyllotactic robustness (Guedon et al. 2013) and, in some cases, SAMs of mutants with perturbed phyllotaxis are indistinguishable from wild-type (Peaucelle et al. 2007; Landrein et al. 2013; Burian et al. 2015). Both stem torsion (Landrein et al. 2013) and pedicel-stem fusions (Burian et al. 2015) contribute to post-meristematic development leading to altered silique phyllotaxy. Upon closer inspection of siliques, it did not appear that changes phyllotactic patterns after repeated *Pst* DC3000 inoculations resulted in silique pedicels fused to stems. However, quantification of epidermal cells in the stem did result in stem torsion and is thus responsible for altered phyllotactic patterning in *Pst* DC3000 inoculated plants.

To investigate if CK plays a critical role in *Pst* DC3000-dependent perturbed phyllotaxy, we inoculated the *ahk2,3* mutant following the robust inoculation regimen presented above. The distribution of uninoculated *ahk2,3* divergence angles showed that without initiation of CK signaling, normal phyllotaxy is perturbed. After repeated *Pst* DC3000 or $MgCl_2$ control inoculations, the phyllotactic pattern of *ahk2,3* resembled the pattern of uninoculated *ahk2,3*. Because phyllotactic patterning of *ahk2,3* is already disrupted, the additional stress of *Pst* DC3000 may not be able to further change phyllotaxy of the *ahk2,3* mutant.

In summary, our data shows that constitutively activated immunity changes phyllotactic patterning originating from reduced SAM area and decreased plastochron. Because constitutive immunity mutants are typically investigated for disease resistance to foliar pathogens, developmental patterns of these plants are usually not studied. Thus, it is possible that exploration of other constitutive immunity mutants in Arabidopsis or other plant species will also reveal irregular shoot architecture.

3.6 FIGURES

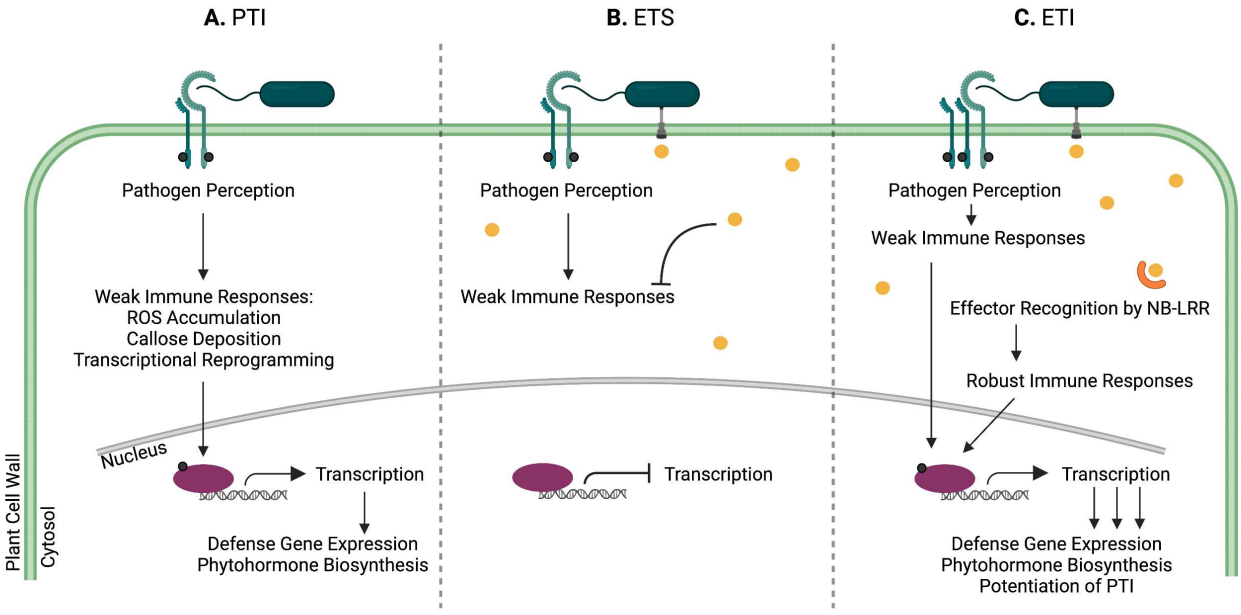

Figure 3.1: Plant immunity and susceptibility, PTI, ETS, and ETI. A. Pattern-Triggered Immunity (PTI) responses are initiated by cell surface receptors (blue transmembrane receptors) recognition of bacterial (teal) peptide recognition. Upon receptor phosphorylation (black dots), an intracellular cascade initiates weak immune responses including reactive oxygen species (ROS) accumulation, callose deposition, and transcriptional reprogramming. Genes related to defense and phytohormone biosynthesis are upregulated during PTI. **B.** During effector triggered susceptibility (ETS), the plant does perceive the pathogen and PTI is induced. However, bacterial effectors (yellow dots) are secreted into the plant cell by the type III secretion system (grey) by the pathogen and suppress PTI responses and cellular reprogramming to benefit pathogen infection leading to plant susceptibility and disease. **C.** During effector triggered immunity (ETI), effector proteins are recognized by specialized plant receptors, NB-LRRs (orange curved receptor), leading to a more robust plant immune response, increased defense gene expression, and potentiation of PTI. This figure was created using BioRender.com and adapted from (Jones and Dangl 2006; Ngou et al. 2021; Yuan, Jiang, et al. 2021; Yuan, Ngou, et al. 2021).

Figure 3.2: Device used to measure silique divergence angles for phyllotactic analysis. The top stages can be moved to accommodate a range of stem heights. The center stage has a circular protractor to measure silique angles. Divergence angle measurements were taken by reading the angle from the first silique, moving the center stage to the base of the next silique along the stem, recording the angle, and then finding the difference between the two. This process was repeated for all the siliques along the primary inflorescence stem.

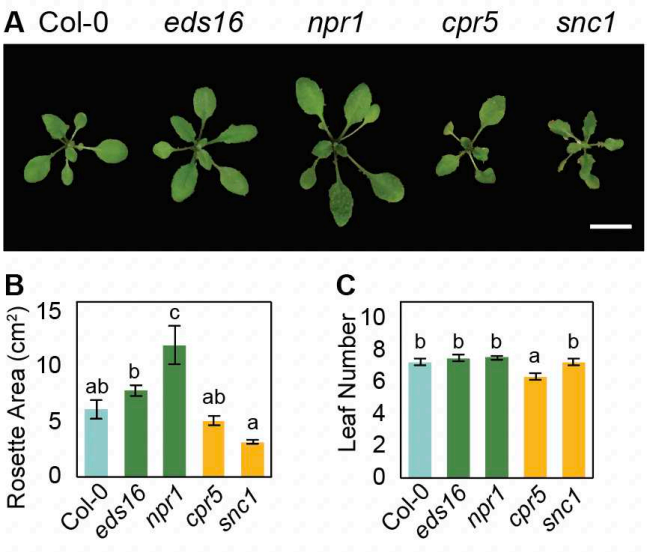

Figure 3.3: Altered SA-dependent immunity changes vegetative plant growth. A. Representative rosettes of Col-0, *eds16* (SA biosynthesis mutant), *npr1* (SA signaling mutant), *cpr5* (constitutive immunity mutant), and *snc1* (constitutive immunity mutant) from a single experiment. Scale bar represents 1 cm. **B.** Average rosette area of each genotype, n > 36 plants per genotype. **C.** Average leaf number per rosette at time of bolting of each genotype, n > 36 plants per genotype. A one-Way ANOVA (p-value ≤ 0.05) was used to determine significance between genotypes. Error bars represent standard error.

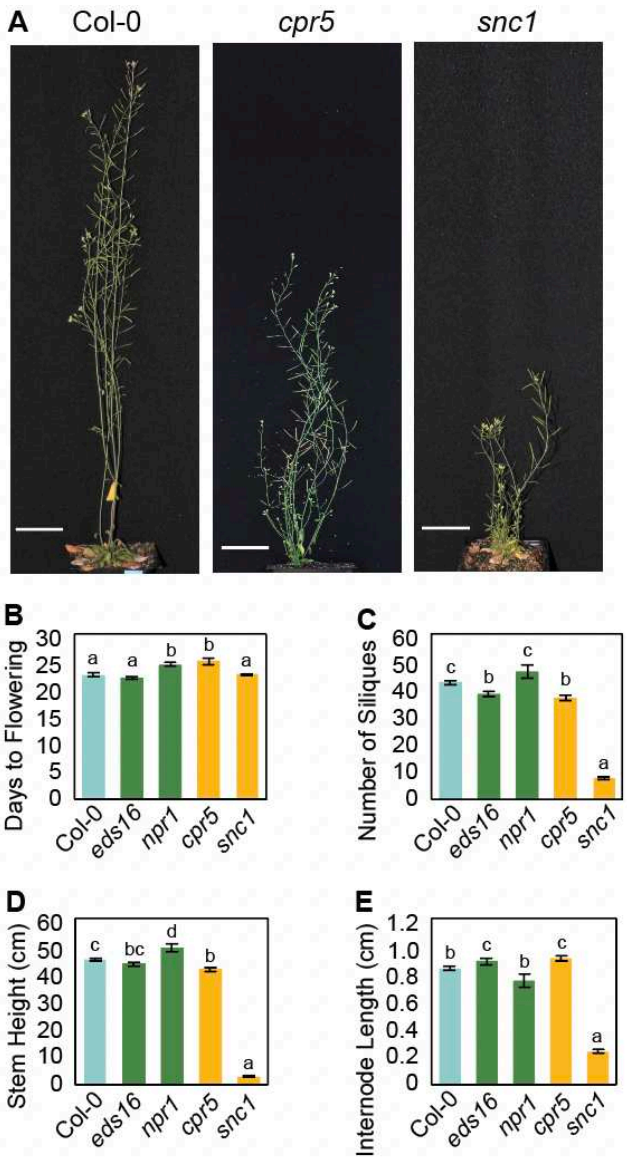

Figure 3.4: Altered SA-dependent immunity changes reproductive plant growth. A. Representative reproductive stage of Col-0 and constitutively activated immunity mutants *cpr5* and *snc1*. Scale bar represents 5 cm. **B.** Average days to flowering of each genotype, counted from the number of days after germination to the appearance of the inflorescence meristem at bolting; n > 36 plants per genotype, from a single experiment. **C.** Total number of siliques along the primary stem; n > 18 plants per genotype of pooled data from two experiments. **D.** Height of the primary stem measured at the end of flowering; n > 18 plants per genotype of pooled data from two experiments. **E.** Average internode length between consecutive siliques along the primary stem; n > 18 plants per genotype of pooled data from two experiments. A one-Way ANOVA (p-value ≤ 0.05) was used to determine significance between genotypes. Error bars represent standard error.

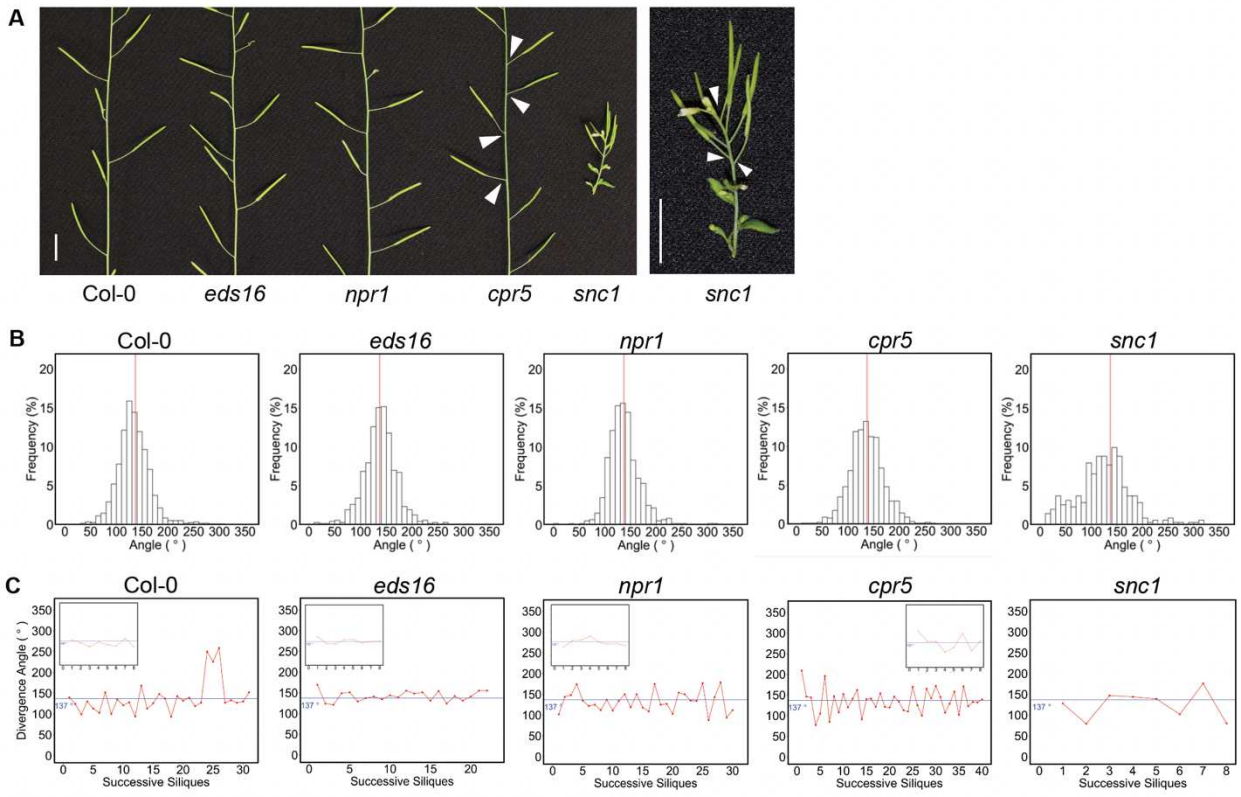

Figure 3.5: Phyllotactic patterning of constitutively activated immunity mutants *cpr5* and *snc1* is quantifiably different from Col-0. A. Representative images of siliques along the primary stem of each genotype. Scale bars represent 1 cm. **B.** Divergence angle distribution of each genotype, pooled data from two experiments. Col-0 n=1171 siliques from 29 plants, 135° average; *eds16* n=731 siliques from 25 plants, 139° average; *npr1* n=602 siliques from 20 plants, 138° average; *cpr5* n=914 siliques from 28 plants; 137° average; *snc1* n=352 siliques from 56 plants, 125° average. The red line denotes 137°. **C.** Consecutive siliques along a single, representative primary stem of each genotype. Insert shows the first 8 consecutive siliques from the representative plant. The blue line represents 137°.

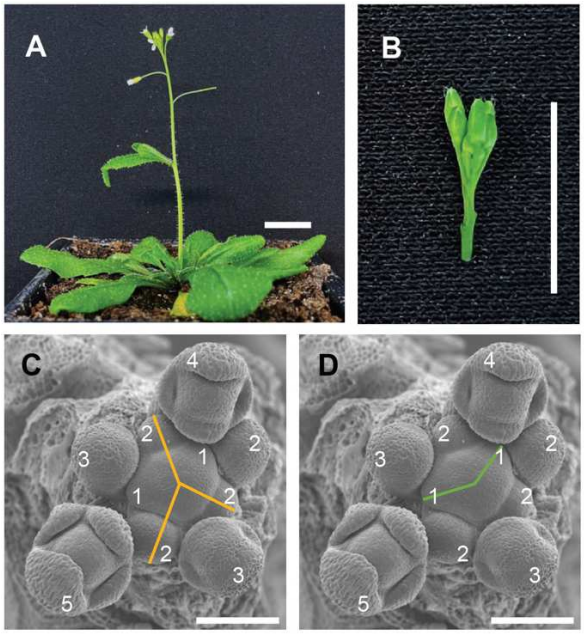

Figure 3.6: SAM dissection preparation and SAM measurements. A. The developmental stage of plants used for SAM dissection, 4 to 5 weeks post germination. Scale bar represents 1 cm. **B.** All open flowers were removed from the primary stem in preparation for further dissection. At this stage, all remaining flower buds between developmental stages 6 and 12 (Smyth, Bowman, and Meyerowitz 1990) were removed to expose the meristem. Scale bar represents 1 cm. **C.** To find the center of the meristem, lines (yellow) were drawn from the edge of the three youngest consecutive stage 2 and 3 inflorescence primordia. This geographical center was used for SAM phyllotactic measurements (Landrein et al. 2015). Scale bar represents 100 µm. **D.** To calculate the SAM area and plastochron ratio, lines (green) from the edge of the two largest stage 1 inflorescence primordia were drawn to the center of the meristem as previously determined. The average of these two lines was used to calculate the area of the SAM. The plastochron ratio was calculated by dividing the length taken from the edge of one inflorescence primordia to the center of the SAM by the length of the next consecutive primordia (Landrein et al. 2015). Scale bar represents 100 µm.

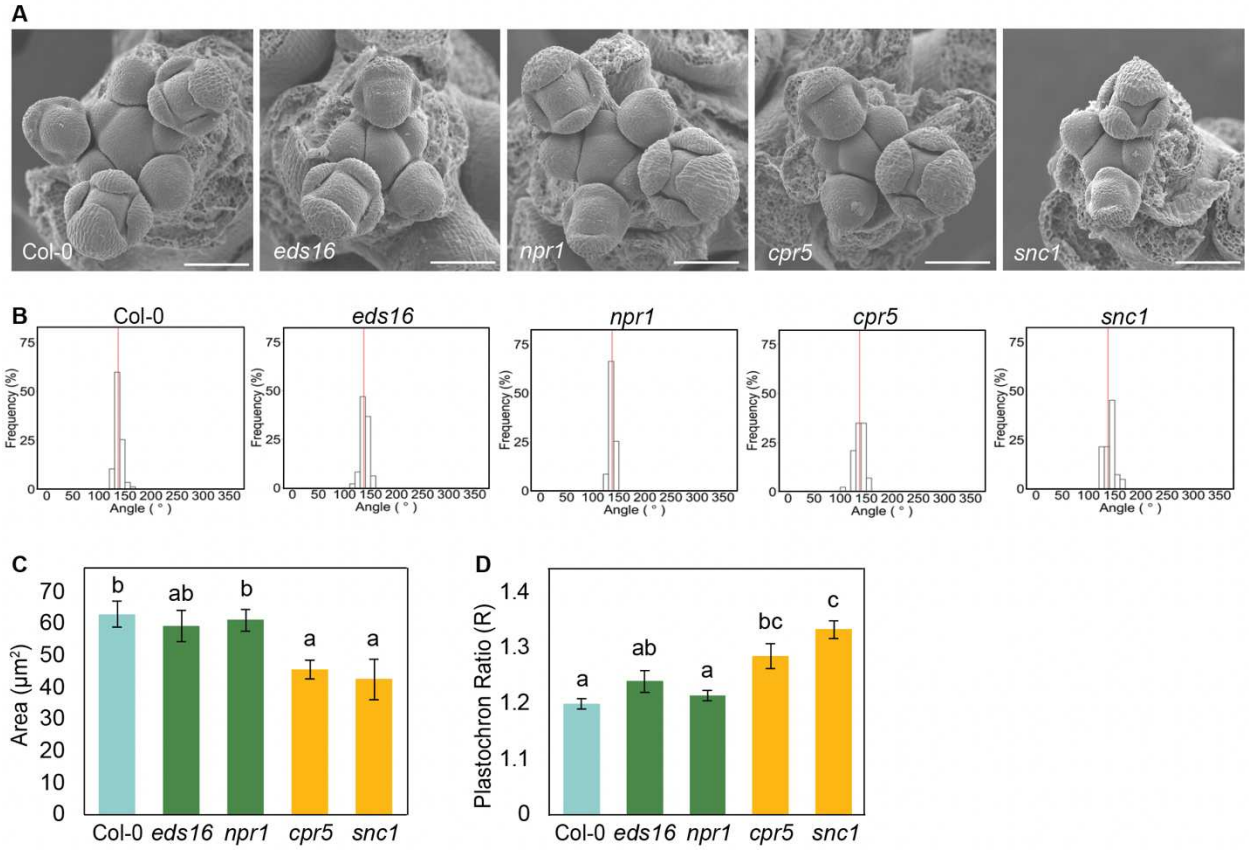

Figure 3.7: Reduced SAM size and increased plastochron leads to altered silique phyllotactic patterning of *cpr5* and *snc1*. A. Representative SAM images for each genotype. Scale bar represents 100 μm. **B.** Divergence angle distributions of the infloresence primordia from one experiment. Col-0 n=87 floral primordia from 12 SAMs, 138° average; *eds16* n=49 floral primordia from 9 SAMs, 138° average; *npr1* n=83 floral primordia from 12 SAMs, 137° average; *cpr5* n=43 floral primordia from 8 SAMs; 136° average; *snc1* n=42 floral primordia from 9 SAMs, 140° average. The red line indicates 137°. **C.** SAM area quantified from SAM images. **D.** SAM plastochron ratio quantified from SAM images. A one-Way ANOVA (p-value ≤ 0.05) was used to determine significance between genotypes. Error bars represent standard error.

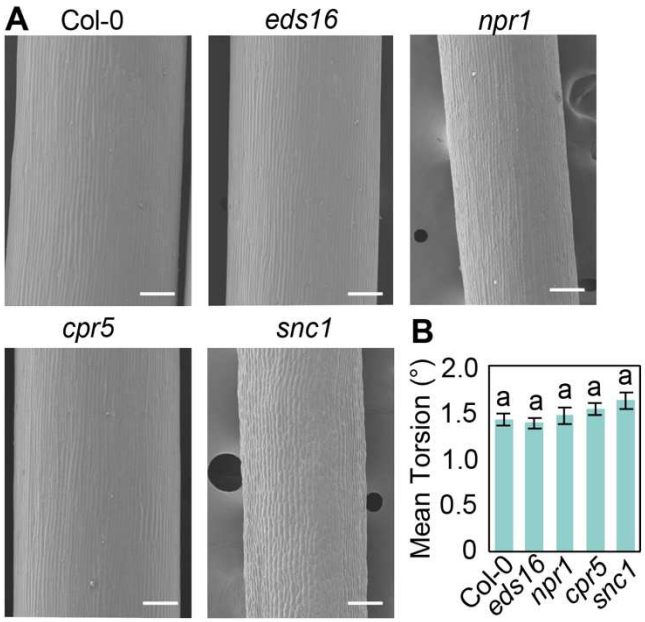

Figure 3.8: Post-meristematic development of stems of constitutively activated immunity mutants *cpr5* and *snc1* does not contribute to change in silique phyllotaxy. A. Representative stems of Col-0 and SA immunity mutants. Col-0 n=22 stems, 330 measurements; *eds16* n=20 stems, 300 measurements; *npr1* n=11 stems; 165 measurements; *cpr5* n=23 stems, 345 measurements; *snc1* n=16, 240 measurements. **B.** Average stem torsion quantified from SEM stem images from one experiment. Error bars represent standard error of the mean. A one-Way ANOVA (p-value ≤ 0.05) was used to determine significance between genotypes.

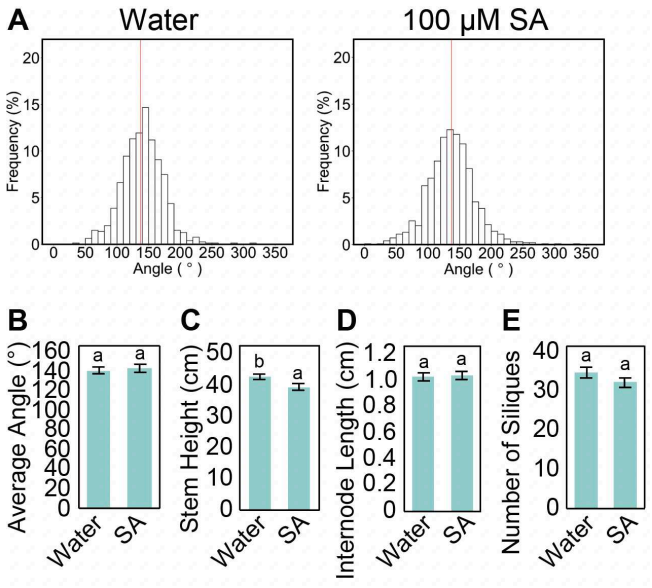

Figure 3.9: SA treatment does not change phyllotactic patterning or shoot growth. A. Silique divergence angle distribution of Col-0 plants treated with water or 100 µM SA from a single experiment. Col-0 water n=805 siliques from 27 plants, 141° average; Col-0 100 µM SA n=986 siliques from 34 plants, 137° average. **B.** Average angle calculated from the divergence angles measured from each plant. **C.** Height of the primary stem at the end of reproductive development, measured at the time of divergence angle measurements. **D.** Average length of internodes between consecutive siliques along the primary stem. **E.** Average of the total number of siliques along the primary stem. A one-Way ANOVA (p-value ≤ 0.05) was used to determine significance between treatments. Error bars represent standard error.

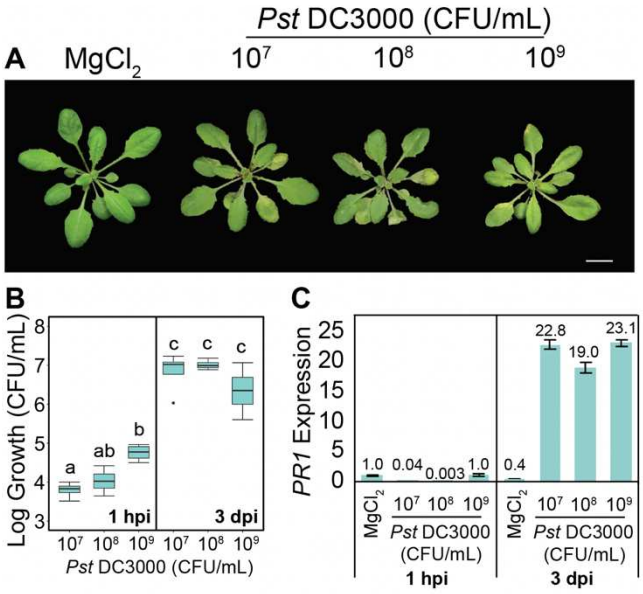

Figure 3.10: *Pst* DC3000 grown in long-day conditions causes disease symptoms and leads to an increase in *PR-1* expression. A. Representative rosettes three days post spray inoculation with *Pst* EV (1 x 10^7 CFU/mL, 1 x 10^8 CFU/mL, or 1 x 10^9 CFU/mL) or control $MgCl_2$. Scale bar represents 1 cm. **B.** *Pst* bacterial growth 1 hour post spray inoculation (hpi), and 3 dpi with *Pst* at 1 x 10^7 CFU/mL, 1 x 10^8 CFU/mL, or 1 x 10^9 CFU/mL. Representative data from a single experiment, repeated three times with 4 technical replicates per treatment, per timepoint. Error bars represent standard error, n=4 per time point. A one-Way ANOVA (p-value ≤ 0.05) was used to determine significance between genotypes. Error bars represent standard error. **C.** qRT-PCR gene expression of *PR1* normalized to 1 hpi $MgCl_2$ after *Pst* inoculation or $MgCl_2$ control 1 hpi and 3 dpi. Error bars represent standard error. Representative data from a single experiment, repeated three times with 3 technical replicates per treatment, per timepoint.

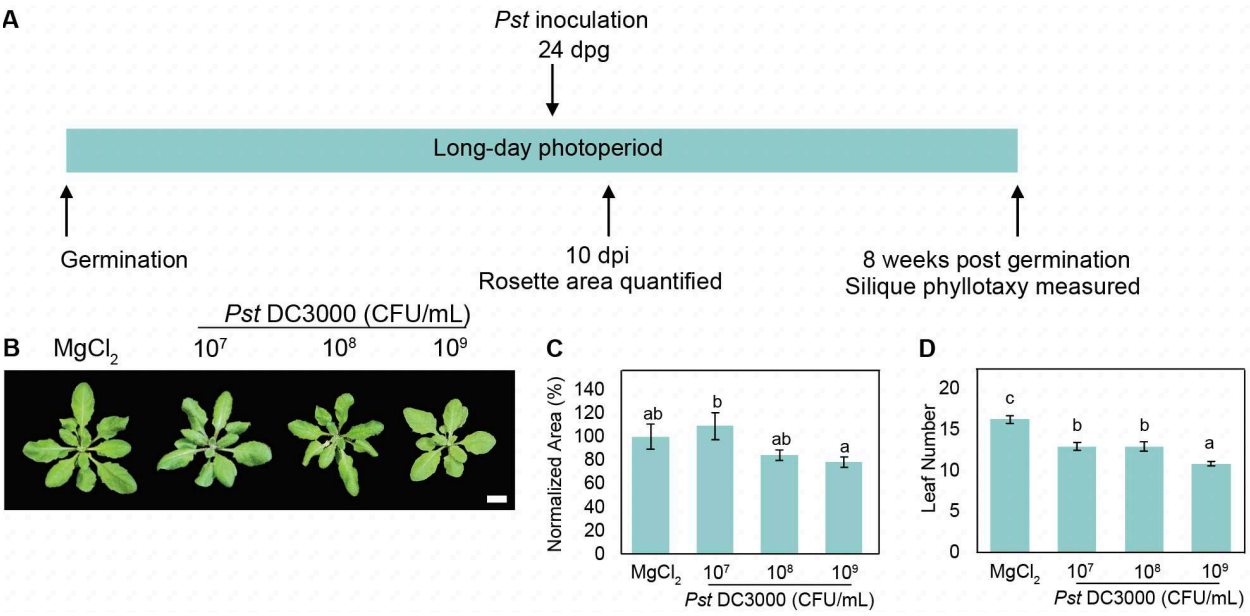

Figure 3.11: A single inoculation of *Pst* DC3000 close to the transition to reproductive development reduces rosette size and leaf number. A. Experimental design for inoculated phyllotaxy experiment: plants were inoculated 24 dpg, close to the transition from vegetative growth to reproductive growth. Rosettes were photographed 10 dpi for rosette area measurements. Silique phyllotaxy was measured 8 weeks post germination. Data was collected from a single experiment. **B.** Representative rosettes 10 dpi with $MgCl_2$, *Pst* EV (1 x 10^7 CFU/mL, 1 x 10^8 CFU/mL, or 1 x 10^9 CFU/mL). Scale bar represents 1 cm. **C.** Normalized rosette area 10 dpi with each treatment, n=18. Percent rosette area growth reduction compared to $MgCl_2$: *Pst* DC3000 10^7 CFU/mL 8.9%; *Pst* DC3000 10^8 CFU/mL 15.6%; *Pst* DC3000 10^9 21.8% CFU/mL. Error bars represent standard error. **D.** Number of rosette leaves at time of rosette area measurements. A one-Way ANOVA (p-value ≤ 0.05) was used to determine significance between genotypes. Error bars represent standard error.

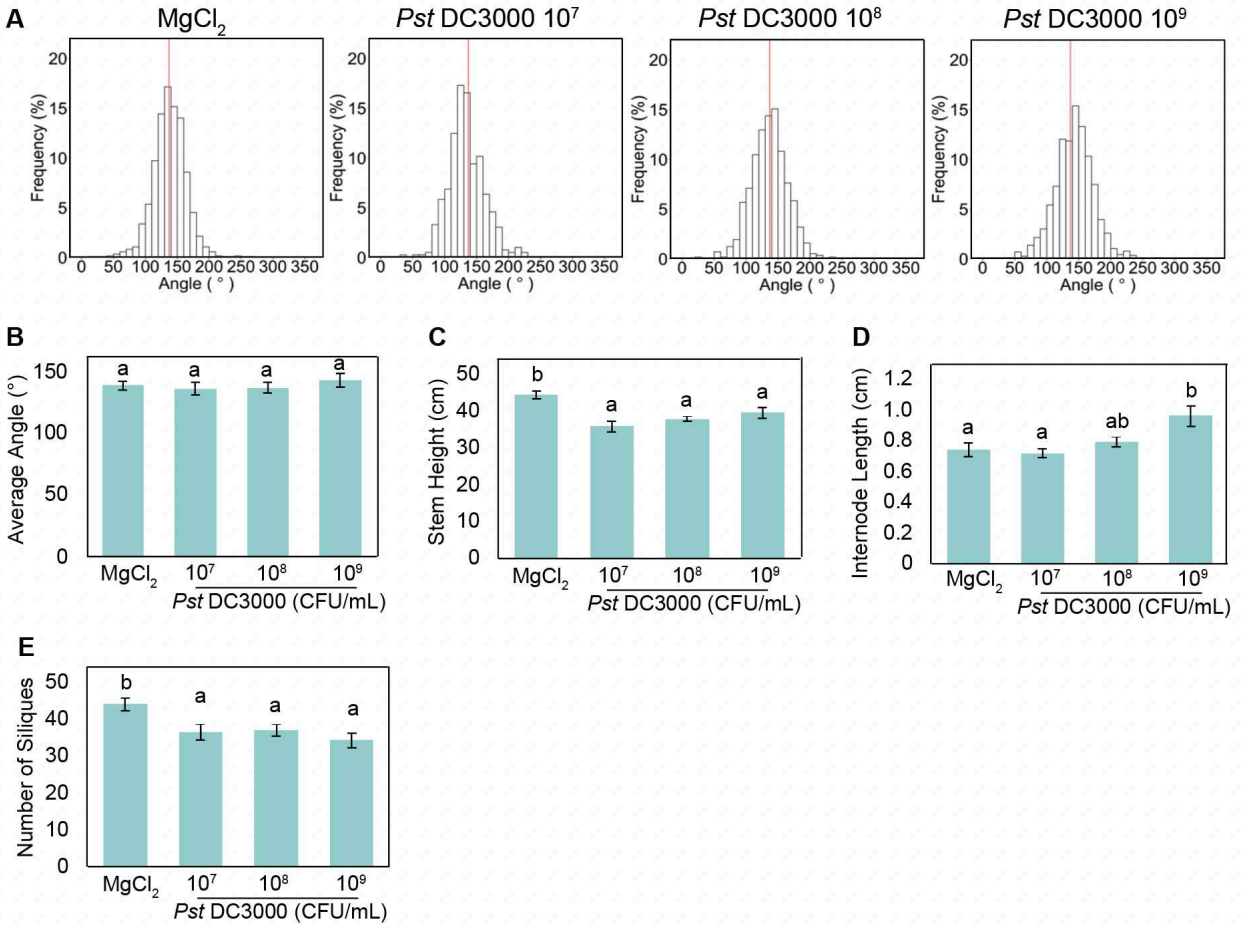

Figure 3.12: A single inoculation of *Pst* DC3000 close to the transition to reproductive development moderately changes silique phyllotaxy pattern and reproductive development but only at a very high concentration. A. Divergence angle distributions measured from siliques along the primary stem after each treatment pooled from three experiments. $MgCl_2$ n=1213 siliques from 32 plants, 139° average; *Pst* DC3000 10^7 CFU/mL n=428 siliques from 12 plants, 135° average; *Pst* DC3000 10^8 CFU/mL n=564 siliques from 17 plants, 137° average; *Pst* DC3000 10^9 CFU/mL n=1165 siliques from 38 plants, 143° average. The red line represents 137°. **B.** Average angle calculated from the divergence angles measured from each plant. **C.** Height of the primary stem at the end of reproductive development, measured at the time of divergence angle measurements. **D.** Average length of internodes between consecutive siliques along the primary stem. **E.** Average of the total number of siliques along the primary stem. A one-Way ANOVA (p-value ≤ 0.05) was used to determine significance between treatments. Error bars represent standard error.

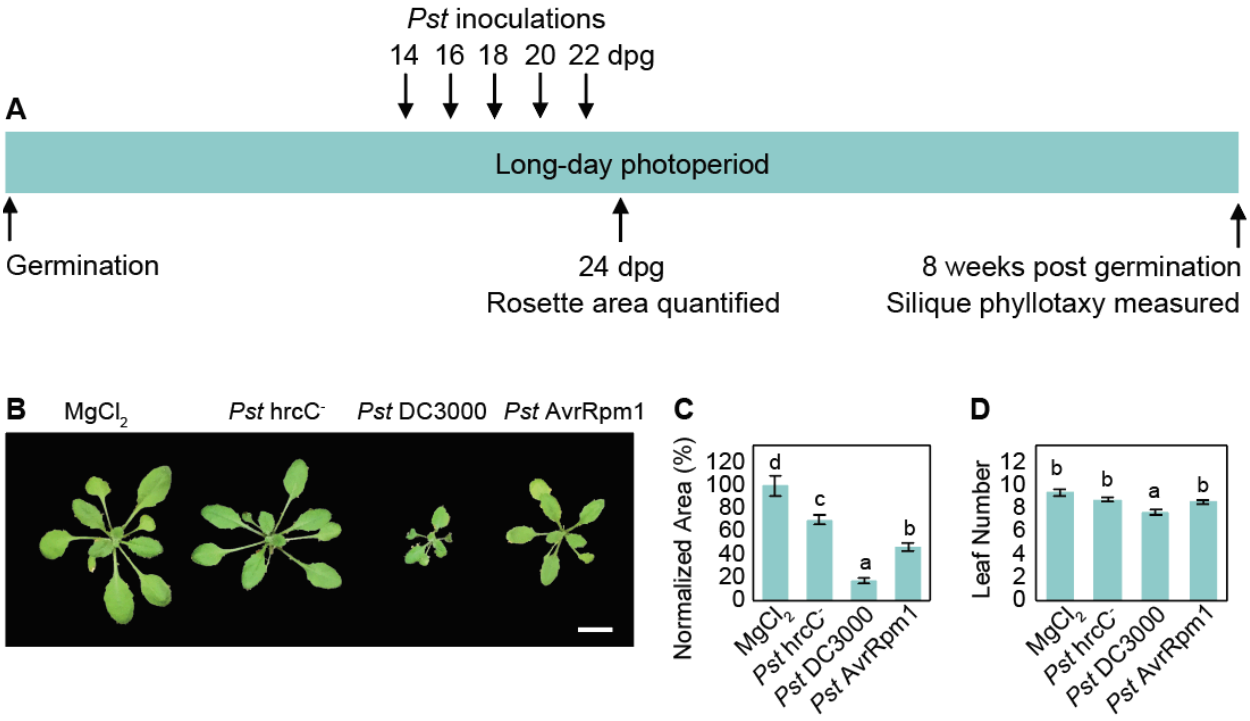

Figure 3.13: Repeated inoculation with *Pst* hrcC$^-$, *Pst* DC3000, or *Pst* AvrRpm1 significantly reduces vegetative growth. A. Experimental design for repeated *Pst* inoculation experiment. Plants were inoculated five times, every other day, beginning at 14 dpg. Rosettes were photographed for area measurements 2 days after the final inoculation, 24 dpi. Silique phyllotaxy measurements were taken at the end of reproductive growth, 8 weeks post germination. **B.** Representative rosettes of repeated inoculations of control $MgCl_2$ and *Pst* hrcC$^-$ or *Pst* DC3000 plants. Scale bar represents 1 cm. **C.** Normalized rosette area showing rosette growth inhibition after repeated inoculations based on measurements taken at 24 dpg, pooled from three experiments. Percent growth reduction compared to $MgCl_2$ control: *Pst* hrcC$^-$ 30.2%; *Pst* DC3000 82.7%; *Pst* AvrRpm1 53.5%. **D.** Average number of rosette leaves at the time of rosette area measurements. A one-Way ANOVA (p-value ≤ 0.05) was used to determine significance between treatments. Error bars represent standard error.

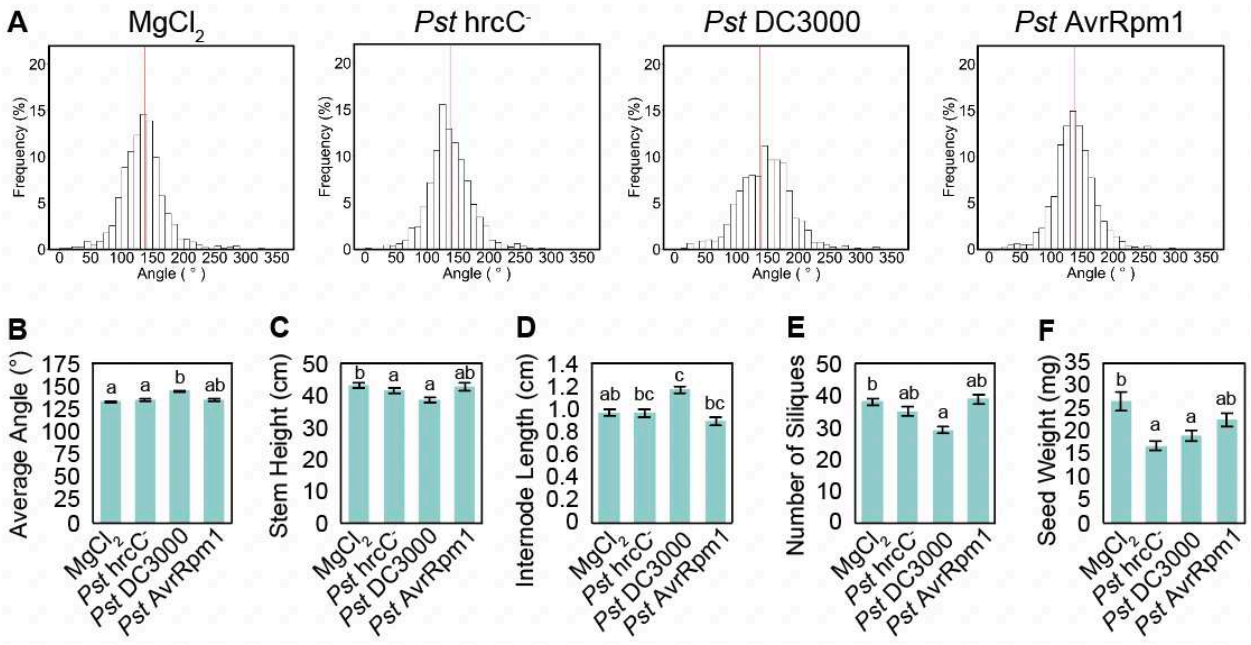

Figure 3.14: Repeated *Pst* DC3000 inoculation changes phyllotactic patterning. A. Phyllotactic divergence angle distributions of siliques along primary stems after repeated treatment. $MgCl_2$ n=1145 siliques from 35 plants, 135° average; *Pst* hrcC$^-$ n=1022 siliques from 33 plants, 137° average; *Pst* EV n=778 siliques from 31 plants, 146° average; *Pst* AvrRpm1 n=1483 siliques from 41 plants, 137° average. The red line represents 137°. Pooled data from three experiments. **B.** Average angle calculated from the divergence angles measured from each plant. **C.** Height of the primary stem at the end of reproductive development, measured at the time of divergence angle measurements. **D.** Average length of internodes between consecutive siliques along the primary stem. **E.** Average of the total number of siliques along the primary stem. **F.** Total seed weight after multiple inoculations. A one-Way ANOVA (p-value ≤ 0.05) was used to determine significance between treatments. Error bars represent standard error.

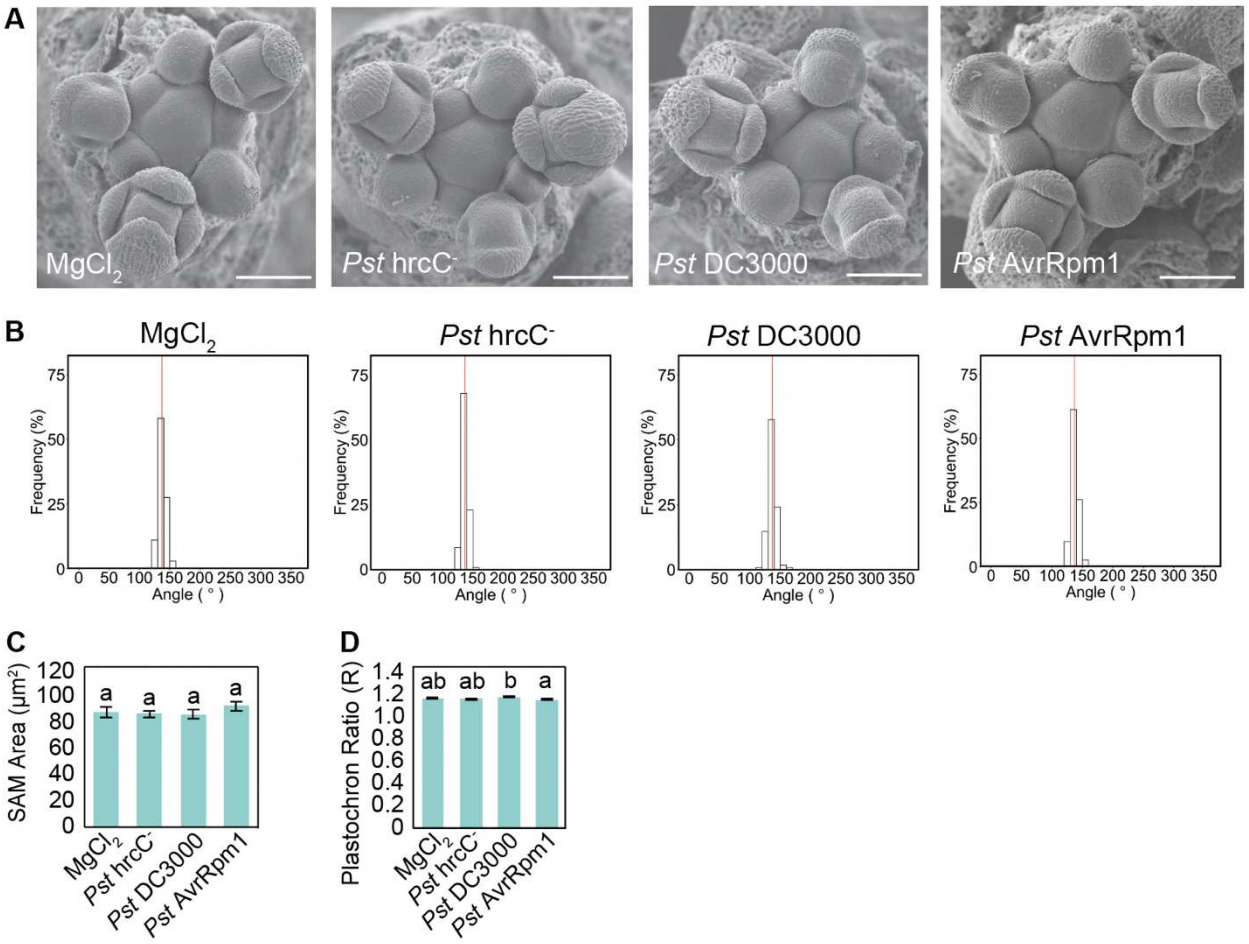

Figure 3.15: Repeated *Pst* inoculations do not change meristematic pattern. A. Representative Col-0 SAM images after each inoculation treatment. Scale bar represents 100 μm. **B.** Divergence angle distributions of the infloresence primordia from a single experiment. $MgCl_2$ n=134 floral primordia from 16 SAMs, 137° average; *Pst* hrcC$^-$ n=131 floral primordia from 15 SAMs, 137° average; *Pst* DC3000 n=116 floral primordia from 15 SAMs, 137° average; *Pst* AvrRpm1 n=111 floral primordia from 15 SAMs, 137° average. The red line indicates 137°. **C.** SAM area quantified from SAM images. **D.** SAM plastochron ratio quantified from SAM images. A one-Way ANOVA (p-value ≤ 0.05) was used to determine significance between treatments. Error bars represent standard error.

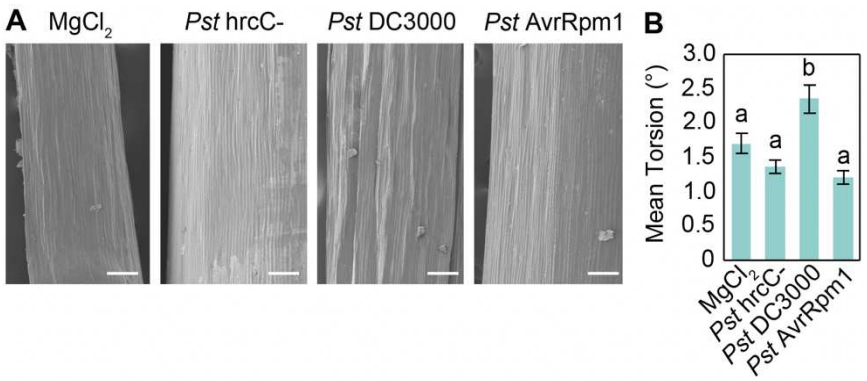

Figure 3.16: Repeated *Pst* DC3000 inoculations increase stem torsion leading to perturbed silique phyllotaxis. A. Representative stems of $MgCl_2$, *Pst* hrcC-, or *Pst* DC3000 inoculated Col-0 stems. $MgCl_2$ n=5 stems, 75 measurements; *Pst* hrcC- n=10 stems, 150 measurements; *Pst* DC3000 n=6 stems; 90 measurements. **B.** Average stem torsion quantified from SEM stem images from a single experiment. Error bars represent standard error of the mean. A one-Way ANOVA (p-value ≤ 0.05) was used to determine significance between genotypes.

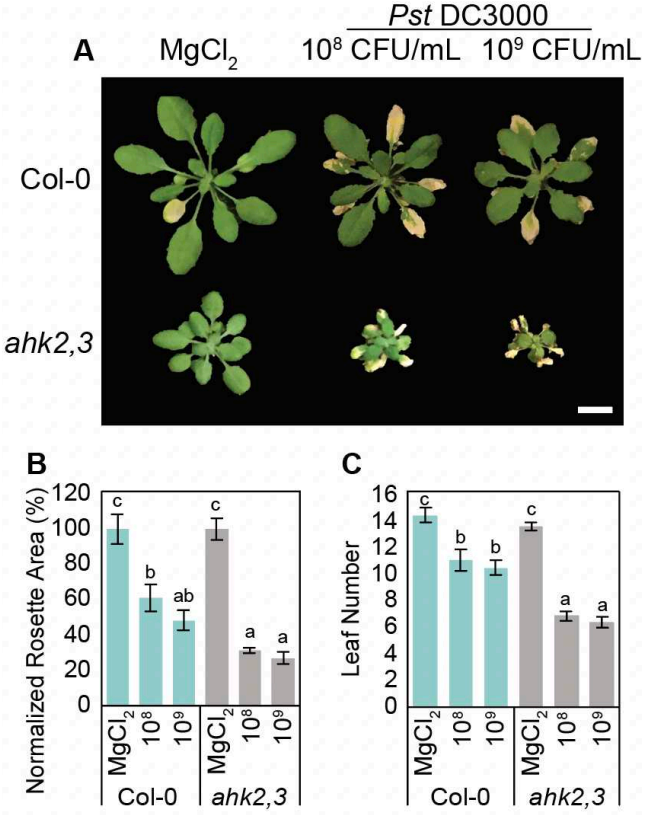

Figure 3.17: Infection with *Pst* DC3000 decreases vegetative growth in a manner-dependent on CK signaling. A Representative rosettes of Col-0 and *ank2,3* after $MgCl_2$ control treatments or *Pst* DC3000 10^8 or 10^9 CFU/mL in short-day conditions. Scale bar represents 1 cm. **B.** Normalized rosette area growth reduction 10 days post inoculation pooled from three experiments. Percent growth reduction compared to Col-0 or *ahk2,3* $MgCl_2$ control: Col-0 10^8 CFU/mL *Pst* DC3000 39.0%; Col-0 10^9 CFU/mL *Pst* DC3000 51.8%; *ahk2,3* 10^8 CFU/mL *Pst* DC3000 68.6%; *ahk2,3* 10^9 CFU/mL *Pst* DC3000 73.1% **C.** Number of rosette leaves at time of area measurements. A one-Way ANOVA (p-value ≤ 0.05) was used to determine significance between treatments. Error bars represent standard error.

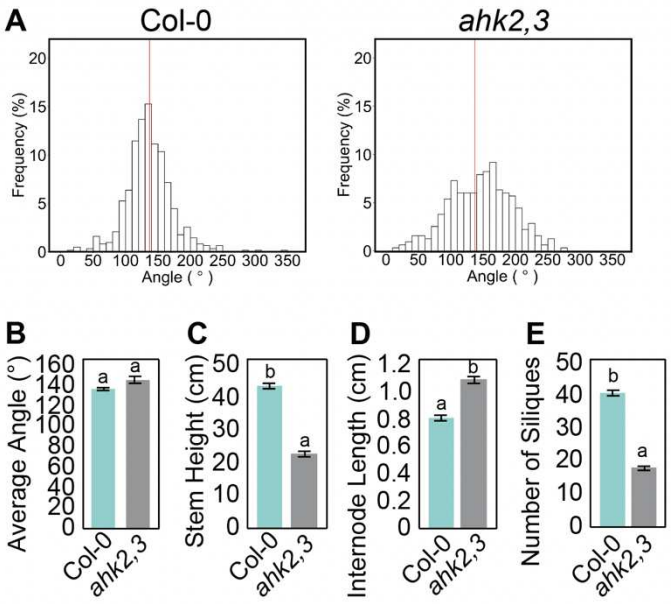

Figure 3.18: The CK signaling mutant *ahk2,3* has altered phyllotactic patterning. A. Divergence angle distributions of siliques along the primary stem. Col-0 n=629 siliques from 18 plants, 137° average; *ahk2,3* n=316 siliques from 18 plants, 146° average, from a single experiment. The red line indicates 137°. **B.** Average angle calculated from the divergence angles measured from each plant. **C.** Height of the primary stem at the end of reproductive development, measured at the time of divergence angle measurements. **D.** Average length of internodes between consecutive siliques along the primary stem. **E.** Average of the total number of siliques along the primary stem. A one-Way ANOVA (p-value ≤ 0.05) was used to determine significance between treatments. Error bars represent standard error.

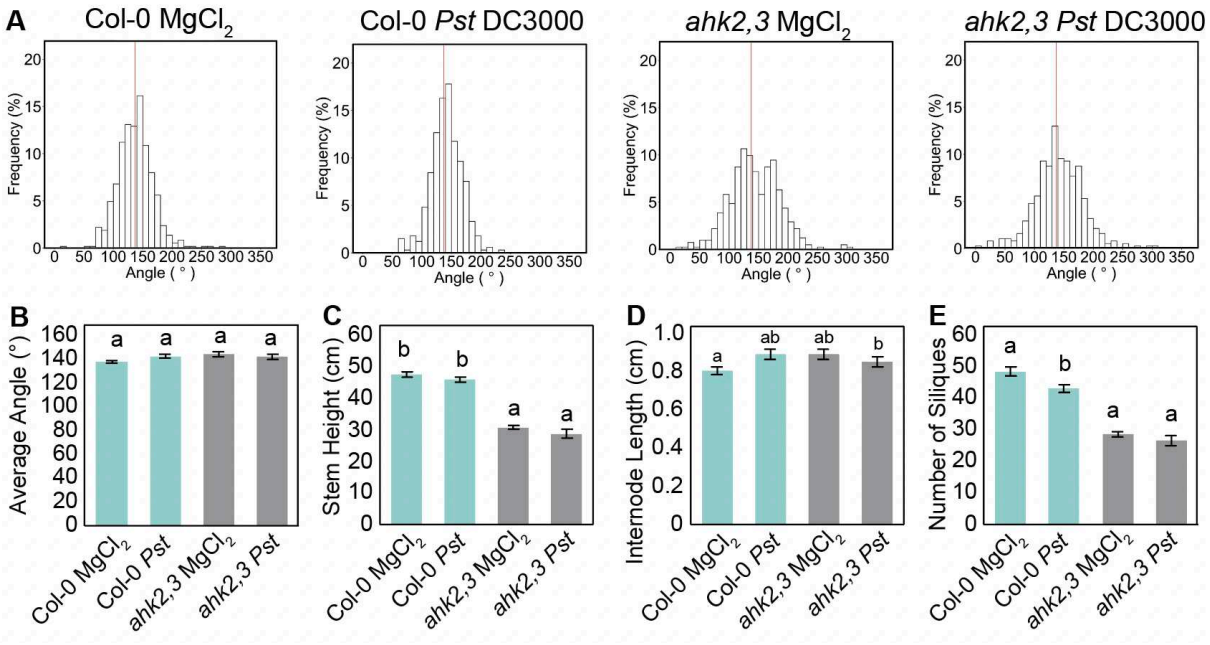

Figure 3.19: *Pst* DC3000 cannot further perturb silique phyllotaxis in the CK signaling mutant *ahk2,3*. A. Divergence angle distributions of siliques along the primary stem. Col-0 $MgCl_2$ n=589 siliques from 14 plants, 138° average; Col-0 *Pst* DC3000 n=332 siliques from 9 plants, 142° average; *ahk2,3* $MgCl_2$ n=413 siliques from 17 plants, 144° average; *ahk2,3 Pst* DC3000 n=377 siliques from 16 plants, 142° average from a single experiment. The red line indicates 137°. **B.** Average angle calculated from the divergence angles measured from each plant. **C.** Height of the primary stem at the end of reproductive development, measured at the time of divergence angle measurements. **D.** Average length of internodes between consecutive siliques along the primary stem. **E.** Average of the total number of siliques along the primary stem. A one-Way ANOVA (p-value ≤ 0.05) was used to determine significance between treatments. Error bars represent standard error.

3.7 TABLES

Table 3.1: Gene specific primers and restriction enzymes for mutant genotyping.

Gene ID	Mutant Name and Allele	Forward (5' → 3')	Reverse (5' → 3')	RE	Digestion Products (bp)
AT1G74710	*enhanced disease susceptibility 16, eds16*	CCTGAGAGACTA TTCCAAAGGAC	ACTCTGAAGATG GGTCACTTCC	-	1027 bp (WT); none (*eds16*)
AT1G64280	*nonexpresser of PR genes 1, npr1-1*	ATAGGAATCCGAG GGGATATACGGTGA	CATCTTCAATTC ATCGGCCGC	HinFI	273 bp (WT); 302 bp (*npr1*)
AT5G64930	*constitutive expression of PR genes 5, cpr5-1*	CGAGTTTGGGTG CAGATATTTTTGG	GGAAACATACTG TTACAACGGTTCG	FokI	320 bp (WT); 283 bp (*cpr5*)
AT4G16890	*suppressor of npr1-1, constitutive 1, snc1-1*	TTGGAATACGTT TGCCATTCGAGG	CCGTGGATCACA AGCCATAA	XbaI	847 bp (WT); 943 bp (*snc1*)

ID: Identification Number; RE: Restriction Enzyme; bp: base pairs. Primers for *eds16* only amplify the wild-type (WT) sequence and no digestion reaction is required for genotyping.

Table 3.2: Plant defense responses to *Pst* DC3000 strains.

***Pst* strain**	**Plant Response**	**Reference**
Pst DC3000 hrcC$^-$ (*Pst* hrcC$^-$)	PTI Weak immune responses ROS burst Callose deposition Increased defense gene expression Increased hormone biosynthesis	(Deng et al. 1998; Jones and Dangl 2006; Tsuda et al. 2008; Ngou et al. 2021; Yuan, Jiang, et al. 2021; Yuan, Ngou, et al. 2021)
Pst DC3000 EV (*Pst* DC3000)	ETS Inhibition of PTI responses Plant susceptibility and disease	(Jones and Dangl 2006; Yao, Withers, and He 2013)
Pst DC3000 AvrRpm1 (*Pst* AvrRpm1)	ETI Strong immune responses Potentiation of PTI Increased defense gene expression Increased hormone biosynthesis	(Jones and Dangl 2006; Kim et al. 2009; Ngou et al. 2021; Yuan, Jiang, et al. 2021; Yuan, Ngou, et al. 2021)

PTI: pattern triggered immunity; ROS: reactive oxygen species; ETS: effector triggered susceptibility; ETI: effector triggered immunity.

Table 3.3: qRT-PCR quality control and gene specific primers for gene expression analysis.

Gene ID	Gene Name	Forward (5' → 3')	Reverse (5' → 3')
AT5G66770	*ACTIN*	GGTTTGGTTTGGT TATCGCCAGGA	TGGCTTCATCTC TTTGGCCTGGA
AT1G13320	*GAPDH (1')*	TAGATCGCTCGGA ACTTGGAAA	CCTCACCAAAAC TCAAATCACTCC
AT1G13320	*GAPDH (3')*	AACTAGGACGGAT CTGGTGCCT	GCTATCCGAACTT CTGCCTCATTAT
AT1G13320	*GAPDH (5')*	AAATTTAACGTGG CCAAAATGATGC	GTTCTCCACAAC CGCTTGGT
AT4G05320	*UBIQUITIN 10, UBQ10*	CGTTAAGACGTTG ACTGGGAAAACT	GCTTTCACGTTAT CAATGGTGTCA
AT2G14610	*PATHOGENESIS-RELATED PROTEIN 1, PR-1*	ACAGTGCAATG GAGTTTGTGGTC	TACACCTCACTT TGGCACATCCGA

REFERENCES

Adler, I., D. Barabe, and R. V. Jean. 1997. 'A history of the study of phyllotaxis', *Annals of Botany*, 80: 231-44.

Argueso, C. T., F. J. Ferreira, P. Epple, J. P. C. To, C. E. Hutchison, G. E. Schaller, J. L. Dangl, and J. J. Kieber. 2012. 'Two-component elements mediate interactions between cytokinin and salicylic acid in plant immunity', *PLOS Genetics*, 8.

Bernoux, M., J. G. Ellis, and P. N. Dodds. 2011. 'New insights in plant immunity signaling activation', *Current Opinion in Plant Biology*, 14: 512-18.

Besnard, F., Y. Refahi, V. Morin, B. Marteaux, G. Brunoud, P. Chambrier, F. Rozier, V. Mirabet, J. Legrand, S. Laine, E. Thevenon, E. Farcot, C. Cellier, P. Das, A. Bishopp, R. Dumas, F. Parcy, Y. Helariutta, A. Boudaoud, C. Godin, J. Traas, Y. Guedon, and T. Vernoux. 2014. 'Cytokinin signalling inhibitory fields provide robustness to phyllotaxis', *Nature*, 505: 417-+.

Besnard, F., F. Rozier, and T. Vernoux. 2014. 'The AHP6 cytokinin signaling inhibitor mediates an auxin-cytokinin crosstalk that regulates the timing of organ initiation at the shoot apical meristem', *Plant Signaling & Behavior*, 9.

Bowling, S. A., J. D. Clarke, Y. D. Liu, D. F. Klessig, and X. N. Dong. 1997. 'The *cpr5* mutant of Arabidopsis expresses both NPR1-dependent and NPR1-independent resistance', *Plant Cell*, 9: 1573-84.

Bowling, S. A., A. Guo, H. Cao, A. S. Gordon, D. F. Klessig, and X. I. Dong. 1994. 'A mutation in Arabidopsis that leads to constitutive expression of systemic acquired-resistance ', *Plant Cell*, 6: 1845-57.

Burian, A., M. Raczynska-Szajgin, D. Borowska-Wykret, A. Piatek, M. Aida, and D. Kwiatkowska. 2015. 'The *CUP-SHAPED COTYLEDON2* and *3* genes have a post-meristematic effect on *Arabidopsis thaliana* phyllotaxis', *Annals of Botany*, 115: 807-20.

Byrne, M. E., A. T. Groover, J. R. Fontana, and R. A. Martienssen. 2003. 'Phyllotactic pattern and stem cell fate are determined by the Arabidopsis homeobox gene *BELLRINGER*', *Development*, 130: 3941-50.

Cao, H., S. A. Bowling, A. S. Gordon, and X. N. Dong. 1994. 'Characterization of an Arabidopsis mutant that is nonresponsive to inducers of systemic acquired-resistance', *Plant Cell*, 6: 1583-92.

Castel, B., P. M. Ngou, V. Cevik, A. Redkar, D. S. Kim, Y. Yang, P. T. Ding, and J. D. G. Jones. 2019. 'Diverse NLR immune receptors activate defence via the RPW8-NLR NRG1', *New Phytologist*, 222: 966-80.

Chickarmane, V. S., S. P. Gordon, P. T. Tarr, M. G. Heisler, and E. M. Meyerowitz. 2012. 'Cytokinin signaling as a positional cue for patterning the apical-basal axis of the growing Arabidopsis shoot meristem', *PNAS*, 109: 4002-07.

Choi, J., S. U. Huh, M. Kojima, H. Sakakibara, K. H. Paek, and I. Hwang. 2010. 'The cytokinin-activated transcription factor ARR2 promotes plant immunity via TGA3/NPR1-dependent salicylic acid signaling in Arabidopsis', *Developmental Cell*, 19: 284-95.

Clarke, J. D., Y. D. Liu, D. F. Klessig, and X. N. Dong. 1998. 'Uncoupling *PR* gene expression from NPR1 and bacterial resistance: Characterization of the dominant Arabidopsis *cpr6-1* mutant', *Plant Cell*, 10: 557-69.

Clarke, J. D., S. M. Volko, H. Ledford, F. M. Ausubel, and X. N. Dong. 2000. 'Roles of salicylic acid, jasmonic acid, and ethylene in *cpr*-induced resistance in Arabidopsis', *Plant Cell*, 12: 2175-90.

Deng, W. L., G. Preston, A. Collmer, C. J. Chang, and H. C. Huang. 1998. 'Characterization of the hrpC and hrpRS operons of *Pseudomonas syringae* pathovars *syringae*, *tomato*, and *glycinea* and analysis of the ability of hrpF, hrpG, hrcC, hrpT, and hrpV mutants to elicit the hypersensitive response and disease in plants', *Journal of Bacteriology*, 180: 4523-31.

Dewdney, J., T. L. Reuber, M. C. Wildermuth, A. Devoto, J. P. Cui, L. M. Stutius, E. P. Drummond, and F. M. Ausubel. 2000. 'Three unique mutants of Arabidopsis identify eds loci required for limiting growth of a biotrophic fungal pathogen', *Plant Journal*, 24: 205-18.

Dietrich, R. A., T. P. Delaney, S. J. Uknes, E. R. Ward, J. A. Ryals, and J. L. Dangl. 1994. 'Arabidopsis mutants simulating disease resistance response', *Cell*, 77: 565-77.

Dietrich, R. A., M. H. Richberg, R. Schmidt, C. Dean, and J. L. Dangl. 1997. 'A novel zinc finger protein is encoded by the Arabidopsis *LSD1* gene and functions as a negative regulator of plant cell death', *Cell*, 88: 685-94.

Gaillochet, C., and J. U. Lohmann. 2015. 'The never-ending story: from pluripotency to plant developmental plasticity', *Development*, 142: 2237-49.

Gallois, J. L., C. Woodward, G. V. Reddy, and R. Sablowski. 2002. 'Combined *SHOOT MERISTEMLESS* and *WUSCHEL* trigger ectopic organogenesis in Arabidopsis', *Development*, 129: 3207-17.

Glazebrook, J. 2005. 'Contrasting mechanisms of defense against biotrophic and necrotrophic pathogens', *Annual Review of Phytopathology*, 43: 205-27.

Goldshmidt, A., J. P. Alvarez, J. L. Bowman, and Y. Eshed. 2008. 'Signals derived from *YABBY* gene activities in organ primordia regulate growth and partitioning of Arabidopsis shoot apical meristems', *Plant Cell*, 20: 1217-30.

Gordon, S. P., V. S. Chickarmane, C. Ohno, and E. M. Meyerowitz. 2009. 'Multiple feedback loops through cytokinin signaling control stem cell number within the Arabidopsis shoot meristem', *PNAS*, 106: 16529-34.

Gruel, J., B. Landrein, P. Tarr, C. Schuster, Y. Refahi, A. Sampathkumar, O. Hamant, E. M. Meyerowitz, and H. Jonsson. 2016. 'An epidermis-driven mechanism positions and scales stem cell niches in plants', *Science Advances*, 2.

Guedon, Y., Y. Refahi, F. Besnard, E. Farcot, C. Godin, and T. Vernoux. 2013. 'Pattern identification and characterization reveal permutations of organs as a key genetically controlled property of post-meristematic phyllotaxis', *Journal of Theoretical Biology*, 338: 94-110.

Heidel, A. J., J. D. Clarke, J. Antonovics, and X. N. Dong. 2004. 'Fitness costs of mutations affecting the systemic acquired resistance pathway in *Arabidopsis thaliana*', *Genetics*, 168: 2197-206.

Higuchi, M., M. S. Pischke, A. P. Mahonen, K. Miyawaki, Y. Hashimoto, M. Seki, M. Kobayashi, K. Shinozaki, T. Kato, S. Tabata, Y. Helariutta, M. R. Sussman, and T. Kakimoto. 2004. 'In planta functions of the Arabidopsis cytokinin receptor family', *PNAS*, 101: 8821-26.

Igari, K., S. Endo, K. Hibara, M. Aida, H. Sakakibara, T. Kawasaki, and M. Tasaka. 2008. 'Constitutive activation of a CC-NB-LRR protein alters morphogenesis through the cytokinin pathway in Arabidopsis', *Plant Journal*, 55: 14-27.

Jiang, C. J., X. L. Liu, X. Q. Liu, H. Zhang, Y. J. Yu, and Z. W. Liang. 2017. 'Stunted growth caused by blast disease in rice seedlings is associated with changes in phytohormone signaling pathways', *Frontiers in Plant Science*, 8.

Jones, J. D. G., and J. L. Dangl. 2006. 'The plant immune system', *Nature*, 444: 323-29.

Kim, M. G., X. Q. Geng, S. Y. Lee, and D. Mackey. 2009. 'The *Pseudomonas syringae* type III effector AvrRpm1 induces significant defenses by activating the Arabidopsis nucleotide-binding leucine-rich repeat protein RPS2', *Plant Journal*, 57: 645-53.

Korves, T. M., and J. Bergelson. 2003. 'A developmental response to pathogen infection in Arabidopsis', *Plant Physiology*, 133: 339-47.

Kuhlemeier, C. 2017. 'Phyllotaxis', *Current Biology*, 27: R882-R87.

Kyozuka, J. 2007. 'Control of shoot and root meristem function by cytokinin', *Current Opinion in Plant Biology*, 10: 442-46.

Landrein, B., R. Lathe, M. Bringmann, C. Vouillot, A. Ivakov, A. Boudaoud, S. Persson, and O. Hamant. 2013. 'Impaired cellulose synthase guidance leads to stem torsion and twists phyllotactic patterns in Arabidopsis', *Current Biology*, 23: 895-900.

Landrein, B., Y. Refahi, F. Besnard, N. Hervieux, V. Mirabet, A. Boudaoud, T. Vernoux, and O. Hamant. 2015. 'Meristem size contributes to the robustness of phyllotaxis in Arabidopsis', *Journal of Experimental Botany*, 66: 1317-24.

Li, X., J. D. Clarke, Y. L. Zhang, and X. N. Dong. 2001. 'Activation of an EDS1-mediated *R*-gene pathway in the *snc1* mutant leads to constitutive, NPR1-independent pathogen resistance', *MPMI*, 14: 1131-39.

Li, Y. G., Y. H. Yang, Y. L. Hu, H. L. Liu, M. He, Z. Y. Yang, F. J. Kong, X. Liu, and X. L. Hou. 2019. 'DELLA and EDS1 form a feedback regulatory module to fine-tune plant growth-defense tradeoff in Arabidopsis', *Molecular Plant*, 12: 1485-98.

MacLean, A. M., Z. Orlovskis, K. Kowitwanich, A. M. Zdziarska, G. C. Angenent, R. G. H. Immink, and S. A. Hogenhout. 2014. 'Phytoplasma effector SAP54 hijacks plant reproduction by degrading MADS-box proteins and promotes insect colonization in a RAD23-dependent manner', *PLOS Biology*, 12.

Mandel, T., F. Moreau, Y. Kutsher, J. C. Fletcher, C. C. Carles, and L. E. Williams. 2014. 'The ERECTA receptor kinase regulates Arabidopsis shoot apical meristem size, phyllotaxy and floral meristem identity', *Development*, 141: 830-41.

Meng, Z., C. Ruberti, Z. Z. Gong, and F. Brandizzi. 2017. 'CPR5 modulates salicylic acid and the unfolded protein response to manage tradeoffs between plant growth and stress responses', *Plant Journal*, 89: 486-501.

Mirabet, V., F. Besnard, T. Vernoux, and A. Boudaoud. 2012. 'Noise and robustness in phyllotaxis', *Plos Computational Biology*, 8.

Naseem, M., N. Philippi, A. Hussain, G. Wangorsch, N. Ahmed, and T. Dandekar. 2012. 'Integrated systems view on networking by hormones in Arabidopsis immunity reveals multiple crosstalk for cytokinin', *Plant Cell*, 24: 1793-814.

Ngou, B. P. M., H. K. Ahn, P. T. Ding, and J. D. G. Jones. 2021. 'Mutual potentiation of plant immunity by cell-surface and intracellular receptors', *Nature*, 592: 110-+.

Pasternak, T., E. P. Groot, F. V. Kazantsev, W. Teale, N. Omelyanchuk, V. Kovrizhnykh, K. Palme, and V. V. Mironova. 2019. 'Salicylic acid affects root meristem patterning via auxin distribution in a concentration-dependent manner', *Plant Physiology*, 180: 1725-39.

Peaucelle, A., and P. Laufs. 2007. 'Phyllotaxy beyond the meristem and auxin comes the miRNA', *Plant Signaling & Behavior*, 2: 293-95.

Peaucelle, A., H. Morin, J. Traas, and P. Laufs. 2007. 'Plants expressing a miR164-resistant *CUC2* gene reveal the importance of post-meristematic maintenance of phyllotaxy in Arabidopsis', *Development*, 134: 1045-50.

Pecher, P., G. Moro, M. C. Canale, S. Capdevielle, A. Singh, A. MacLean, A. Sugio, C. H. Kuo, J. R. S. Lopes, and S. A. Hogenhout. 2019. 'Phytoplasma SAP11 effector destabilization of TCP transcription factors differentially impact development and defence of Arabidopsis versus maize', *PLOS Pathogens*, 15.

Reddy, G. V., M. G. Heisler, D. W. Ehrhardt, and E. M. Meyerowitz. 2004. 'Real-time lineage analysis reveals oriented cell divisions associated with morphogenesis at the shoot apex of *Arabidopsis thaliana*', *Development*, 131: 4225-37.

Schindelin, Johannes, Ignacio Arganda-Carreras, Erwin Frise, Verena Kaynig, Mark Longair, Tobias Pietzsch, Stephan Preibisch, Curtis Rueden, Stephan Saalfeld, Benjamin Schmid, Jean-Yves Tinevez, Daniel James White, Volker Hartenstein, Kevin Eliceiri, Pavel Tomancak, and Albert Cardona. 2012. 'Fiji: an open-source platform for biological-image analysis', *Nature Methods*, 9: 676-82.

Smyth, D. R., J. L. Bowman, and E. M. Meyerowitz. 1990. 'Early flower development in Arabidopsis', *Plant Cell*, 2: 755-67.

Szczesny, T., A. L. Routier-Kierzkowska, and D. Kwiatkowska. 2009. 'Influence of *clavata3-2* mutation on early flower development in Arabidopsis thaliana: quantitative analysis of changing geometry', *Journal of Experimental Botany*, 60: 679-95.

Talbot, M. J., and R. G. White. 2013. 'Methanol fixation of plant tissue for scanning electron microscopy improves preservation of tissue morphology and dimensions', *Plant Methods*, 9.

Tsuda, K., M. Sato, J. Glazebrook, J. D. Cohen, and F. Katagiri. 2008. 'Interplay between MAMP-triggered and SA-mediated defense responses', *Plant Journal*, 53: 763-75.

van Wersch, R., X. Li, and Y. L. Zhang. 2016. 'Mighty dwarfs: Arabidopsis autoimmune mutants and their usages in genetic dissection of plant immunity', *Frontiers in Plant Science*, 7.

Vernoux, T., G. Brunoud, E. Farcot, V. Morin, H. Van den Daele, J. Legrand, M. Oliva, P. Das, A. Larrieu, D. Wells, Y. Guedon, L. Armitage, F. Picard, S. Guyomarc'h, C. Cellier, G. Parry, R. Koumproglou, J. H. Doonan, M. Estelle, C. Godin, S. Kepinski, M. Bennett, L. De Veylder, and J. Traas. 2011. 'The auxin signalling network translates dynamic input into robust patterning at the shoot apex', *Molecular Systems Biology*, 7.

Wu, H. J., X. Y. Qu, Z. C. Dong, L. J. Luo, C. Shao, J. Forner, J. U. Lohmann, M. Su, M. C. Xu, X. B. Liu, L. Zhu, J. Zeng, S. M. Liu, Z. X. Tian, and Z. Zhao. 2020. 'WUSCHEL triggers innate antiviral immunity in plant stem cells', *Science*, 370: 227-+.

Yang, F., H. T. Bui, M. Pautler, V. Llaca, R. Johnston, B. H. Lee, A. Kolbe, H. Sakai, and D. Jackson. 2015. 'A maize glutaredoxin gene, *Abphyl2*, regulates shoot meristem size and phyllotaxy', *Plant Cell*, 27: 121-31.

Yao, Jian, John Withers, and Sheng Yang He. 2013. '*Pseudomonas syringae* infection assays in Arabidopsis.' in Alain Goossens and Laurens Pauwels (eds.), *Jasmonate Signaling: Methods and Protocols* (Humana Press: Totowa, NJ).

Yuan, M. H., Z. Y. Jiang, G. Z. Bi, K. Nomura, M. H. Liu, Y. P. Wang, B. Y. Cai, J. M. Zhou, S. Y. He, and X. F. Xin. 2021. 'Pattern-recognition receptors are required for NLR-mediated plant immunity', *Nature*, 592: 105-+.

Yuan, M. H., B. P. M. Ngou, P. T. Ding, and X. Xiu-Fan. 2021. 'PTI-ETI crosstalk: an integrative view of plant immunity', *Current Opinion in Plant Biology*, 62.

Zhang, Y. L., S. Goritschnig, X. N. Dong, and X. Li. 2003. 'A gain-of-function mutation in a plant disease resistance gene leads to constitutive activation of downstream signal transduction pathways in *suppressor of npr1-1, constitutive 1*', *Plant Cell*, 15: 2636-46.

Zhao, Z., S. U. Andersen, K. Ljung, K. Dolezal, A. Miotk, S. J. Schultheiss, and J. U. Lohmann. 2010. 'Hormonal control of the shoot stem-cell niche', *Nature*, 465: 1089-U154.

CHAPTER 4

Spatiotemporal distribution of phytohormones in *Solanum lycopersicum* cv. Micro-Tom[4]

4.1 SUMMARY

Hormones have been widely characterized in *Arabidopsis thaliana* (hereafter Arabidopsis)*;* however, Arabidopsis is not a useful system in studying some physiological processes such as fleshy fruit development. *Solanum lycopersicum* cv. Micro-Tom (hereafter Micro-Tom) is a useful model to study fleshy fruit development as the genome has been fully sequenced and annotated, the plants are relatively small, can be grown close together, and many hormone mutations and transgenic lines have been introgressed in the Micro-Tom background. In this study, I collected above- and below-ground tissues from Micro-Tom plants to evaluate hormone abundance at multiple stages of plant development. Using a single-phase hormone extraction protocol that was previously developed by the Proteomics and Metabolomics Facility at Colorado State University, extracts from Micro-Tom samples were simultaneously quantified by selected reaction monitoring (SRM) mass spectrometry. Of the eighteen hormone species in five of the nine plant hormone families, we selected four to six important hormones based on concentration and previous studies to describe hormonal role at each stage of Micro-Tom development.

4.2 INTRODUCITON

Tomato is a vegetable crop of considerable importance to US agriculture as one of the top three vegetables in terms of area harvested and total production, reaching nearly $2 billion in sales (USDA 2022). Many resources have been established in tomatoes including a fully

[4] Data from this chapter will be used for a future publication with the following authors: Hannah M. Berry, Grace A. Johnston, and Cristiana T. Argueso.

sequenced and annotated genome (The Tomato Genome 2012), protocols for functional genomics (Saito et al. 2009; Sahu et al. 2012; Okabe et al. 2011; Matsukura et al. 2008), and extensive germplasm collections ('The C. M. Rick Tomato Genetics Resource Center'), making it a valuable model species for research. In particular, Micro-Tom is of particularly useful for addressing research questions as these plants are small, they can be grown in close proximity to one another, they have a relatively short life cycle, the fruits turn red during ripening, and many hormone mutations have been introgressed into the background (Dan, Fei, and Rothan 2007; Campos et al. 2010; Carvalho et al. 2011).

Plant hormones are essential integrators of responses to biotic and abiotic signals through the regulation of important physiological processes (Davies 2010). Many plant hormones have been recognized and characterized for quite some time including auxins, cytokinins (CKs), ethylene, gibberellic acid (GA), and abscisic acid (ABA), while additional hormones have been identified more recently including salicylic acid (SA), jasmonic acid (JA), brassinosteroids (BRs), and strigolactones (SLs). As major regulators of plant processes ranging from plant development to defense, the molecular mechanisms for hormone perception, signaling, and crosstalk with other hormones has been a focus in the hormone biology field, with major progress made in recent years (Durbak, Yao, and McSteen 2012; Santner and Estelle 2009). Most of these studies have been done in Arabidopsis, however, Arabidopsis is not an adequate system for studying all plant physiological processes. In particular, Arabidopsis, does not produce fleshy fruits, and therefore cannot be used to address plant processes that regulate fleshy fruit development. With the tools available in Micro-Tom, it is an ideal tool to evaluate hormone signaling in a model crop species.

An important aspect of plant hormone biology is the accurate quantification of plant hormone species. The distribution of hormones within tomato fruit tissues is essential in each stage of fruit development. While the roles hormones play throughout tomato plant and fruit development have been characterized to some extent, data has been limited to a few hormones

at a time (de Jong et al. 2011), due to the lack of technologies to properly address these questions in a comprehensive manner. Methods for extraction of multiple hormone species in a single protocol have been developed (Pan, Welti, and Wang 2010), however, these protocols are still limited as focus has been on acidic hormones, and therefore do not represent a complete panel of the major classes of plant hormone species. Additionally, their use is typically demonstrated on tissues from a single growth stage (Muller, Duchting, and Weiler 2002; Kojima et al. 2009; Balcke et al. 2012; Van Meulebroek et al. 2012; Simura et al. 2018), a limited number of tissue types (i.e. leaves and roots) (Forcat et al. 2008; Trapp et al. 2014; Sheflin et al. 2019), or are optimized for one to two hormone families (Novak et al. 2008; Liang et al. 2012; Dobrev, Hoyerova, and Petrasek 2017). Only a single paper has addressed phytohormone distribution throughout development of rice (Cai et al. 2016). Rice is a model species in plant biology and this study provides valuable insight into hormonal regulation at multiple stages of plant development, however, like Arabidopsis, this is not an adequate system to address fleshy fruit development. Furthermore, rice is a monocot, and hormones have been shown to play different roles in plant immunity and development compared to dicot species including Arabidopsis and tomato (Yang, Yang, and He 2013; De Vleesschauwer, Xu, and Höfte 2014).

Here, we have used a method developed by the Proteomics and Metabolomics Facility (PMF) at Colorado State University to quantify eighteen hormone species from five of the major hormone classes using a single extraction protocol (Sheflin et al. 2019). While previous studies have shown the validity of using a single extraction protocol to quantify a variety of plant hormones, we show that a single method can be used across a diverse range of plant tissues including roots, leaves, stems, flowers, and fruits. Our focus on hormone quantification of above- and below-ground plant tissues has resulted in a data set providing valuable insight into hormone localization across multiple Micro-Tom developmental stages. We have used these data to evaluate hormones that play a major role at each developmental stage and to establish

the Plant Hormone Atlas, a web-based tool that will be available to plant researchers through The Bio-Array Resource for Plant Biology.

4.3 METHODS

Plant growth conditions

Plants were grown in long-day conditions, with a photoperiod of 16:8 hour day:night, in a controlled environment greenhouse. Temperature, relative humidity, and light were monitored using an Onset HOBO data logger (Table 4.1). Two-week old seedlings were transplanted to individual gallon-sized pots and randomized across the bench. Plants were randomly assigned to each developmental stage for tissue collection. All pots were watered daily at 10 am on a drip irrigation system.

Tissue collection

Plants were randomized across the greenhouse bench and randomly assigned to a developmental stage before sample collection. All plant tissues for hormone quantification were collected between 12 and 2 pm. Harvested tissue was weighted, flash frozen in liquid nitrogen, and stored at -80°C until lyophilization and hormone extraction.

Seedling tissue was collected and pooled from 15-20 individuals for each sample before the first appearance of true leaves, 14 days post germination (dpg). Seedlings were removed from soil, roots gently washed in cool water, and cotyledons, hypocotyls, and roots were separated using a sterile blade.

One plant was used to collect pairs of tissue types for the young developmental stage (i.e., the tap and lateral roots were collected from one plant, first leaf and first stem were collected from a second plant, etc.). Plants were carefully removed from gallon pots and roots

gently washed in a bucket of water for all root samples. Young plant tissue was collected from plants with 4 leaves, before the development of flower buds, 4-5 weeks post germination.

A single plant was used to collect each tissue type for the adult and fruiting developmental stages. Adult plant tissue was collected the day after the first flower opened, 6-7 weeks post germination. Fruiting tissue was collected according to fruit size, 10 to 12 weeks after germination. Whole immature fruits were collected with diameters 0.5-0.9 cm, 1.0-1.4 cm, and 1.5-1.9 cm. Pericarp, placenta, and seed and locular tissue was collected from fully expanded green fruits exceeding 2 cm in diameter; breaker fruits, just as color began to change; and ripe fruits, 10-days post breaker stage.

Phytohormone extraction and quantification

Five technical replicates for each tissue type were prepared by adding 10-20 mg lyophilized tissue to 2 mL polypropylene tubes. Tissue samples with less than 10 mg of tissue, including youngest leaves and youngest stems, were pooled to reach appropriate tissue amounts. Lyophilized tissue was homogenized using 3 mm round stainless-steel beads using a Qiagen TissueLyser II (Qiagen). Phytohormone internal standards (IS), extraction methods, detection parameters, and quantification calculations were performed as previously described (Sheflin et al. 2019).

Data Analysis

Skyline software (Version 19.1.0.193, MacCoss Lab, Department of Genome Sciences, University of Washington) (MacLean et al. 2010) was used to identify and calculate peak areas of internal standards used for quantification. Each sample peak was normalized to the appropriate IS. Data was analyzed using Excel to calculate the linear regression of the analytical standards and used for quantification (ng/mL) of each phytohormone and adjusted for sample weight (ng/g Dry Weight, DW).

The limit of detection (LOD) is defined as the concentration where signal intensity is 3 times that of the noise. The limit of quantification (LOQ) is the concentration where signal intensity is 10 times the noise. Values below the LOD were excluded from the data analysis. LOD and LOQ values for each hormone are listed in Table 4.2.

4.4 RESULTS

Hormone Quantification from Solanum lycopersicon cv. Micro-Tom

Eighteen hormone species from five of the major hormone classes were quantified throughout tomato plant development. The quantified hormones were as follows: ABA and ABA catabolites phaseic acid (PA) and dihydrophaseic acid (DPA); auxins indole-3-acetic acid (IAA), indole-3-acetamide (IAmide), indole-3-acetylnitrile (IAnitrile), indole-3-acetyl alanine (IA-alanine), indole-3-butyric acid (IBA), indole-3-acrylic acid (IAcrA), and indole-3-carboxyclic acid (ICA); CKs *trans*-zeatin (*t*Z) and *trans*-zeatin riboside (*t*Z-R); JA, (+)-7-*iso*-jasmonoyl-L-isoleucine (JA-Ile), methyl-Jasmonic Acid (meJA), and JA precursor 12-oxo-phytodienoic acid (OPDA); SA and methyl SA (meSA).

To visualize hormone abundance between tissues within each developmental stage, the quantified hormones were presented in stacked bar charts (Figure 4.1A-D) and as heat maps for each hormone (Figure 4.2). This representation showed that the bioactive JA derivative JA-Ile was highly abundant in all tissue types at each developmental stage. JA is commonly associated with defense responses but also plays a role in plant development in young plant tissues and in flower and pollen development (Creelman and Mullet 1995). JA-Ile has also been shown to be a negative regulator of Arabidopsis seed dormancy (Singh et al. 2017). It was therefore not surprising to see that some of the lowest concentrations of JA-Ile to be present in developing tomato fruits (Figure 4.2). Based on the relative abundance in the stacked bar charts (Figure 4.1A-D) and heat maps (Figure 4.2), hormones of interest were selected for further description at each developmental stage.

The seedling developmental stage is characterized by high levels of growth-related hormones

Micro-Tom seedling tissue was collected 14 dpg, just before the true leaves appeared (Figure 4.3A). Cotyledons, hypocotyls, and roots were separated and pooled into 5 biological replicates for quantification. Phytohormone quantification revealed all auxin species were present and quantifiable in all seedling tissues, with notable patterns in biologically active IAA (Figure 4.4). The highest level of IAA was found in roots (12.48 ng/g DW) and lowest in cotyledons (5.74 ng/g DW) (Figure 4.3B). Previously, IAA quantification from pea seedlings showed the same pattern with highest levels in root tissue, followed by hypocotyl and cotyledon tissues (Schneider, Kazakoff, and Wightman 1985). Because of the importance of IAA in developing seedling tissues, these data were incorporated into a biological illustration of the seedling with a darker green color representing higher concentrations of IAA in each of the quantified tissues (Figure 4.3C). The IAA precursor and storage form IBA is required to fuel seedling growth and cell expansion in seedling development (Strader et al. 2011). Appropriate levels of IBA and IAA act together to regulate development of cotyledon vasculature, root cell expansion and length, and root meristem size (Strader et al. 2011). In tomato seedlings, IBA was present at highest levels in hypocotyl tissue (53.54 ng/g DW) and lowest in cotyledons (16.11 ng/g DW) (Figure 4.1B). This balance of IAA and IBA in tomato seedling tissues likely promotes normal seedling development.

In addition to auxins, ABA was also present in seedling tissues contributing to seedling development (Figure 4.4). ABA is known to play a major role in abiotic stress responses, and through hormone crosstalk, acts in biotic defense responses (Shigenaga and Argueso 2016), however, knowledge of the role of ABA during unstressed plant growth and development is limited (Nambara and Marion-Poll 2005). Notably, ABA has been shown to antagonize the effects of GA, including during the promotion of seedling growth (Cutler et al. 2010). In tomato seedling tissues, the highest levels of ABA were found in cotyledons (200.64 ng/g DW) and lowest in roots (49.28 ng/g DW) (Figure 4.3B). Previous studies have shown that ABA is

synthesized in leaf tissue, and synthesis is robustly upregulated during drought stress as ABA is associated with regulating stomatal closure (Ikegami et al. 2009). The *notabilis* (*not*) tomato mutant is deficient in an enzyme critical for ABA biosynthesis resulting in a wilted phenotype as these plants are unable to regulate stomatal closure and retain water (Burbidge et al. 1999). It is possible that in developing Micro-Tom seedlings there are relatively high concentrations of ABA to retain water at this vulnerable developmental stage.

JA is most notably responsible for plant defense responses to necrotrophic pathogens and insect herbivory (Shigenaga and Argueso 2016), but also plays a role in plant growth and development (Creelman and Mullet 1995; Santino et al. 2013). Biologically active JA-Ile was present at high levels in all Micro-Tom seedling tissues (Figure 4.3B). In a previous study with soybean seedlings, the precursors to JA-Ile, JA and MeJA, levels were found to be highest in the youngest tissues, particularly in the hypocotyl hook (Creelman and Mullet 1995). In tomato seedlings, JA-Ile was present in highest levels in roots. While JA has previously been shown to be lowest in roots as a whole, the root tips do have higher quantities of JA (Creelman and Mullet 1995). Due to the small size of tomato seedling roots, the higher level of JA-Ile in root tissue may be a result of the increased ratio of root tip to total root in these samples.

Characterization of hormones during vegetative plant growth show high concentrations of growth-related hormones

Micro-Tom young plants were defined at the 4-leaf stage where the first leaf was fully expanded, between 4.8 and 5.6 cm, and the fourth leaf was between 3.9 and 5.1 cm in length, 4-5 weeks post germination (Figure 4.5A). Hormone quantification at the 4-leaf stage shows notable patterns in CKs *t*Z and *t*Z-R; SA, and MeJA (Figure 4.6).

SA is most commonly associated with plant immune responses to biotrophic pathogens and abiotic stressors (Shigenaga and Argueso 2016). Some studies have also shown SA to play a role in plant development with impacts on seed germination and flower development

(Shigenaga and Argueso 2016). Highest levels of SA were present in younger stem tissues 3 and 4 with concentrations of 1034.93 and 1933.06 ng/g DW, respectively, while SA was present at a lower concentration in all leaf tissues and decreasing with increased leaf age (Figure 4.5B). Additionally, SA is found in relatively high concentrations in tap and lateral roots 717.24 ng/g DW and 645.08 ng/g DW, respectively (Figure 4.5B). These data suggest that elevated concentrations of SA may plays a role in regulating plant development in younger shoot tissues and roots.

The precursor to JA-Ile, MeJA, is a volatile compound that acts as a signaling molecule in plant immunity to necrotrophic pathogens (Shigenaga and Argueso 2016). In vegetative Micro-Tom tissues, meJA gradually increased inversely to age in stem tissues and had a maximum concentration of 27.79 ng/g DW in stem 3 and 27.65 ng/g DW in stem 4 (Figure 4.5B). In roots and leaf tissues, meJA concentrations were relatively consistent and considerably lower than in stems, suggesting that meJA plays a larger role in stems than in roots and leaves at this developmental stage (Figure 4.5B). Research shows that JA is highest in tissues that are rapidly growing (Creelman and Mullet 1995), it is therefore not surprising to see the highest concentrations of meJA in areas of high growth such as young stems.

The most abundant and active form of CK in Arabidopsis is *t*Z, followed by isopentenyl adenine (iP) (Kieber and Schaller 2014; Kiba et al. 2013; Osugi et al. 2017). In vegetative tomato plants, *t*Z was most abundant in younger stem tissues and roots (Figure 4.5B). In stem 3, just below the third leaf, *t*Z concentration was highest (59.08 ng/g DW), followed by stem 4, just under the fourth leaf (27.76 ng/g DW) (Figure 4.5B). In root tissues, *t*Z was highest in the tap root (32.882 ng/g DW) (Figure 4.5B). In vegetative tomato plants, *t*ZR was most present in young stem tissues (95.81 ng/g DW, stem 4) and roots (65.58 ng/g DW in tap roots and 87.50 ng/g DW in lateral roots) (Figure 4.5B). It was initially thought that CKs were synthesized in roots and transported to shoots, however, more recent work has shown that cytokinins are synthesized throughout the plant and long distance transport of *t*ZR occurs through the xylem

(Kieber and Schaller 2014). Additionally, *t*ZR accumulates in roots after nitrate treatment, suggesting *t*ZR may be responsible for nutrient signaling shootward to coordinate plant development (Kieber and Schaller 2014). Because of the known transport of *t*ZR and association with plant growth and development, *t*ZR data was integrated into a biological illustration of a young Micro-Tom plant, where a darker yellow-orange color was associated with increased *t*ZR content in each tissue type collected (Figure 4.5C).

Hormones associated with the transition to reproductive development are present in higher concentrations in flowering Micro-Tom plants

The transition from vegetative growth to flowering marks a pivotal time in plant development and is associated with large changes in transcription and metabolism (Molinero-Rosales et al. 2004). While more is known about regulatory mechanisms that play a role in the floral transition of Arabidopsis, considerably less is known about the transition to reproductive development in tomatoes (Molinero-Rosales et al. 2004). Micro-Tom tissue collected during this stage occurred the day after the first flower opened, 6-7 weeks post germination (Figure 4.7A). These plants had between 6 to 7 leaves per plant and were between 9 and 10 cm in height at the time of tissue collection (Figure 4.9A-B). In addition to root, stem, and leaf tissue, developing flower buds at three stages defined by bud size (A: 0.2-0.5 cm; B: 0.6-0.7 cm; and C: 0.8 cm), and fully opened flowers were collected for hormone quantification (Figure 4.7A). In these data, SA, JA, ABA, DPA, IAnitrile, and IBA were selected for further analysis (Figure 4.7B, Figure 4.8).

Some research has shown the importance of SA in regulating flowering in Arabidopsis (Martinez et al. 2004). Though direct mechanisms are not known, SA likely integrates environmental cues to initiate the floral transition (Martinez et al. 2004). SA was highest in young leaf tissue (440.29 ng/g DW) with elevated levels in all tissues collected (Figure 4.7B). Because of the link to floral transition, SA data was used to color a Micro-Tom illustration at this

developmental stage where a darker teal color corresponded to increased SA concentration (Figure 4.7C).

In plant development, JA plays a large role in plant fertility, filament elongation, pollen viability, flower development, and fruit ripening (Browse 2009; Santino et al. 2013). In Arabidopsis, high levels of JA-dependent defense response genes are expressed in reproductive tissues, likely as a preventative measure against insect herbivory or pathogen attack (Browse 2009). JA mutations in Arabidopsis are commonly associated with decreased pollen development and are male sterile (Feys et al. 1994; Sanders et al. 1999; Sanders et al. 2000; Stintzi and Browse 2000). In tomatoes, however, mutations in JA signaling are female sterile, and pollen viability is reduced compared to wild-type (Li et al. 2004; Browse 2009). Fruit does develop after pollination in JA signaling tomato mutants, but the fruits are significantly smaller with undeveloped seeds, indicating JA signaling plays a critical role in reproductive development in tomatoes (Li et al. 2004). Quantification data showed JA was present uniformly in all tissues of adult Micro-Tom plants ranging from 5.05 ng/g DW in lateral roots to 10.59 ng/g DW in oldest stems (Figure 4.7B).

While ABA is most commonly associated with responses to abiotic stressors, ABA and an ABA catabolism product, DPA, are also involved in plant developmental processes such as bud and seed dormancy, leaf senescence, stomatal opening regulation, and stress responses to abiotic stimuli (Fedoroff 2002). ABA concentrations were highest in adult young stems (83.90 ng.g DW) (Figure 4.7B). ABA is biosynthesized in plastids of leaf tissues and is transported to the roots (Ikegami et al. 2009). It is possible that the highest concentrations of ABA were found in the youngest stems of adult Micro-Tom if ABA was actively being transported to the roots through the vasculature system. As these stem sections were small, the relative abundance of ABA may be artificially high during ABA transport in comparison to sites of ABA biosynthesis. DPA was highest in adult young leaves (72.73 ng/g DW) (Figure 4.7B). ABA crosstalk with other plant hormones promotes defense responses to abiotic and biotic stimuli, and negatively

regulate growth processes including those associated with GA (Cutler et al. 2010). Therefore, it is possible that as ABA is being produced in leaves, it is also being rapidly degraded in favor of Micro-Tom development.

The role of auxins throughout plant growth and development have been widely characterized and reviewed (Benjamins and Scheres 2008; Mockaitis and Estelle 2008; Chapman and Estelle 2009; Zhao 2010; Korasick, Enders, and Strader 2013). The pool of biologically active IAA is relatively small in comparison to auxins in inactive precursors, including IBA, and auxin conjugates (Korasick, Enders, and Strader 2013). In the adult Micro-Tom stage, IAnitrile and IBA were selected due to their relative abundance at this stage (Figure 4.7B). Previous studies have shown that concentrations of IAA were elevated in immature tomato ovaries but decreased during anthesis and increased again after pollination (Matsuo et al. 2018). Here, IAnitrile concentrations were highest in adult old leaves and flower buds B (70.84 ng/g DW and 70.59 ng/g DW, respectively) (Figure 4.7B). Similarly, IBA concentrations were highest in old leaves (18.32 ng/g DW) (Figure 4.7B). As a biologically inactive precursors to IAA, the pattern of IAnitrile in developing flower buds reflect the pattern of IAA, just before the flower opens.

CK, auxin, and ABA are found in high concentrations in fruit tissues of fruiting Micro-Tom plants

The role of phytohormones in tomato fruit development has been shown to be dependent on crosstalk between ethylene, auxin, GA, ABA, and CKs (Gillaspy, Bendavid, and Gruissem 1993; Srivastava and Handa 2005; McAtee et al. 2013; Kou et al. 2021). Old and young leaf tissues were collected from fruiting Micro-Tom plants, approximately 10 weeks after germination (Figure 4.10A). A single plant was used to collect each tissue sample. Fruits at multiple stages of rapid growth were characterized based on fruit diameter (Figure 4.10A). Rapidly expanding whole fruit were collected for hormone extraction and quantification at the following sizes: whole fruit A 0.5-0.9 cm; whole fruit B 1-1.4 cm; and whole fruit C 1.5-1.9 cm

(Figure 4.10A). At the end of the rapid growth phase, green fruits exceeding a diameter of 2 cm were collected for green fruit tissues where placenta, seed and locular tissue, and pericarp were collected separately (Figure 4.10A). At the onset of fruit ripening, breaker stage fruits were collected, and 10 days post breaker stage, ripe fruits were harvested (Figure 4.10A). As with the green fruit, breaker and ripe fruit tissues were separated prior to hormone extraction. In our data, we identified *t*ZR, IAA, IAcn, and ABA to be of interest and further discussion (Figure 4.10B, Figure 4.11).

CK is a critical hormone in regulating tomato fruit development (Gillaspy, Bendavid, and Gruissem 1993). High concentrations of CK are associated with appropriate development of seeds and for cell division in surrounding tissues (Gillaspy, Bendavid, and Gruissem 1993). In this study, the highest concentrations of *t*-ZR were in green seed and locular tissue (18.26 ng/g DW) (Figure 4.10B). Previous data shows that the highest concentrations of CK were found in developing seeds with little being found in the pericarp (Abdelrahman 1977; Bohner and Bangerth 1988), supporting our findings.

In plant growth, ABA is most commonly associated with maintaining seed dormancy and inhibiting germination, though ABA does promote embryo growth in early embryogenesis (Nambara and Marion-Poll 2005). Upon cues for seeds to germinate, ABA levels decrease leading to an increase in ABA catabolism products PA and DPA (Nambara and Marion-Poll 2005). PA maintains some level of biological activity, albeit to a lesser extent than ABA (Rodriguez 2016). During seed development, ABA acts to upregulate genes associated with desiccation tolerance and seed dormancy (Fedoroff 2002). As mature seeds exit dormancy during germination, ABA levels decrease as seeds imbibe water and GA promotes germination and growth (Fedoroff 2002). In these data, ABA concentrations were highest in breaker seeds and locular tissue (163.16 ng/g DW) followed by green fruit seed and locular tissue (123.37 ng/g DW). At these stages, seeds are developing and preparing for dormancy, and therefore high concentrations of ABA are to be expected in these tissues. Additionally, endogenous levels of

ABA have been shown to peak during cell enlargement and decrease during later stages of fruit development (Gillaspy, Bendavid, and Gruissem 1993). Furthermore, ABA promotes ethylene synthesis necessary for fruit ripening and promotes anthocyanin accumulation, a distinct marker of ripening fruit (Zhang, Yuan, and Leng 2009; Karppinen et al. 2018). Taken together, these findings show the diverse roles of ABA throughout multiple stages of fruit ripening. We therefore used these data to show relative abundance in a fruiting tomato plant where a darker orange is associated with higher concentrations of ABA (Figure 4.10C).

Auxin is associated with cell expansion in fruit tissues, but is highest in seeds (Gillaspy, Bendavid, and Gruissem 1993). Previous data has also identified elevated levels of IAA in mature fruit stages however these data did not make the distinction between the placenta, pericarp, and seed and locular fruit tissues (Matuso 2018). In our data, IAA and IAnitrile concentrations are elevated in the rapid growth stages but are highest in green seed and locular tissue, 5.48 ng/g DW, and 36.82 ng/g DW, respectively (Figure 4.10B). At the end of fruit development, auxin peaks coinciding with embryo development, however, auxin concentrations are very low in tissues surrounding seeds including pericarp and placenta tissues (Gillaspy, Bendavid, and Gruissem 1993). Again, in these data, concentrations of IAA in ripe placenta (0.06 ng/g DW) and of IAnitrile in ripe pericarp (0.29 ng/g DW) were the lowest compared to other tissues (Figure 4.10B), following previously published trends of auxin concentrations in tomato fruit development.

4.5 DISCUSSION

Fruit development can be characterized into climacteric and non-climacteric, where climacteric fruits, such as tomatoes, bananas, and apples, rely on ethylene for fruit ripening, while ABA plays critical roles during non-climacteric fruit ripening (Cherian, Figueroa, and Nair 2014). Studies of non-climacteric fruits including strawberries (Gu et al. 2019) sweet cherries (Teribia, Tijero, and Munne-Bosch 2016), and peppers (Osorio et al. 2012) have quantified

hormones during fruit development but have neglected other aspects of plant development including vegetative and root tissues. Further investigation into hormonal regulation in additional tissues in non-climacteric model fruit species are valuable to furthering our understanding of mechanisms underlying developmental processes prior to fruit development.

Here we have shown that a single-phase extraction can quantify many plant hormone species from a diverse set of tissue types throughout tomato plant development. Previous reports have been limited to a few tissue types, a single developmental stage, or have optimized protocols for specific hormones. A single paper, other than this one, has characterized hormones throughout rice plant development in multiple tissue types, providing a critical tool for the study of another important agricultural crop (Cai et al. 2016).

Due to quantification limitations, we were unable to quantify members in four of the nine plant hormones including ethylene, BRs, GA, and SLs. The importance of ethylene in climacteric fruit ripening has been extensively reviewed (Giovannoni 2001; Cara and Giovannoni 2008; Klee and Giovannoni 2011; Agarwal et al. 2012; Karlova et al. 2014; Kumar, Khurana, and Sharma 2014; Quinet et al. 2019). However, as a volatile plant hormone, direct quantification of ethylene requires gas chromatography and specialized collection chambers to capture samples for ethylene quantification (Pereira et al. 2017; Yoon and Chen 2017). Addition of an IS for the ethylene precursor, 1-aminocyclopropane-1-carboxylic acid (ACC), to our hormone panel will provide valuable insight into the roles of ethylene throughout tomato plant development beyond its known roles in fruit ripening and in relation to other plant hormones. Furthermore, ACC has been shown to act as a signaling molecule and play a role in plant growth independently of ethylene (Polko and Kieber 2019) and the addition of ACC quantification to the current hormone panel would provide valuable information in ACC-growth regulatory mechanisms throughout tomato plant development. In addition to ethylene and ACC, ISs for BRs should be added to our current hormone panel to gain a more comprehensive view of all hormones during development. While characterization of BRs in fruit development is

limited, mutations resulting in reduced BR content have delayed flowering and reduced fruit yield (Srivastava and Handa 2005) indicating BRs do play vital roles in tomato fruit development. GA was originally quantified in this data set, however, upon further inspection, we found inconsistencies in quantification of our IS samples, resulting in inaccurate linear curves, from which we could not accurately quantify GA concentrations. With this knowledge, we removed GA species from our data analysis. Any future studies using this protocol may want to modify the extraction protocol to optimize the extraction for GA. SLs play critical roles in plant architecture, however, little is currently known about their crosstalk with other hormones due to their relatively new identification as a plant hormone (Gomez-Roldan et al. 2008; Umehara et al. 2008; Lopez-Obando et al. 2015). SL quantification has proven difficult as the concentrations are typically low in comparison to other plant hormones and their detection can be masked by other substances (Boutet-Mercey et al. 2018). At this time, addition of SL quantification into broader hormone panels has not yet been done. Regarding their role in shoot branching and architecture, further development of SL localization and signaling in agricultural species will be valuable information.

During ripening, tomato fruits undergo a major shift accumulating sugars, volatile compounds, and flavonoids (Gillaspy, Bendavid, and Gruissem 1993; Carrari et al. 2006; Osorio et al. 2011; McAtee et al. 2013). Through selection of larger, shelf stable, and transportable tomatoes, tomato fruits have become flavorless with less nutritional content (Klee 2010). Because of this trend, there has been a renewed focus on integrating flavor compounds back into tomatoes through research surrounding sugars, acids, and volatiles associated with flavor (Tieman et al. 2006; Mathieu et al. 2009; Klee and Tieman 2013, 2018). Ethylene (Cara and Giovannoni 2008; Klee and Giovannoni 2011; Agarwal et al. 2012; Quinet et al. 2019) and ABA (Barickman, Kopsell, and Sams 2017a, 2017b; Wu et al. 2018a) have primarily been associated with the development of sugars and other flavor-related compounds. However, the connection

between flavor and auxins (Wu et al. 2018b), BRs (Wang et al. 2019; Hu et al. 2020), CKs, and GA is limited or yet to be determined.

Studies combining transcriptomic and metabolomic data provide a robust tool for precision genomic editing that could result in the development of elite lines faster than traditional breeding methods (Osorio et al. 2012; Zhu et al. 2018; Gu et al. 2019). Increasingly, there are more databases to address questions regarding tomato genetics and development. Among them are the Sol Genomics Network (SGN) providing the genome sequence, structural, and functional annotation of the Heinz 1706 cultivar (The Tomato Genome 2012; Fernandez-Pozo et al. 2015); KaFTom database, a database of full-length cDNA from Micro-Tom (Aoki et al. 2010; Yano et al. 2007); MiBASE database containing expressed sequence tag data from Micro-Tom (Yano et al. 2006); TOMATOMA database for information about mutations established in the Micro-Tom background (Shikata et al. 2016); and TOMATOMICS for integrated omics information (Kudo et al. 2017). Together, these resources provide valuable information about multiple tomato cultivars, to which our data provides another layer of -omics data.

In conjunction with transcriptomic data at these Micro-Tom developmental stages, we can further establish hormone crosstalk and hormonal regulation of plant development. Furthermore, by challenging Micro-Tom plants to pathogen attack or abiotic stressors, we can identify changes in hormone patterns to address crosstalk and the balance between growth and defense. This data set provides a comprehensive foundation to address the role of hormones and their respective crosstalk throughout tomato plant development. However, further investigation into specific crosstalk interactions will further expand the usefulness of this data. Because many mutations in hormone biosynthesis and signaling have been introgressed into the Micro-Tom background (Carvalho et al. 2011), we have begun work on establishing double mutant lines deficient in two hormone biosynthesis and signaling pathways to further address hormone crosstalk during tomato development and defense. Although hormonal crosstalk is ubiquitous to plant life, we are far from fully understanding the complex interactions especially

regarding how different hormonal pathways contribute to determine plant growth, development, and defense. Investigation into hormonal crosstalk throughout tomato plant and fruit development and pathogen infection will allow for a more comprehensive map of hormonal networks.

4.6 FIGURES

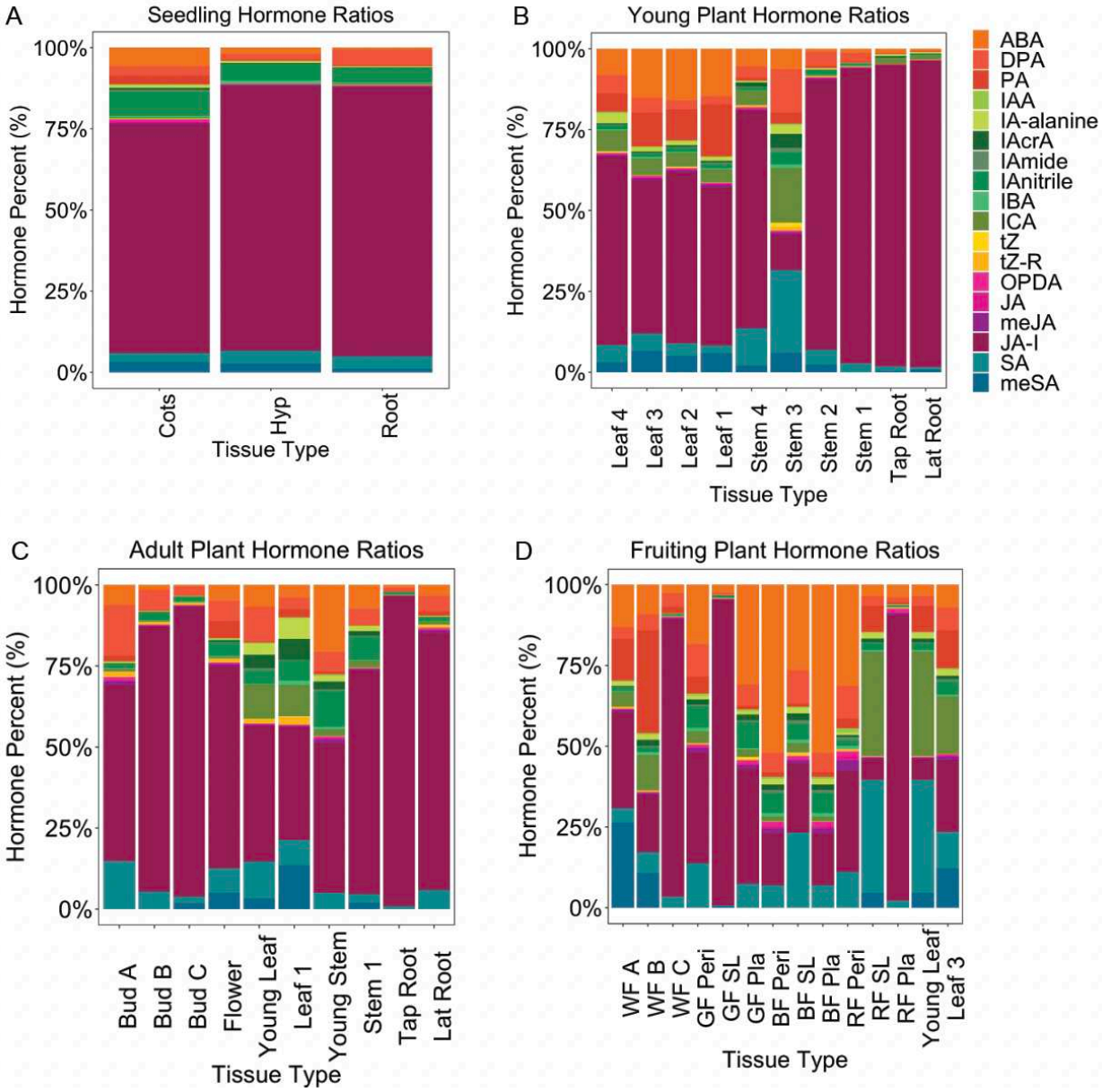

Figure 4.1: Hormones are present in different ratios between developmental stages and tissue types. A. Percent of hormones quantified in cotyledons (Cots), hypocotyls (Hyp), and root tissues at the seedling stage. **B.** Percent of quantified hormones from tissues collected in the young developmental stage. **C.** Percent of quantified hormones from tissues collected from the adult developmental stage. **D.** Percent of hormones quantified from the fruiting plant stage. WF A, B, C: whole fruit A, B, C; GF Peri: green fruit pericarp; GF SL: green fruit seed and locular tissue; GF Pla: green fruit placenta; BF Peri: breaker fruit pericarp; BF SL: breaker fruit seed and locular tissue; BF Pla: breaker fruit placenta; RF Peri: red fruit pericarp; RF SL: red fruit seed and locular tissue; RF Pla: red fruit placenta.

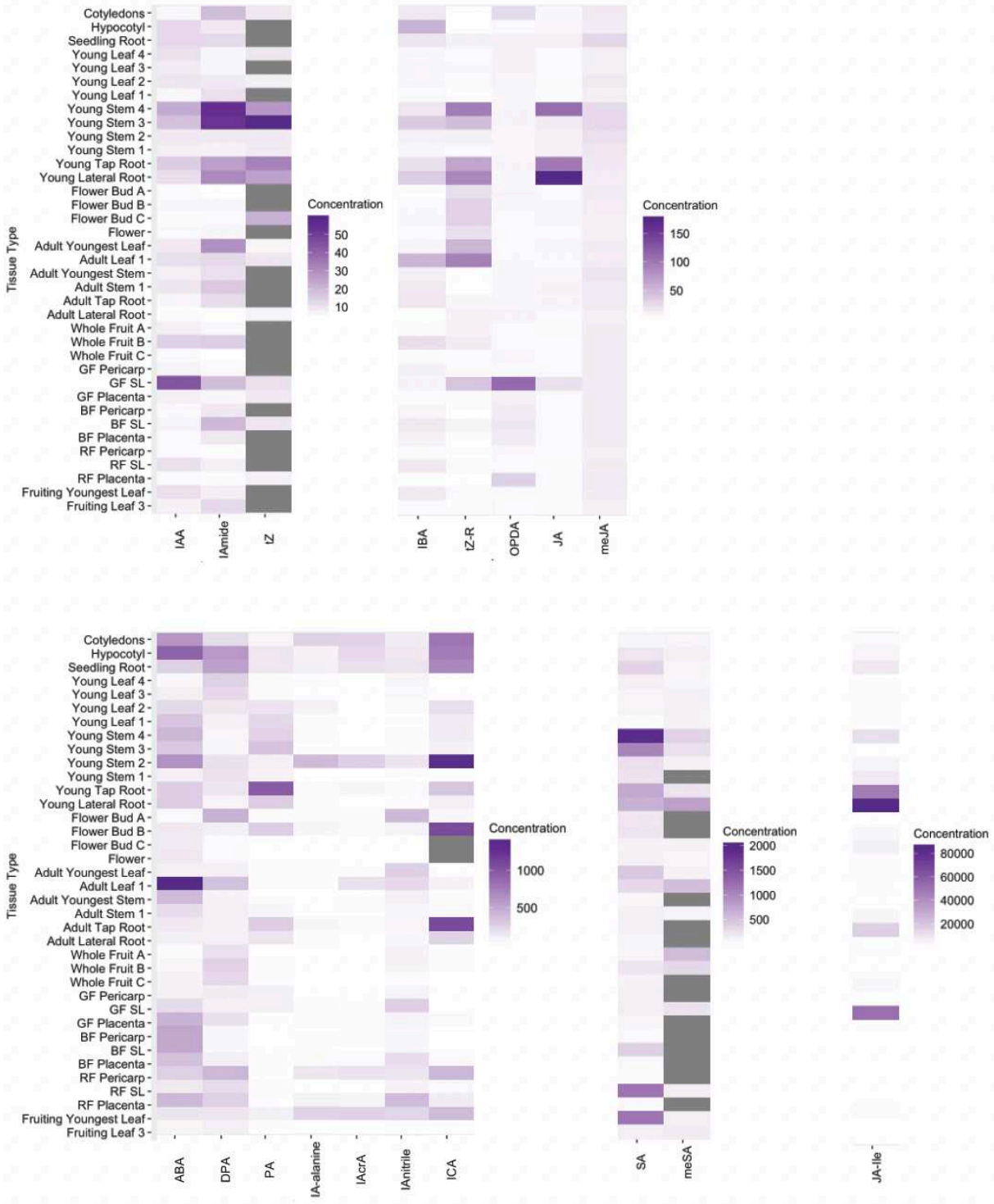

Figure 4.2: Hormones are present at different levels in different tissues across tomato plant and fruit development. Concentrations in ng/g dry weight. GF Pericarp: green fruit pericarp; GF SL: green fruit seed and locular tissue; GF Placenta: green fruit placenta; BF Pericarp: breaker fruit pericarp; BF SL: breaker fruit seed and locular tissue; BF Placenta: breaker fruit placenta; RF Pericarp: red fruit pericarp; RF SL: red fruit seed and locular tissue; RF Placenta: red fruit placenta.

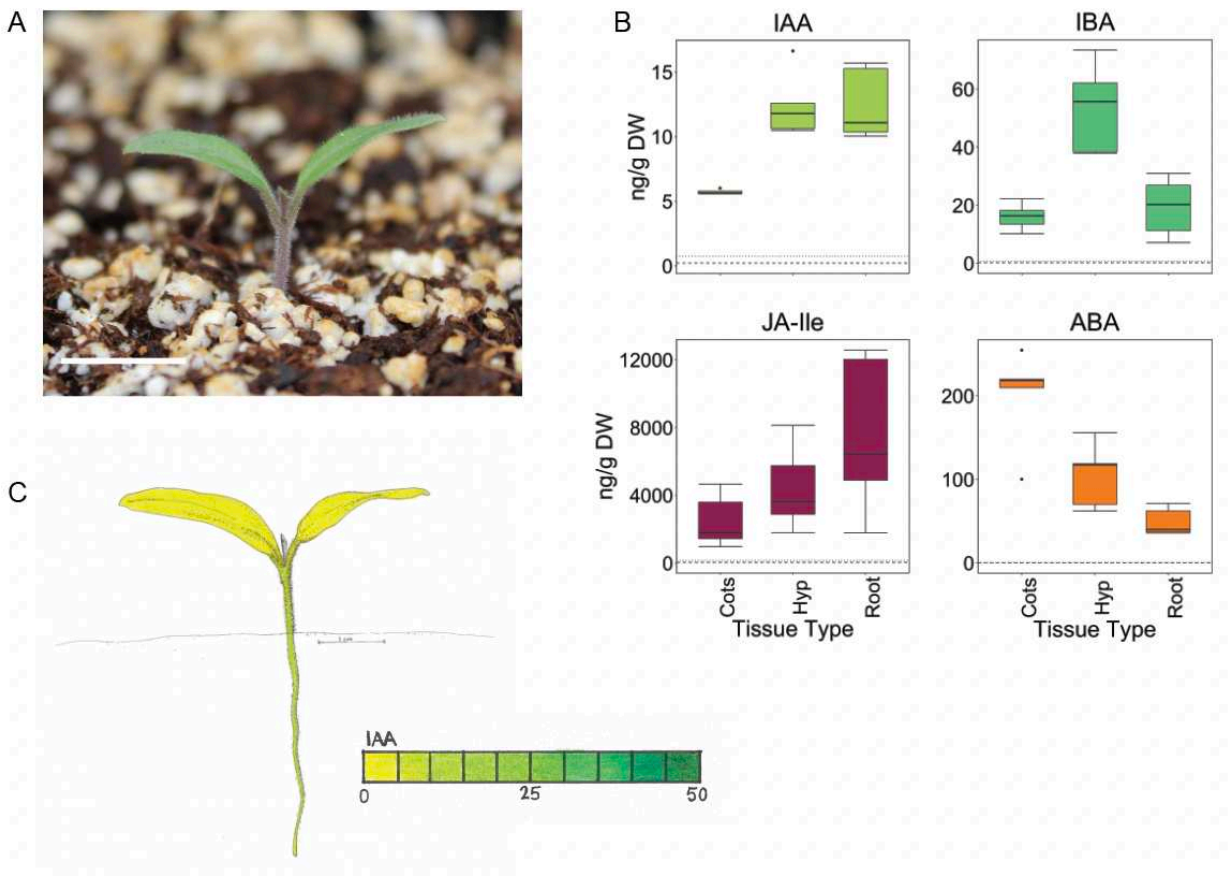

Figure 4.3: Seedling Micro-Tom plants have elevated concentrations of auxins and other other growth-related hormones. A. Representative image of a two-week old Micro-Tom seedling used for tissue collection. Scale bar represents 1 cm. **B.** Hormone quantification concentrations in ng/g Dry Weight (DW) of key hormone players in the seedling developmental stage. Data was collected from 5 biological replicates of tissue pooled from multiple plants. Cots: cotyledons; Hyp: hypocotyl. **C.** Hormone atlas illustration of seedling Micro-Tom stage, false colored with IAA hormone data. A darker color represents higher concentrations of IAA in quantified tissues.

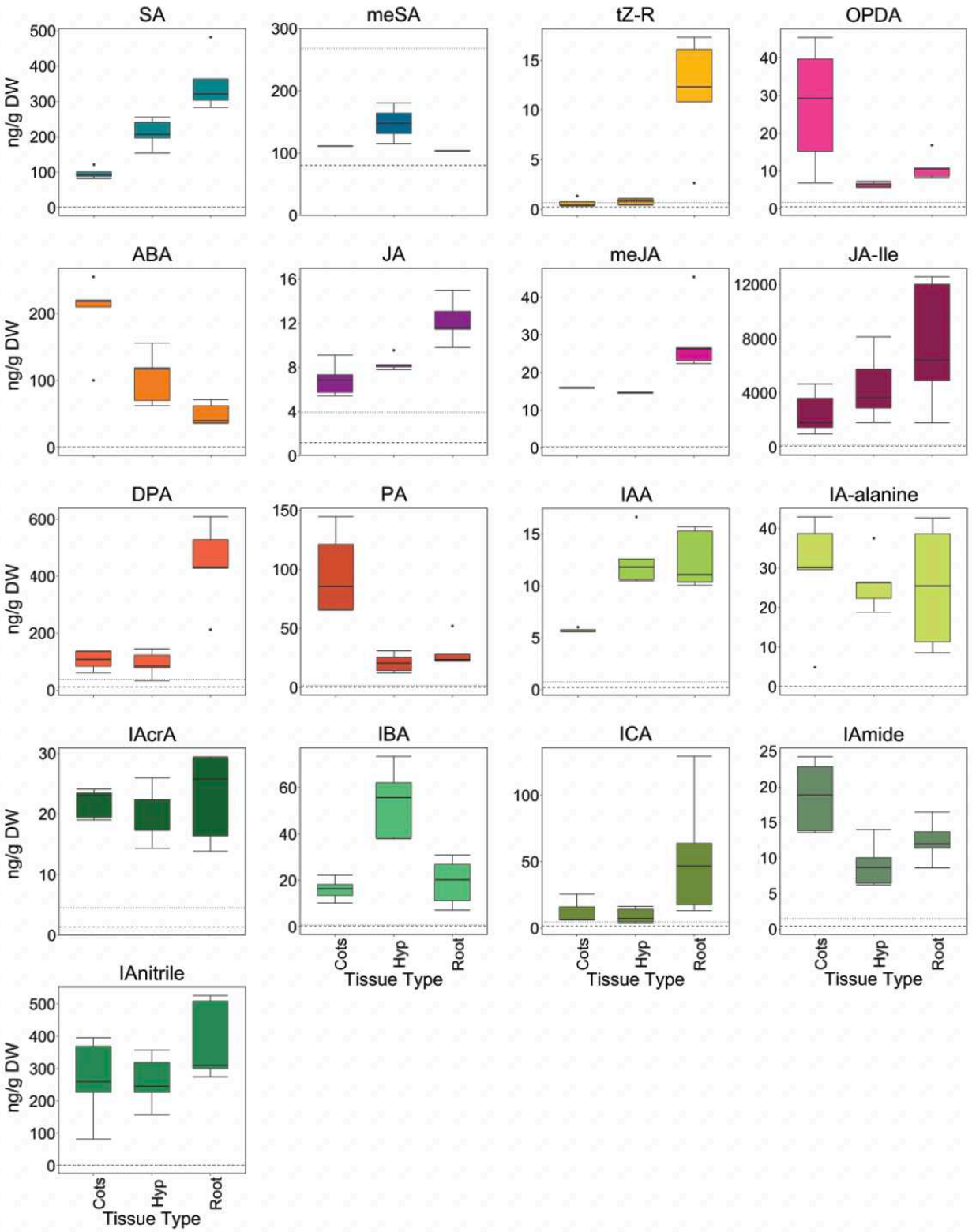

Figure 4.4: Quantified hormones from seedling Micro-Tom tissues. Hormone quantification concentrations in ng/g DW of all hormone species measured. Cots: cotyledons; Hyp: hypocotyl.

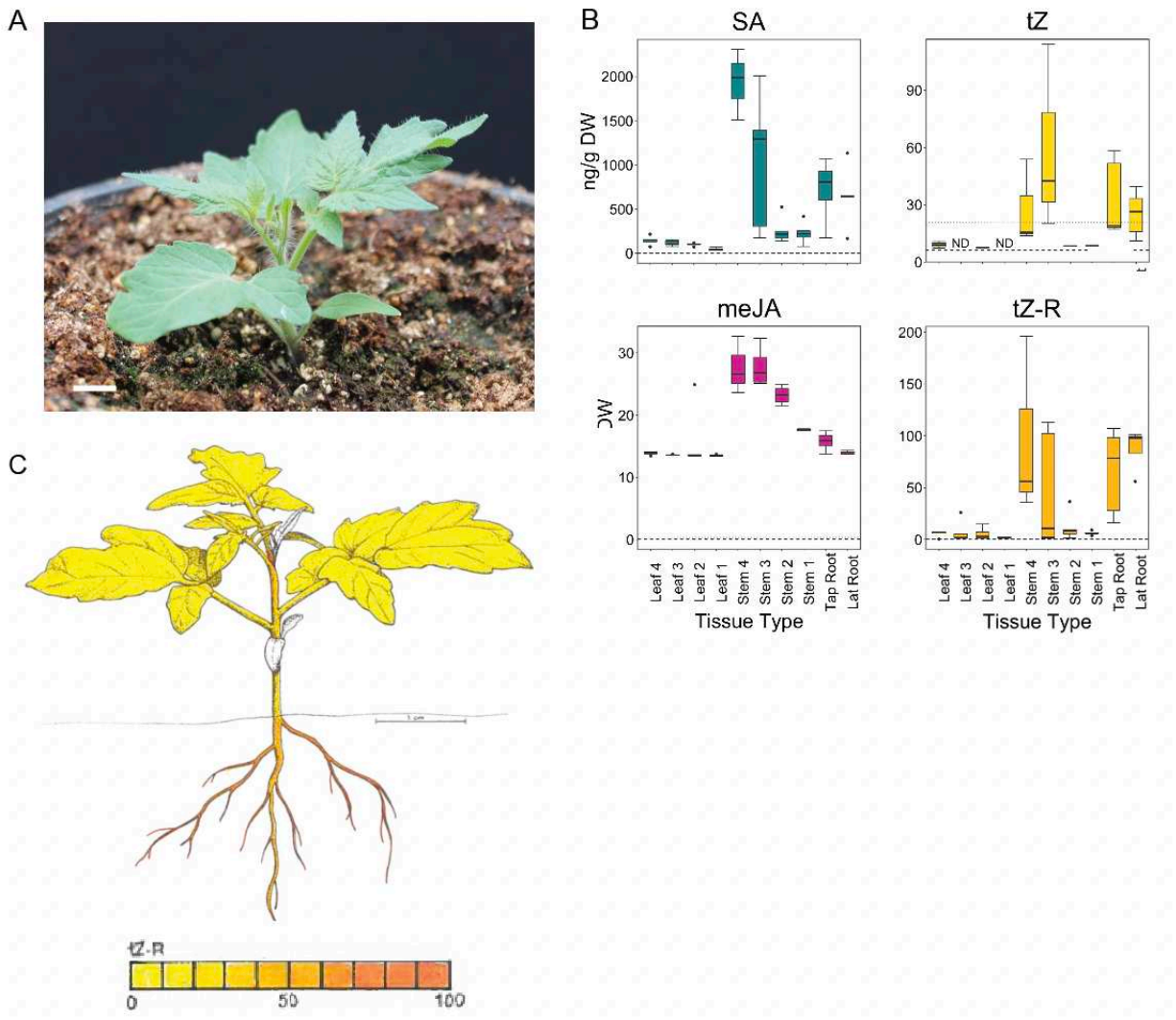

Figure 4.5: Elevated concentrations of CKs were found in four-leaf young Micro-Tom plants. A. A representative image of a vegetative Micro-Tom plant, approximately 4 weeks post germination, used for tissue collection. Scale bar represents 1 cm. **B.** Hormone quantification concentrations in ng/g DW of key hormone players in young plant tissues. Data was collected from 5 biological replicates of tissue pooled from multiple plants. Lat Root: Lateral Root. **C.** Hormone atlas illustration of the young Micro-Tom stage false colored with *tZ* hormone data. A darker color represents higher concentrations of *tZ* within quantified tissues.

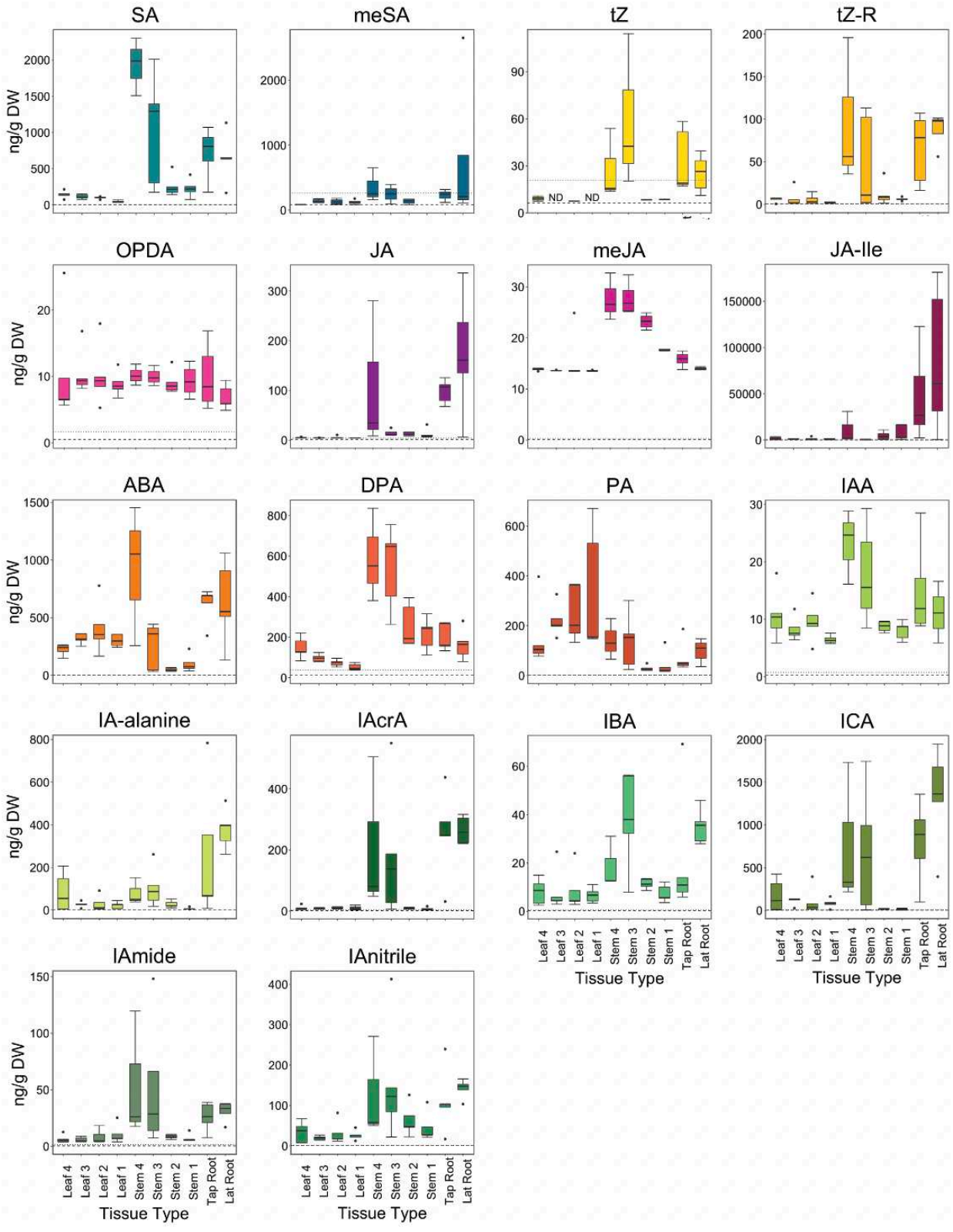

Figure 4.6: Quantified hormones from young Micro-Tom tissues. Hormone quantification concentrations in ng/g DW of all hormones measured. Lat Root: Lateral Root.

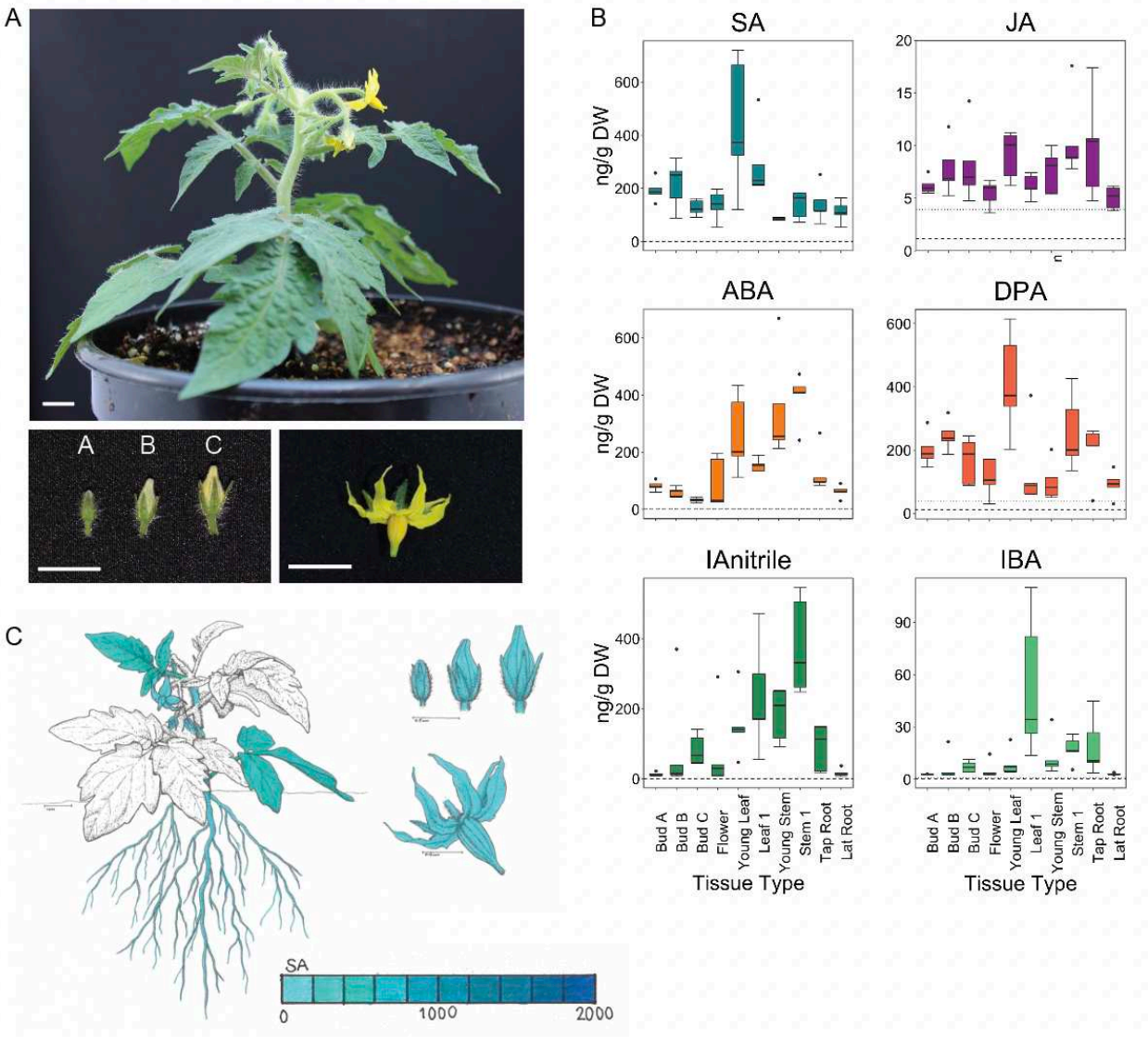

Figure 4.7. Adult Micro-Tom plants are characterized by elevated concentrations of auxins, ABAs, SA, and JA. A. Representative images of reproductive Micro-Tom tissues and plant used for tissue collection, between 6 and 7 weeks post germination. Buds A were between 0.2-0.5 cm, Buds B between 0.6-0.7 cm, and Buds C 0.8 cm. All scale bars represent 1 cm. **B.** Hormone quantification concentrations in ng/g DW of key hormone players in the adult reproductive developmental stage. Data was collected from 5 biological replicates of tissue pooled from multiple plants. Lat Root: Lateral Root. **C.** Hormone atlas illustration of adult Micro-Tom stage false colored with SA hormone data. A darker color represents higher concentrations of SA within quantified tissues.

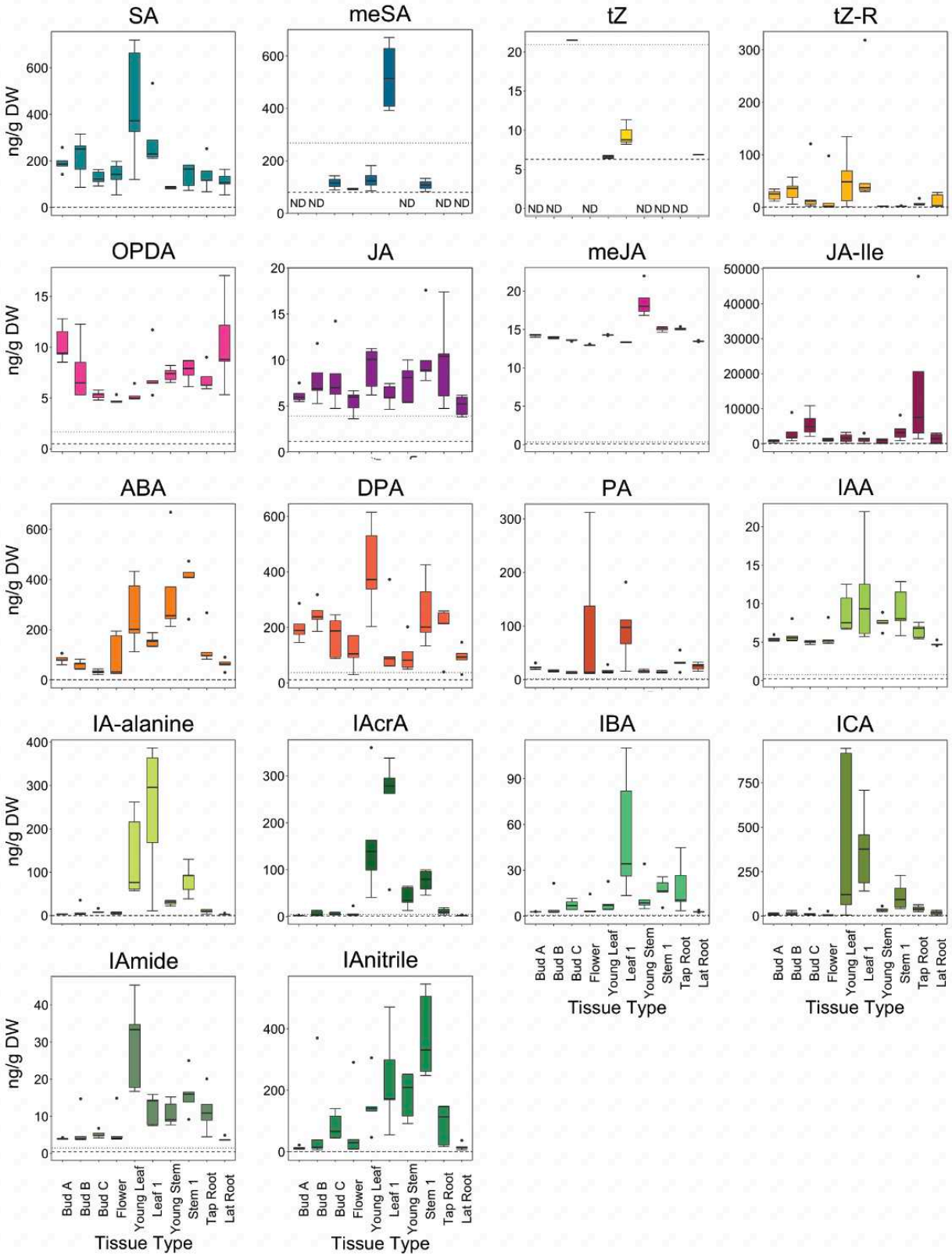

Figure 4.8: Quantified hormones from adult Micro-Tom tissues. Hormone quantification concentrations in ng/g DW of all hormone species measured. Lat Root: Lateral Root.

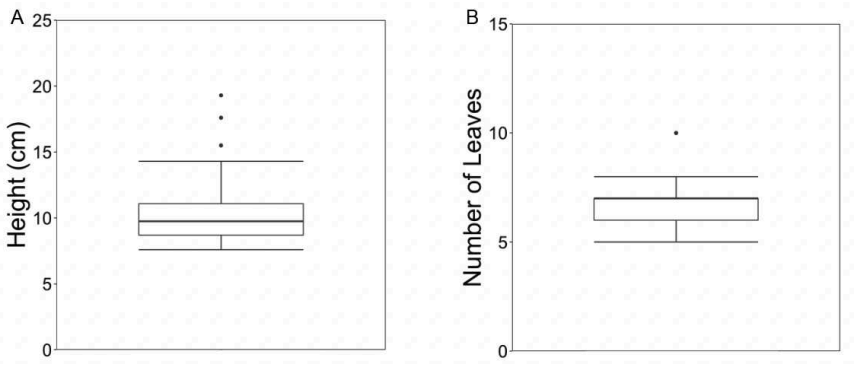

Figure 4.9: Plant height and leaf number of adult plants. A. Stem height of adult plants collected for tissue. **B.** Number of leaves present in adult plants at the time of tissue collection.

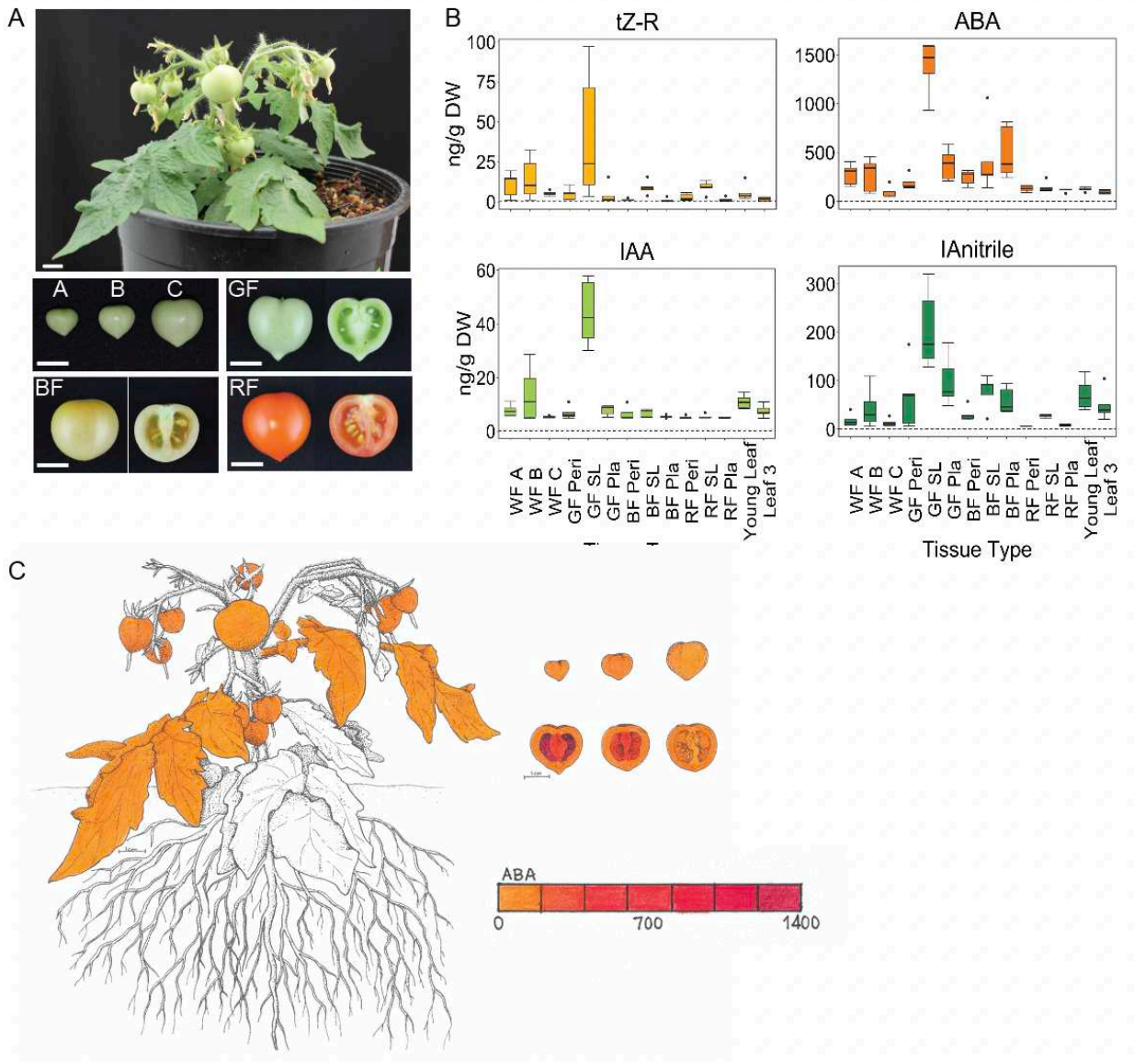

Figure 4.10: Micro-Tom fruiting tissue is predominately characterized by growth-related hormones. A. Representative images of a fruiting Micro-Tom plant and tissues collected for hormone quantification, between 10 and 12 weeks after germination. Whole fruits A were between 0.5-0.9 cm, whole fruits B between 1-1.4 cm, and whole fruits C 1.5-1.9 cm. GF, Green Fruit tissues were collected from fully expanded fruits 2 cm or larger. BF, Breaker Fruit tissues were collected from fully expanded fruits at the first appearance of yellow color. RF, Red Fruit tissues were collected from fruits 10 days post breaker stage. All scale bars represent 1 cm. **B.** Hormone quantification concentrations in ng/g DW of key hormones during fruit development. Data was collected from 5 biological replicates of tissue pooled from multiple plants. WF: whole fruit; GF Peri: green fruit pericarp; GF SL: green fruit seed and locular tissue; GF Pla: green fruit placenta; BF Peri: breaker fruit pericarp; BF SL: breaker fruit seed and locular tissue; BF Pla: breaker fruit placenta; RF Peri: red fruit pericarp; RF SL: red fruit seed and locular tissue; RF Pla: red fruit placenta. **C.** Hormone atlas illustration of fruiting Micro-Tom stage false colored with ABA hormone quantification data. A darker color represents higher concentrations of ABA within quantified tissues.

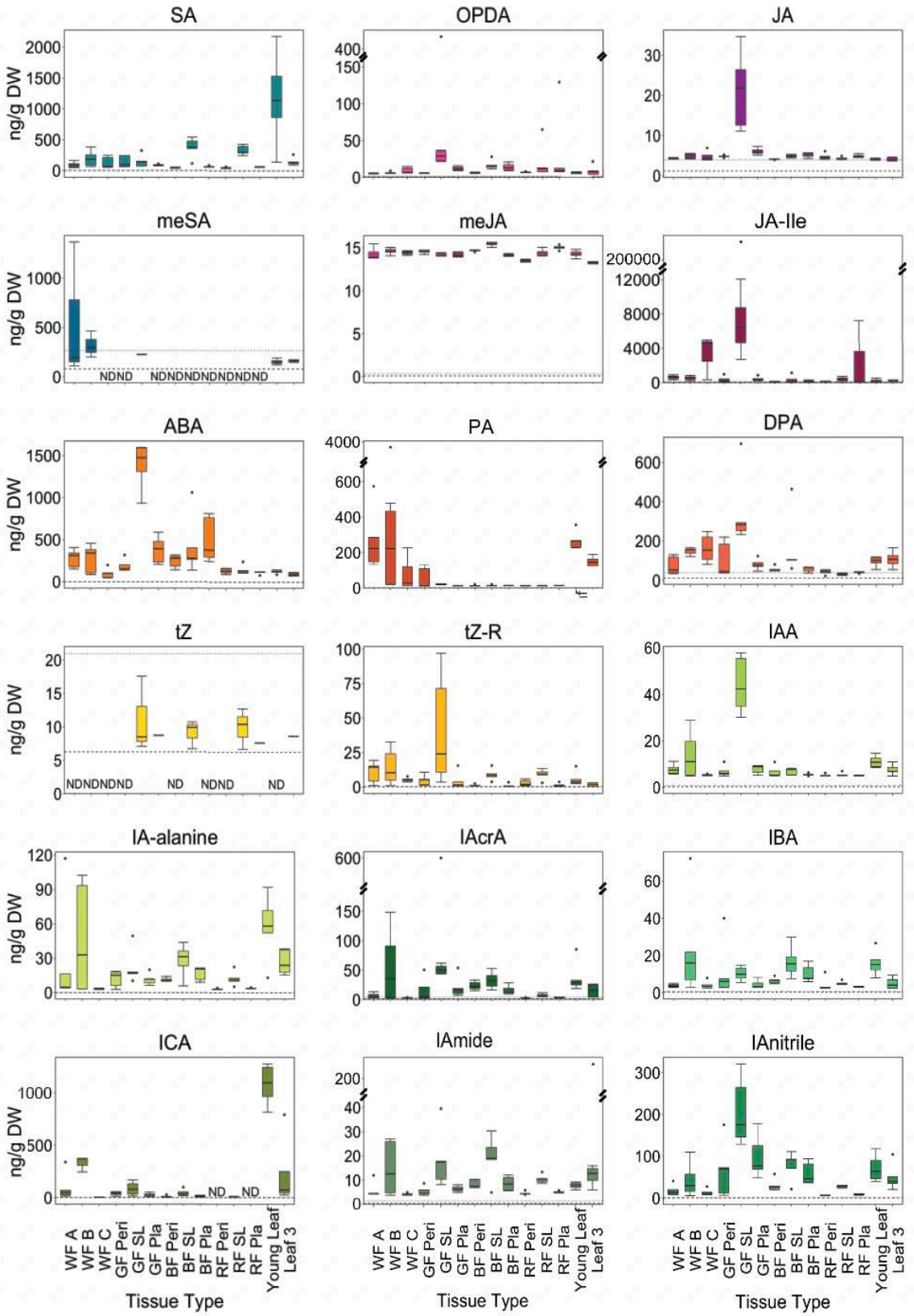

Figure 4.11: Quantified hormones from adult Micro-Tom tissues. Hormone quantification concentrations in ng/g DW of all hormone species measured. WF: whole fruit; GF Peri: green

fruit pericarp; GF SL: green fruit seed and locular tissue; GF Pla: green fruit placenta; BF Peri: breaker fruit pericarp; BF SL: breaker fruit seed and locular tissue; BF Pla: breaker fruit placenta; RF Peri: red fruit pericarp; RF SL: red fruit seed and locular tissue; RF Pla: red fruit placenta.

4.7 TABLES

Table 4.1: Greenhouse temperatures across tomato growth and tissue collection timeline.

Season	Weeks Post Germination (wpg)	Average High Temp (°C)	Average Low Temp (°C)
Winter	1	23.40	14.75
Winter	2	23.65	13.91
Winter	3	24.57	15.28
Winter	4	23.46	13.92
Winter	5	23.44	14.00
Winter	6	23.20	13.81
Winter	7	25.15	13.61
Winter	8	22.97	13.78
Winter	10	23.89	14.88
Spring	12	29.84	14.05

The average daytime high and average nighttime low temperatures recorded during each week of tomato plant growth and tissue collection.

Table 4.2: Limit of detection (LOD) and limit of quantification (LOQ) values (ng/g DW) for each hormone measured.

Hormone	LOD	LOQ
ABA	0.18	0.59
PA	0.44	1.48
DPA	11.32	37.75
IAA	0.23	0.75
IA-amide	0.44	1.46
IA-alanine	0.01	0.02
IA-nitrile	0.23	0.78
IAcrA	1.35	4.51
IBA	0.20	0.66
ICA	1.35	4.51
tZ	6.29	20.95
tZ-R	0.21	0.69
JA	1.18	3.93
OPDA	0.50	1.68
meJA	0.10	0.34
JA-Ile	1275.25	4250.84
SA	0.43	1.45
meSA	80.40	268.02

REFERENCES

Abdelrahman, M. 1977. 'Patterns of hormones, respiration and ripening enzymes during development, maturation ripening of cherry tomato fruits', *Physiologia Plantarum*, 39: 115-18.

Agarwal, G., D. Choudhary, V. P. Singh, and A. Arora. 2012. 'Role of ethylene receptors during senescence and ripening in horticultural crops', *Plant Signaling & Behavior*, 7: 827-46.

Aoki, K., K. Yano, A. Suzuki, S. Kawamura, N. Sakurai, K. Suda, A. Kurabayashi, T. Suzuki, T. Tsugane, M. Watanabe, K. Ooga, M. Torii, T. Narita, T. Shin-i, Y. Kohara, N. Yamamoto, H. Takahashi, Y. Watanabe, M. Egusa, M. Kodama, Y. Ichinose, M. Kikuchi, S. Fukushima, A. Okabe, T. Arie, Y. Sato, K. Yazawa, S. Satoh, T. Omura, H. Ezura, and D. Shibata. 2010. 'Large-scale analysis of full-length cDNAs from the tomato (*Solanum lycopersicum*) cultivar Micro-Tom, a reference system for the Solanaceae genomics', *BMC Genomics*, 11.

Balcke, G. U., V. Handrick, N. Bergau, M. Fichtner, A. Henning, H. Stellmach, A. Tissier, B. Hause, and A. Frolov. 2012. 'An UPLC-MS/MS method for highly sensitive high-throughput analysis of phytohormones in plant tissues', *Plant Methods*, 8.

Barickman, T. C., D. A. Kopsell, and C. E. Sams. 2017a. 'Abscisic acid improves tomato fruit quality by increasing soluble sugar concentrations', *Journal of Plant Nutrition*, 40: 964-73.

Barickman, T. C., D. A. Kopsell, and C. E. Sams. 2017b. 'Effects of abscisic acid and calcium on tomato fruit aroma volatiles', *Journal of Plant Nutrition*, 40: 2096-100.

Benjamins, R., and B. Scheres. 2008. 'Auxin: The looping star in plant development', *Annual Review of Plant Biology*, 59: 443-65.

Bohner, J., and F. Bangerth. 1988. 'Effects of fruit-set sequence and defoliation on cell number, cell-size and hormone levels of tomato fruits (*Lycopersicon-esculentum* Mill) within a truss', *Plant Growth Regulation*, 7: 141-55.

Boutet-Mercey, S., F. Perreau, A. Roux, G. Clave, J. P. Pillot, I. Schmitz-Afonso, D. Touboul, G. Mouille, C. Rameau, and F. D. Boyer. 2018. 'Validated method for strigolactone quantification by ultra high-performance liquid chromatography - electrospray ionisation tandem mass spectrometry using novel deuterium labelled standards', *Phytochemical Analysis*, 29: 59-68.

Browse, J. 2009. 'Jasmonate passes muster: A receptor and targets for the defense hormone', *Annual Review of Plant Biology*, 60: 183-205.

Burbidge, A., T. M. Grieve, A. Jackson, A. Thompson, D. R. McCarty, and I. B. Taylor. 1999. 'Characterization of the ABA-deficient tomato mutant *notabilis* and its relationship with maize Vp14', *Plant Journal*, 17: 427-31.

'The C. M. Rick Tomato Genetics Resource Center'. [http://tgrc.ucdavis.edu].

Cai, W. J., T. T. Ye, Q. Wang, B. D. Cai, and Y. Q. Feng. 2016. 'A rapid approach to investigate spatiotemporal distribution of phytohormones in rice', *Plant Methods*, 12.

Campos, M. L., R. F. Carvalho, V. A. Benedito, and L. E. P. Peres. 2010. 'Small and remarkable', *Plant Signaling & Behavior*, 5: 267-70.

Cara, B., and J. J. Giovannoni. 2008. 'Molecular biology of ethylene during tomato fruit development and maturation', *Plant Science*, 175: 106-13.

Carrari, F., C. Baxter, B. Usadel, E. Urbanczyk-Wochniak, M. I. Zanor, A. Nunes-Nesi, V. Nikiforova, D. Centero, A. Ratzka, M. Pauly, L. J. Sweetlove, and A. R. Fernie. 2006. 'Integrated analysis of metabolite and transcript levels reveals the metabolic shifts that underlie tomato fruit development and highlight regulatory aspects of metabolic network behavior', *Plant Physiology*, 142: 1380-96.

Carvalho, R. F., M. L. Campos, L. E. Pino, S. L. Crestana, A. Zsogon, J. E. Lima, V. A. Benedito, and L. E. P. Peres. 2011. 'Convergence of developmental mutants into a single tomato model system: 'Micro-Tom' as an effective toolkit for plant development research', *Plant Methods*, 7.

Chapman, E. J., and M. Estelle. 2009. 'Mechanism of auxin-regulated gene expression in plants.' in, *Annual Review of Genetics*.

Cherian, S., C. R. Figueroa, and H. Nair. 2014. ''Movers and shakers' in the regulation of fruit ripening: a cross-dissection of climacteric versus non-climacteric fruit', *Journal of Experimental Botany*, 65: 4705-22.

Creelman, R. A., and J. E. Mullet. 1995. 'Jasmonic acid distribution and action in plants - Regulation during development and response to biotic and abiotic stress', *PNAS*, 92: 4114-19.

Cutler, S. R., P. L. Rodriguez, R. R. Finkelstein, and S. R. Abrams. 2010. 'Abscisic acid: Emergence of a core Signaling network.' in S. Merchant, W. R. Briggs and D. Ort (eds.), *Annual Review of Plant Biology, Vol 61*.

Dan, Y., Z. Fei, and C. Rothan. 2007. 'MicroTom - A new model system for plant genomics', *Genes, Genomes and Genomics*, 1: 167-79.

Davies, PeterJ. 2010. 'The plant hormones: Their nature, occurrence, and functions.' in PeterJ Davies (ed.), *Plant Hormones* (Springer Netherlands).

de Jong, M., M. Wolters-Arts, J. L. Garcia-Martinez, C. Mariani, and W. H. Vriezen. 2011. 'The *Solanum lycopersicum* AUXIN RESPONSE FACTOR 7 (SlARF7) mediates cross-talk between auxin and gibberellin signalling during tomato fruit set and development', *Journal of Experimental Botany*, 62: 617-26.

De Vleesschauwer, David, Jing Xu, and Monica Höfte. 2014. 'Making sense of hormone-mediated defense networking: from rice to Arabidopsis', *Frontiers in Plant Science*, 5: 611.

Dobrev, P. I., K. Hoyerova, and J. Petrasek. 2017. 'Analytical determination of auxins and cytokinins.' in T. Dandekar and M. Naseem (eds.), *Auxins and Cytokinins in Plant Biology: Methods and Protocols*.

Durbak, A., H. Yao, and P. McSteen. 2012. 'Hormone signaling in plant development', *Current Opinion in Plant Biology*, 15: 92-96.

Fedoroff, Nina V. 2002. 'Cross-talk in abscisic acid signaling', *Science's STKE*, 2002: re10-re10.

Fernandez-Pozo, N., N. Menda, J. D. Edwards, S. Saha, I. Y. Tecle, S. R. Strickler, A. Bombarely, T. Fisher-York, A. Pujar, H. Foerster, A. M. Yan, and L. A. Mueller. 2015. 'The Sol Genomics Network (SGN)-from genotype to phenotype to breeding', *Nucleic Acids Research*, 43: D1036-D41.

Feys, B. J. F., C. E. Benedetti, C. N. Penfold, and J. G. Turner. 1994. 'Arabidopsis mutants selected for resistance to the phytotoxin coronatine are male-sterile, insensitive to methyl jasmonate, and resistant to a bacterial pathogen', *Plant Cell*, 6: 751-59.

Forcat, S., M. H. Bennett, J. W. Mansfield, and M. R. Grant. 2008. 'A rapid and robust method for simultaneously measuring changes in the phytohormones ABA, JA and SA in plants following biotic and abiotic stress', *Plant Methods*, 4.

Gillaspy, G., H. Bendavid, and W. Gruissem. 1993. 'Fruits - A developmental perspective', *Plant Cell*, 5: 1439-51.

Giovannoni, J. 2001. 'Molecular biology of fruit maturation and ripening', *Annual Review of Plant Physiology and Plant Molecular Biology*, 52: 725-49.

Gomez-Roldan, V., S. Fermas, P. B. Brewer, V. Puech-Pages, E. A. Dun, J. P. Pillot, F. Letisse, R. Matusova, S. Danoun, J. C. Portais, H. Bouwmeester, G. Becard, C. A. Beveridge, C. Rameau, and S. F. Rochange. 2008. 'Strigolactone inhibition of shoot branching', *Nature*, 455: 189-U22.

Gu, T. T., S. F. Jia, X. R. Huang, L. Wang, W. M. Fu, G. T. Huo, L. J. Gan, J. Ding, and Y. Li. 2019. 'Transcriptome and hormone analyses provide insights into hormonal regulation in strawberry ripening', *Planta*, 250: 145-62.

Hu, S. S., L. H. Liu, S. Li, Z. Y. Shao, F. L. Meng, H. R. Liu, W. Y. Duan, D. Y. Liang, C. Q. Zhu, T. Xu, and Q. M. Wang. 2020. 'Regulation of fruit ripening by the brassinosteroid biosynthetic gene *SlCYP90B3* via an ethylene-dependent pathway in tomato', *Horticulture Research*, 7.

Ikegami, K., M. Okamoto, M. Seo, and T. Koshiba. 2009. 'Activation of abscisic acid biosynthesis in the leaves of *Arabidopsis thaliana* in response to water deficit', *Journal of Plant Research*, 122: 235-43.

Karlova, R., N. Chapman, K. David, G. C. Angenent, G. B. Seymour, and R. A. de Maagd. 2014. 'Transcriptional control of fleshy fruit development and ripening', *Journal of Experimental Botany*, 65: 4527-41.

Karppinen, K., P. Tegelberg, H. Haggman, and L. Jaakola. 2018. 'Abscisic acid regulates anthocyanin biosynthesis and gene expression associated with cell wall modification in ripening bilberry (*Vaccinium myrtillus* L.) fruits', *Frontiers in Plant Science*, 9.

Kiba, T., K. Takei, M. Kojima, and H. Sakakibara. 2013. 'Side-chain modification of cytokinins controls shoot growth in Arabidopsis', *Developmental Cell*, 27: 452-61.

Kieber, J. J., and G. E. Schaller. 2014. 'Cytokinins', *Arabidopsis Book*, 12: e0168.

Klee, H. J. 2010. 'Improving the flavor of fresh fruits: genomics, biochemistry, and biotechnology', *New Phytologist*, 187: 44-56.

Klee, H. J., and J. J. Giovannoni. 2011. 'Genetics and control of tomato fruit ripening and quality attributes.' in B. L. Bassler, M. Lichten and G. Schupbach (eds.), *Annual Review of Genetics, Vol 45*.

Klee, H. J., and D. M. Tieman. 2013. 'Genetic challenges of flavor improvement in tomato', *Trends in Genetics*, 29: 257-62.

Klee, H. J., and D. M. Tieman. 2018. 'The genetics of fruit flavour preferences', *Nature Reviews Genetics*, 19: 347-56.

Kojima, M., T. Kamada-Nobusada, H. Komatsu, K. Takei, T. Kuroha, M. Mizutani, M. Ashikari, M. Ueguchi-Tanaka, M. Matsuoka, K. Suzuki, and H. Sakakibara. 2009. 'Highly sensitive and high-throughput analysis of plant hormones using MS-probe modification and liquid chromatography tandem mass spectrometry: An application for hormone profiling in *Oryza sativa*', *Plant and Cell Physiology*, 50: 1201-14.

Korasick, D. A., T. A. Enders, and L. C. Strader. 2013. 'Auxin biosynthesis and storage forms', *Journal of Experimental Botany*, 64: 2541-55.

Kou, X. H., S. Yang, L. P. Chai, C. E. Wu, J. Q. Zhou, Y. F. Liu, and Z. H. Xue. 2021. 'Abscisic acid and fruit ripening: Multifaceted analysis of the effect of abscisic acid on fleshy fruit ripening', *Scientia Horticulturae*, 281.

Kudo, T., M. Kobayashi, S. Terashima, M. Katayama, S. Ozaki, M. Kanno, M. Saito, K. Yokoyama, H. Ohyanagi, K. Aoki, Y. Kubo, and K. Yano. 2017. 'TOMATOMICS: A web batabase for integrated omics information in tomato', *Plant and Cell Physiology*, 58.

Kumar, R., A. Khurana, and A. K. Sharma. 2014. 'Role of plant hormones and their interplay in development and ripening of fleshy fruits', *Journal of Experimental Botany*, 65: 4561-75.

Li, L., Y. F. Zhao, B. C. McCaig, B. A. Wingerd, J. H. Wang, M. E. Whalon, E. Pichersky, and G. A. Howe. 2004. 'The tomato homolog of *CORONATINE-INSENSITIVE1* is required for the maternal control of seed maturation, jasmonate-signaled defense responses, and glandular trichome development', *Plant Cell*, 16: 126-43.

Liang, Y., X. C. Zhu, M. P. Zhao, and H. W. Liu. 2012. 'Sensitive quantification of isoprenoid cytokinins in plants by selective immunoaffinity purification and high performance liquid chromatography-quadrupole-time of flight mass spectrometry', *Methods*, 56: 174-79.

Lopez-Obando, M., Y. Ligerot, S. Bonhomme, F. D. Boyer, and C. Rameau. 2015. 'Strigolactone biosynthesis and signaling in plant development', *Development*, 142: 3615-19.

MacLean, Brendan, Daniela M Tomazela, Nicholas Shulman, Matthew Chambers, Gregory L Finney, Barbara Frewen, Randall Kern, David L Tabb, Daniel C Liebler, and Michael J MacCoss. 2010. 'Skyline: an open source document editor for creating and analyzing targeted proteomics experiments', *Bioinformatics*, 26: 966-68.

Martinez, C., E. Pons, G. Prats, and J. Leon. 2004. 'Salicylic acid regulates flowering time and links defence responses and reproductive development', *Plant Journal*, 37: 209-17.

Mathieu, S., V. D. Cin, Z. J. Fei, H. Li, P. Bliss, M. G. Taylor, H. J. Klee, and D. M. Tieman. 2009. 'Flavour compounds in tomato fruits: identification of loci and potential pathways affecting volatile composition', *Journal of Experimental Botany*, 60: 325-37.

Matsukura, C., K. Aoki, N. Fukuda, T. Mizoguchi, E. Asamizu, T. Saito, D. Shibata, and H. Ezura. 2008. 'Comprehensive resources for tomato functional genomics based on the miniature model tomato Micro-Tom', *Current Genomics*, 9: 436-43.

Matsuo, S., K. Kikuchi, K. Nagasuga, H. Ueno, and S. Imanishi. 2018. 'Transcriptional regulation of auxin metabolic-enzyme genes during tomato fruit development', *Scientia Horticulturae*, 241: 329-38.

McAtee, P., S. Karim, R. Schaffer, and K. David. 2013. 'A dynamic interplay between phytohormones is required for fruit development, maturation, and ripening', *Frontiers in Plant Science*, 4.

Mockaitis, K., and M. Estelle. 2008. 'Auxin receptors and plant development: A new signaling paradigm', *Annual Review of Cell and Developmental Biology*, 24: 55-80.

Molinero-Rosales, N., A. Latorre, M. Jamilena, and R. Lozano. 2004. '*SINGLE FLOWER TRUSS* regulates the transition and maintenance of flowering in tomato', *Planta*, 218: 427-34.

Muller, A., P. Duchting, and E. W. Weiler. 2002. 'A multiplex GC-MS/MS technique for the sensitive and quantitative single-run analysis of acidic phytohormones and related compounds, and its application to *Arabidopsis thaliana*', *Planta*, 216: 44-56.

Nambara, E., and A. Marion-Poll. 2005. 'Abscisic acid biosynthesis and catabolism', *Annual Review of Plant Biology*, 56: 165-85.

Novak, O., E. Hauserova, P. Amakorova, K. Dolezal, and M. Strnad. 2008. 'Cytokinin profiling in plant tissues using ultra-performance liquid chromatography-electrospray tandem mass spectrometry', *Phytochemistry*, 69: 2214-24.

Okabe, Y., E. Asamizu, T. Saito, C. Matsukura, T. Ariizumi, C. Bres, C. Rothan, T. Mizoguchi, and H. Ezura. 2011. 'Tomato TILLING technology: Development of a reverse genetics tool for the efficient isolation of mutants from Micro-Tom mutant libraries', *Plant and Cell Physiology*, 52: 1994-2005.

Osorio, S., R. Alba, C. M. B. Damasceno, G. Lopez-Casado, M. Lohse, M. I. Zanor, T. Tohge, B. Usadel, J. K. C. Rose, Z. J. Fei, J. J. Giovannoni, and A. R. Fernie. 2011. 'Systems biology of tomato fruit development: Combined transcript, protein, and metabolite analysis of tomato transcription factor (*nor*, *rin*) and ethylene receptor (*Nr*) mutants reveals novel regulatory interactions', *Plant Physiology*, 157: 405-25.

Osorio, S., R. Alba, Z. Nikoloski, A. Kochevenko, A. R. Fernie, and J. J. Giovannoni. 2012. 'Integrative comparative analyses of transcript and metabolite profiles from pepper and tomato ripening and development stages uncovers species-specific patterns of network regulatory behavior', *Plant Physiology*, 159: 1713-29.

Osugi, A., M. Kojima, Y. Takebayashi, N. Ueda, T. Kiba, and H. Sakakibara. 2017. 'Systemic transport of trans-zeatin and its precursor have differing roles in Arabidopsis shoots', *Nature Plants*, 3.

Pan, X. Q., R. Welti, and X. M. Wang. 2010. 'Quantitative analysis of major plant hormones in crude plant extracts by high-performance liquid chromatography-mass spectrometry', *Nature Protocols*, 5: 986-92.

Pereira, L., M. Pujol, J. Garcia-Mas, and M. A. Phillips. 2017. 'Non-invasive quantification of ethylene in attached fruit headspace at 1p.p.b. by gas chromatography-mass spectrometry', *Plant Journal*, 91: 172-83.

Polko, J. K., and J. J. Kieber. 2019. '1-aminocyclopropane 1-carboxylic acid and its emerging role as an ethylene-independent growth regulator', *Frontiers in Plant Science*, 10.

Quinet, M., T. Angosto, F. J. Yuste-Lisbona, R. Blanchard-Gros, S. Bigot, J. P. Martinez, and S. Lutts. 2019. 'Tomato fruit development and metabolism', *Frontiers in Plant Science*, 10.

Rodriguez, P. L. 2016. 'Abscisic acid catabolism generates phaseic acid, a molecule able to activate a subset of ABA receptors', *Molecular Plant*, 9: 1448-50.

Sahu, P. P., S. Puranik, M. Khan, and M. Prasad. 2012. 'Recent advances in tomato functional genomics: utilization of VIGS', *Protoplasma*, 249: 1017-27.

Saito, T., E. Asamizu, T. Mizoguchi, N. Fukuda, C. Matsukura, and H. Ezura. 2009. 'Mutant resources for the miniature tomato (*Solanum lycopersicum* L.) 'Micro-Tom'', *Journal of the Japanese Society for Horticultural Science*, 78: 6-13.

Sanders, P. M., A. Q. Bui, K. Weterings, K. N. McIntire, Y. C. Hsu, P. Y. Lee, M. T. Truong, T. P. Beals, and R. B. Goldberg. 1999. 'Anther developmental defects in *Arabidopsis thaliana* male-sterile mutants', *Sexual Plant Reproduction*, 11: 297-322.

Sanders, P. M., P. Y. Lee, C. Biesgen, J. D. Boone, T. P. Beals, E. W. Weiler, and R. B. Goldberg. 2000. 'The Arabidopsis *DELAYED DEHISCENCE1* gene encodes an enzyme in the jasmonic acid synthesis pathway', *Plant Cell*, 12: 1041-61.

Santino, A., M. Taurino, S. De Domenico, S. Bonsegna, P. Poltronieri, V. Pastor, and V. Flors. 2013. 'Jasmonate signaling in plant development and defense response to multiple (a)biotic stresses', *Plant Cell Reports*, 32: 1085-98.

Santner, A., and M. Estelle. 2009. 'Recent advances and emerging trends in plant hormone signalling', *Nature*, 459: 1071-78.

Schneider, E. A., C. W. Kazakoff, and F. Wightman. 1985. 'Gas chromatography-mass spectrometry evidence for several endogenous auxins in pea seedling organs', *Planta*, 165: 232-41.

Sheflin, A. M., J. S. Kirkwood, L. M. Wolfe, C. E. Jahn, C. D. Broeckling, D. P. Schachtman, and J. E. Prenni. 2019. 'High-throughput quantitative analysis of phytohormones in sorghum leaf and root tissue by ultra-performance liquid chromatography-mass spectrometry', *Analytical and Bioanalytical Chemistry*, 411: 4839-48.

Shigenaga, A. M., and C. T. Argueso. 2016. 'No hormone to rule them all: Interactions of plant hormones during the responses of plants to pathogens', *Seminars in Cell & Developmental Biology*, 56: 174-89.

Shikata, M., K. Hoshikawa, T. Ariizumi, N. Fukuda, Y. Yamazaki, and H. Ezura. 2016. 'TOMATOMA update: phenotypic and metabolite information in the Micro-Tom mutant resource', *Plant and Cell Physiology*, 57.

Simura, J., I. Antoniadi, J. Siroka, D. Tarkowska, M. Strnad, K. Ljung, and O. Novak. 2018. 'Plant hormonomics: multiple phytohormone profiling by targeted metabolomics', *Plant Physiology*, 177: 476-89.

Singh, P., A. Dave, F. E. Vaistij, D. Worrall, G. H. Holroyd, J. G. Wells, F. Kaminski, I. A. Graham, and M. R. Roberts. 2017. 'Jasmonic acid-dependent regulation of seed dormancy following maternal herbivory in Arabidopsis', *New Phytologist*, 214: 1702-11.

Srivastava, A., and A. K. Handa. 2005. 'Hormonal regulation of tomato fruit development: A molecular perspective', *Journal of Plant Growth Regulation*, 24: 67-82.

Stintzi, A., and J. Browse. 2000. 'The Arabidopsis male-sterile mutant, *opr3*, lacks the 12-oxophytodienoic acid reductase required for jasmonate synthesis', *PNAS*, 97: 10625-30.

Strader, L. C., D. L. Wheeler, S. E. Christensen, J. C. Berens, J. D. Cohen, R. A. Rampey, and B. Bartel. 2011. 'Multiple facets of Arabidopsis seedling development require indole-3-butyric acid-derived auxin', *Plant Cell*, 23: 984-99.

Teribia, N., V. Tijero, and S. Munne-Bosch. 2016. 'Linking hormonal profiles with variations in sugar and anthocyanin contents during the natural development and ripening of sweet cherries', *New Biotechnology*, 33: 824-33.

The Tomato Genome, Consortium. 2012. 'The tomato genome sequence provides insights into fleshy fruit evolution', *Nature*, 485: 635-41.

Tieman, D. M., M. Zeigler, E. A. Schmelz, M. G. Taylor, P. Bliss, M. Kirst, and H. J. Klee. 2006. 'Identification of loci affecting flavour volatile emissions in tomato fruits', *Journal of Experimental Botany*, 57: 887-96.

Trapp, M. A., G. D. De Souza, E. Rodrigues, W. Boland, and A. Mithofer. 2014. 'Validated method for phytohormone quantification in plants', *Frontiers in Plant Science*, 5.

Umehara, M., A. Hanada, S. Yoshida, K. Akiyama, T. Arite, N. Takeda-Kamiya, H. Magome, Y. Kamiya, K. Shirasu, K. Yoneyama, J. Kyozuka, and S. Yamaguchi. 2008. 'Inhibition of shoot branching by new terpenoid plant hormones', *Nature*, 455: 195-U29.

USDA, National Agricultural Statistics Service. 2022. "Vegetables 2021 Summary." In, edited by USDA.

Van Meulebroek, L., J. Vanden Bussche, K. Steppe, and L. Vanhaecke. 2012. 'Ultra-high performance liquid chromatography coupled to high resolution Orbitrap mass spectrometry for metabolomic profiling of the endogenous phytohormonal status of the tomato plant', *Journal of Chromatography A*, 1260: 67-80.

Wang, S. F., J. W. Liu, T. Zhao, C. X. Du, S. M. Nie, Y. Y. Zhang, S. Q. Lv, S. H. Huang, and X. F. Wang. 2019. 'Modification of threonine-1050 of SlBRI1 regulates BR signalling and increases fruit yield of tomato', *BMC Plant Biology*, 19.

Wu, Q., X. Y. Tao, X. Z. Ai, Z. S. Luo, L. C. Mao, T. J. Ying, and L. Li. 2018a. 'Contribution of abscisic acid to aromatic volatiles in cherry tomato (*Solanum lycopersicum* L.) fruit during postharvest ripening', *Plant Physiology and Biochemistry*, 130: 205-14.

Wu, Q., X. Y. Tao, X. Z. Ai, Z. S. Luo, L. C. Mao, T. J. Ying, and L. Li. 2018b. 'Effect of exogenous auxin on aroma volatiles of cherry tomato (Solanum lycopersicum L.) fruit during postharvest ripening', *Postharvest Biology and Technology*, 146: 108-16.

Yang, Dong-Lei, Yinong Yang, and Zuhua He. 2013. 'Roles of plant hormones and their interplay in rice immunity', *Molecular Plant*, 6: 675-85.

Yano, K., K. Aoki, K. Suda, T. Suzuki, N. Sakurai, T. Narita, T. Shin-I, Y. Kohara, H. Ezura, and D. Shibata. 2007. 'KaFTom: Full-length cDNA database of a miniature tomato cultivar Micro-Tom', *Plant and Cell Physiology*, 48: S255-S55.

Yano, Kentaro, Manabu Watanabe, Naoki Yamamoto, Taneaki Tsugane, Koh Aoki, Nozomu Sakurai, and Daisuke Shibata. 2006. 'MiBASE: A database of a miniature tomato cultivar Micro-Tom', *Plant Biotechnology*, 23: 195-98.

Yoon, G. M., and Y. C. Chen. 2017. 'Gas chromatography-based ethylene measurement of Arabidopsis seedlings.' in B. M. Binder and G. E. Schaller (eds.), *Ethylene Signaling: Methods and Protocols*.

Zhang, M., B. Yuan, and P. Leng. 2009. 'The role of ABA in triggering ethylene biosynthesis and ripening of tomato fruit', *Journal of Experimental Botany*, 60: 1579-88.

Zhao, Y. D. 2010. 'Auxin biosynthesis and its role in plant development.' in S. Merchant, W. R. Briggs and D. Ort (eds.), *Annual Review of Plant Biology, Vol 61*.

Zhu, G. T., S. C. Wang, Z. J. Huang, S. B. Zhang, Q. G. Liao, C. Z. Zhang, T. Lin, M. Qin, M. Peng, C. K. Yang, X. Cao, X. Han, X. X. Wang, E. van der Knaap, Z. H. Zhang, X. Cui, H. Klee, A. R. Fernie, J. Luo, and S. W. Huang. 2018. 'Rewiring of the fruit metabolome in tomato breeding', *Cell*, 172: 249-+.

CHAPTER 5

The Plant Hormone Atlas: An artistic perspective of scientific data throughout tomato plant development[5,6]

5.1 SUMMARY

Biological and botanical art have been part of human history worldwide starting with cave drawings during the Paleolithic era. While the first known documents containing botanical drawings did not resemble the plants of interest, global exploration and scientific advancement moved artists to study botanical specimens with more care and detail, resulting in scientifically accurate art. Art and science have commonly been thought of as opposites, however, combining art into science is becoming more common. In my research, I have combined my two interests of botanical illustration and plant hormone research to create the Plant Hormone Atlas. This project was presented at the Art Lab Fort Collins, a public gallery space in Fort Collins, Colorado. Starting with more traditional botanical illustrations, I integrated hormone quantification data into the drawings for display. Additionally, I included two interactive components to the gallery show: “Paint by Hormone” and “Color Your Own Plant Hormone Atlas” both of which participants were encouraged to engage with during their visit to further connect with the art and the science of this project.

[5] Berry, Hannah. *The Plant Hormone Atlas: An Artistic Perspective of Scientific Data throughout Tomato Plant Development*. 25-26 Oct 2021, Art Lab Fort Collins, Fort Collins, CO.
[6] This project was funded by NSF Grant Number 1818211.

5.2 THE EVOLUTION OF BOTANICAL ILLUSTRATION: FROM PREHISTORIC PAINTINGS TO MODERN DIGITAL RENDERINGS

Humans have relied on plants for food, medicine, fuel, and shelter for thousands of years. Therefore, it is not surprising that Paleolithic drawings of the natural world have been found in caves around the world, demonstrating the origins and importance of biological art in human history. The oldest of these paintings have been found in Chauvet Cave in Southern France dating to 30,000 years old (Groeneveld 2017). These paintings are remarkably well preserved and depict hundreds of drawings from handprints to geometric forms to animals (Groeneveld 2017). Interestingly, most of the animals painted on these walls were not hunted and include drawings of lions and bears, deviating from depictions of prey animals in later periods (Groeneveld 2017).

Ealy illustrations of plants and trees have been associated with the agricultural societies of Mesopotamia and ancient Egypt (Buck 2013) and the Johnson Papyrus is the oldest surviving manuscript of botanical illustrations dating to the early 5th century (Simblet 2010). While this is an important piece of history, the artist never referenced the comfrey plant for the drawing, resulting in an inaccurate depiction of the plant (Simblet 2010). In the illustrated Herbals of ancient Greek, Arabic, and Latin texts, the focus was on plants of medicinal use and the drawings were originally done directly from nature (Collins 2000; Sherwood 2005). However, these drawings were copied in later versions of the texts, eventually becoming unrealistic and sometimes unrecognizable depictions of the plants of interest (Collins 2000; Sherwood 2005). While the West experienced the Dark Ages and a decline in botanical art, Chinese and Japanese botany did not encounter a similar halt in scientific and botanical progress. Instead, medical botany continued to develop in the East, accompanied by precise illustrations of thousands of named plants with detailed descriptions (Sherwood 2005). The artistic style of Eastern botanical illustrations is different from those of the West with an emphasis on brush strokes and calligraphy techniques (Rix 2013).

In the early Renaissance, artists began drawing from life, establishing texts containing realistic drawings (Simblet 2010). This trend continued to illustrations of animals and the human form, tying illustration to multiple scientific fields of study (Simblet 2010). Furthermore, the publication of two books in High Renaissance Germany depicted plants in such detail and accuracy that these illustrations could be used in place of living specimens (Simblet 2010). During the Renaissance, Leonardo da Vinci and other artists furthered the scientific illustration field by integrating artistic sensibility with scientific precision (Buck 2013). Influenced by his interests in the golden ratio, da Vinci's "Vitruvian Man" is one of the most recognizable drawings in the world, and other diagrams of the human form greatly contributed to developments in medical illustration (Kron and Krishnan 2019). While da Vinci's achievements in many interests are frequently recognized, his study of flowers are commonly overlooked in the context of botanical art (Rix 2013). da Vinci's drawings demonstrate his careful observation of botanical subjects depicting scientific accuracy and beauty (Rix 2013).

In the early 1600's, florilegia, or flower books, became popular as flowers were grown increasingly for their beauty, novelty, and rarity, instead of their medicinal uses (Saunders 1995). The drawings in florilegia were emphasized over text and often these books were made as catalogues of single gardens (Saunders 1995). During European's exploration of the world, many voyages commissioned artists and naturalists who documented flora and fauna of faraway places in impeccable detail (Saunders 1995; Simblet 2010; Rix 2013). Correlating with increased exploration, biological discoveries, increased wealth, and the development of printing techniques, the Golden Age of Botanical Art of the 18th century marks a significant peak in the artform (Sherwood 2005; Simblet 2010; Rix 2013). During this time, plants around the globe were extensively documented, contributing to the growing scientific knowledge of plant biodiversity (Sherwood 2005; Simblet 2010; Rix 2013).

Even with developments in photography, botanical illustration has maintained prominence because the artist can more easily highlight features for identification and

demonstrate a plant's appearance over time such as throughout development or in different seasons (Saunders 1995; Sherwood 2005; Sherwood and Rix 2008). There are two basic styles of botanical illustration: the illusionistic pictorial representation, generally colored with watercolor; and the outline schematic representation, typically drawn with pen and ink (Saunders 1995). Both styles usually feature the plant on an isolated background and is considered to be the "more scientific" presentation of botanical illustration than drawings with backgrounds showing the ecosystem or environment in which the plant grows (Saunders 1995). Until recently, there was not a permanent, open to the public, location to view botanical art, specifically watercolor pieces due to the fragile nature of the medium (Sherwood and Rix 2008). Opened in 2008, The Shirley Sherwood Gallery of Botanical Art at the Royal Botanic Gardens, Kew is the largest collection of botanical art in the world with over 200,000 botanical paintings from over 300 artists from 36 countries (The Shirley Sherwood Collection ; Sherwood and Rix 2008). It remains the only gallery in the world dedicated to botanical art (Sherwood and Rix 2008).

In the United States, there are a handful of Certificate and Masters' programs teaching specialized techniques for medical, biological, and botanical illustration. Botanical gardens across the country, including the Denver Botanic Gardens in Denver, CO (Denver Botanic Gardens), and The North Carolina Botanical Garden associated with the University of North Carolina at Chapel Hill in Chapel Hill, NC (North Carolina Botanical Garden), offer certificate programs focusing on techniques specialized for botanical illustration. Additionally, the Guild of Natural Science Illustrators (GNSI) and the American Society of Botanical Artists (ASBA) hold annual conferences bringing together scientific illustrators from around the world for workshops, symposia, and training sessions (Guild of Natural Science Illustrators ; American Society of Botanical Artists). With technological advances, techniques using digital software have been added to some programs, though the classic techniques using watercolor and pen and ink are still emphasized in coursework and by botanical art masters.

5.3 NO LONGER OPPOSITES: MERGING ART INTO SCIENCE

Science and art are commonly seen as opposites (Snow 1956) reinforced by ideas of right vs. left brained thinking, however, in reality, art and science are closely related. “A picture is worth a thousand words” is a saying we all know well, and this sentiment has been adapted by both scientific and nonscientific publications. For example, when the first volume of the journal *Nature* was published in 1869, accurate visual representations of the scientific data within was a critical component to the editors and has continued to be a focus of the publication (Belknap 2019).

Both fields of art and science aim to describe and understand the world around us, however, through different approaches (Paterson et al. 2020). Because art and science activate different responses, emotional and logical, respectively, it has been hypothesized that the combination of art and science could elicit a stronger response to global problems such as climate change and thus, transdisciplinary collaborations are becoming more common (Paterson et al. 2020). In the plant biology field, the Bio-Analytical Resource for Plant Biology (Toufighi et al. 2005) has established itself as a resource for visualizing transcriptomic data in many plant species including Arabidopsis, tomato, soybean, rice, and more (Winter et al. 2007). The electronic fluorescent pictograph (eFP) (Winter et al. 2007) tool integrates data into diagrams of plant tissues, cell types, and cellular organelles, combining art and science into an ever-growing body of resources for plant biologists.

5.4 INTEGRATING ART AND SCIENCE IN THE CONTEXT OF TOMATO PLANT HORMONE RESEARCH

Nearly every aspect in a plant’s life is regulated by plant hormones. Just like in our bodies, these small molecules travel throughout the plant to influence growth, development, and responses to the environment (Gaillochet and Lohmann 2015; Shigenaga and Argueso 2016; Kieber and Schaller 2018). Hormones are commonly grouped by major biological function;

primarily growth-related hormones: auxin (Aux), cytokinin (CK), gibberellic acid (GA), brassinosteroids (BRs), and strigolactones (SLs); and primarily stress-related hormones: salicylic acid (SA), jasmonic acid (JA), ethylene (ET), and abscisic acid (ABA). While these groupings can be helpful, the reality of hormone involvement during a plant's life is much more complex where growth-related hormones play critical roles in plant immunity and defense-related hormones contribute to the regulation of plant growth and development (Shigenaga and Argueso 2016). With funding from the National Science Foundation (NSF), we measured 5 of the main plant hormone groups (ABA, Aux, CK, SA, and JA) in roots and shoots throughout *Solanum lycopersicum* cv. Micro-Tom (hereafter Micro-Tom) tomato plant development to establish the Plant Hormone Atlas, which combines biological illustration with scientific data (see Chapter 4). In this exhibit, we aimed to showcase scientific developments in plant hormone quantification at Colorado State University through visual data representation and an interactive installation at the Art Lab Fort Collins in Old Town Fort Collins, Colorado.

An important aspect of plant hormone biology is the accurate quantification of plant hormone species. Plant hormone quantification during development and/or environmental stress provides insight into changes in physiological processes and the regulation of these processes by plant hormones. The distribution of hormones within tomato fruit tissues is essential in each stage of fruit development (Gorguet, van Heusden, and Lindhout 2005; Srivastava and Handa 2005; Quinet et al. 2019). In the last decade, advances in mass spectrometry (MS) have allowed for significant increases in selectivity and sensitivity, leading to protocols for the simultaneous quantification of several plant hormones (Kojima et al. 2009; Pan, Welti, and Wang 2010; Van Meulebroek et al. 2012; Simura et al. 2018). Data collected for the Plant Hormone Atlas will be used to develop a web-based tool for researchers in search of tissue-specific hormone data.

Because of our interest in quantifying hormones throughout tomato plant development, we identified four stages of interest: seedling, 4-leaf vegetative, flowering adult, and fruiting

plants. Drawing from live plants and photographs, I illustrated these four developmental stages (Figure 5.1A-D) to be used as the base drawings for hormone data integration. After analyzing the hormone quantification data (see Chapter 4), I began to add hormone data into my illustrations using a color gradient where a lighter color correlated to a lower hormone concentration and a darker color corresponded to a higher concentration. While we quantified 18 hormone species (Chapter 4), for the Plant Hormone Atlas gallery show, we focused on five hormones, one from each major hormone family: ABA; Aux indole-3-acetic acid (IAA); CK *trans*-Zeatin (*tZ*); SA, and JA (Figure 5.2A-D). All four developmental stages with all five of these hormones were presented during the gallery event to show the concentration and localization changes of these hormones throughout Micro-Tom development.

I have always enjoyed participating in art instillations when visiting galleries and art spaces. Because of the scientific basis of this gallery show, I wanted to make the project more accessible to the public, leading to two interactive components of the gallery show. On large canvases, I drew a tomato flower, leaf, and three sliced fruits at green, breaker, and ripe stages (Figure 5.3A). To these drawings, I drew outlines roughly proportionate to the concentrations of ABA, IAA, SA, tZ, and JA quantified in these tissues (Figure 5.3B). As participants visited the gallery, I encouraged everyone to fill in the outlined spaces with paint pens in a “Paint by Hormone” activity and documented the progression of these pieces over the course of the gallery event (Figure 5.3C-E). After the event, I completed these pieces by filling in remaining white spaces, redrawing the black outlines, and adding stippling for depth and dimension (Figure 5.4A-E). These pieces were gifted to Dr. Cris Argueso and the Argueso Lab for display.

In promoting the gallery event, I printed postcards with my original botanical illustrations to easily share information about the time and location of the show. With left over postcards, I added a section where participants could color their own Plant Hormone Atlas by coloring the postcards with colored pencils. I wanted visitors to be as creative as they wanted, resulting in a beautiful range of drawings (Figure 5.5A). Some early participants added their postcards to the

wall, which evolved into a second art instillation piece, which further encouraged participation in this activity.

5.5 ARTIST STATEMENT

Throughout my educational career, I have been torn between art and science. Fostered by my parents, both of whom are in artistic professions, art was my first passion in life. Through art, I have been able to express my inner child, continuously learn new skills, and challenge my creativity. On the other hand, science has provided me answers to my insatiable curiosity. Since childhood, I have known that science, specifically biology and environmental science, would be integral parts of my future career, and ultimately led me to the Program in Cell and Molecular Biology at Colorado State University for my Ph.D. studies. However, my need for a creative outlet has never dissipated.

During my undergraduate studies at North Carolina State University, I was introduced to biological and botanical art through a course in biological illustration. After a year of classes focused on science, this was my first college level art class, and I immediately connected to the art form. After this class, I received an NSF Research Experience for Undergraduates (REU) internship through the University of New Mexico in Albuquerque, NM, as an Art in Ecology student. As an artist-in-residence of sorts, I illustrated the biological foci of the ecology projects of my fellow REU students, ranging from creosote bush to prairie dogs. After my summer in the Chihuahuan desert, I returned to the biological illustration studio at NCSU during my free time, which led me to a teaching assistant position for the studio section of the course for two semesters. Although unknown to me prior to 2011, biological illustration, and in particular botanical illustration, has become a wonderful outlet for my creativity. By sharing my scientific illustrations, I have been able to integrate and share my scientific data in a special way. I was extremely lucky to have an advisor who encouraged me to integrate my botanical illustration skills into my dissertation. Through The Plant Hormone Atlas, I have combined my interest in

plant hormone research and botanical illustration in a harmonious balance between my two passions.

5.6 DISCUSSION

Art is a powerful way to connect with people around the world and within a community, and botanical art is entering a second Golden Age with more people becoming interested in the artform. This art in science outreach event reached approximately 40 people between the two gallery nights. While most of the participants were associated with Colorado State University, a number of visitors did see the gallery as they were walking by and stopped in. Due to the timing of the event (late October and Monday-Tuesday) the exposure of the event was limited as there were fewer people walking past the Art Lab at this time. If we were to present this work at the gallery for a second time, a weekend opening during warmer months would likely bring in more people.

Regardless of participation numbers, I interacted with nearly every visitor, introduced my art in science project, the goals of the gallery presentation, addressed questions, and encouraged participation in the interactive parts of the exhibit (Figure 5.6). I recognize that the integration of art into a Ph.D. dissertation for a Cell and Molecular Biology program is unusual. Showcasing my artistic abilities along with my scientific research was such a valued component of my graduate school career and I appreciate the opportunity to present my research in such a unique way.

5.7 FIGURES

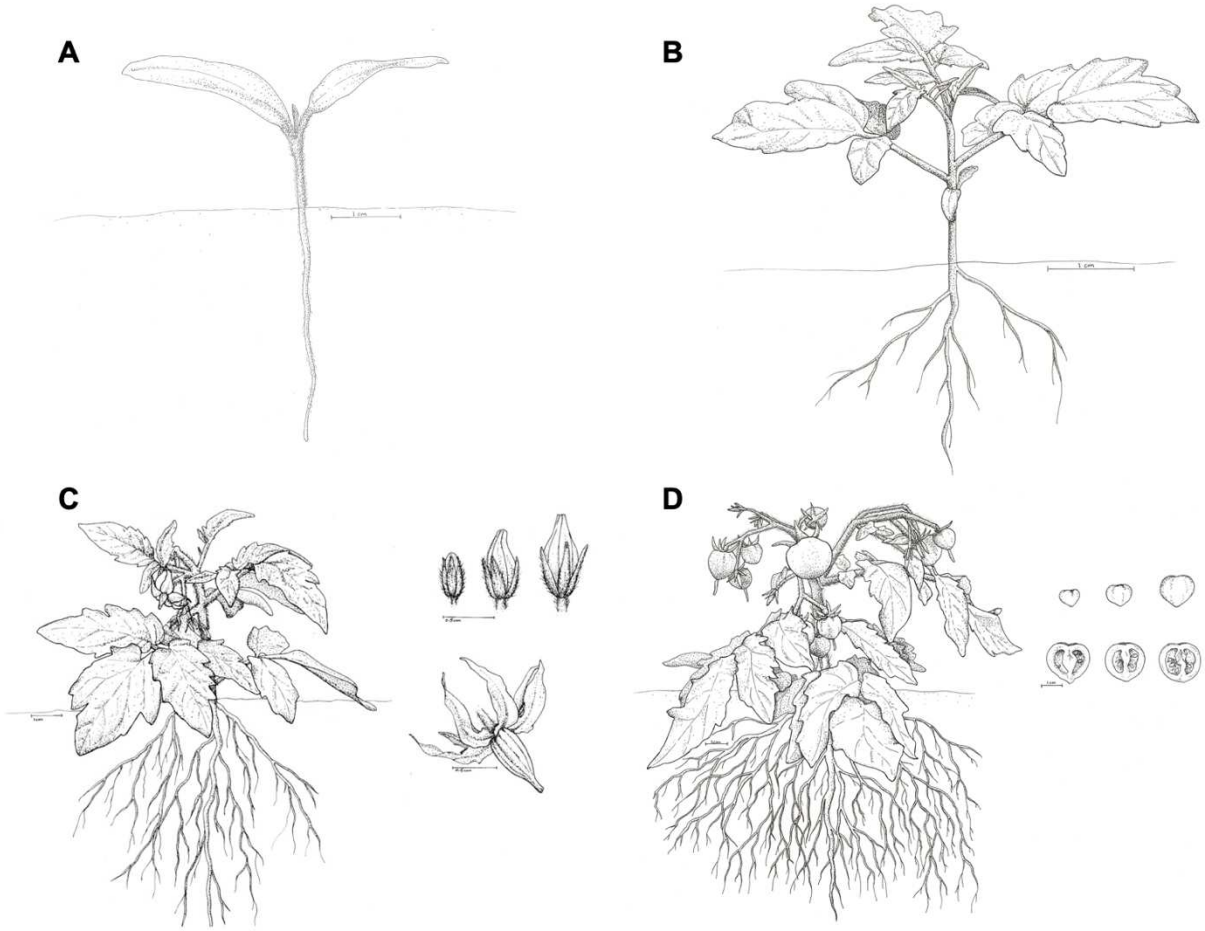

Figure 5.1: Botanical illustrations of Micro-Tom developmental stages. A. The seedling Micro-Tom developmental stage. **B.** The 4-leaf vegetative Micro-Tom developmental stage. **C.** The adult developmental stage, marked by the opening of the first flower with expanded illustrations of bud developmental stages and an open flower depicting different tissues collected for hormone quantification. **D.** The fruiting developmental stage showing different fruit stages and tissues collected for hormone quantification. Scale bars represent 1 cm. All biological illustrations were drawn by Hannah Berry.

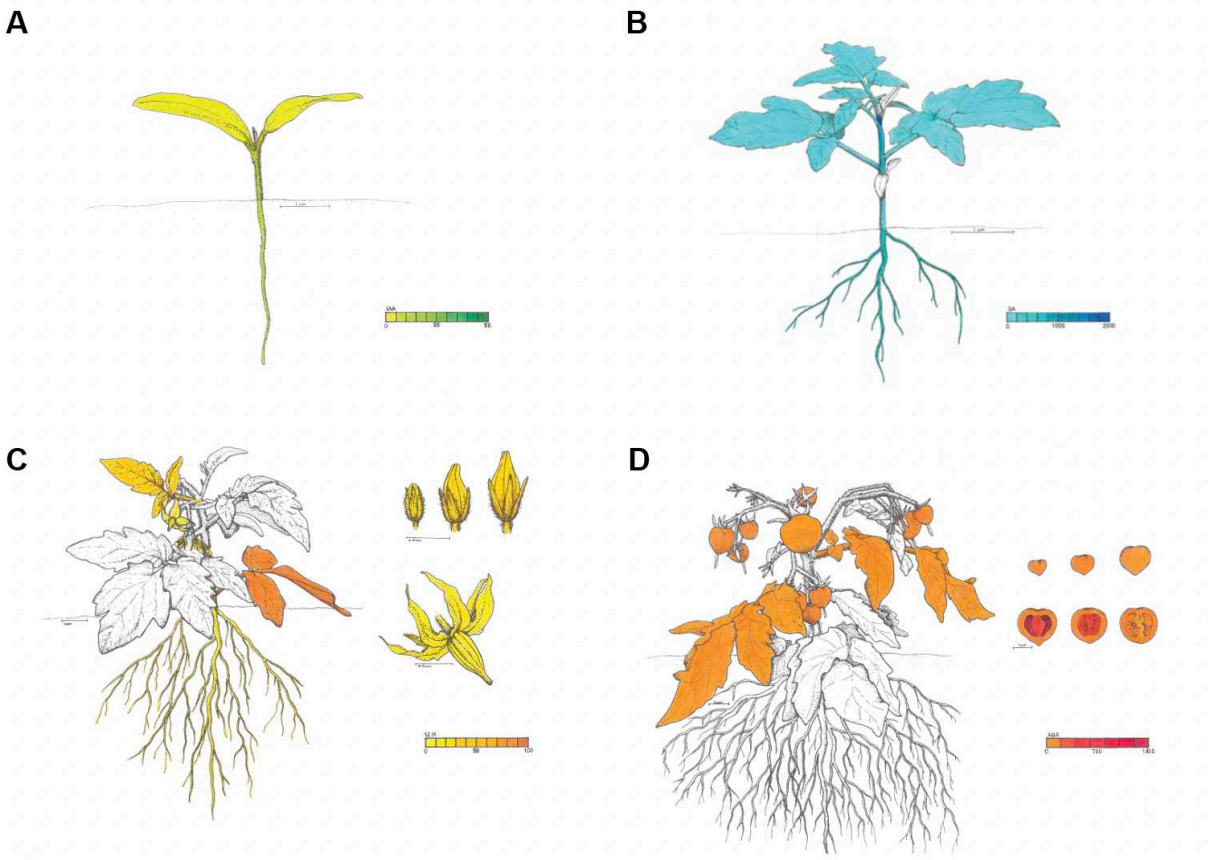

Figure 5.2: Botanical illustrations with integrated hormone data. A. Micro-Tom seedling developmental stage colored with an IAA concentration gradient. **B.** Micro-Tom young plant colored with a SA concentration gradient. **C.** Flowering Micro-Tom and flower bud developmental stages colored with the CK *t*-Z concentration gradient. **D.** Fruiting Micro-Tom and fruit development stages colored with an ABA concentration gradient. For all illustrations, the lack of color indicates the tissue was not collected at that developmental stage and therefore no data is available. In these cases, lack of color does not indicate the hormone was not detected in these tissues.

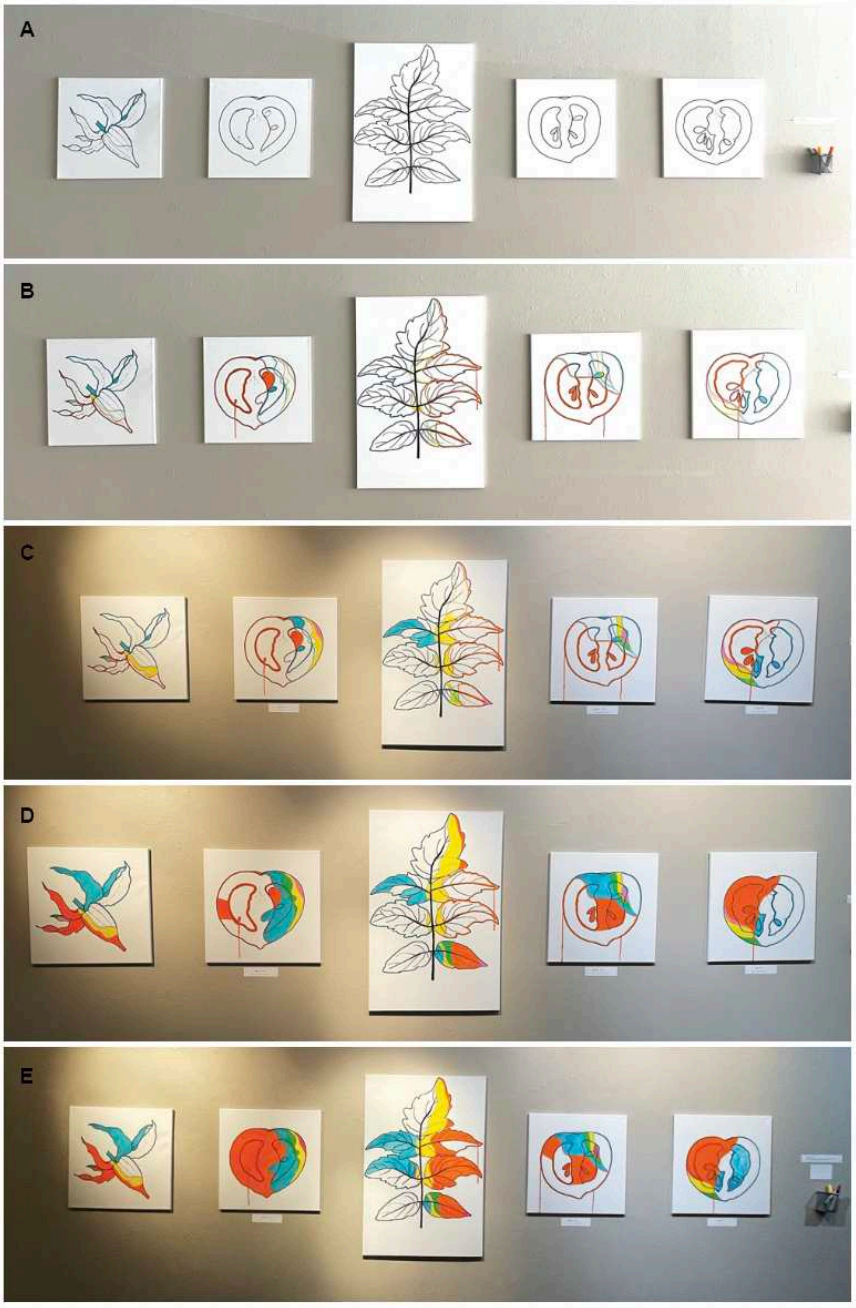

Figure 5.3: Evolution of the paint-by-hormone interactive gallery display. A. Illustrations were drawn in Sharpie on canvas. Drawings left to right: open flower, green fruit, leaf, breaker fruit, ripe fruit. Paint pens were provided to the right of the drawings for participant use to fill in areas of the drawings. **B.** Outlines roughly proportionate to the hormones ABA (orange), IAA (green), *t*Z (yellow), SA (blue), and JA (pink) found in each of these tomato tissues were added to the drawings for the public to fill in. **C.** Progress towards completion of paint-by-hormone pieces at the end of the first gallery night. **D.** Progression of paint-by-hormone drawings during the second night of the gallery event. **E.** Paint-by-hormone illustrations at the end of the second gallery night.

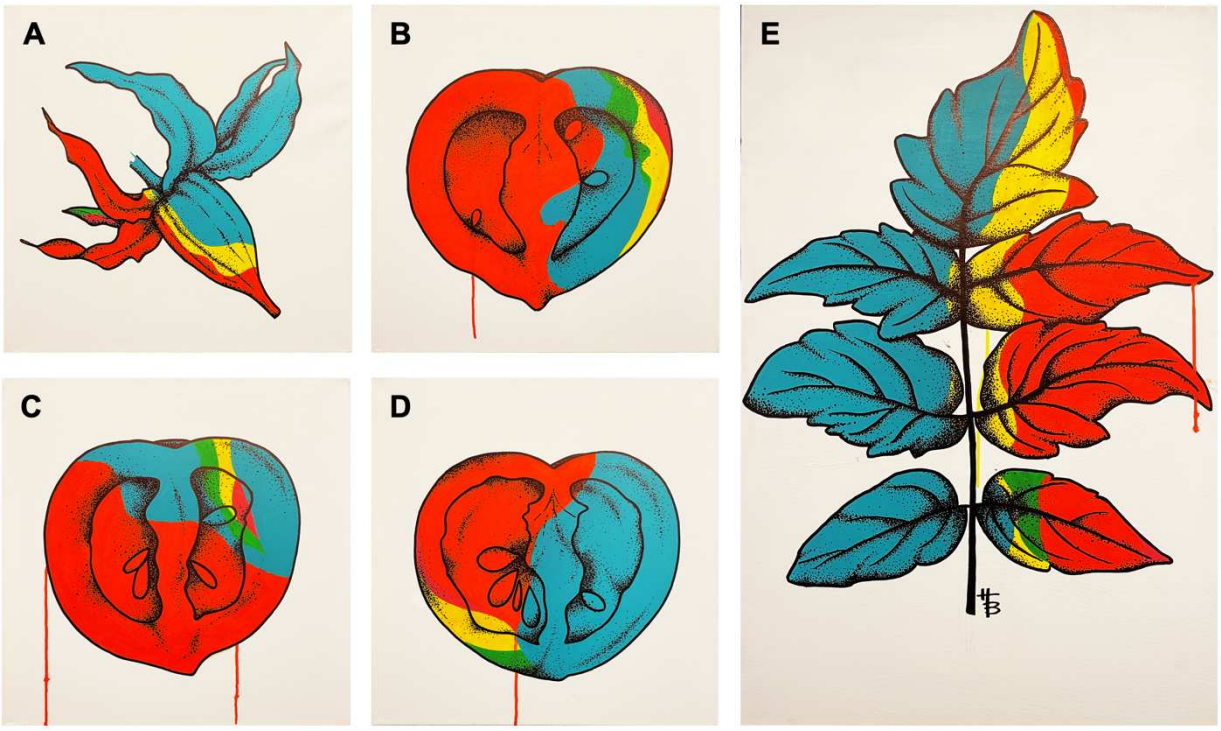

Figure 5.4: Completed paint-by-hormone drawings. A. Micro-Tom flower. **B.** Micro-Tom green fruit. **C.** Micro-Tom breaker fruit. **D.** Micro-Tom ripe fruit. **E.** Micro-Tom fully expanded leaf. Each color represents a different hormone quantified in our hormone panel: orange: ABA; yellow: CK; blue: SA; green: IAA; pink: JA. The amount of each color is roughly proportionate to the amount of each hormone quantified from these tissues. For the tomato fruits, these proportions correspond to the fruit as a whole, and the colors are not proportionate to each tissue type within the fruit.

Figure 5.5: Color your own Plant Hormone Atlas postcards. A. Compilation of colored postcards by participants of the gallery event.

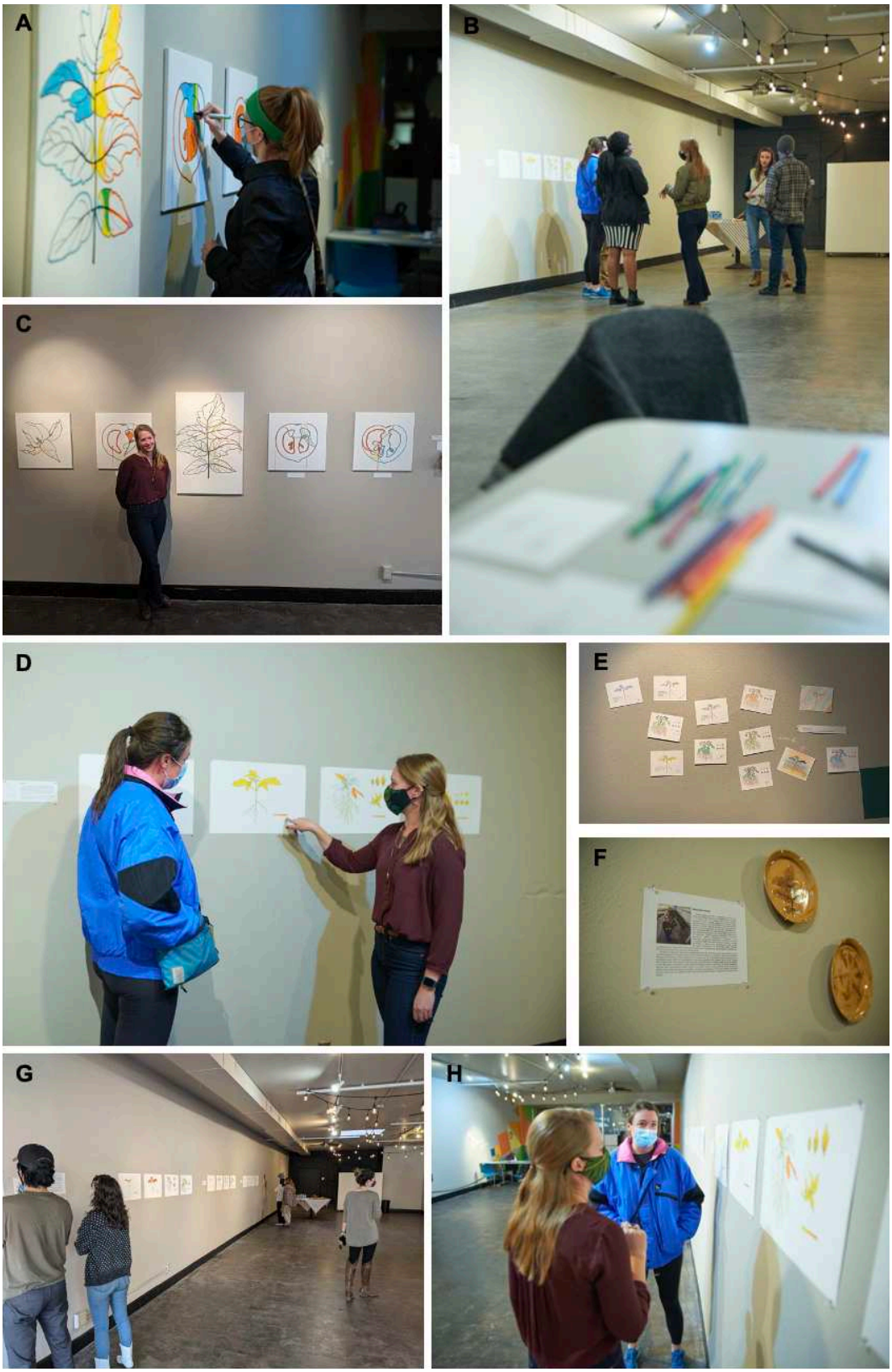

Figure 5.6: Participant interaction with biological illustrations, Paint-by-Hormone, and color your own Plant Hormone Atlas during the gallery event. A. Participant Julie Barnum

adds color to the paint-by-number instillation. **B.** Visitors to the gallery talk to Hannah Berry about the art show. **C.** Artist and scientist Hannah Berry presents her work at the Art Lab in Fort Collins, CO. **D.** Hannah Berry explains how she interpreted hormone quantification data to integrate into her biological illustrations to Jemma Fadum. **E.** Color your own Plant Hormone Atlas postcards left by visitors. **F.** Artist statement and tomato-inspired pottery pieces from Hannah Berry. **G.** Members of the Argueso Lab look around the gallery space and discuss the art pieces. **H.** Hannah Berry and Jemma Fadum chat about the exploration of art in science.

REFERENCES

American Society of Botanical Artists. 'About ASBA'. https://asba-art.org/about.

Belknap, G. 2019. 'The evolution of scientific illustration', *Nature*, 575: 25-28.

Buck, Jutta. 2013. 'The history of botanical art', *The Botanical Artist*, 19: 32-32.

Collins, Minta. 2000. *Medieval Herbals: The Illustrated Traditions* (The British Library: London, UK).

Denver Botanic Gardens. 'School of Botanical Art & Illustration'. https://www.botanicgardens.org/education/school-botanical-art-illustration.

Gaillochet, C., and J. U. Lohmann. 2015. 'The never-ending story: from pluripotency to plant developmental plasticity', *Development*, 142: 2237-49.

Gorguet, B., A. W. van Heusden, and P. Lindhout. 2005. 'Parthenocarpic fruit development in tomato', *Plant Biology*, 7: 131-39.

Groeneveld, Emma. 2017. "Chauvet Cave." In *World History Encyclopedia*.

Guild of Natural Science Illustrators. 'GNSI'. https://www.gnsi.org.

Kieber, J. J., and G. E. Schaller. 2018. 'Cytokinin signaling in plant development', *Development*, 145.

Kojima, M., T. Kamada-Nobusada, H. Komatsu, K. Takei, T. Kuroha, M. Mizutani, M. Ashikari, M. Ueguchi-Tanaka, M. Matsuoka, K. Suzuki, and H. Sakakibara. 2009. 'Highly sensitive and high-throughput analysis of plant hormones using MS-probe modification and liquid chromatography tandem mass spectrometry: an application for hormone profiling in *Oryza sativa*', *Plant and Cell Physiology*, 50: 1201-14.

Kron, Tomas, and Prem Krishnan. 2019. 'Leonardo DaVinci's contributions to medical physics and biomedical engineering: celebrating the life of a 'Polymath'', *Australasian Physical & Engineering Sciences in Medicine*, 42: 403-05.

North Carolina Botanical Garden. 'Botanical Art & Illustration'. https://ncbg.unc.edu/learn/adult-programs/botanical-art-illustration/.

Pan, X. Q., R. Welti, and X. M. Wang. 2010. 'Quantitative analysis of major plant hormones in crude plant extracts by high-performance liquid chromatography-mass spectrometry', *Nature Protocols*, 5: 986-92.

Paterson, Shona K., Martin Le Tissier, Hester Whyte, Lisa B. Robinson, Kristin Thielking, Mrill Ingram, and John McCord. 2020. 'Examining the potential of art-science collaborations in the anthropocene: a aase study of Catching a Wave', *Frontiers in Marine Science*, 7.

Quinet, M., T. Angosto, F. J. Yuste-Lisbona, R. Blanchard-Gros, S. Bigot, J. P. Martinez, and S. Lutts. 2019. 'Tomato fruit development and metabolism', *Frontiers in Plant Science*, 10.

Rix, Martyn. 2013. *The Golden Age of Botanical Art* (The University of Chicago Press: Chicago).

Saunders, Gill. 1995. *Picturing Plants: An Analytical History of Botanical Illustrations* (University of California Press: Los Angeles, CA).

Sherwood, Shirley. 2005. *A New FLowering: 1000 Years of Botanical Art* (The Ashmolean Museum: Oxford).

Sherwood, Shirley, and Martyn Rix. 2008. *Treasures of Botanical Art* (Royal Botanic Gardens, Kew: Richmond Surrey, UK).

Shigenaga, A. M., and C. T. Argueso. 2016. 'No hormone to rule them all: Interactions of plant hormones during the responses of plants to pathogens', *Seminars in Cell & Developmental Biology*, 56: 174-89.

Simblet, Sarah. 2010. *Botany for the Artist: An Inspirational Guide to Drawing Plants* (DK Publishing: New York, NY).

Simura, J., I. Antoniadi, J. Siroka, D. Tarkowska, M. Strnad, K. Ljung, and O. Novak. 2018. 'Plant hormonomics: multiple phytohormone profiling by targeted metabolomics', *Plant Physiology*, 177: 476-89.

Snow, C. P. 1956. *The Two Cultures* (Cambridge University Press: Cambridge).

Srivastava, A., and A. K. Handa. 2005. 'Hormonal regulation of tomato fruit development: A molecular perspective', *Journal of Plant Growth Regulation*, 24: 67-82.

The Shirley Sherwood Collection. 'Botanical Art: Collection and Gallery'. https://shirleysherwood.com.

Toufighi, K., S. M. Brady, R. Austin, E. Ly, and N. J. Provart. 2005. 'The botany array resource: e-Northerns, expression angling, and promoter analyses', *Plant Journal*, 43: 153-63.

Van Meulebroek, L., J. Vanden Bussche, K. Steppe, and L. Vanhaecke. 2012. 'Ultra-high performance liquid chromatography coupled to high resolution Orbitrap mass spectrometry for metabolomic profiling of the endogenous phytohormonal status of the tomato plant', *Journal of Chromatography A*, 1260: 67-80.

Winter, D., B. Vinegar, H. Nahal, R. Ammar, G. V. Wilson, and N. J. Provart. 2007. 'An "Electronic Fluorescent Pictograph" browser for exploring and analyzing large-scale biological data sets', *PLOS One*, 2.

CHAPTER 6

Conclusions and Future Directions

6.1 INTRODUCTION

As sessile organisms, plants must balance responses to abiotic and biotic stressors in their environment with plant growth and development. Phytohormones are critical regulators of these responses, and through signaling plasticity, plant immunity is tightly regulated upon pathogen perception (Bernoux, Ellis, and Dodds 2011). Mutations resulting in increased accumulation or signaling of the defense-related hormone salicylic acid (SA) have increased disease resistance to a broad range of hemi-biotrophic and biotrophic pathogens. However, these mutants often have a severe reduction in overall plant growth as well as additional developmental abnormalities including loss of apical dominance, reduced seed yield, and ectopic meristem development (Bowling et al. 1997; Clarke et al. 1998; Li et al. 2001; Igari et al. 2008). This phenomenon, known as the growth defense tradeoff, has been characterized in *Arabidopsis thaliana* (hereafter Arabidopsis) as well as crop species (Ning, Liu, and Wang 2017).

The growth defense tradeoff was initially thought to be a result of metabolic resource limitations, but recent studies have demonstrated that growth and defense can be uncoupled resulting in increased defense without negative impacts to plant growth and development (Herms and Mattson 1992; Moreno et al. 2009; Hu et al. 2013; Huot et al. 2014; Leone et al. 2014; Campos et al. 2016; Kliebenstein 2016; Schuman and Baldwin 2016; Major et al. 2017). The hormone cytokinin (CK) was first identified in 1955 as a critical regulator of cell division (Miller et al. 1955) and has since been associated with regulation of leaf senescence, meristem maintenance, and vasculature development (Argueso, Ferreira, and Kieber 2009). Furthermore, recent advancements have revealed the importance of CK in plant immune responses to

biotrophic pathogens via crosstalk with SA (Choi et al. 2010; Argueso et al. 2012; Naseem et al. 2012). While the mechanisms of regulating the switch between growth and defense are not completely understood, plant hormones are essential regulators of plant development and biotic and abiotic stressors. In this dissertation, I have focused on impacts to plant development in response to SA-associated constitutive and activated immunity and a family of CK-regulated transcription factors that may act as a switch between growth and defense processes.

6.2 CYTOKININ RESPONSE FACTORS AS MEDIATORS OF PLANT GROWTH AND DEFENSE

Perception of CK initiates a phosphorelay mechanism resulting in the upregulation of multiple transcription factors including CYTOKININ RESPONSE FACTORS (CRFs) (Argueso, Ferreira, and Kieber 2009; Hwang, Sheen, and Muller 2012; Rashotte et al. 2006). CRFs are found in all land plant species and are defined by a CRF domain at the N-terminal end and an APETALA2/ETHYLENE RESPONSE FACTOR (AP2/ERF) DNA-binding domain near the center of the protein (Rashotte and Goertzen 2010). Previous data has suggested that CRFs may act as a switch between CK-regulated growth and SA-associated defense responses as lines overexpressing *CRFs* are less susceptible to pathogen infection than wildtype (Kwon 2016; Liang et al. 2010). Of the six main CRFs in Arabidopsis, *CRF2* and *CRF5* are known to be rapidly and robustly upregulated after CK treatment, followed by *CRF6* at a later timepoint, while expression of the other *CRFs* were not regulated by CK signaling (Rashotte et al. 2003; Raines et al. 2016).

In Chapter 2, I showed that CRFs are differentially regulated by CK and SA treatments and by pathogen inoculations. Furthermore, I showed that overexpression of *CRF1* or *CRF5* reduces plant susceptibility to *Pseudomonas syringae* pv. *tomato* DC3000 (*Pst* DC3000), however, *CRF* overexpression does result in suppressed growth and reduced plant fertility.

The mutant *CONSTITUTIVE EXPRESSION OF PR GENES 5* (*cpr5*) has elevated levels of SA and *PATHOGENESIS RELATED-1* (*PR-1*) gene expression and has distinct autoimmunity phenotypes including reduced rosette size, spontaneous lesion formation, and reduced seed yield (Bowling et al. 1997). These phenotypes are shared with *CRF5ox* lines, therefore we crossed *cpr5* and *CRF5ox* 3G to determine if *CRF5* and *CPR5* act in the same pathway to regulate plant growth and immunity. The resulting line, *cpr5, CRF5ox*, had a further decrease in rosette area compared to either parental line, and a more severe delay in flowering time. Because of the change in phenotype, we determined that *CPR5* and *CRF5* act in different pathways.

To further characterize *cpr5, CRF5ox*, we performed an RNA-seq experiment to evaluate changes in gene expression related to SA and CK biosynthesis and signaling. SA biosynthesis and signaling genes are up-regulated in *cpr5*, *CRF5ox* 3G, and *cpr5, CRF5ox* compared to Col-0, while CK biosynthesis and signaling genes are generally down-regulated in these lines. Because of previous reports showing that SA plays an inhibitory role on CK (Argueso et al. 2012), these expression patterns support SA inhibition on CK. Furthermore, gene ontology (GO) analysis of differentially expressed genes (DEGs) in *cpr5*, *CRF5ox* 3G, and *cpr5, CRF5ox* compared to Col-0 showed increases in terms associated with defense responses to bacterial and fungal pathogens, and responses to SA and jasmonic acid (JA), another defense-related hormone. Further investigation into these genes revealed that *cpr5* and *CRF5ox* 3G had a combinatorial effect on gene expression patterns in *cpr5, CRF5ox*, and while *CPR5* and *CRF5* act in different pathways, they regulate a similar subset of genes. Because of these data, I proposed a model for which CRF5 acts in balancing CK-mediated plant growth and SA-associated plant defense responses, thus acting as a switch between these two processes.

6.3 PLANT ARCHITECTURE AND REGULATION BY SALICYLIC ACID

Plant architecture is a critical component of agricultural yield and is a necessary consideration in engineering crop lines with increased resistance to abiotic and biotic stressors without severe compromises to seed yield. CK and auxin, another growth-related hormone, have been shown to maintain pluripotent cell populations, cell division, and cell differentiation in the shoot and root apical meristems (SAM and RAM) (Gaillochet and Lohmann 2015). Together, they regulate shoot architecture originating at the SAM via CK inhibitory fields (Besnard, Rozier, and Vernoux 2014; Besnard et al. 2014) and auxin maxima (Vernoux et al. 2000; Reinhardt et al. 2003; Mallory, Bartel, and Bartel 2005; Lohmann et al. 2010; Vernoux et al. 2011; Fujita and Kawaguchi 2018), resulting in precise placement of primordia around the meristem. This regular patterning of consecutive organs around a central point is known as phyllotaxis. Arabidopsis follows a spiral phyllotactic pattern where consecutive organs are separated by 137.5°. Mutations displaying altered phyllotactic pattern can result from increased meristem size (Landrein et al. 2015; Mandel et al. 2014; Yang et al. 2015), disrupted CK and auxin crosstalk (Besnard, Rozier, and Vernoux 2014), mis-regulation of stem cell populations (Gallois et al. 2002; Byrne et al. 2003; Goldshmidt et al. 2008; Szczesny, Routier-Kierzkowska, and Kwiatkowska 2009), or post-meristematic development (Peaucelle et al. 2007; Landrein et al. 2013; Burian et al. 2015).

SA accumulating mutants *snc1*, *cpr5*, and *cpr6* have constitutively activated defense and distinct developmental phenotypes including reduced plant growth, loss of apical dominance, and spontaneous lesion development (Bowling et al. 1997; Clarke et al. 1998; Li et al. 2001), but developmental patterns have not been characterized. Notably, these phenotypes resemble that of some auxin deficient mutants (Wang et al. 2007). Auxin-responsive genes were down-regulated in plants treated with SA, however, auxin concentrations remained the same as untreated plants (Wang et al. 2007). This data showed that a transient increase in SA signaling does not influence auxin accumulation. On the other hand, constitutive immunity mutants had a

significant reduction in auxin concentrations indicating that elevated endogenous SA does have a negative impact on auxin accumulation (Wang et al. 2007). This lends us to the idea that constitutively high levels of SA in these constitutive immunity mutants could also have a negative impact on CK biosynthesis or accumulation contributing to these distinct developmental phenotypes. In Chapter 3, I quantified silique phyllotactic patterns along the primary stem of Col-0 wild type, constitutive immunity mutants *snc1* and *cpr5*, and mutants *ENHANCED DISEASE SUSCEPTIBILITY 16* (*eds16*) and *NONEXPRESSER OF PR GENES 1* (*npr1*) resulting in decreased SA biosynthesis and signaling, respectively. Both *snc1* and *cpr5* mutants had altered phyllotactic patterning resulting from reduced SAM area and increased plastochron. This implements SA in meristematic regulation, likely through crosstalk with CK and/or auxin.

Because constitutive activation of defense changed phyllotaxis, I next investigated if activation of immunity, which leads to increased SA biosynthesis and signaling, could also change plant architecture. Using multiple strains of *Pst* DC3000 initiating a low level of plant defense, plant susceptibility, or a robust defense response, I evaluated developmental patterns of siliques and of the SAM. Here, I found that the increased SA accumulation and signaling resulting from activated immunity cannot overcome robust meristematic maintenance and patterning. Additionally, the SAM size and plastochron were not changed, even after repeated treatment of any *Pst* strain. Only after repeated inoculation with high concentrations of *Pst* DC3000 were phyllotactic patterns changed, however, these changes were a result of post-meristematic development seen in stem torsion analysis. Overall, in Chapter 2, I show that constitutively high levels of SA change phyllotactic patterns originating in the SAM but activation of defense in response to pathogen perception cannot change the robustly controlled and guarded meristem to change plant development.

6.4 SPATIOTEMPORAL DISTRIBUTION OF PLANT HORMONES THORUGHOUT TOMATO PLANT DEVELOPMENT

Hormones play a critical role in fruit development, and multiple studies have demonstrated that the balance of auxin, CK, gibberellic acid (GA), ethylene, and abscisic acid (ABA) is tightly controlled throughout fruit development (Gillaspy, Bendavid, and Gruissem 1993; Srivastava and Handa 2005; McAtee et al. 2013; Kou et al. 2021). While Arabidopsis is an excellent resource to evaluate hormone signaling and crosstalk pathways, it does not set fleshy fruit and thus falls short as a model species to evaluate the hormonal role of fruit development. Therefore, I used *Solanum lycopersicum* cv. MicroTom (hereafter Micro-Tom) to quantify plant hormones at multiple stages of plant and fruit development.

Limitations in hormone extraction and quantification methods prevented the simultaneous evaluation of all plant hormones from a small amount of tissue. As more recent protocols have been developed to achieve this goal, studies have focused on limited tissue types or a single stage of plant development (Kojima et al. 2009; Pan, Welti, and Wang 2010; Van Meulebroek et al. 2012; Simura et al. 2018). Here, I quantified 18 hormone species from 5 major hormone families from above- and below-ground tissues from four stages of Micro-Tom in Chapter 4 using a protocol previously established by the Proteomics and Metabolomics Facility at Colorado State University (Sheflin et al. 2019).

Based on the overall hormone patterns, I identified key hormones at each developmental stage (seedling, four-leaf vegetative, flowering adult, or fruiting stages) for further discussion. While the data in this chapter is descriptive in nature, my data reinforces previously found results and provides a single data set covering many tissue types and multiple stages of plant development. In combination with transcriptomic data, spatiotemporal resolution of hormones will likely provide insight into phytohormone functions in Micro-Tom development. Furthermore, this data will be developed into a resource for plant biologists to investigate hormone-related hypotheses.

As many mutations in hormone biosynthesis or signaling pathways have been introgressed into the Micro-Tom background, we can evaluate hormone crosstalk during development and defense. I have been working on crossing these mutant lines to establish a double mutant population to address how the loss of two hormones changes plant development and defense responses to *Pst* DC3000. Due to some challenges, I was unable to evaluate these questions, however, these populations will be a valuable resource for our lab when developed further.

6.5 FUTURE DIRECTIONS IN PLANT ARCHITECTURE

As the human population rises, agricultural yields are expected to fall short of global demand. Shoot architecture is of significant agricultural importance as modifications in SAM development ultimately dictates shoot architectural patterns and seed yield (Li, Meng, et al. 2022). It is therefore imperative that shoot architecture traits are evaluated and considered during the establishment of new crop lines, in addition to shoot and root size phenotypes. Considering the hormonal role in SAM maintenance and primordia spacing and development, crosstalk between these regulatory hormones provides a starting point for maximizing agricultural yields. Recent advancements have shown growth and defense can be uncoupled in Arabidopsis, rice, and wheat through mutant combinations, optimized expression of select transcription factors, and targeted genetic modification (Goto et al. 2015; Campos et al. 2016; Liu et al. 2019; Li, Lin, et al. 2022). Because CRFs are present in all land plant species and play a role in plant growth and defense, they are of interest for optimizing growth and defense in species beyond Arabidopsis. Furthermore, integration of transcriptomic networks in conjunction with hormone quantification data will provide additional insight for establishing crop lines with ideal plant architecture, growth, and immunity.

REFERENCES

Argueso, C. T., F. J. Ferreira, P. Epple, J. P. C. To, C. E. Hutchison, G. E. Schaller, J. L. Dangl, and J. J. Kieber. 2012. 'Two-component elements mediate interactions between cytokinin and salicylic acid in plant immunity', *PLOS Genetics*, 8.

Argueso, C. T., F. J. Ferreira, and J. J. Kieber. 2009. 'Environmental perception avenues: the interaction of cytokinin and environmental response pathways', *Plant Cell and Environment*, 32: 1147-60.

Bernoux, M., J. G. Ellis, and P. N. Dodds. 2011. 'New insights in plant immunity signaling activation', *Current Opinion in Plant Biology*, 14: 512-18.

Besnard, F., Y. Refahi, V. Morin, B. Marteaux, G. Brunoud, P. Chambrier, F. Rozier, V. Mirabet, J. Legrand, S. Laine, E. Thevenon, E. Farcot, C. Cellier, P. Das, A. Bishopp, R. Dumas, F. Parcy, Y. Helariutta, A. Boudaoud, C. Godin, J. Traas, Y. Guedon, and T. Vernoux. 2014. 'Cytokinin signalling inhibitory fields provide robustness to phyllotaxis', *Nature*, 505: 417-+.

Besnard, F., F. Rozier, and T. Vernoux. 2014. 'The AHP6 cytokinin signaling inhibitor mediates an auxin-cytokinin crosstalk that regulates the timing of organ initiation at the shoot apical meristem', *Plant Signaling & Behavior*, 9.

Bowling, S. A., J. D. Clarke, Y. D. Liu, D. F. Klessig, and X. N. Dong. 1997. 'The *cpr5* mutant of Arabidopsis expresses both NPR1-dependent and NPR1-independent resistance', *Plant Cell*, 9: 1573-84.

Burian, A., M. Raczynska-Szajgin, D. Borowska-Wykret, A. Piatek, M. Aida, and D. Kwiatkowska. 2015. 'The *CUP-SHAPED COTYLEDON2* and *3* genes have a post-meristematic effect on *Arabidopsis thaliana* phyllotaxis', *Annals of Botany*, 115: 807-20.

Byrne, M. E., A. T. Groover, J. R. Fontana, and R. A. Martienssen. 2003. 'Phyllotactic pattern and stem cell fate are determined by the Arabidopsis homeobox gene *BELLRINGER'*, *Development*, 130: 3941-50.

Campos, M. L., Y. Yoshida, I. T. Major, D. D. Ferreira, S. M. Weraduwage, J. E. Froehlich, B. F. Johnson, D. M. Kramer, G. Jander, T. D. Sharkey, and G. A. Howe. 2016. 'Rewiring of jasmonate and phytochrome B signalling uncouples plant growth-defense tradeoffs', *Nature Communications*, 7.

Choi, J., S. U. Huh, M. Kojima, H. Sakakibara, K. H. Paek, and I. Hwang. 2010. 'The cytokinin-activated transcription factor ARR2 promotes plant immunity via TGA3/NPR1-dependent salicylic acid signaling in Arabidopsis', *Developmental Cell*, 19: 284-95.

Clarke, J. D., Y. D. Liu, D. F. Klessig, and X. N. Dong. 1998. 'Uncoupling *PR* gene expression from NPR1 and bacterial resistance: Characterization of the dominant Arabidopsis *cpr6-1* mutant', *Plant Cell*, 10: 557-69.

Fujita, H., and M. Kawaguchi. 2018. 'Spatial regularity control of phyllotaxis pattern generated by the mutual interaction between auxin and PIN1', *PLOS Computational Biology*, 14.

Gaillochet, C., and J. U. Lohmann. 2015. 'The never-ending story: from pluripotency to plant developmental plasticity', *Development*, 142: 2237-49.

Gallois, J. L., C. Woodward, G. V. Reddy, and R. Sablowski. 2002. 'Combined *SHOOT MERISTEMLESS* and *WUSCHEL* trigger ectopic organogenesis in Arabidopsis', *Development*, 129: 3207-17.

Gillaspy, G., H. Bendavid, and W. Gruissem. 1993. 'Fruits - A developmental perspective', *Plant Cell*, 5: 1439-51.

Goldshmidt, A., J. P. Alvarez, J. L. Bowman, and Y. Eshed. 2008. 'Signals derived from *YABBY* gene activities in organ primordia regulate growth and partitioning of Arabidopsis shoot apical meristems', *Plant Cell*, 20: 1217-30.

Goto, S., F. Sasakura-Shimoda, M. Suetsugu, M. G. Selvaraj, N. Hayashi, M. Yamazaki, M. Ishitani, M. Shimono, S. Sugano, A. Matsushita, T. Tanabata, and H. Takatsuji. 2015. 'Development of disease-resistant rice by optimized expression of *WRKY45*', *Plant Biotechnology Journal*, 13: 753-65.

Herms, D. A., and W. J. Mattson. 1992. 'The dilemma of plants - To grow or defend', *Quarterly Review of Biology*, 67: 283-335.

Hu, P., W. Zhou, Z. W. Cheng, M. Fan, L. Wang, and D. X. Xie. 2013. 'JAV1 controls jasmonate-regulated plant defense', *Molecular Cell*, 50: 504-15.

Huot, B., J. Yao, B. L. Montgomery, and S. Y. He. 2014. 'Growth-defense tradeoffs in plants: A balancing act to optimize fitness', *Molecular Plant*, 7: 1267-87.

Hwang, I., J. Sheen, and B. Muller. 2012. 'Cytokinin signaling networks.' in S. S. Merchant (ed.), *Annual Review of Plant Biology, Vol 63*.

Igari, K., S. Endo, K. Hibara, M. Aida, H. Sakakibara, T. Kawasaki, and M. Tasaka. 2008. 'Constitutive activation of a CC-NB-LRR protein alters morphogenesis through the cytokinin pathway in Arabidopsis', *Plant Journal*, 55: 14-27.

Kliebenstein, D. J. 2016. 'False idolatry of the mythical growth versus immunity tradeoff in molecular systems plant pathology', *Physiological and Molecular Plant Pathology*, 95: 55-59.

Kojima, M., T. Kamada-Nobusada, H. Komatsu, K. Takei, T. Kuroha, M. Mizutani, M. Ashikari, M. Ueguchi-Tanaka, M. Matsuoka, K. Suzuki, and H. Sakakibara. 2009. 'Highly sensitive and high-throughput analysis of plant hormones using MS-probe modification and liquid chromatography tandem mass spectrometry: An application for hormone profiling in *Oryza sativa*', *Plant and Cell Physiology*, 50: 1201-14.

Kou, X. H., S. Yang, L. P. Chai, C. E. Wu, J. Q. Zhou, Y. F. Liu, and Z. H. Xue. 2021. 'Abscisic acid and fruit ripening: Multifaceted analysis of the effect of abscisic acid on fleshy fruit ripening', *Scientia Horticulturae*, 281.

Kwon, T. 2016. 'Cytokinin Response Factor 2 positively regulates salicylic acid-mediated plant immunity in *Arabidopsis thaliana*', *Plant Biotechnology*, 33: 207-+.

Landrein, B., R. Lathe, M. Bringmann, C. Vouillot, A. Ivakov, A. Boudaoud, S. Persson, and O. Hamant. 2013. 'Impaired cellulose synthase guidance leads to stem torsion and twists phyllotactic patterns in Arabidopsis', *Current Biology*, 23: 895-900.

Landrein, B., Y. Refahi, F. Besnard, N. Hervieux, V. Mirabet, A. Boudaoud, T. Vernoux, and O. Hamant. 2015. 'Meristem size contributes to the robustness of phyllotaxis in Arabidopsis', *Journal of Experimental Botany*, 66: 1317-24.

Leone, M., M. M. Keller, I. Cerrudo, and C. L. Ballare. 2014. 'To grow or defend? Low red : far-red ratios reduce jasmonate sensitivity in Arabidopsis seedlings by promoting DELLA degradation and increasing JAZ10 stability', *New Phytologist*, 204: 355-67.

Li, S. N., D. X. Lin, Y. W. Zhang, M. Deng, Y. X. Chen, B. Lv, B. S. Li, Y. Lei, Y. P. Wang, L. Zhao, Y. T. Liang, J. X. Liu, K. L. Chen, Z. Y. Liu, J. Xiao, J. L. Qiu, and C. X. Gao. 2022. 'Genome-edited powdery mildew resistance in wheat without growth penalties', *Nature*, 602: 455-+.

Li, S. P., S. J. Meng, J. F. Weng, and Q. Y. Wu. 2022. 'Fine-tuning shoot meristem size to feed the world', *Trends in Plant Science*, 27: 355-63.

Li, X., J. D. Clarke, Y. L. Zhang, and X. N. Dong. 2001. 'Activation of an EDS1-mediated *R*-gene pathway in the *snc1* mutant leads to constitutive, NPR1-independent pathogen resistance', *MPMI*, 14: 1131-39.

Liang, Y. S., N. Ermawati, J. Y. Cha, M. H. Jung, M. Su'udi, M. G. Kim, S. H. Ha, C. G. Park, and D. Son. 2010. 'Overexpression of an AP2/ERF-type transcription factor *CRF5* confers pathogen resistance to Arabidopsis plants', *Journal of the Korean Society for Applied Biological Chemistry*, 53: 142-48.

Liu, M. M., Z. Y. Shi, X. H. Zhang, M. X. Wang, L. Zhang, K. Z. Zheng, J. Y. Liu, X. M. Hu, C. R. Di, Q. Qian, Z. H. He, and D. L. Yang. 2019. 'Inducible overexpression of *Ideal Plant Architecture1* improves both yield and disease resistance in rice', *Nature Plants*, 5: 389-400.

Lohmann, D., N. Stacey, H. Breuninger, Y. Jikumaru, D. Muller, A. Sicard, O. Leyser, S. Yamaguchi, and M. Lenhard. 2010. '*SLOW MOTION* is required for within-plant auxin homeostasis and normal timing of lateral organ initiation at the shoot meristem in Arabidopsis', *Plant Cell*, 22: 335-48.

Major, I. T., Y. Yoshida, M. L. Campos, G. Kapali, X. F. Xin, K. Sugimoto, D. D. Ferreira, S. Y. He, and G. A. Howe. 2017. 'Regulation of growth-defense balance by the JASMONATE ZIM-DOMAIN (JAZ)-MYC transcriptional module', *New Phytologist*, 215: 1533-47.

Mallory, A. C., D. P. Bartel, and B. Bartel. 2005. 'MicroRNA-directed regulation of Arabidopsis *AUXIN RESPONSE FACTOR17* is essential for proper development and modulates expression of early auxin response genes', *Plant Cell*, 17: 1360-75.

Mandel, T., F. Moreau, Y. Kutsher, J. C. Fletcher, C. C. Carles, and L. E. Williams. 2014. 'The ERECTA receptor kinase regulates Arabidopsis shoot apical meristem size, phyllotaxy and floral meristem identity', *Development*, 141: 830-41.

McAtee, P., S. Karim, R. Schaffer, and K. David. 2013. 'A dynamic interplay between phytohormones is required for fruit development, maturation, and ripening', *Frontiers in Plant Science*, 4.

Miller, C. O., F. Skoog, M. H. Vonsaltza, and F. M. Strong. 1955. 'Kinetin, a cell division factor from deoxyribonucleic acid', *Journal of the American Chemical Society*, 77: 1392-92.

Moreno, J. E., Y. Tao, J. Chory, and C. L. Ballare. 2009. 'Ecological modulation of plant defense via phytochrome control of jasmonate sensitivity', *PNAS*, 106: 4935-40.

Naseem, M., N. Philippi, A. Hussain, G. Wangorsch, N. Ahmed, and T. Dandekar. 2012. 'Integrated systems view on networking by hormones in Arabidopsis immunity reveals multiple crosstalk for cytokinin', *Plant Cell*, 24: 1793-814.

Ning, Y. S., W. D. Liu, and G. L. Wang. 2017. 'Balancing immunity and yield in crop plants', *Trends in Plant Science*, 22: 1069-79.

Pan, X. Q., R. Welti, and X. M. Wang. 2010. 'Quantitative analysis of major plant hormones in crude plant extracts by high-performance liquid chromatography-mass spectrometry', *Nature Protocols*, 5: 986-92.

Peaucelle, A., H. Morin, J. Traas, and P. Laufs. 2007. 'Plants expressing a miR164-resistant *CUC2* gene reveal the importance of post-meristematic maintenance of phyllotaxy in Arabidopsis', *Development*, 134: 1045-50.

Raines, T., C. Shanks, C. Y. Cheng, D. McPherson, C. T. Argueso, H. J. Kim, J. M. Franco-Zorrilla, I. Lopez-Vidriero, R. Solano, R. Vankova, G. E. Schaller, and J. J. Kieber. 2016. 'The cytokinin response factors modulate root and shoot growth and promote leaf senescence in Arabidopsis', *Plant Journal*, 85: 134-47.

Rashotte, A. M., S. D. B. Carson, J. P. C. To, and J. J. Kieber. 2003. 'Expression profiling of cytokinin action in Arabidopsis', *Plant Physiology*, 132: 1998-2011.

Rashotte, A. M., and L. R. Goertzen. 2010. 'The CRF domain defines Cytokinin Response Factor proteins in plants', *BMC Plant Biology*, 10.

Rashotte, A. M., M. G. Mason, C. E. Hutchison, F. J. Ferreira, G. E. Schaller, and J. J. Kieber. 2006. 'A subset of Arabidopsis AP2 transcription factors mediates cytokinin responses in concert with a two-component pathway', *PNAS*, 103: 11081-85.

Reinhardt, D., E. R. Pesce, P. Stieger, T. Mandel, K. Baltensperger, M. Bennett, J. Traas, J. Friml, and C. Kuhlemeier. 2003. 'Regulation of phyllotaxis by polar auxin transport', *Nature*, 426: 255-60.

Schuman, M. C., and I. T. Baldwin. 2016. 'The layers of plant responses to insect herbivores.' in M. R. Berenbaum (ed.), *Annual Review of Entomology, Vol 61*.

Sheflin, A. M., J. S. Kirkwood, L. M. Wolfe, C. E. Jahn, C. D. Broeckling, D. P. Schachtman, and J. E. Prenni. 2019. 'High-throughput quantitative analysis of phytohormones in sorghum leaf and root tissue by ultra-performance liquid chromatography-mass spectrometry', *Analytical and Bioanalytical Chemistry*, 411: 4839-48.

Simura, J., I. Antoniadi, J. Siroka, D. Tarkowska, M. Strnad, K. Ljung, and O. Novak. 2018. 'Plant hormonomics: Multiple phytohormone profiling by targeted metabolomics', *Plant Physiology*, 177: 476-89.

Srivastava, A., and A. K. Handa. 2005. 'Hormonal regulation of tomato fruit development: A molecular perspective', *Journal of Plant Growth Regulation*, 24: 67-82.

Szczesny, T., A. L. Routier-Kierzkowska, and D. Kwiatkowska. 2009. 'Influence of *clavata3-2* mutation on early flower development in Arabidopsis thaliana: quantitative analysis of changing geometry', *Journal of Experimental Botany*, 60: 679-95.

Van Meulebroek, L., J. Vanden Bussche, K. Steppe, and L. Vanhaecke. 2012. 'Ultra-high performance liquid chromatography coupled to high resolution Orbitrap mass spectrometry for metabolomic profiling of the endogenous phytohormonal status of the tomato plant', *Journal of Chromatography A*, 1260: 67-80.

Vernoux, T., G. Brunoud, E. Farcot, V. Morin, H. Van den Daele, J. Legrand, M. Oliva, P. Das, A. Larrieu, D. Wells, Y. Guedon, L. Armitage, F. Picard, S. Guyomarc'h, C. Cellier, G. Parry, R. Koumproglou, J. H. Doonan, M. Estelle, C. Godin, S. Kepinski, M. Bennett, L. De Veylder, and J. Traas. 2011. 'The auxin signalling network translates dynamic input into robust patterning at the shoot apex', *Molecular Systems Biology*, 7.

Vernoux, T., J. Kronenberger, O. Grandjean, P. Laufs, and J. Traas. 2000. '*PIN-FORMED 1* regulates cell fate at the periphery of the shoot apical meristem', *Development*, 127: 5157-65.

Wang, D., K. Pajerowska-Mukhtar, A. H. Culler, and X. N. Dong. 2007. 'Salicylic acid inhibits pathogen growth in plants through repression of the auxin signaling pathway', *Current Biology*, 17: 1784-90.

Yang, F., H. T. Bui, M. Pautler, V. Llaca, R. Johnston, B. H. Lee, A. Kolbe, H. Sakai, and D. Jackson. 2015. 'A maize glutaredoxin gene, *Abphyl2*, regulates shoot meristem size and phyllotaxy', *Plant Cell*, 27: 121-31.